Two isoforms of pyruvate kinase enzymes in *Pseudomonas aeruginosa* with distinct functional and structural properties

Yassmin Abdelhamid Abdeldayem Karin

University of Cambridge

Department of Biochemistry

Murray Edwards College

April 2019

This dissertation is submitted for the degree of

Doctor of Philosophy

Declaration

The work presented in this dissertation was conducted at the Department of Biochemistry, University of Cambridge between April 2015 and December 2018 under the supervision of Dr. Martin Welch. This thesis is the result of my own work and includes nothing which is the outcome of work done in collaboration except as declared in the Preface and specified in the text. It is not substantially the same as any that I have submitted, or, is being concurrently submitted for a degree or diploma or other qualification at the University of Cambridge or any other University or similar institution except as declared in the Preface and specified in the text. I further state that no substantial part of my thesis has already been submitted, or, is being concurrently submitted for any such degree, diploma or other qualification at the University of Cambridge or any other University or similar institution except as declared in the Preface and specified in the text. The length of this thesis does not exceed the prescribed word limit stated by the Biology Degree Committee.

Two isoforms of pyruvate kinase enzymes in *Pseudomonas aeruginosa* with distinct functional and structural properties

Yassmin Abdelhamid Abdeldayem Karin

In most organisms, phosphofructokinase (PFK) and pyruvate kinase (PK) are the key glycolytic regulatory enzymes. However, the opportunistic human pathogen, *Pseudomonas aeruginosa*, relies entirely on the Entner-Doudoroff pathway for glycolysis, and consequently, does not encode a PFK homologue. It does encode two PK isozymes though, denoted PykA and PykF. This arrangement is uncommon in bacteria, although when it does arise, PykF is usually the dominant isozyme. In this project, I investigated the genetic, functional and structural characteristics of PykA and PykF in *P. aeruginosa*. The *P. aeruginosa* PykA and PykF enzymes are phylogenetically distinct, and display a number of unusual properties compared with the isozymes previously characterized from other species.

I found that a *pykA* mutant (but not a *pykF* mutant) of *P. aeruginosa* showed decreased growth on glucose and glycerol, suggesting that PykA is the dominant enzyme in this pathogen. However, a mutant defective in both *pykA* and *pykF* could be complemented (i.e., made to grow normally on glucose or glycerol) by expression of either enzyme *in trans*, indicating that both enzymes have the potential to be active. Consistent with the notion that PykA is the dominant enzyme in *P. aeruginosa*, I also found that PykA (but not PykF) was highly expressed under all conditions tested. Biochemical characterization revealed that purified PykA and PykF share similar catalytic activity, but were differentially regulated by a number of metabolites, most notably by intermediates from the anabolic pentose phosphate pathway. This suggests that *P. aeruginosa* coordinates glycolysis with the availability of key gluconeogenic precursors, which seems to be a common emerging theme for this pathogen. Given that PykA appears to play an important physiological role, it also represents an excellent target for the development of new antimicrobial agents. With this in mind, I found that a natural product, shikonin, inhibits PykA and prevents growth on glucose.

I also solved the x-ray crystal structures of *P. aeruginosa* PykA and PykF. The PykA structure revealed a proven regulator, glucose-6-phosphate (G6P), bound to an allosteric site and a substrate analogue, malonate, bound in the active site. Only one structure has previously been solved for a microbial PK containing a bound regulator – that of the PK from *Mycobacterium tuberculosis* (Mtb). Interestingly, the G6P binding site in *P. aeruginosa* PykA was clearly distinct from the G6P binding site in Mtb PK. Based on my results, I propose a mechanism by which the conformational change might be transmitted from the allosteric G6P site to the active site of PykA. By contrast, the *P. aeruginosa* PykF structure was solved in the apo-state, with no bound ligands. However, this too proved to be distinct from the structure proposed for PykF from *Escherichia coli*.

Acknowledgements

Contents

Chapter 1: Introduction

Chapter 2: Materials and methods

Chapter 4: Biochemical characterization of PykA and PykF

Chapter 5: Crystal structures of PykA and PykF

List of Figures

Chapter 5

List of Tables

List of Appendixes

Abbreviations

μm	Micromolar
6PG	6-phosphogluconate
Å	Angstrom
ADP	Adenosine diphosphate
AMP	Adenosine monophosphate
ATP	Adenosine triphosphate
AUC	Analytical ultracentrifugation
bp	base pair
CAG-DPKP	cAMP/cGMP dependent protein kinase phosphorylation
Carb^R	Carbenicillin resistant
Cm^R	Chloramphenicol resistant
dH$_2$O	Deionized water
DMSO	Dimethyl sulfoxide
DNA	Deoxyribonucleic acid
dNTP	Deoxynucleotide triphosphate
EDP	Entner-Doudoroff Pathway
EDTA	Ethylenediamine tetraacetic acid
EMPP	Embden-Meyerhof-Parnas Pathway
F1,6P	Fructose 1,6-bisphosphate
F6P	Fructose 6-phosphate
G3P	Glyceraldehyde 3-phosphate
G6P	Glucose 6-phosphate
GDP	Guanosine diphosphate
GTP	Guanosine triphosphate
IPTG	Isopropyl β-D-1-thiogalactopyranoside
kb	kilobase pair
kDa	Kilodaltons
KDPG	2-*keto*-3-deoxy-6-phosphogluconate
LB	Luria-Bertani (broth or agar)
LDH	Lactate dehydrogenase
M	Molar
MLI	sodium malonate
mM	Millimolar
MUG	4-methylumbelliferyl-β-D-galactopyranoside
NAD (H)	Nicotinamide adenine dinucleotide (reduced form)
Ni-NTA	Nickel-nitrilotriacetic acid
nm	nanometre
nM	nanomolar
OD	Optical density
ORF	Open reading frame

PAO1	A laboratory wild-type strain of *P. aeruginosa*
PBS	Phosphate buffer saline
PCR	Polymerase chain reaction
PDB	Protein data bank
PEG	Polyethylene glycol
PEP	Phospho*enol*pyruvate
PK	Pyruvate kinase
PPP	Pentose-phosphate Pathway
PVDF	Polyvinylidene difluoride
PykA	Pyruvate kinase type II
PykF	Pyruvate kinase type I
R5P	Ribose 5-phosphate
RFU	Relative fluorescence unit
RL5P	Ribulose 5-phosphate
rpm	revolutions per minute
SDS	Sodium dodecyl sulphate
SDS-PAGE	SDS polyacrylamide gel electrophoresis
TCA	Trichloroacetic acid cycle
Tet^R	Tetracycline resistant
TKP	Tyrosine kinase phosphorylation
UWGC	University of Washington Genome Centre
WT	Wild-type
X5P	Xylulose 5-phosphate

Chapter 1

1   Introduction

1.1   *Pseudomonas aeruginosa*

1.1.1 General features

Pseudomonas aeruginosa is a rod-shape, Gram-negative, motile bacteria that can grow in aerobic as well as anaerobic conditions. It is a metabolically versatile organism that is often present in the soil, but it can also thrive on natural and artificial surfaces including in medical facilities (Gellatly and Hancock, 2013). *P. aeruginosa* is an opportunistic pathogen, meaning that it is not a threat to healthy individuals, whereas infections by *P. aeruginosa* mostly develop when the immune system is compromised (Lyczak et al., 2000).

P. aeruginosa infections are commonly seen in patients with cystic fibrosis. The disease itself is genetic and caused by a mutation of the CFTR (cystic fibrosis transmembrane conductance regulator) gene that is responsible for the normal transport of chloride ions across the epithelial cell membranes. The mutation of the CFTR, therefore, alters the ionic balance across the epithelium leading to accumulation of thick mucus that is difficult to clear (Riordan et al., 1989). CF affects different parts of the body, including the lungs where the disease usually gets complicated by secondary bacterial infections of *P. aeruginosa*. The persistent infection of the CF lungs by *P. aeruginosa* causes irreversible tissue damage, leading to severe impairment of patient quality of life and, eventually, to death (Flume et al., 2007).

1.1.2   Virulence factors

The *P. aeruginosa* genome encodes numerous virulence factors that facilitate the establishment and persistence of infections, as well as evasion of the host immune system (Bianconi et al., 2015). These virulence determinants can be used by *P. aeruginosa* to mediate both acute and chronic infections. Figure 1.1 illustrates the major virulence factors associated with *P. aeruginosa* infections.
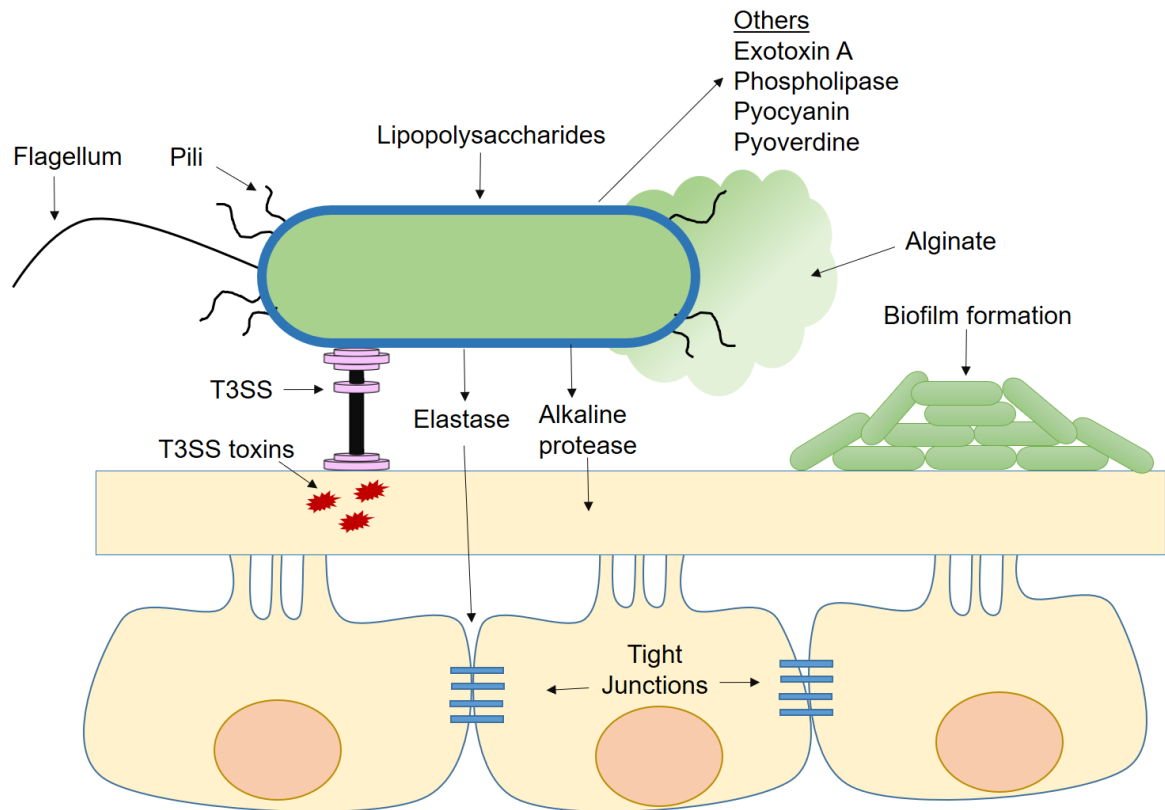
Figure 1.1: Major virulence factors in *P. aeruginosa* (adapted from Gellatly and Hancock, 2013). The pathogenicity of *P. aeruginosa* is attributed to multiple virulence factors that can be cell surface-associated (lipopolysaccharide layer, flagellum, pili, T3SS), secreted (proteases, alginate, exotoxin A, pyocyanin, pyoverdine, phosholipases) or behaviour-related (biofilm).

1.1.2.1 Biofilm formation

Biofilm formation is the transition of bacteria from a free swimming lifestyle (planktonic state) into cell aggregations (sessile state) that are embedded in an extracellular polymeric substance (EPS). With this, the bacteria can adhere to the host cells, while being protected from the surrounding environment (O'Toole et al., 2000). The EPS is considered as reservoir of nutritional metabolites and also acts as a shield against environmental stressors and antimicrobial agents (Mann and Wozniak, 2012). In *P. aeruginosa* biofilms, the EPS is made of exopolysaccharides (Psl, Pel, alginate) (Periasamy et al., 2015), biosurfactant rhamnolipid (Davey et al., 2003), extracellular DNA from dead bacteria (Whitchurch et al., 2002) and proteins such as flagella and type IV pili (Klausen et al., 2003).

Within *P. aeruginosa* biofilms, cell-to-cell communication is facilitated by a social phenomenon known as quorum sensing. Using this social behaviour, bacteria use chemical signals to regulate the expression of large number of operons, in response to population density (Smith et al., 2002). For example, there are nearly 40 identified genes in *P. aeruginosa* (including metabolic and virulence genes) that are controlled only by quorum sensing signals of acyl-homoserine lactone (Whiteley et al., 1999).

When *P. aeruginosa* grows in biofilms, the cells become more tolerant to hostile conditions, but become less virulent (Winstanley et al., 2016). *P. aeruginosa* can form mucoid biofilms in the airways of CF patients and these biofilms are resilient to nutrient limitations, oxidative stress and antimicrobial treatment (Mah et al., 2003). Mucoid biofilms are typically developed due to mutation of *mucA*. When MucA is functional, it interacts with and sequesters AlgU (a sigma factor required for alginate production) leading to suppression of alginate expression. In contrast, defective MucA is unable to bind or sequester AlgU and this in turn enhances alginate biosynthesis (Martin et al., 1993). After the biofilms are formed, *P. aeruginosa* infections become persistent and the pathogen dominates the pulmonary tissue over other species (McDaniel et al., 2015).

1.1.2.2 The type III secretion system (T3SS)

The T3SS is a hollow needle-like structure present at the cell surface of *P. aeruginosa*, through which the pathogen delivers its effectors (ExoS, ExoT, ExoU, ExoY) directly into the host cytoplasm (Coburn et al., 2007). The effectors of T3S are toxigenic with broad anti-host properties and they act by enhancing tissue destruction (Finck-Barbançon et al., 1997), reducing wound healing and opposing phagocytosis (Garrity-Ryan et al., 2000). Moreover, they are responsible of dissemination of *P. aeruginosa* cells from the primary colonization sites into the bloodstream leading to septicaemia (Koh et al., 2005). Thus, *P. aeruginosa* infections associated with a functional T3SS are an indication of a poor clinical prognosis (Roy-Burman et al., 2001).

1.1.2.3 Motility appendages

P. aeruginosa has one long polar flagellum and few short type IV pili, present at the cell surface, which are primarily used for motility activities. These proteinaceous appendages are also considered indispensable for virulence as they promote attachment to the host cells, establishment of biofilms and cause inflammation (Haiko and Westerlund-Wikström, 2013). Whilst acute infections of *P. aeruginosa* are mostly associated with flagellated cells, flagella-encoding genes are down-regulated in chronic infections such as those associated with CF (Wolfgang et al., 2004).

Compared with flagella, pili are more selective in targeting cell types (Ramphal and Vishwanath, 1987) and they are known to enhance formation of microcolonies that are commonly found in the sputum of CF patients (Lam et al., 1980; Matz et al., 2004). Microcolonies are formed by the aggregation and concentration of bacteria on host tissues as means of protection from the host immune response and antimicrobial therapy (Craig et al., 2004). The absence of pili from *P. aeruginosa* cells is a sign of reduced pathogenicity (Tang et al., 1995).

1.1.2.4 Proteases

P. aeruginosa produces a number of proteases that are capable of causing profound destruction of host cells, such as alkaline protease, LasA (metallopeptidase) and LasB (zinc metalloprotease) (Alhazmi, 2015). Protease production is commonly associated with severe infections of the respiratory tract, cornea and burn wounds (Hobden, 2002; Bielecki et al., 2008; Blackwood et al., 1983). Alkaline protease causes destruction of the host fibronectins and the protein complement systems leading to severe impairment of the host immune response (Laarman et al., 2012). LasB and LasA are elastases and both can be found in sputum samples from CF patients, especially during acute pulmonary exacerbation episodes (Hollsing et al., 1987). However, the destructive ability of LasB is more potent than that of LasA (Matsumoto, 2004) and bacterial cells that lack LasB can be easily phagocytosed and cleared by the host immune system (Mariencheck et al., 2003; Kuang et al., 2011).

1.1.2.5 Lipopolysaccharide

The outer membrane of *P. aeruginosa* is made of a complex lipopolysaccharide layer, which is comprised of hydrophobic lipid A, an oligosaccharide core and a distal polysaccharide O-antigen (Pier, 2007). The lipid A and the O-antigen are amongst the most antigenic factors of *P. aeruginosa*, and can strongly provoke all types of host immune response (Heine et al., 2001). The elicited immune response from these components underlies the extensive tissue inflammation, high morbidity and mortality rates that are commonly associated with *P. aeruginosa* infections (Li et al., 1997). Due to the high antigenicity of the LPS components, multiple attempts were made to include these structures in immunization of CF patients, however, all remained unsuccessful (Döring and Pier, 2008).

1.1.2.6 Production of alginate

Alginate is a mucoid exopolysaccharide substance produced by some pseudomonads including *P. aeruginosa* (Gacesa and Wusteman, 1990; Fett et al., 1995). Mucoid strains of *P. aeruginosa* can be isolated from the lungs of the CF patients and are associated with poor clinical prognosis (Pedersen, 1992). Alginate plays a prominent role during biofilm formation because it facilitates adhesion of bacterial cells to the host tissue and it also protects the cells from external antimicrobial penetration (Boyd and Chakrabarty, 1995; May et al., 1991). Production of alginate together with the LPS layer cause synergistic effects on the immune response owing to their high antigenicity (McCaslin et al., 2015).

1.1.3 Antibiotic resistance of *P. aeruginosa*

P. aeruginosa is one of the "ESKAPE" pathogens, which are known to be highly resistant to antibiotics, and they require urgent development of antimicrobials. Besides, *P. aeruginosa*, ESKAPE pathogens also include *Enterococcus faecium*, *Staphylococcus aureus*, *Klebsiella pneumoniae*, *Acinetobacter baumannii*, and *Enterobacter* species (Santajit and Indrawattana, 2016). The antimicrobial resistance of *P. aeruginosa* is primarily due to intrinsic and/or acquired factors.

1.1.3.1 Intrinsic causes

a) Low outer membrane permeability

The outer membrane of *P. aeruginosa* is one of the main barriers that prevents antimicrobials from penetrating the bacterial cell. The pathogen has an outer cell membrane that impedes the entry of antimicrobials to the inner side of the cell (Livermore, 1984). Compared with *E. coli*, the outer membrane of *P. aeruginosa* is one hundred times more impermeable to hydrophilic agents (Yoshimura and Nikaido, 1982). The reduced permeability of the outer membrane in *P. aeruginosa* is attributed to the scarcity and inefficiency of the large channel porin (OprF) and the presence of many narrow channel porins (OprD and OprB) (Nikaido et al., 1991). With this, the pathogen is highly resistant to antimicrobials, unless the outer membrane barrier is perturbed by cationic antimicrobial peptides (Scott et al., 1999) or the narrow channel porins are widened by mutation (Huang and Hancock, 1996).

b) Efflux pumps

P. aeruginosa has a number of drug efflux systems including MexAB-OprM, MexXY-OprM, MexCD-OprJ, MexEF-OprN and MexJK-OprM (Schweizer, 2003). In the first system, MexB functions as the main pump that transports the antibiotic from the cytoplasm to the periplasm. The drug is subsequently uptaken by the MexA linker protein and is delivered to the outer membrane. The MexAB system then collaborates with the OprM outer membrane protein to expel the antibiotic from the outer membrane to the exterior (Zhao et al., 1998). The other systems operate in a similar fashion, some using alternatives to OprM (Aires et al., 1999). Using the multi-drug efflux systems, *P. aeruginosa* can get rid of antibiotics, biocides, detergents and other small inhibitors (Schweizer, 2003). On the other hand, mutation of the drug efflux pumps increases the susceptibility of *P. aeruginosa* to a wealth of antibiotics (Hancock and Speert, 2000).

c) Production of β-lactamase

The resistance of *P. aeruginosa* to β-lactam antimicrobials is mainly attributed to the production of β-lactamase. The enzyme cleaves the β-lactam ring of pencillins, cephalosporins and carbapenems leading to loss of bioactivity (Newsom et al., 1970). The enzyme is expressed in the cell periplasm and is encoded by the *ampC* gene (Jacoby,

2009). Expression of the β-lactamase is induced upon exposure to β-lactam containing antibiotics and carbapenems (Hancock and Speert, 2000). Resistance to β-lactams is due to an interplay between the β-lactamase activity and the drug efflux pumps (Masuda et al., 1999). In strains that lack or exhibit inducible β-lactamase activity, the MexAB-OprM efflux system contributes greatly to enhanced β-lactam resistance, whereas in strains that overexpress the β-lactamase, there is little contribution from the efflux pump (Nakae et al., 1999).

1.1.3.2 Acquired causes

P. aeruginosa applies many adaptive mechanisms in order to evade treatments by antibiotics. These acquired mechanisms explain in part the discrepancy between the poor treatment outcomes of CF patients and the susceptibility of the laboratory strains to antibiotics (Alhazmi, 2015). *P. aeruginosa* acquires antibiotic resistance primarily after continuous exposure of the bacteria to environmental stresses, or after the administration of sub-lethal doses of antibiotics, or during biofilm formation. These factors can either promote antibiotic resistance via horizontal gene transfer or induce other mutational modifications that reduce susceptibility of the bacteria to antibiotics (Gilleland et al., 1989).

Resistance to cationic antimicrobial peptides is one of the commonly seen examples of an acquired resistance of *P. aeruginosa*, which occurs independent of genetic mutations (Gellatly and Hancock, 2013). The continuous exposure of *P. aeruginosa* to polymyxins together with magnesium restrictions stimulate multiple sensor kinases in the cell, which lead to changes of the cell surface and insensitivity to cationic antimicrobial peptides (McPhee et al., 2006). An example of a mutation-induced antibiotic resistance is the mutation of *mexZ*, the transcriptional regulator. The *mexZ* gene normally represses expression of the MexXY efflux pump, whereas mutation of it causes overexpression of the MexXY system and confers resistance to aminoglycosides (Yamamoto et al., 2009).

Persister cells are a subpopulation of bacteria that mostly evolve due to an inactive metabolic state, known as dormancy, and they are characterized by resistance to antimicrobial treatment (Wood et al., 2013). Persister cells of *P. aeruginosa* are primarily

present in the lungs of CF patients and they contribute to the failure of antibiotic treatment in these individuals (Mulcahy et al., 2010). In contrast to bacteria with inherent antibiotic resistance, persisters cannot grow in the presence of antibiotics (Wood et al., 2013). Moreover, antibiotic resistance in these cells is temporary and emerges independently on horizontal gene transfer or genetic mutations (Miyaue et al., 2018). The drug tolerance of persister cells is mainly associated with changes in the toxin-antitoxin systems (Grady and Hayes, 2003). In normal conditions, toxins are inactive by binding to their cognate antitoxins. In contrast, under stress conditions, the antitoxins are easily degraded because they are more labile than their toxins and this allows toxins to exert their harmful effects in the cell including inhibition of cell growth, promotion of dormancy and induction of drug resistance (Page and Peti, 2016).

1.2 Glycolysis in bacteria

Glycolysis is one of the most conserved metabolic processes in a living organism. It supplies the cell with the energy and essential metabolites that are required for cell function, whilst converting glucose into pyruvate (Noor et al., 2010). The Embden-Meyerhof-Parnas pathway (EMPP), the Entner-Doudoroff pathway (EDP) and the pentose-phosphate pathway (PPP) are the primary glycolytic routes in bacteria (Conway, 1992). The sequence of lower reactions of the EMPP and the EDP is the same and they differ only in the upper part of each pathway. The PPP is more distinctive than the EMPP and the EDP and runs parallel to these. The PPP can be split into an upper oxidative and a lower non-oxidative phase. *P. aeruginosa* relies exclusively on the EDP for glycolysis, so this chapter is focused mainly on the role of EDP in metabolism.

1.2.1 General characteristics of the EDP

The EDP is a primitive glycolytic pathway that was first described in *Pseudomonas saccharophila* (Entner and Doudoroff, 1952; Kresge et al., 2005). The pathway is commonly found in Gram-negative bacteria and to a lesser extent in Gram-positive species (Kersters and De Ley, 1968). It was also recently described as a metabolic pathway in cyanobacterium *Synechocystis* and, the plant, *Hordeum vulgare* (Chen et al., 2016). The EDP is evolutionarily more ancient than the EMPP because it is mostly found in primitive, deep-rooted and slow-evolving organisms than does EMPP (Romano and

Conway, 1996). However, phylogeny analysis based on the availability of the EMPP and the EDP enzymes revealed the EMPP is more widely distributed among the different bacterial families compared with the EDP (Figure 1.2). Moreover, the key enzymes of both pathways can sometimes co-exist in some species (Flamholz et al., 2013), such as *E. coli*. In *E. coli*, the EMPP and the EDP operate alternately according to the cell's metabolic demands (Fraenkel, 1986).
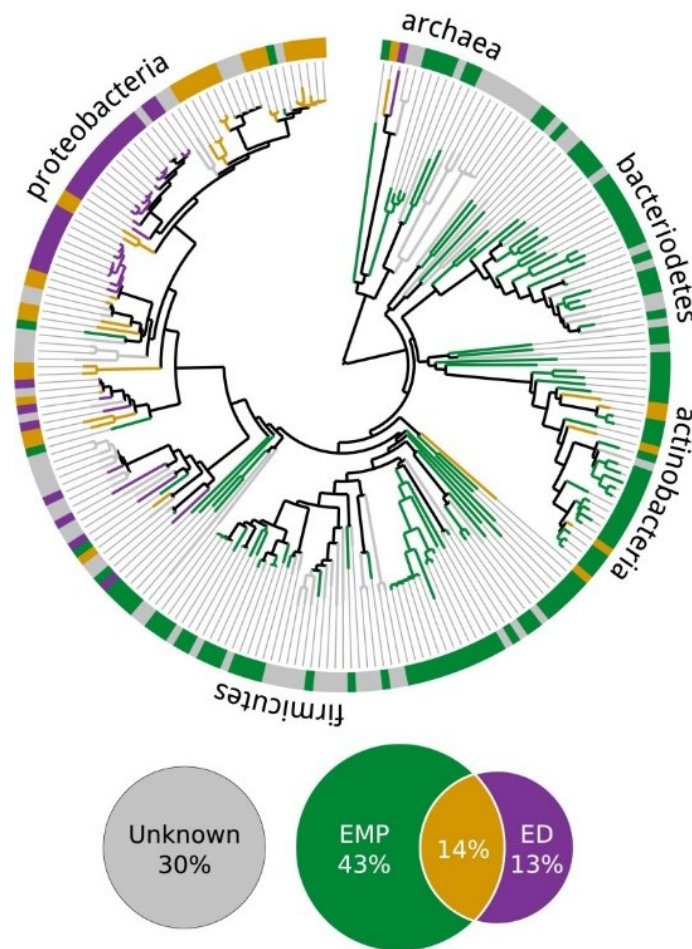
Figure 1.2: Distribution of the EDP and the EMPP among bacterial families (adapted from Flamholz et al., 2013). Organisms are classified as ED-capable (encoding 6-phosphogluconate dehydratase and 2-*keto*-3-deoxy-6-phosphogluconate aldolase, which are specific to the EDP) and EMP-capable (encoding 6-phosphofructokinase, which is specific to the EMPP). Each group of organisms also encodes a pyruvate kinase enzyme, given its essentiality for both pathways. The bottom Venn diagram demonstrates the percentage of each pathway in a non-redundant set of prokaryotes. The EMPP and the EDP are present among 57% and 27% of prokaryotes, respectively. Of these organisms, only 13% rely exclusively on the EDP for metabolism.

1.2.2 The key reactions of the EDP and the EMPP

The EDP operates using a unique set of enzymes other than those used by the EMPP (Conway, 1992). The 6-phosphogluconate dehydratase (Edd, EC 4.2.1.12) and the 2-*keto*-3-deoxy-6-phosphogluconate (KDPG) aldolase (Eda, EC 4.1.2.14) are the key enzymes of the EDP, whereas the 6-phosphofructokinase (Pfk, EC 2.7.1.11) is specific for the EMPP.

The general scheme of the EDP and EMPP is quite similar and differs at the upper part of glycolysis (Figure 1.3). In both pathways, a six-carbon phosphorylated metabolite is first formed and then cleaved by an aldolase enzyme yielding two three-carbon products (Peekhaus and Conway, 1998). In the EDP, the Edd catalyses the dehydration of 6-phosphogluconate (6PG) to produce KDPG; the six-carbon metabolite of the EDP (Kovachevich and Wood, 1955a). KDPG is subsequently cleaved by KDPG aldolase (Eda) to yield two three-carbon products; pyruvate and glyceraldehyde 3-phosphate (G3P) (Kovachevich and Wood, 1955b). Alternatively in the EMPP, Pfk catalyses the phosphorylation of fructose 6-phosphate (F6P) to yield fructose 1,6-bisphosphate (F1,6P); the six-carbon metabolite of the EMPP. The F1,6P is then cleaved into two three-carbon products; dihydroxyacetone phosphate (DHAP) and G3P (Drechsler et al., 1959). After the aldolase step, both the EDP and the EMPP share the same set of lower glycolytic pathway reactions to synthesize pyruvate.

1.2.3 Types of EDP in bacteria

Although the EDP is a primitive form of glycolysis, its operation is more complicated than it initially seems to be. There are several operational modes of the EDP that correlate perfectly with the lifestyle of different organisms (Conway, 1992). Among all modes, pseudomonads operate the EDP in a unique cyclic fashion that is not present in other EDP-dependent microorganisms.
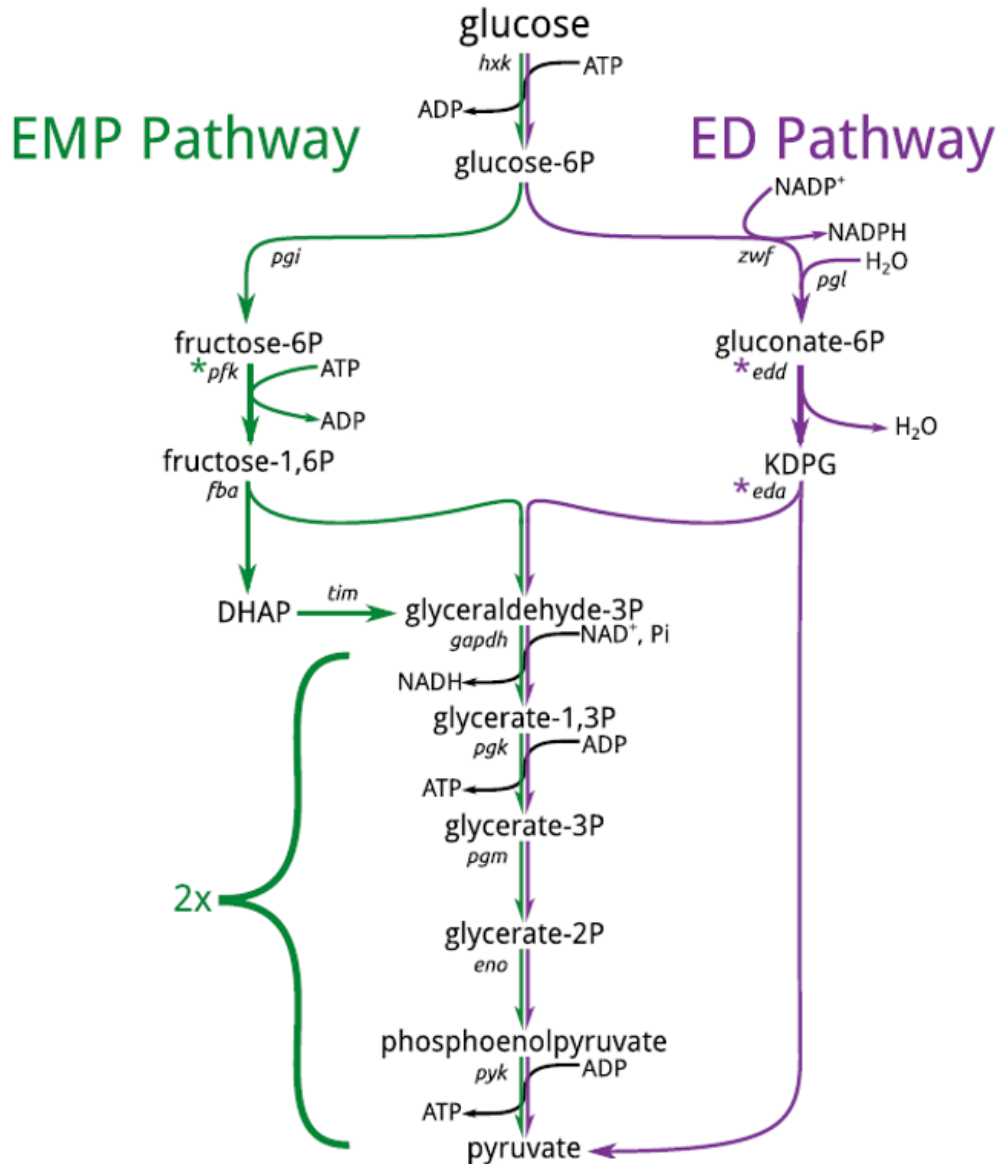
Figure 1.3: Schematic representation of the EDP and the EMPP (adpated from Flamholz et al., 2013). The EDP and the EMPP are represented by purple and green arrows, respectively. Each pathway has an upper unique part (from glucose 6-phosphate to glyceraldehyde 3-phosphate) and a common lower part (from glyceraldehyde 3-phosphate to pyruvate). Asterisks highlight the unique enzymes of each pathway. Edd and Eda are specific to the EDP, whereas Pfk is specific to the EMPP. Abbreviations: *hxk*, hexokinase; *zwf*, glucose 6-phosphate dehydrogenase; *pgl*, phosphogluconolactonase; *edd*, phosphogluconate dehydratase; *eda*, KDPG aldolase; *pgi*, phosphoglucose isomerase; *pfk*, 6-phosphofructokinase; *fba*, fructose bisphosphate aldolase; *tim*, triosephosphate isomerase; *gapdh*; glyceraldehyde 3-phosphate dehydrogenase; *pgk*, phosphoglycerate kinase; *pgm*, phosphoglycerate mutase; *eno*, enolase; *pyk*, pyruvate kinase.

1.2.3.1 The cyclic EDP

The cyclic EDP is an inducible pathway that is commonly present in pseudomonads, where the induced enzymes vary according to the inducer molecule (Udaondo et al., 2018). The cyclic EDP operates by using side branches of the EDP that mainly serve gluconeogenesis. Thus, this special operation of the EDP requires a series of gluconeogenic enzymes to be present and these include the triose phosphate isomerase, fructose 1,6-bisphosphate aldolase, fructose 1,6-bisphosphatase, phosphoglucose isomerase and glucose 6-phosphate dehydrogenase (Conway, 1992).

P. aeruginosa lacks *pfk* (Lessie and Phibbs, 1984) and phosphogluconate dehydrogenase (Temple et al., 1998), which are necessary for the regular operation of the EMPP and the oxidative PPP, respectively (Figure 1.4). Instead, it relies heavily on the EDP for metabolism which can operate both in a linear and cyclic fashion (Kersters and De Ley, 1968). In the linear EDP, G3P feeds downwards into the lower glycolytic branch of the EDP to yield pyruvate which in turn joins the tricarboxylic acid (TCA) cycle. In contrast, in the cyclic EDP, the G3P feeds into the side branches of the EDP (the reversal of the EMPP and the non-oxidative PPP), yielding back glucose 6-phosphate (Phibbs, 1988; Lessie and Phibbs, 1984; Tiwari and Campbell, 1969; Conway, 1992).

Amongst bacterial species, the cyclic operation of the EDP is common in pseudomonads. Despite the availability of the EDP enzymes in other species, they cannot operate the EDP in a cyclic way. For example, in *E. coli*, the EDP functions only in one direction using glyceraldehyde 3-phosphate dehydrogenase (Hillman and Fraenkel, 1975). The latter enzyme converts G3P into 1,3-bisphosphoglycerate, thus directs the carbon flux mainly towards lower glycolysis (Daldal and Fraenkel, 1983; Chambost and Fraenkel, 1980).

1.2.3.2 The inducible linear EDP (IL-EDP)

The genes encoding the IL-EDP require induction by certain metabolites and the pathway under this mode operates unidirectionally (Figure 1.5). The IL-EDP is more common among enteric bacteria, where glycolysis depends mainly on other metabolic routes, whereas the EDP has only a secondary role. *E. coli* is one of the enteric species that

can operate the IL-EDP. In *E. coli*, the EMPP and the PPP are the main metabolic pathways, but when gluconate is available, the metabolism switches to the EDP (Eisenberg and Dobrogosz, 1967). The presence of gluconate in the cell induces the synthesis of the EDP enzymes, gluconate transporters and gluconate metabolic enzymes (Istúriz et al., 1986). Moreover, when glucose and gluconate are both available in the cells, they are co-metabolized and boost the cell yield in *E. coli* compared with when glucose is the sole carbon source. Thus, by using the IL-EDP, the enteric bacteria gains far more advantages than by using the EMPP alone (Fliege et al., 1992). The end products of the IL-EDP depend on the oxygen levels in the cell. If oxygen and gluconate are present, the carbon flux feeds into the TCA cycle, whereas under anaerobic conditions with gluconate, the EDP yields ethanol and CO_2 as fermentation end products (Istúriz et al., 1986).
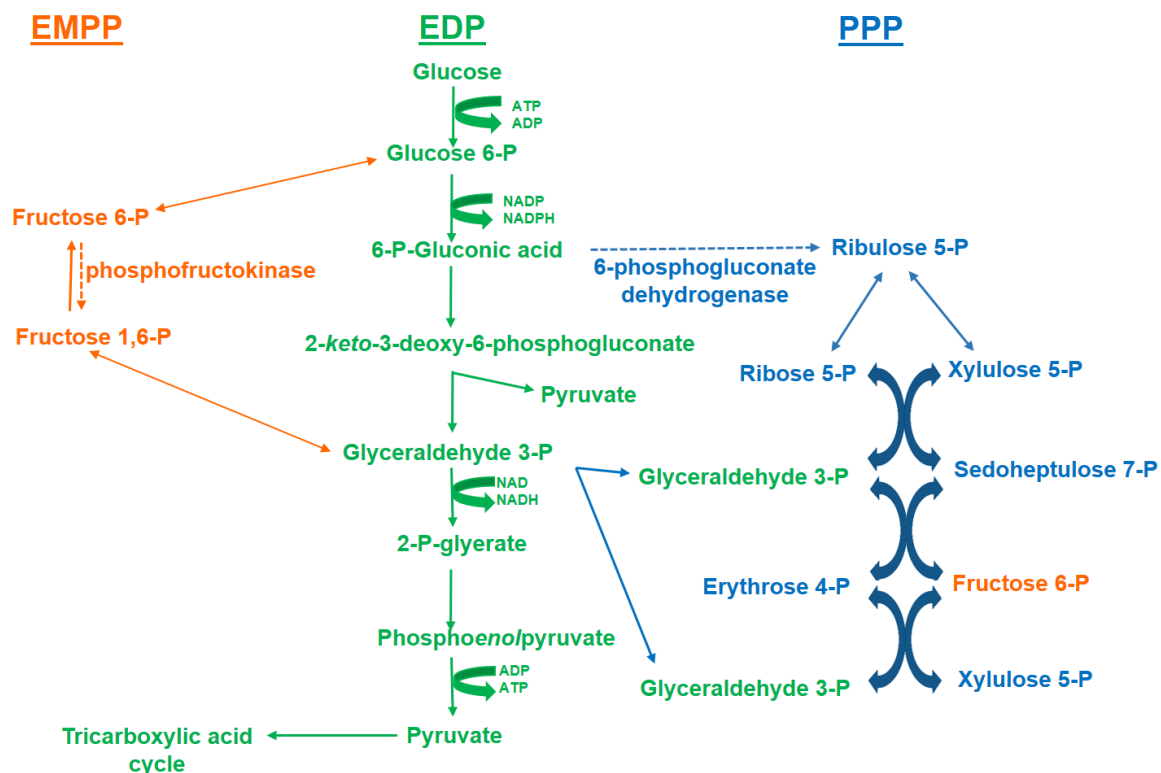
Figure 1.4: Schematic representation of the EDP in *P. aeruginosa*. *P. aeruginosa* lacks phosphofructokinase and 6-phosphogluconate dehydrogenase that operate the EMPP and the oxidative PPP, respectively. *P. aeruginosa*, however, relies heavily on the EDP for metabolism that operates in a linear and a cyclic fashion. In the linear EDP (green), the carbon flux feeds unidirectional from glucose 6-phosphate to the tricarboxylic acid cycle, whereas in the cyclic mode, the carbon flux is recycled from glyceraldehyde 3-phosphate into the gluconeogenic direction of EMPP (orange) and non-oxidative PPP (blue).

1.2.3.3 The constitutive linear EDP (CL-EDP)

The genes encoding the CL-EDP are constitutively expressed and the pathway itself operates in one direction (Figure 1.5). This pathway is used by both aerobic and anaerobic bacteria with end products that are adjustable accordingly. For example, the facultative anaerobe *Zymomonas mobilis* produces ethanol and CO_2 as end products from the CL-EDP, whereas the aerobe *Neisseria gonorrhoeae* produces acetate and CO_2 as end products from same pathway (Baratti and Bu'lock, 1986; Morse et al., 1974; Rogers et al., 1979).

1.2.4 Main products of the EDP

Although the main purpose of the EDP and the EMPP is to provide energy and biosynthetic materials, their end products are dissimilar. Whilst the EDP produces one ATP, one NADH and one NADPH, the EMPP produces two ATPs and two NADH molecules (Flamholz et al., 2013). Thus, the EMPP surpasses the EDP in providing energy and biomass precursors to the cell (Bar-Even et al., 2012), whereas the EDP provides more tolerance to oxidative stress via NADPH production (Kim et al., 2008).

1.2.4.1 Energy yield

The EDP invests one ATP during the phosphorylation of glucose into glucose 6-phosphate in order to yield KDPG. The latter is cleaved into G3P and pyruvate, and G3P undergoes substrate-level phosphorylation during lower glycolysis to produce two ATPs. Thus, the net energy production from the EDP is one ATP molecule (Bar-Even et al., 2012). By contrast, glycolysis by the EMPP consumes two ATP molecules during the phosphorylation of glucose into glucose 6-phosphate and the phosphorylation of fructose 6-phosphate into fructose 1,6-bisphosphate. The latter is then cleaved into G3P and DHAP, and both undergo substrate-level phosphorylation providing four ATP molecules. With this, the net yield of the EMPP is two ATP molecules (Bar-Even et al., 2012; Kim and Gadd, 2008).
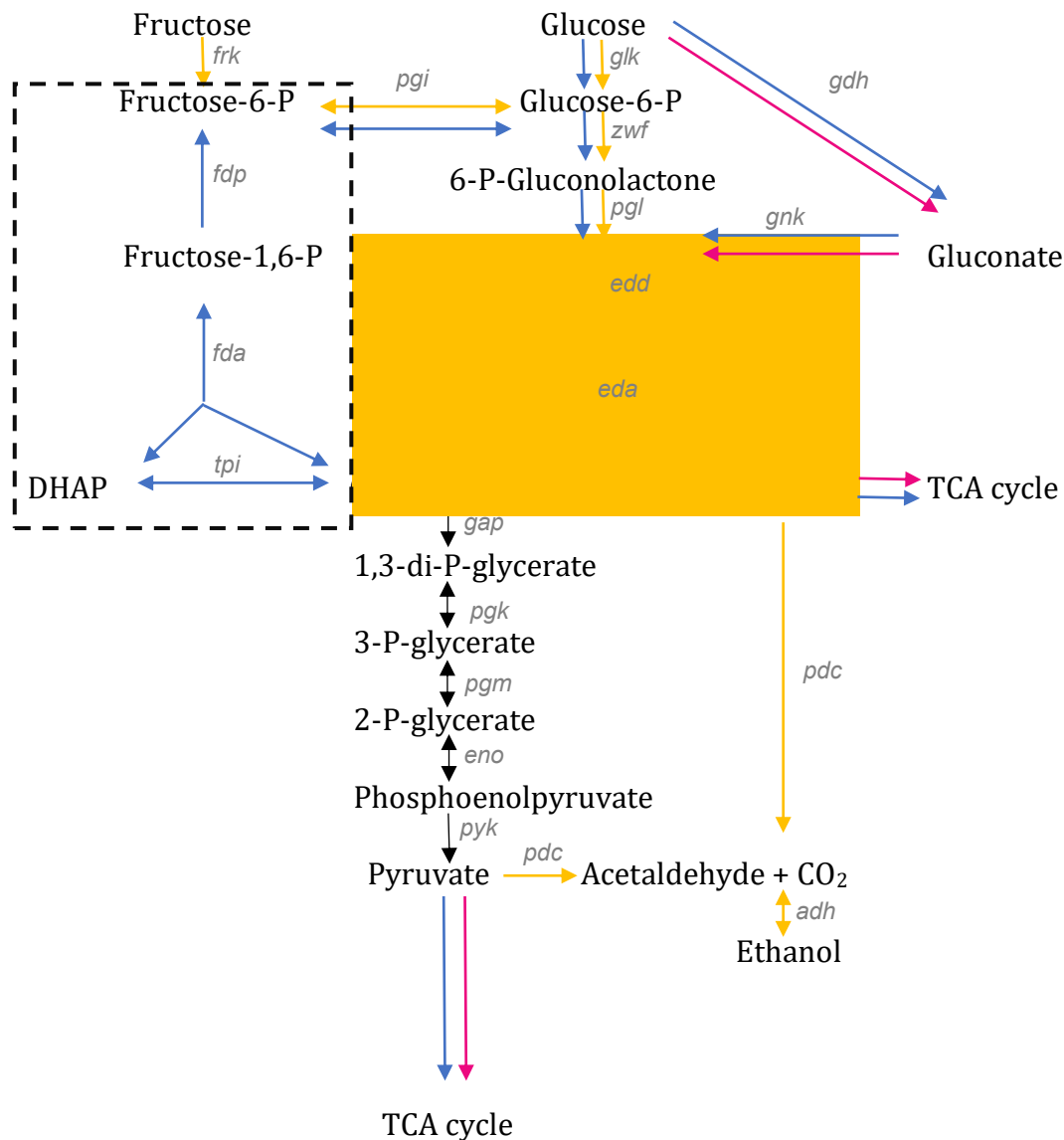
Figure 1.5: Types of EDP in bacteria (combined figures from Conway, 1992). The EDP can operate in constitutive-linear (yellow), inducible-linear (red) or inducible-cyclic (blue) manner. The yellow box highlights the common reactions in all types of EDP and the dashed box bounds the cyclic operation of the EDP which is common in *Pseudomonas* species. Abbreviations: glucokinase (*glk*), glucose dehydrogenase (*gdh*), gluconokinase (*gnk*), fructokinase (*frk*), triose phosphate isomerase (*tpi*), fructose bisphosphate aldolase (*fda*), fructose bisphosphatase (*fdp*), phosphoglucose isomerase (*zwf*), 6-phosphogluconolactonase (*pgl*), 6-phosphogluconate dehydratase (*edd*), 2-*keto*-3-deoxy-6-phosphogluconate aldolase (*eda*), glyceraldehyde 3-phosphate dehydrogenase (*gap*), phosphoglycerate kinase (*pgk*), phosphoglycerate mutase (*pgm*), enolase (*eno*), pyruvate kinase (*pyk*), pyruvate dehydrogenase (*pdc*), alcohol dehydrogenase (*adh*), DHAP (dihydroxyacetone phosphate), tricarboxylic acid cycle (TCA cycle).

15

The energy yield from the EDP and the EMPP is directly correlated with their prevalence in bacteria. Thus, the EDP is mostly present in aerobic and facultative anaerobic bacteria where the ATP requirements are relatively low. In contrast, the EMPP is more prevalent in fermentative anaerobic strains where the ATP requirement is much greater and can only be driven from high energy producing reactions such as substrate-level phosphorylation (Hofmann, 1976; Ronimus and Morgan, 2001; Flamholz et al., 2013). Although the EDP seems to be less energy-efficient than the EMPP, it still has an interesting wide prevalence among prokaryotes (Fuhrer et al., 2005). This is mostly attributed to the low protein needs for production of energy in EDP-dependent organisms, compared with the EMPP-dependent organisms where more protein is invested in production of enzymes that operate the pathway (Flamholz et al., 2013).

1.2.4.2 High reducing power

Microorganisms that depend on the EDP are more resistant to external and internal stress compared with those which use the EMPP (Kim et al., 2008; Chavarría et al., 2013). Although both pathways can generate NADH (reduced nicotinamide adenine dinucleotide), the EDP can additionally provide the cell with NADPH (reduced nicotinamide adenine dinucleotide phosphate) during the oxidation of glucose 6-phosphate into 6-phosphogluconolactone (Levy, 2006). Through the reducing power of NADPH, bacteria like *Pseudomonas aeruginosa* can cope better with the surrounding hostile environmental conditions. For example, *P. putida* (EDP-dependent) was more tolerant to redox stress than *E. coli* (EMPP-dependent), when both were exposed to a sulfhydryl-oxidizing agent. Moreover, switching to the EMPP in *P. putida* (by knocking-in phosphofructokinase) caused a significant drop in the growth rate due to the decline in the NADPH production (Chavarría et al., 2013).

1.3 Pyruvate kinase

1.3.1 The reaction of pyruvate kinase

Pyruvate kinase (PK, E.C. 2.7.1.40) is an ancient enzyme that is indispensable for glycolysis of prokaryotes and eukaryotes (Hattori et al., 1995) and it is located at the node between the lower arm of glycolysis and the TCA cycle. PK catalyses the production of pyruvate in two steps (Figure 1.6). The first step is the transfer of a phosphoryl group from phospho*enol*pyruvate (PEP) to adenosine diphosphate (ADP) yielding adenosine triphosphate (ATP) and enolate (Seeholzer et al., 1991) and the second step is the conversion of enolate to pyruvate by proton transfer (Rose, 1970).

1.3.2 The effects of PK mutation in bacteria

Besides the role of PK in energy production, the substrate and product of PK also feed into multiple metabolic pathways (Prichard and Schofield, 1968). Moreover, the central location of PK enables the enzyme to regulate the carbon flux and to act as a switch point between glycolysis and gluconeogenesis in many organisms (Al-Zaid Siddiquee et al., 2004). Thus, mutation of PK is always associated with physiological disturbances including dysregulation of genes, impairment of growth, as well as decline in pathogenic traits. The effects of PK mutation in bacteria and yeast can be found in Table 1.1.
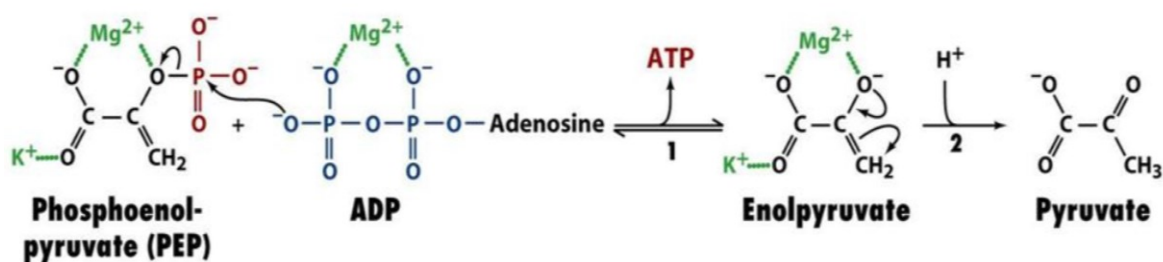
Figure 1.6: The reaction catalysed by PK (adapted from Voet et al., 2012). The enzyme catalyses the transfer of a phosphoryl group from PEP to ADP to yield pyruvate and ATP. The availability of the metal ions is important to facilitate the transfer of the phosphoryl group.

Table 1.1: The effects of PK mutation in bacteria and yeast.

Organism	Effects of PK mutation	Reference
Staphylococcus aureus (*pyK*)	No growth	(Zoraghi et al., 2010)
Mycobacterium tuberculosis (*pyK*)	- Change in colony morphology - Up-regulation of protein expression of isocitrate dehydrogenase and oxidative stress proteins - Down-regulation of protein expression of isocitrate lyase, PEP carboxylase and fatty acid biosynthesis.	(Chavadi et al., 2009)
Escherichia coli (*pykF*)	-Down-regulation of glycolytic genes, acetate-forming flux and lactate-forming flux - Up-regulation of PPP and FruR regulator	(Siddiquee et al., 2004)
Yersinia pseudotuberculosis (*pykF*)	- Decreased growth rate, glucose uptake, dissemination into host cells and persistence in deeper tissue.	(Bücker et al., 2014)
Bacillus subtilis (*pyK*)	- Decreased growth rate, acetate production and recombinant protein expression	(Fry et al., 2000; Pan et al., 2008, 2010)
Corynebacterium glutamicum (*pyK*)	- Decreased growth rate and lactate production - Increased glucose consumption and production of glutamate and aspartate	(Sawada et al., 2010; Chai et al., 2016)
Saccharomyces cerevisiae (*pyK1*)	- Decreased growth on glucose, glycerol and fermentable carbohydrates	(Sprague, 1977)

1.3.3 General kinetics of PK

PK is a cooperative enzyme that is homotropically regulated by its substrate (PEP) and heterotropically regulated by different ligands other than the substrate. The homotropic activation is achieved when one PEP molecule binds to the active site of one subunit and this in turn improves the binding of the next PEP molecules to the adjacent enzyme subunits. Therefore, titration of PEP produces a characteristic sigmoidal allosteric response in most PK enzymes. The sigmoidal response to PEP is additionally, associated with a Hill coefficient >1 which confirms positive enzyme cooperativity. There are a few exceptions to this pattern in the mammalian PK (PKM1) and plant PK, where the PK enzymes display hyperbolic kinetics to titration of PEP (Hill coefficient=1) instead of the typical sigmoidal response (Muirhead et al., 1986; Smith et al., 2000).

The majority of PKs are heterotropically regulated by allosteric ligands which can bind to sites other than the active site (Figure 1.7). Binding of these ligands to PKs greatly boosts enzyme-substrate binding as these regulators are thought to cause major conformational changes in the enzyme that, in turn, alter the configuration of the active site (Fenton, 2008). In the presence of an allosteric regulator, the cooperativity of PK is reduced (the Hill coefficient is decreased) and the sigmoidal response to PEP saturation changes to a hyperbolic one. Allosteric regulation, however, does not change the maximal velocity of the enzyme (V_{max}) nor the enzyme turnover number (k_{cat}), although it decreases the value of the apparent binding affinity of the enzyme ($S_{0.5}$) (Malcovati and Valentini, 1982). The nature of the allosteric ligands is variable, but PKs are mostly regulated by mono- and di-phosphorylated carbohydrates (Jurica et al., 1998). Whereas PKs respond to PEP titration with sigmoidal kinetics, they display "Michaelis-Menten" hyperbolic kinetics to ADP titration.

1.3.4 Dependence of PK activity on metal ions

The availability of divalent cations (usually magnesium, Mg^{2+}) is an absolute requirement for a PK reaction (Baek and Nowak, 1982). The ion functions as a mediator between the active site of the enzyme and the substrates (PEP and ADP) and it orients the phosphoryl groups of PEP and ADP in the active site, where the transfer of the phosphoryl group take places. On the other hand, the phosphotransfer fails if there are

no divalent ions in the reaction (Mesecar and Nowak, 1997; Muirhead et al., 1986). Apart from the dependence of all PK on divalent ions, a subset of PK also require an additional source of monovalent ions (mainly K^+) in order to reach maximal enzymatic activity (Kachmar and Boyer, 1953). In this group of enzymes, K^+ is essential for acquisition of the active conformation of the enzyme. It is also responsible for the conversion of the PK reaction from an ordered kinetics (where binding of the substrates is sequential) into random kinetics (where binding of the substrates is independent on each other). Therefore, the maximal activity of the PK and the binding affinity to the substrates is increased by K^+ (Oria-Hernández et al., 2005).
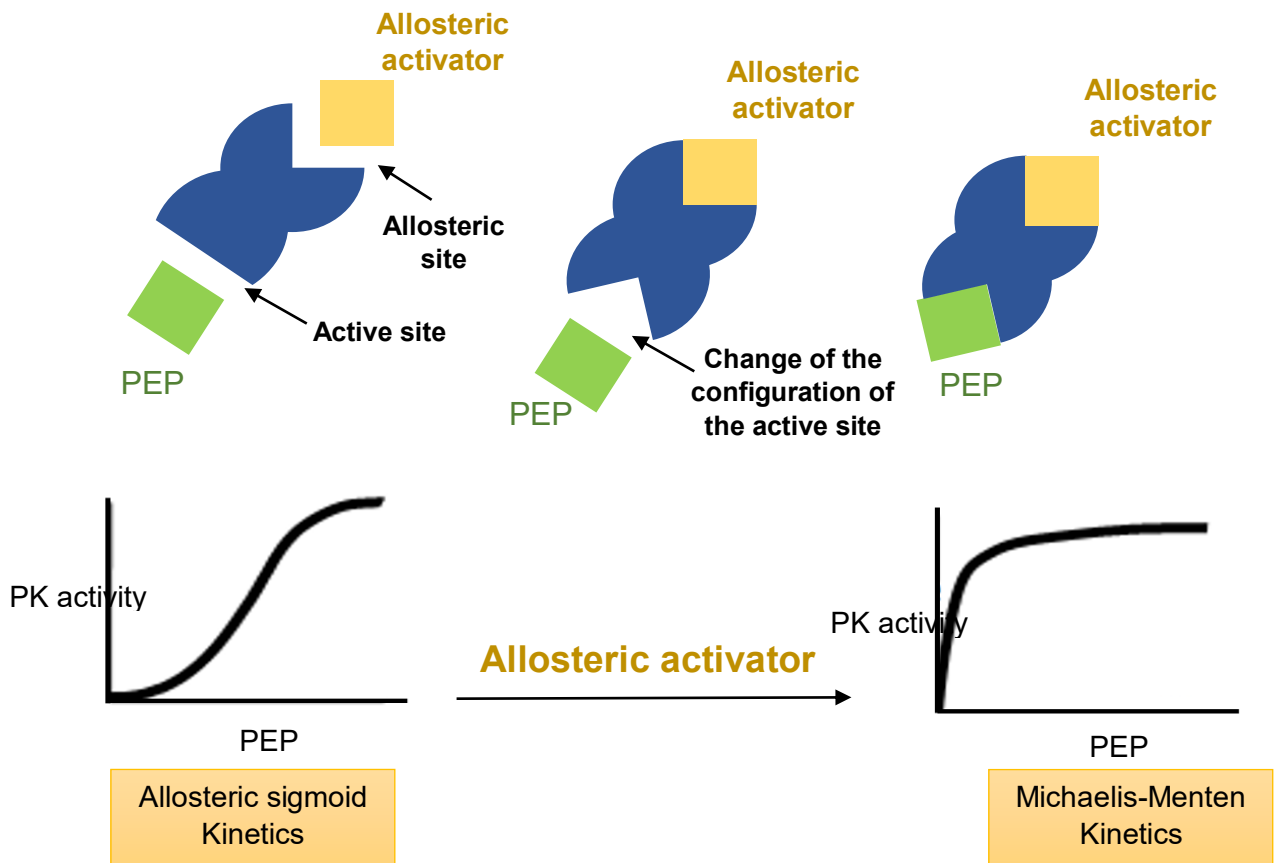
Figure 1.7: The allosteric regulation of PK. The figure illustrates the effects of an allosteric activator on the PK enzyme kinetics. When the activator is absent, PK responds with allosteric sigmoid kinetics to PEP titration. Whereas when the activator is present and binds to the allosteric site, it causes major conformational changes of the active site that in turn facilitates the binding of the PEP to the active site. Thus, the allosteric sigmoidal kinetics of the enzyme with regards to PEP saturation (without the activator) converts to Michaelis-Menten hyperbolic kinetics (with the activator).

1.3.5 PykA and PykF isoforms in bacteria

Almost all bacteria encode one PK, whilst a few can have more than one PK isoform (Muñoz and Ponce, 2003). Among the latter group are bacterial species which encode PykA (pyruvate kinase II) and PykF (pyruvate kinase I) isoforms. The PykA and PykF isoforms have been studied extensively in *E. coli* (Waygood et al., 1975, 1976), *Salmonella enterica* Serovar Typhimurium (Garcia-Olalla and Garrido-Pertierra, 1987), *Yersinia* species (Bücker et al., 2014; Hofmann et al., 2013) and *P. aeruginosa* (this study). The *pykA* and *pykF* genes are usually unlinked on the chromosome and they are often regulated independently (Pertierra and Cooper, 1977). Moreover, the PykA and PykF share a relatively low amino acid sequence homology (below 40%) when compared with each other in the same organism, whereas they have a higher sequence homology to other group members of the same isoform (Table 1.2).

Table 1.2: Percentage of amino acid sequence identity of PykA and PykF among selected Gram-negative bacteria.

	P. aeruginosa PykA	*E. coli* PykA	*S. typhimurium* PykA	*Y. pestis* PykA	*Y. pestis* PykF	*E. coli* PykF	*S. typhimurium* PykF	*P. aeruginosa* PykF
P. aeruginosa **PykA**	100	57.1	57.1	56.4	37.9	36.6	36.8	37.3
E. coli **PykA**		100	98.5	90.6	36.7	36.5	36.3	39.3
S. typhimurium **PykA**			100	90.6	37.1	36.7	36.3	39.3
Y. pestis **PykA**				100	37.5	37.3	36.9	38
Y. pestis **PykF**					100	85.7	86.8	37.3
E. coli **PykF**						100	95.7	36.9
S. typhimurium **PykF**							100	37.3
P. aeruginosa **PykF**								100

1.3.5.1 Genetic and biochemical characterization

Results from previous work show that *pykF* is the dominant isoform in most bacteria that encode both isozymes. Genetic characterization of *pykA* and *pykF* mutants revealed that *pykF* contributes more to pyruvate biosynthesis than *pykA* and that pyruvate biosynthesis disappears completely when *pykF* is knocked-out. Moreover, the specific activity of PykF is several fold higher than PykA, when measured in the wild-type strain (Ponce et al., 1995).

The PykA and PykF isoforms also show a typical response to allosteric regulators; PykA activity is often activated by ribose 5-phosphate (R5P) and adenosine monophosphate (AMP), whereas PykF is positively regulated by fructose 1,6-bisphosphate (F1,6P). When these regulators are present, PykA and PykF lose cooperativity (indicated by a drop in the Hill coefficient); the allosteric kinetics with respect to PEP titration becomes hyperbolic, and the PEP binding affinity increases (indicated by a drop in the $S_{0.5}$ values) (Malcovati and Valentini, 1982; Waygood et al., 1976; Garcia-Olalla and Garrido-Pertierra, 1987; Waygood et al., 1975). The distinguishable allosteric regulation of PykA and PykF confirms that these isozymes have non-interconvertible roles in metabolism (Garcia-Olalla and Garrido-Pertierra, 1987).

1.3.5.2 Genetic regulation

The genetic control of *pykF* has been described before, whereas the regulation of *pykA* has not been characterized. Most likely, this is because so far *pykF* is the only essential PK in bacterial species that encode both *pykA* and *pykF* isoforms. The *pykF* gene was found to be controlled by two unrelated regulators; CsrA and FruR. CsrA is a global RNA-binding regulator which positively controls expression of the glycolytic genes (among many others), while having negative control on gluconeogenic genes (Romeo and Babitzke, 2018). In *E. coli*, PykF activity is strongly related to *csrA* and when the *csrA* is inactivated, the enzymatic activity of PykF is lost. On the other hand, mutation of *csrA* was found not to impact PykA activity at all (Sabnis et al., 1995).

FruR is a transcriptional regulator that has a central role in the regulation of carbon metabolism in enteric bacteria (Ramseier et al., 1995). In contrast to CsrA, FruR regulates *pykF* negatively. In *E. coli*, FruR binds to the promoter region of the *pykF* gene and represses its activity, under both glycolytic and gluconeogenic conditions (Bledig et al., 1996). Moreover, the negative impacts of FruR on *pykF* transcription were alleviated after inactivation of *fruR* or the addition of F1,6P; the key glycolytic metabolite in *E. coli*.

Although the regulation of PK itself has not been yet characterized in pseudomonads, regulation of other enzymes (before and after the PK reaction) has been demonstrated. For example, the transcription of some EDP enzymes is tightly controlled by HexR and RccR. Both regulators share high sequence homology and can bind KDPG, a key metabolite of the EDP. Generally, HexR regulates the enzymes before the PK step of the EDP, whereas RccR regulates enzymes before and after the PK step. In *P. putida* and *P. fluorescens*, HexR represses the expression of glucose 6-phosphate dehydrogenase (*zwf*), 6-phosphogluconate dehydratase (*edd*) and glyceraldehyde 3-phosphate dehydrogenase (*gap*) when KDPG is not abundant, such as during growth in media containing carbon sources other than glucose (Daddaoua et al., 2009; Campilongo et al., 2017). In contrast, when KDPG is present as during growth in glucose, HexR leaves its target operators and alternatively binds KDPG, thus the transcription of *zwf*, *edd* and *gap* is turned on (Daddaoua et al., 2009).

Unlike HexR, RccR targets the genes of an entirely different set of metabolic enzymes (*pckA*: phospho*enol*pyruvate carboxykinase, *gap*: glyceraldehyde 3-phosphate dehydrogenase, *aceA*: isocitrate lyase, *glcB*: malate synthase, *aceE/F*: pyruvate dehydrogenase subunits) and can simultaneously repress and activate their expression (Campilongo et al., 2017). According to the available carbon source, RccR inversely regulates pyruvate metabolism (*aceE*) and gluconeogenesis/glyoxylate shunt (*pckA*, *gap*, *aceA*, *glcB*). For example, when RccR binds KDPG (e.g. cells growing in glucose), the affinity of RccR to enzymes of the gluconeogenesis/glyoxylate shunt is increased and therefore their expression is suppressed. At the same time, the negative effect of RccR on pyruvate metabolism is removed, and vice versa when cells grow in acetate (Campilongo et al., 2017).

1.3.6 X-ray crystal structure of PK

There are many PK structures from prokaryotes and eukaryotes that are already published on the Protein Data Bank (PDB) (Figure 1.8). More than 80% of these structures belong to eukaryotes. In contrast, the number of bacterial PK models are limited with only one structure from Gram-negative species; PykF from *E. coli*. The *E. coli* PykF is present with four PDB models and none of them contains a bound regulator to the enzyme, apart from metal ions. The *E. coli* PykF was either modelled unbound as in PDB 1PKY or bound with sulphate ions (1E0T, 1EOU and 4YNG). So far, the only available prokaryotic PK structure with bound regulators (not ions) belongs to PK of *M. tuberculosis*.
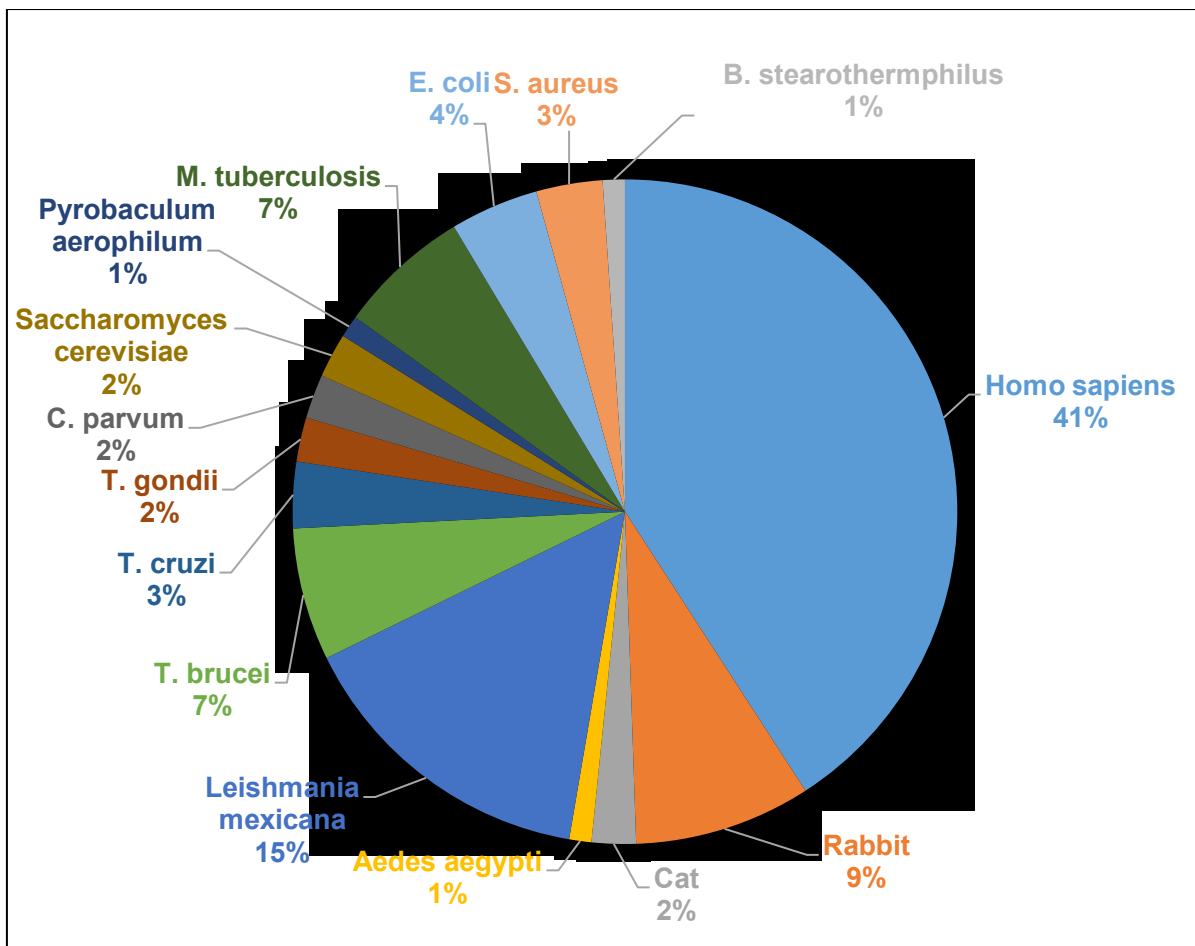
Figure 1.8: PK structures in the PDB. Pie chart showing the distribution of the published PK structures in the PDB (updated last on 11-April-2019). Of PykA and PykF isoforms, only *E. coli* PykF has been deposited representing 4% of the deposited models, and there is no published structure for a PykA isoform.

1.3.6.1 The structure of a PK subunit

PK is a tetramer of four identical subunits (Valentini et al., 1979) where each subunit is subdivided into three domains; A, B and C (Mattevi et al., 1995; Zhong et al., 2017) (Figure 1.9A, 1.9B). Some PK structures may have additional domains which can be in a form of a short N-terminal domain or a long extra C-terminal domain (Figure 1.9C, 1.9D). The N-terminal domain is mostly present in PK structures from mammals, yeast and some parasites (Muirhead et al., 1986; Wooll et al., 2001; Jurica et al., 1998; Cook et al., 2012; Allen and Muirhead, 1996), whereas the C-terminal domain is more common among bacterial PKs (Zoraghi et al., 2011; Axerio-Cilies et al., 2012; Suzuki et al., 2008).

Of the three main domains, the A domain is the largest and is centrally positioned between the B and C domains. The A domain is comprised of a typical triosephosphate isomerase (TIM)-barrel fold where eight β-strands alternate with eight α-helices along the peptide backbone. The A domain is linked to the B domain and the C domain at its C-terminus and its N-terminus, respectively. The B domain, also called the lid domain, is the smallest among the three domains and is rich in β-sheets. The active site of all PK lies at the cleft between the A and the B domains. The C domain is mostly made of a four to five (α + β) open sheet structure (Larsen et al., 1994). The predicted allosteric site of almost all PKs lies within the structure of the C domain. Within a complete PK tetramer, the opposing A domains communicate across the A-A interface, whereas the opposing C domains interact via the C-C interface (Mattevi et al., 1995).
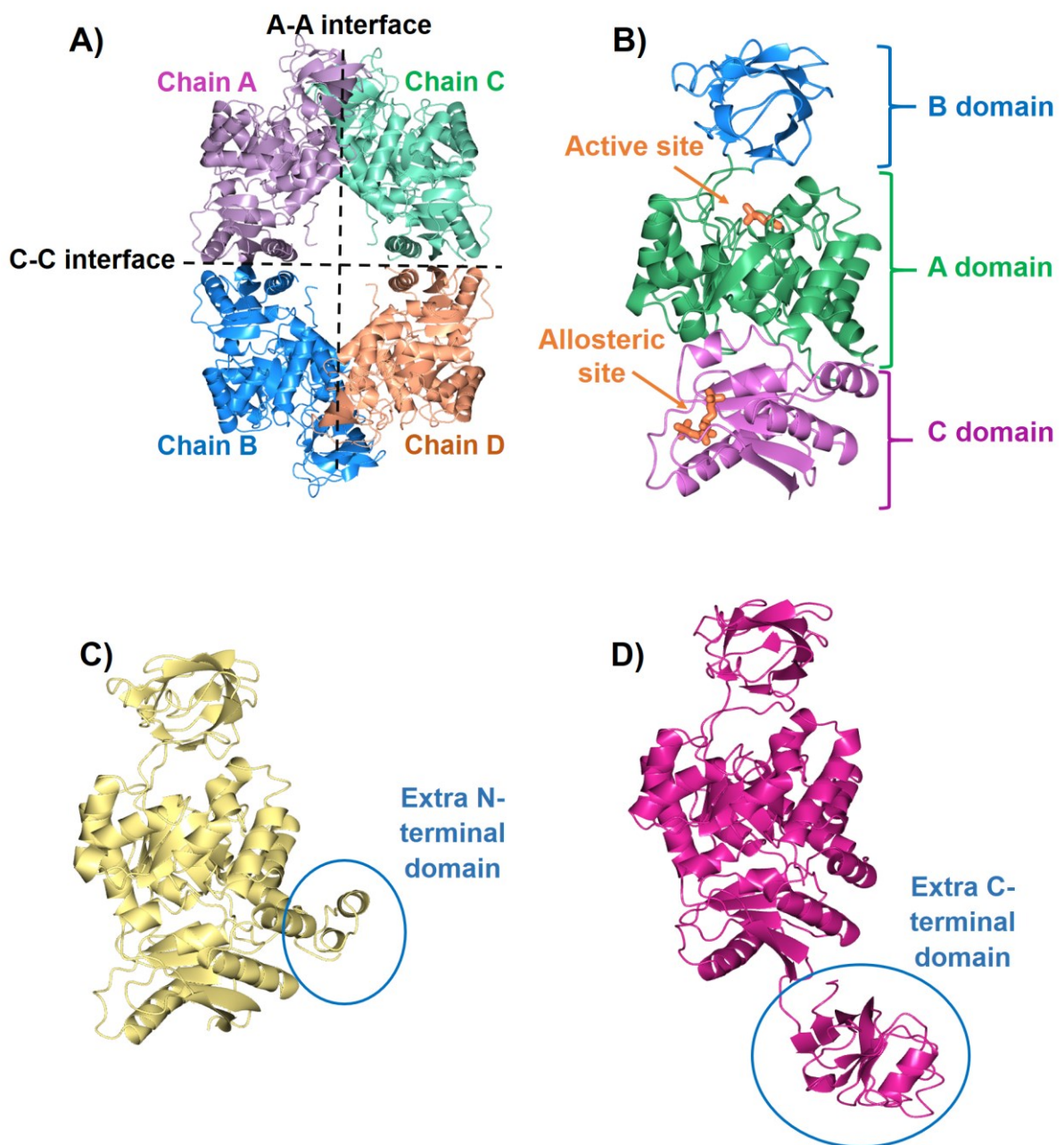
Figure 1.9: Structure of PK. A) A PykF tetramer from *E. coli*, (PDB 1PKY). The tetramer is made of four identical subunits that are coloured differently. Dashed lines highlight the intersubunit interfaces. B) The three-domain organization of a PK subunit from *Saccharomyces cerevisiae* (PDB 1A3W). The active site and the allosteric site are occupied by phosphoglycolic acid and F1,6P, respectively as shown by coral cylinders. C) A PK subunit from rabbit muscle (PDB 1F3W) showing the extra N-terminal domain. D) A PK subunit from *S. aureus* (PDB 3T05) showing the extra C-terminal domain. Ligands of figure C (K^+, Mn^{2+} and pyruvic acid) and figure D (PO_4) are not shown. All images are generated using CCP4mg.

1.3.6.2 The active site of PK

The active site of PK lies in the cleft between the A and B domains (Muirhead et al., 1986) and is comprised of strictly conserved residues in all organisms (Jurica et al., 1998; Muñoz and Ponce, 2003). Although, the active site is present in the A domain, the catalytic reaction of many PK enzymes is associated with movement of the B domain. For example, in rabbit muscle PK, when the substrate is present in the active site, the B domain rotates around the A domain with a hinge-bending motion in order to narrow the active site cleft (Larsen et al., 1997).

Almost all published PK structures on the PDB have a substrate analogue bound in the active site, with the exception of PK of *Trypanosoma brucei* (PDB 4HYV), which instead has PEP (the natural substrate) bound to the enzyme (Figure 1.10) (Zhong et al., 2013). At the active site of the 4HYV model, Arg50, Lys239, Mg^{2+} and K^+ create a positively charged pocket that facilitates orientation and transfer of the phosphoryl group from PEP to ADP (Jurica et al., 1998). These positive charges are important in the reaction as they neutralize the negatively charged phosphate. Therefore, the electrophilic phosphate becomes available for nucleophilic attack on ADP and the reaction completes producing an ATP and eventually, pyruvate (Westheimer, 1987).
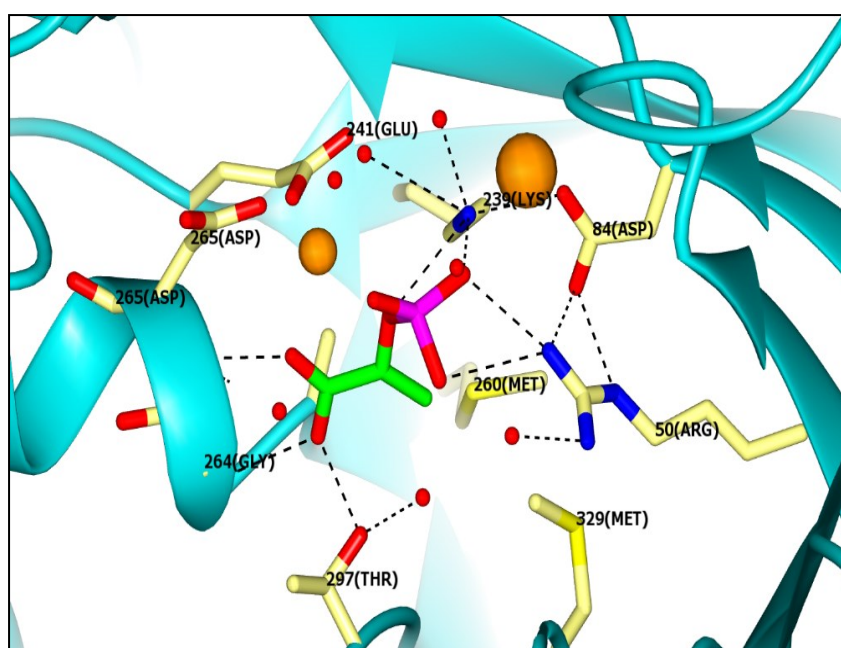
Figure 1.10: The active site of PK. A Close-up view of *T. brucei* PK (PDB 4HYV, Chain B) showing PEP (coloured sticks), Mg^{2+} (small coral sphere), K^+ (large coral sphere) and water (small red spheres) bound in the active site. The figure was generated using CCP4mg.

1.3.6.3 The allosteric site of PK

The predicted allosteric site of almost all PK lies within the C domain, nearly 40Å away from the active site (Jurica et al., 1998; Morgan et al., 2014; Zhong et al., 2013). However, another allosteric site has been identified recently in the PK of *M. tuberculosis*, which is found in the vicinity between the A and the C domains (Zhong et al., 2017). Most of the published structures for prokaryotic PK are modelled with phosphate or sulphate ions bound to the allosteric site. Among prokaryotes, there is only one PK from *M. tuberculosis* (several models) with regulators bound. In PK of *M. tuberculosis*, there is an AMP bound to the predicted allosteric site, whereas the G6P is bound to a distinct position than the AMP binding site (Zhong et al., 2017). By contrast, so far there is no PK from Gram-negative species modelled with a bound regulator in the allosteric site.

In most of the PK structures (prokaryotic and eukaryotic), occupation of the allosteric site by ligands drives structural changes within the C domain and across the domain interfaces. Of these changes, the disposition of a mobile loop is most commonly seen (Figure 1.11). The loop is present between the last two β-strands of the C domain and when the allosteric site is empty, it is placed away from the allosteric pocket. However, when the ligand occupies the allosteric pocket, the loop shifts towards the bound ligand.
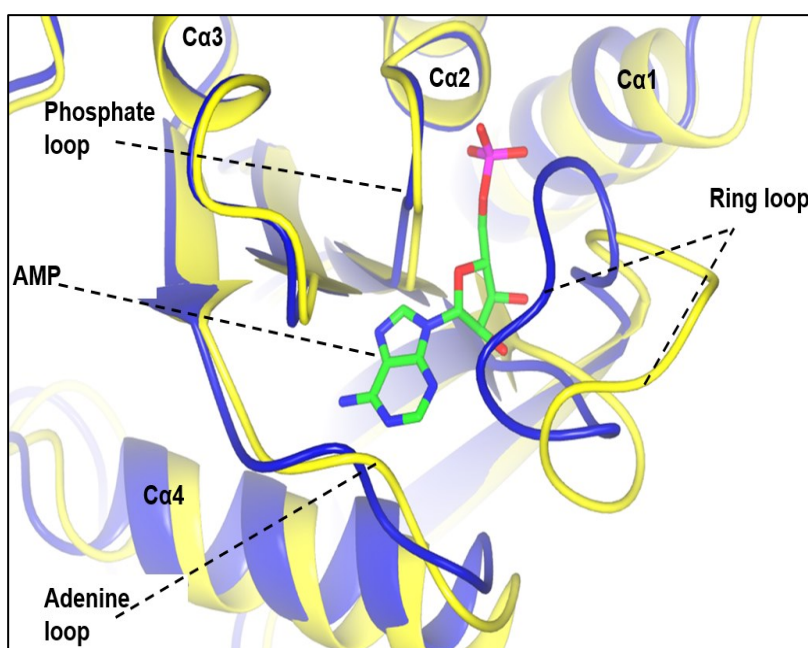
Figure 1.11: Structural changes in the allosteric site of PK after binding to a regulator. Superposition of unbound (PDB 5WRP, yellow, chain B) and AMP-bound (PDB 5WSB, blue, chain D) PK from *M. tuberculosis*. The figure shows movement of the mobile loop after binding to AMP. The figure was generated using CCP4mg.

1.3.6.4 The mechanism of allosteric regulation of PK

Without a positive regulator, PKs adopt a configuration of low substrate affinity known as T-state (tensed state). After the activator binds to the allosteric site, major conformational adjustments take place across the tetramer that facilitate binding of the substrate and the enzyme converts to an R-state (relaxed state), (Mattevi et al., 1995; Valentini et al., 2000; Zhong et al., 2017; Monod et al., 1965). The transition from the T-state to the R-state is important for understanding the mechanism of transfer of the allosteric signals across the subunits.

The switch from the less active T-state to the active R-state is an attention-grabbing phenomenon as it explains the rapid response of many PKs to metabolic signals in the cell. Figure 1.12 shows that there are two established theories which describe the transition from the T-state to the R-state; the "Domain and subunit rotation" and the "Rigid body reorientation" (Donovan et al., 2016). In the first model, the enzyme-ligand complex at the allosteric site induces rotations of the individual domains in each subunit besides the rotation of each subunit independently. This mode is proposed for the allosteric regulation of PK from *E. coli* by F1,6P, although so far there is no bacterial PK structure with bound regulators other than the PK of *M. tuberculosis* (Mattevi et al., 1995; Valentini et al., 2000; Mattevi et al., 1996). The second model, however, explains that the transmission of the allosteric signal throughout the tetramer is due to the reorientation of the individual subunits as a whole rigid bodies, while using a pivot point at the intersection of the A and C domains. This model is proposed for the regulation of PK in *Leishmania mexicana* by F2,6P (Morgan et al., 2014).

Analysis of the intersubunit interfaces is crucial for understanding the mechanism of the allosteric signal transduction (Wooll et al., 2001). This is because the transition from the unbound to the ligand-bound PK is usually associated with building or breaking of interactions across the A-A or the C-C interfaces. For example, the binding of the allosteric ligand to PK from *Leishmania mexicana* lead to formation of eight salt bridges across the C-C interface which contributed significantly to the stability of the enzyme (Morgan et al., 2010). Moreover, the transition from the T- to the R- states in PK of *L. mexicana* was associated with changes also at the A-A interface (Naithani et al., 2015). Enzyme kinetics and site-directed mutagenesis confirmed that the intersubunit

interactions play a central role in the allosteric regulation of PK (Friesen and Lee, 1998; Fenton and Blair, 2002).
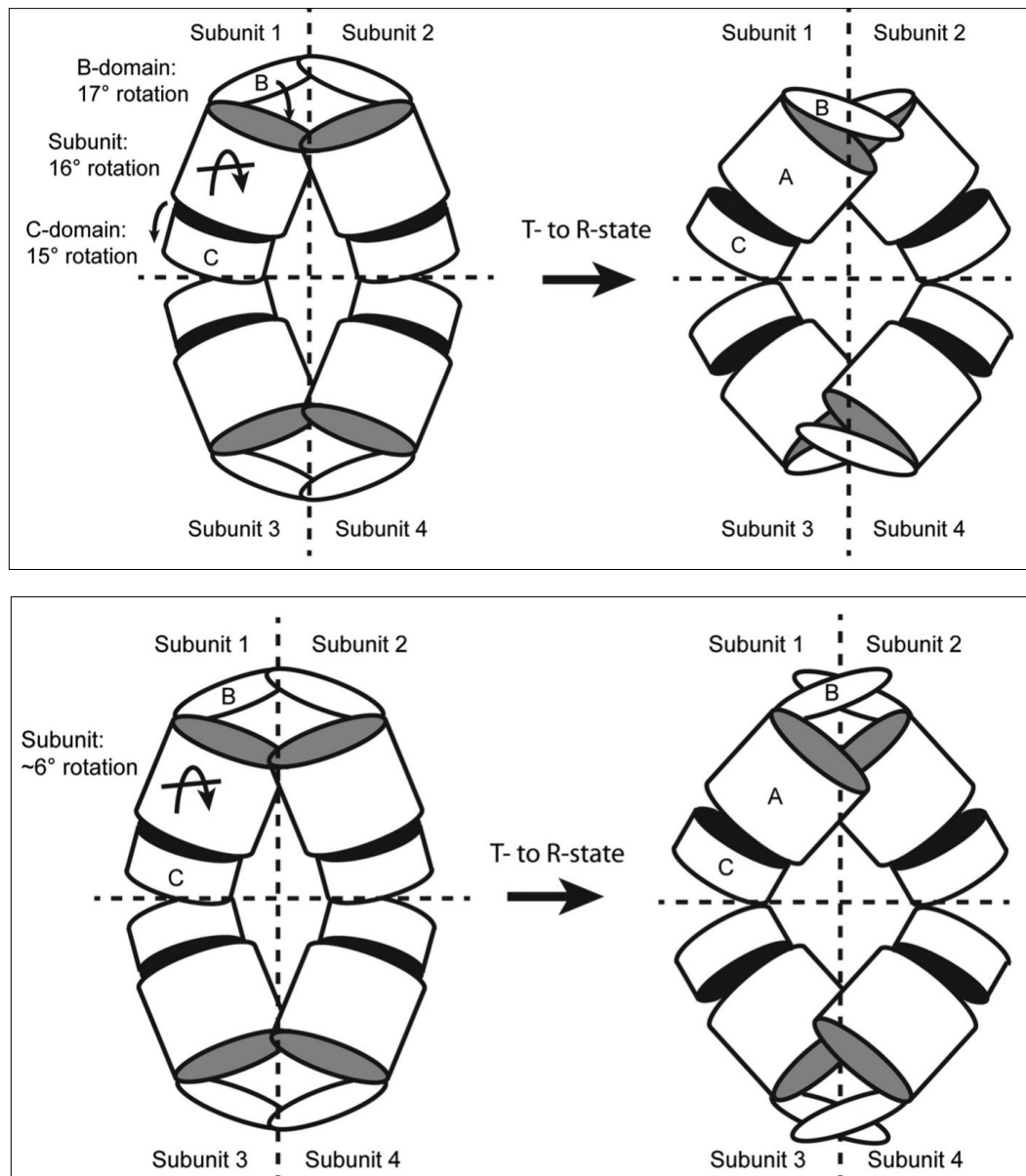
Figure 1.12: The transition of a PK from the T-state to the R-state (adapted from Donovan et al., 2016). The transition of a PK from the T-state (unbound) to the R-state (bound) is explained by the domain and subunit rotation model (top) and by the rigid body reorientation model (bottom). In the first model, binding of the ligand induces rotational movement of all domains and the whole subunits (e.g. PK of *E. coli*), whereas in the second model, the ligand-enzyme complex causes rotation of the whole subunits only around a pivot point (e.g. PK of *L. mexicana*). In the two models, binding of the ligand to the allosteric site significantly improves binding affinity of the enzyme to the substrate.

1.4 Objectives of this study

PK is a key regulatory enzyme with a central position between upper glycolysis and TCA cycle. Thus, PK activity has been linked with major metabolic changes in the cell and more recently, with pathogenicity. Most of bacteria have a single PK and a few encode two PK isozymes, denoted as PykA and PykF. In the latter group of organisms, PykF is usually the dominant isoform, whereas PykA has a less important role. Moreover in species encoding both isoforms, PykA and PykF are found to follow a typical pattern of allosteric regulation; PykA is activated by AMP and/or R5P and PykF is activated by F1,6P. With respect to structural data, most (81%) relate to eukaryotic PKs and only 19% relate to bacterial enzymes. Of these bacterial structures, some pertain to PykF, and there are no structures currently available for any PykA enzyme.

P. aeruginosa encodes one PykA isozyme (PA4329) and one PykF isozyme (PA1498). Neither of these isozymes have been characterised to date. As *P. aeruginosa* relies exclusively on the EDP for metabolism (unlike most other bacteria), it is likely that PK regulation is different in this organism. It is my thesis that one or both of these enzymes plays a critical role in controlling flux through the EDP in *P. aeruginosa*, and that is because of the way in which this organism is "wired up" for the EDP. Also, the regulation of these isoforms in *P. aeruginosa* is likely to differ significantly from that reported in other species. Thus, the main aim of this project was to characterise the genetic, biochemical and structural properties of PykA and PykF in *P. aeruginosa*. To realise this aim, I pursued the following specific objectives:

- To characterize the expression profile(s) of each isoform and to examine the impact of mutating *pykA* and *pykF* on cell growth, pyruvate biosynthesis and virulence phenotypes.
- To characterize the kinetic and regulatory properties of purified PykA and PykF, and to identify non-physiological inhibitors of the enzymes with potential antimicrobial activity.
- To solve the x-ray crystal structures of PykA and PykF with a view to understanding better the link between structure, function and regulation of these enzymes.

Chapter 2

2 Materials and methods

2.1 General microbiological procedures

2.1.1 Bacterial strains

Bacterial strains used in this work are listed in Table 2.1

Table 2.1: Bacterial strains and mutants used in this work.

Strains	Description	Source
P. aeruginosa strains		
PAO1	Wild-type	B. Iglewski, University of Rochester, USA
PW8308	PAO1 harbouring transposon (ISlacZ/hah) insertion in *pykA*, Tet^R	UWGC mutant bank
PW3705	PAO1 harbouring transposon (IS*phoA*/hah) insertion in *pykF*, Tet^R	UWGC mutant bank
PAF0	A double mutant defective in *pykA* and *pykF*, generated by phage transduction, Tet^R	This study
PW8308-cre	PW8308 with the tetracycline resistance cassette removed by Cre-mediated excision	This study
PW8308C	PW8308 containing pUCP20-*pykA*, Tet^R, Carb^R	This study
PW3705C	PW3705 containing pUCP20-*pykF*, Tet^R, Carb^R	This study
PAF1	PAF0 containing pUCP20-*pykA*, Tet^R, Carb^R	This study
PAF2	PAF0 containing pUCP20-*pykF*, Tet^R, Carb^R	This study
PpykA	PAO1 containing pLP170-*pykA*, Carb^R	This study
PpykF	PAO1 containing pLP170-*PA1499*, Carb^R	This study
K3-3105-D4	Clinical isolate	Papworth Hospital
K9-1306-C6	Clinical isolate	Papworth Hospital

E. coli strains		
JM109	*endA1 gyrA96 recA1 thi hsdR17*(r_K^-, m_K^+) *relA1 sup*E44 *Δ(lac-pro*AB*) [F' tra*D36 *pro*AB$^+$ *lac*I^q *lacZ*ΔM15*]*	(Yanisch-Perron et al., 1985)
BL21(DE3)	F$^-$ *ompT gal dcm lon hsdS$_B$*($r_B^- m_B^-$) λ(DE3 [*lacI lacUV5-T7p07 ind1 sam7 nin5*]) [*malB$^+$*]$_{K-12}$(λ^S) pLysS[*T7p20 ori*$_{p15A}$](Cm^R)	Novagen
BL21-PykA	BL21 containing pET19m-*pykA* Carb^R, Cm^R	This study
BL21-PykF	BL21 containing pET19m-*pykF*, Carb^R, Cm^R	This study

2.1.2 Plasmids and bacteriophages

Table 2.2 shows the list of plasmids and bacteriophage used in this study.

Table 2.2: Plasmids and bacteriophage used in this work.

	Description	Source
Plasmids		
pFLP2-cre	Site specific excision vector with Cre-recombinase, Carb^R	Welch lab stocks
pUCP20	*Escherichia coli-Pseudomonas* shuttle vector, Carb^R	(West et al., 1994)
pLP170	*lacZ* transcriptional fusion vector, Carb^R	(Preston et al., 1997)
pET19m	A vector for inducible protein expression of N-terminally His-tagged proteins, Carb^R	Welch lab stocks
pUCP20-*pykA*	pUCP20 containing a PCR-amplified fragment of *pykA*, Carb^R	This work

Table 2.2: Continued		
Plasmids	**Description**	**Source**
pUCP20-*pykF*	pUCP20 containing a PCR-amplified fragment of *pykF* and *PA1499*, Carb^R	This work
pLP170-*pykA*	*pykA* reporter plasmid, Carb^R	This work
pLP170-*PA1499*	*pykF* reporter plasmid, Carb^R	This work
pET19m-*pykA*	Vector for inducible expression of N-terminally His-tagged PykA, Carb^R	This work
pET19m-*pykF*	Vector for inducible expression of N-terminally His-tagged PykF, Carb^R	This work
Bacteriophages		
ØPA3	Generalized transducing phage of *P. aeruginosa*	(Monson et al., 2011)

2.1.3   Preparation and concentration of antibiotics

All antibiotics are prepared in 50% (v/v) ethanol in dH$_2$O and filter-sterilized using 0.22 μm syringe filter units (Millipore). Antibiotic stocks were kept in aliquots and stored at -20°C.

Table 2.3: Concentration of antibiotics used in this work.

	Stock (mg/ml)	Final concentration (μg/ml)	
		P. aeruginosa	*E. coli*
Carbenicillin	50	250	50
Chloramphenicol	34		34
Tetracycline	10	50	

2.1.4   Media, solutions and buffers

2.1.4.1 Growth media

Liquid and solid media used in this study are detailed in Table 2.4 and Table 2.5, respectively. Glassware and media constituents were autoclaved at 115°C for 15 min (standard), unless otherwise stated.

Table 2.4: List of liquid growth media used in this study.

Liquid media	Per litre
LB broth (lennox)	10 g tryptone 5 g yeast extract 5 g NaCl
M9 minimal media, 1X	200 ml 5X M9 minimal salts 2 mM magnesium sulfate 0.1 mM calcium chloride And one of the following carbon sources: 20 mM glucose 40 mM acetate 20 mM succinate 30 mM glycerol 15 mM ribose
M9 Minimal salts, 5X (BD Difco)	33.9 g disodium phosphate 15 g monopotassium phosphate 5 g ammonium chloride 2.5 g sodium chloride

Table 2.5: List of solid media used in this study.

LB agar (LBA)	
Purpose	Routine growth media
Preparation	LB broth containing 1.5% (w/v) agar

M9 minimal media agar, 1X	
Purpose	Comparison of growth in different carbon sources
Preparation	M9 minimal media containing 1.5% (w/v) agar

PPGAS (Proteose Peptone Glucose Ammonium Salt) agar	
Purpose	Detection of rhamnolipid production
Components	<u>PPGAS salts</u> 20 mM ammonium chloride 20 mM potassium chloride 120 mM Tris-HCl pH 7.5 1.6 mM magnesium sulfate 0.5% (w/v) glucose 1% (w/v) proteose peptone 1.5% (w/v) agar <u>CTAB (Cetyltrimethylammonium Bromide)</u> 20 mg/ml <u>MB (Methylene blue)</u> 0.5 mg/ml
Preparation	The PPGAS salts were prepared in 200 ml dH$_2$O and autoclaved as standard. The CTAB and MB stocks were prepared independently, filter-sterilized and stored at room temperature. For preparation of the PPGAS minimal media, 58.8 ml of PPGAS salts were mixed with 600 μl of CTAB and 600 μl of MB in a sterilized bottle. The 60 ml of PPGAS agar was poured into a sterile square Petri-dish.

Skim Milk Agar	
Purpose	Detection of caseinase production
Components	<u>Tryptone soy agar (TSA)</u> 50 g/L Tryptone soy agar <u>Skim milk (SM)</u> 2% (w/v) skim milk
Preparation	The TSA was prepared in water and autoclaved as standard. The SM was prepared independently and autoclaved by special cycle for milk. The skim milk agar was prepared fresh by mixing

160 ml of TSA with 40 ml of SM. The mixture was shaken gently and 60 ml was dispensed into a sterile square Petri-dish.

Gelatin agar media	
Purpose	Detection of gelatinase production
Components	13 g/L nutrient broth 1.6% (w/v) agar 30 g/L gelatin
Preparation	60 ml of prepared agar was dispensed into a sterile square Petri-dish.

Swarming assay	
Purpose	Detection of swarming activity
Components	8 g/L Nutrient Broth 5 g/L Glucose 5 g/L agar
Preparation	60 ml of prepared agar was dispensed into a sterile square Petri-dish.

Swimming assay	
Purpose	Detection of swarming activity
Components	20 g/L LB media 3 g/L agar
Preparation	60 ml of prepared agar was dispensed into a sterile square Petri-dish.

2.1.4.2 Solutions, buffers and gels

Table 2.6: Components of solutions, buffers and gels used in this study.

Solution or Buffer	Per litre
Phosphate buffered saline (PBS)	Ten tablets of 10 g PBS (Dulbecco A)
Phage buffer	10 mM Tris-HCl pH 7.5 10 mM magnesium sulfate 0.01% (w/v) gelatin
TAE buffer	40 mM Tris-HCl pH 8 20 mM acetic acid 1 mM EDTA
Lysis buffer	50 mM Tris-HCl pH 7.5 300 mM sodium chloride 10 mM imidazole 10% (v/v) glycerol
Equilibration buffer	50 mM Tris-HCl pH 8 200 mM sodium chloride 10% (v/v) glycerol 10 mM imidazole
Elution buffer	50 mM Tris-HCl pH 8 200 mM sodium chloride 10% (v/v) glycerol 250 mM imidazole
Dialysis buffer	20 mM Tris-HCl pH 7.5 100 mM sodium chloride 5% (v/v) glycerol 1 mM DTT 0.1 mM EDTA
Resolving buffer, 5X	151 g Tris-HCl 0.5% (w/v) SDS pH 8.8

Table 2.6: Continued Solution or Buffer	Per litre
Stacking buffer, 5X	60 g Tris-HCl 0.5% (w/v) SDS pH 6.8
Resolving phase, 15% (per 10 ml)	5 ml 30% (v/v) Bis-acrylamide (Severn Biotech) 5 ml 5X resolving buffer 50 µl 20% (w/v) SDS 100 µl 8% (w/v) ammonium persulfate 5 µl tetramethylethylenediamine
Resolving phase, 9% (per 10 ml)	3 ml 30% (v/v) Bis-acrylamide (Severn Biotech) 5 ml 5X resolving buffer 2 ml dH$_2$O 50 µl 20% (w/v) SDS 100 µl 8% (w/v) ammonium persulfate 5 µl tetramethylethylenediamine
Stacking phase, 6% (per 10 ml)	2 ml 30% (v/v) Bis-acrylamide (Severn Biotech) 1 ml 5X stacking buffer 50 µl 20% (w/v) SDS 100 µl 8%(w/v) ammonium persulfate 5 µl tetramethylethylenediamine
SDS PAGE running buffer (per Litre)	25 mM Tris-HCl pH 8.3 0.2 M Glycine 0.1% (w/v) SDS
SDS loading buffer, 4X	200 mM Tris-HCl pH 6.8 40% (v/v) glycerol 8% (w/v) SDS 0.4% (w/v) bromophenol blue 400 mM DTT

Table 2.6: Continued Solution or Buffer	Per litre
Coomassie stain (per Litre)	1 g/L Coomassie Brilliant Blue G (sigma) 50% (v/v) methanol 10% (v/v) acetic acid
Destain I (per Litre)	50% (v/v) methanol 7% (v/v) acetic acid
Destain II (per Litre)	10% (v/v) methanol 7% (v/v) acetic acid

2.1.5   Growth and phenotypic assays

2.1.5.1 Storage of bacterial culture

Bacterial strains were stored at -80°C after mixing an equal volume of an overnight culture with 50% (v/v) sterile glycerol solution. Agar plates containing viable colonies of *P. aeruginosa* and *E. coli* were stored at room temperature and 4°C, respectively for up to two weeks.

2.1.5.2 Growth on LBA

Colonies of *P. aeruginosa* and *E. coli* were grown in 10 cm diameter Petri-dishes containing 25 ml LBA. Antibiotics were added as appropriate. Plates were incubated overnight at 37°C. For growing cells from a frozen culture, a small part of the frozen stock was defrosted on the surface of the agar at room temperature. After melting, the culture was streaked onto the agar using a flame-sterilized inoculation loop.

2.1.5.3 Overnight cultures in LB

A single colony was picked from an LBA plate and used to inoculate 10 ml LB broth in a 30 ml universal tube. Antibiotics were added as appropriate. Bacterial cultures were incubated overnight at 37°C on a rotating drum. Three biological replicates were prepared if needed by inoculating three independent colonies into three different overnight cultures.

2.1.5.4 Growth in M9 minimal media

Growth was carried out in a 250 ml conical flask containing 50 ml of M9 minimal media supplemented with the desired carbon source. First, overnight cultures were prepared in LB as above. Then, bacterial cells were pelleted down (3,200 x g, 20°C, 5 min) and the pellets were washed three times in PBS. The cells were inoculated into the minimal media with the desired carbon source to reach an initial OD_{600} of 0.05. When microaerobic growth was desired, a 1 cm thick layer of sterile mineral oil was added on top of the cell suspension. Flasks containing cell cultures were incubated in a shaking water bath at 37°C and 210 rpm for aerobic growth or at 37°C and 80 rpm for microaerobic growth. Antibiotics were added as appropriate. Three biological replicates were used for each growth condition. Samples of 1 ml bacterial culture were collected every hour for measurement of cell density at 595 nm.

2.1.5.5 Growth on M9 minimal agar

An overnight culture was first prepared in LB as above. The culture was serially diluted in sterile PBS up to 10^{-6}. A 10 μl of the last dilution was spotted onto M9 minimal agar containing the desired carbon source and left to dry. The spot was streaked into single colonies using a sterile inoculation loop. The plates were incubated at 37°C for 24 – 48 hr.

2.1.5.6 Production of rhamnolipids

An overnight culture was first prepared in LB as above. The OD_{600} of an overnight culture was adjusted to 1 and 5 μl were spotted onto PPGAS agar. The spot was left to dry and plates were incubated upright (agar at the bottom of the plate) at 37°C for 48 hr. The rhamnolipid production was visualized as blue halos around the growing colonies.

2.1.5.7 Caseinase production

Directly from an overnight culture in LB, a 5 μl spot was transferred onto skim milk agar. The spot was left to dry and plates were incubated upright (agar at the bottom of the plate) at 37°C for 48 hr. Caseinase production was indicated by halo formation around the growing colonies.

2.1.5.8 Gelatinase production

Directly from an overnight culture in LB, a 5 μl spot was transferred onto gelatin agar. The spot was left to dry and plates were incubated upright (agar at the bottom of the plate) at 37°C for 48 hr. Gelatinase production was indicated by halo formation after the plate was flooded with saturated ammonium sulphate solution.

2.1.5.9 Swarming activity

The OD_{600} of an overnight culture was adjusted to 1 and 5 μl were spotted on top of the swarming agar. Plates were left to dry and incubated upright (agar at the bottom of the plate) at 37°C for 15 – 24 hr.

2.1.5.10 Swimming activity

The OD_{600} of an overnight culture was adjusted to 1 and 5 μl were inoculated at the bottom of the swimming agar. Plates were left to dry and incubated upright (agar at the bottom of the plate) at 37°C for 15 – 24 hr.

2.1.5.11 Biofilm assay

Overnight cultures were first prepared in LB as above. The cultures were sedimented and the pellets were washed three times in M9 minimal media supplemented with 20 mM glucose. The cells were adjusted to an OD_{600} of 0.1 using M9 minimal media with glucose and 100 μl were transferred to a sterile 96-well plate. For biofilm formation in LB, cells were taken directly from the overnight cultures and the OD_{600} was adjusted to 0.1 in LB. Plates were sealed with a sterile breathable adhesive membrane (StarLab) and incubated for 24 hr at 37°C on a static surface. The planktonic culture was aspirated without disruption of the adhered cells to the sides of the well. The cells adhering to the plate were washed three times using 200 μl dH_2O, followed by addition of 100 μl of 0.1% (w/v) crystal violet were added to stain the biofilms (15 min, static, room temperature). The stain was aspirated and the biofilms were washed three times using 200 μl dH_2O and left to dry. The crystal violet stain absorbed to the attached biomass was solubilized by adding 120 μl of 30% (v/v) acetic acid for 15 min. The biofilm formation was quantified by measuring the absorbance of the solubilized crystal violet at 595 nm.

2.1.5.12 Growth assays with potential inhibitors

The effects of synthetic inhibitors (shikonin and R396907) on cell growth was measured using a sterile 96-well microtiter plate. An overnight culture was prepared in LB (for growth curves in LB) or M9 minimal media with 20 mM glucose (for growth curves in glucose). The cells were sub-cultured in 10 ml of the same media to reach an OD_{600} of 0.05. A serial fold dilution (0 – 500 μm) of each inhibitor was prepared in DMSO and 2 μl of each dilution was transferred into the microtiter plate. The sub-culture (200 μl) was added into the microtiter plate and mixed gently with the inhibitors. For the control wells, 2 μl of DMSO was used. A sterile breathable membrane (StarLab) was used to seal the plate that were incubated at 37°C in FLUOstar Omega microplate reader (BMG LABTECH) static with 5 sec shaking prior to readings. Four readings per well were taken every 15 min at 595 nm. Three biological replicates were used for each growth condition.

2.1.5.13 Measurement of β-galactosidase activity

Bacterial strains were grown in M9 Minimal media supplemented with the desired carbon source as indicated in section 2.1.5.4. One ml sample was collected every hour and used for both measuring planktonic growth and $β$-galactosidase activity. With regards to the latter, 100 μl aliquots were collected in a sterile 96-well plate that was kept on ice during collection of the samples and then stored at -80°C until measurement. At the time of the assay, the frozen plates were left to thaw at room temperature for 30 min. β-galactosidase activity was measured according to the protocol of Ramsay (Ramsay, 2013), while using 4-methylumbelliferyl-β-D-galactopyranoside (MUG) as a substrate. Part of the stored aliquots (10 μl) was transferred into a fresh 96-well plate and 100 μl of the reaction mixture was added. The reaction mixture was prepared by adding 99.5 μl of 20 mg/ml chicken lysozyme in PBS to 0.5 μl of 50 mg/ml MUG dissolved in DMSO. The β-galactosidase activity was measured using Gemini XPS fluorimeter (Molecular Devices) at 360 nm excitation, 450 nm emission, 435 nm cut-off and 8 reads/well. The measurements were taken during the linear phase at 37°C every 30 sec for a total of 30 min.

2.2   DNA techniques

2.2.1   Gene cloning

Cloning experiments were performed using a standard protocol (Sambrook et al., 1989). Genomic DNA was extracted from PAO1 and used as a template for DNA amplifications. The desired gene was amplified from the genomic DNA using a Polymerase chain reaction (PCR). After PCR amplification of the gene, the DNA fragments were purified using agarose gel and digested using the appropriate restriction enzymes. The plasmid was also digested using the same restriction enzymes and both restricted gene and vector were purified before being ligated. Ligation was performed by mixing and incubation of the digested gene fragment, digested plasmid and DNA ligase enzyme. After ligation was performed, the desired construct was transformed into the appropriate bacterial host. All DNA products were kept at -20°C.

2.2.1.1   DNA extraction

The genomic DNA was extracted from overnight bacterial cultures using the GeneJET Genomic DNA Purification Kit. Plasmid DNA was purified from overnight bacterial cultures using The GeneJET Plasmid Miniprep kit. The extracted DNA was quantified using a NanoDrop ND-1000 spectrophotometer (NanoDrop Technologies, Wilmington, DE).

2.2.1.2   Polymerase chain reaction (PCR)

PCR reactions were performed using Veriti Thermal cycler. Components of the PCR reaction are listed in Table 2.7. Steps of the PCR reaction can be found in Table 2.8. Conditions of the PCR reaction varied according to the length of the amplified gene and the annealing temperature of the primers. The list of synthetic oligonucleotides primers can be found in Table 2.9. Primers were purchased from Sigma-Aldrich.

2.2.1.3   Colony PCR

Colony PCR was used to confirm the presence of insert DNA in plasmid constructs. A small portion of the colony containing the desired construct was picked and resuspended in 100 µl of dH_2O. The colony suspension was boiled at 95°C for 10 min and

the cell debris was removed by centrifugation (3,200 x g, 5 min, 4°C). The supernatant was used (1 μl) as a gene template in a standard PCR reaction.

Table 2.7: Components of the PCR reaction.

Ingredients	Volume (μl)
DNA template	0.5
5X HF or GC Phusion buffer	10
Taq polymerase	0.5
25 mM dNTPs	1
10 μM Forward Primer	2.5
10 μM Reverse Primer	2.5
DMSO	0-5
Nuclease-free water	Up to 50

Table 2.8: Steps of the PCR reaction.

Step	Temperature (°C)	Time	Number of cycles
Initial denaturation	98	1 min	1
Denaturation	98	10 sec	
Annealing	55-70	30 sec	35
Extension	72	30s/kb of amplicon	
Final extension	72	5 min	1

Table 2.9: List of primers used in this work.

Primer	Sequence (5'-3')	Site	Product
For complementation of *pykA* and *pykF* mutants			
cPykA F	GATCGAATTCCTGCATACCCACGCGGCGATGCC	*Eco*RI	pUCP20-*pykA*
cPykA R	AAAAAAGGATCCTTATACCAGCAGGTCGCCGACGTGC	*Bam*HI	pUCP20-*pykA*
cPykF F	GATCGAATTCCTACCCAACACCGCCAACGCCCAG	*Eco*RI	pUCP20-*pykF*
cPykF R	AAAAAAAGCTTCACCATCACCATCATCACTCAGAGATCTCCCAGCGGCG	*Hind*III	pUCP20-*pykF*
For transcriptional analysis of *pykA* and *pykF*			
pPykA F	GATCGAATTCCTGCATACCCACGCGGCGATGCC	*Eco*RI	pLP170-*pykA*
pPykA R	CATGGGATCCGTGCGGCGAACGGACATGCAAAG	*Bam*HI	pLP170-*pykA*
pPA1499 F	GATCGAATTCCTACCCAACACCGCCAACGCCCAG	*Eco*RI	pLP170-*PA1499*
pPA1499 R	CATGGGATCCCGCGTGGATCGGTACTCATGACAG	*Bam*HI	pLP170-*PA1499*
For overexpression of PykA and PykF			
rPykA F	AAAAAACATATGATGTCCGTTCGCCGCACCAAAATCG	*Nde*I	pET19m-*pykA*
rPykA R	AAAAAAGGATCCTTATACCAGCAGGTCGCCGACGTGC	*Bam*HI	pET19m-*pykA*
rPykF F	GATGACCATATGACAGCCGACAAGAAAGCCAAGA	*Nde*I	pET19m-*pykF*
rPykF R	CTGAAAGCTTAAGGTCTTTCCCGGATGGATGGAG	*Hind*III	pET19m-*pykF*

2.2.1.4 Agarose gel electrophoresis

Agarose gel electrophoresis was performed to separate the PCR products according to their size. The DNA samples were mixed with 6X DNA loading dye (Thermo Scientific, R0611) and loaded into 1% (w/v) agarose gel. The agarose gel was prepared by dissolving 0.6 g agarose in 60 ml 1X Tris-Acetate-EDTA (TAE) buffer using gentle heating. The agarose was supplemented with 0.5 μg/ml ethidium bromide and allowed to set. The gel was submerged under TAE buffer in a gel tray and 50 μl of DNA samples were loaded into each well. A DNA hyperLadder (10 kb, Bioline) was used as a sizing reference. DNA electrophoresis was performed at 80 V for 45-90 min depending on the size of the DNA. The DNA was visualized and photographed using a UV transilluminator. Bands with desired DNA size were excised using a scalpel and the DNA was purified using a GeneJET Gel Extraction Kit.

2.2.1.5 Digestion of DNA

The DNA was digested using the indicated restriction endonucleases at 37°C for 2 – 3 h. Table 2.10 lists the components of DNA digestion reaction. The digested DNA was purified using GeneJET PCR Purification Kit to avoid generation of random constructs and quantified by NanoDrop ND-100 spectrophotometer. If needed, agarose gel electrophoresis was performed to confirm successful digestion and products were purified from the agarose gel.

Table 2.10: Components of the DNA digestion reaction.

Components	Restriction of PCR amplicon (μl)	Restriction of plasmid (μl)
Enzyme 1	2	2
Enzyme 2	2	2
PCR product	41	___
Plasmid	___	10
CutSmart buffer	5	5
dH$_2$O	Up to 50	Up to 50

2.2.1.6 Ligation of DNA

The digested amplicon and digested plasmid were ligated using T4 DNA ligase. The reaction was conducted in 20 µl using 3:1 insert to plasmid molar ratio, 1 µl T4 DNA ligase and 2 µl T4 ligase buffer. The ligation reaction was incubated for 1 hr on ice and 1 hr at room temperature. Products of ligation were stored at -20°C.

2.2.1.7 Transformation

All bacterial transformations were performed using electroporation (Eppendorf Electroporator). The JM109 strain was used as an initial host for all constructs in this study. The transformed JM109 was confirmed to contain the desired constructs by growth on LBA with selective antibiotics, colony PCR and gene sequencing. Positive constructs were extracted and introduced into the appropriate final hosts (*P. aeruginosa* strains or *E. coli* BL21 strain).

A) Transformation of *E. coli* by electroporation

A sub-culture was prepared by inoculation of 100 µl of overnight culture into a 10 ml fresh LB. The sub-culture was incubated on a rotating drum at 37°C until reaching an OD_{600} of 0.4-0.5. Cells were then placed on ice for 30 min before being sedimented at 3,200 x *g*, 4°C for 10 min. The cell pellet was washed three times using sterile 10% ice-cold glycerol. The pellet was resuspended in 500 µl sterile 10% ice-cold glycerol for transformation. In an ice-cold electroporation cuvette, 100 µl of the final cell suspension were mixed with 2 µl of the ligation mixture and incubated for 10 min on ice. Cells were transformed by electroporation using Eppendorf Electroporator at 2.5 kV (25 µF, 200 Ω, 5 ms time constant). Immediately after electroporation, 1 ml of pre-warmed LB was added to the transformed cells and the cells were incubated for 1 h at 37°C on a rotating drum. Finally, 100 µl were spread onto LBA plates supplemented with appropriate selective antibiotic. The plates were incubated overnight at 37°C.

B) Transformation of *P. aeruginosa* cells by electroporation

Similar to transformation of *E. coli* except that all transformation steps were performed at 20°C.

2.2.1.8 Gene sequencing

Gene sequencing was carried out by GATC Biotech and samples were prepared as per the company's instructions.

2.3   Preparation of vectors and strains

2.3.1   Construction of pUCP20-*pykA* and pUCP20-*pykF* complementation vectors

For complementation of *pykA*, the ORF and 500 bp upstream region of *pykA* were PCR-amplified using cPykA F and cPykA R primers. The PCR products corresponding to this region were purified and the amplified DNA fragment and pUCP20 plasmid were digested independently using *Eco*RI and *Bam*HI restriction endonucleases. The restricted fragments were ligated to yield the complementation plasmid pUCP20-*pykA*.

The design of the complementation construct of the *pykF* gene was slightly different. The *pykF* ORF is predicted to form an operon with *PA1499*. Therefore, I PCR-amplified the entire region spanning upstream of *PA1499* to the 3' end of *pykF*, using the cPykF F and the cPykF R primers. After purification of the DNA fragment from the agarose gel, it was digested by *Eco*RI and *Hind*III restriction enzymes and ligated to the corresponding sites in similarly digested pUCP20. The ligation produced the complementation plasmid pUCP20-*pykF*.

The pUCP20-*pykA* and pUCP20-*pykF* were introduced into JM109 independently and cells were spread onto LBA containing carbenicillin to select for positive transformants. The desired pUCP20 constructs were confirmed using colony PCR and gene sequencing before the plasmids were extracted and re-introduced into the relevant PK mutants. The complementation plasmid pUCP20-*pykA* was introduced into PW8308 and PAF0 to produce PW8308C and PAF1, respectively. Likewise, pUCP20-*pykF* was introduced into PW3705 and PAF0 to produce PW3705C and PAF2, respectively. Cells were spread onto LBA containing carbenicillin to select for positive transformants.

2.3.2 Construction of pLP170-*pykA* and pLP170-*PA1499* transcriptional reporters

Transcriptional reporters of *pykA* and *pykF* were prepared using pLP170 vector. This vector encodes a promoterless *lacZ* gene. The promoter of *PA4329* (*pykA*) was PCR-amplified using pPykA F and pPykA R primers, and the promoter of *PA1499* (predicted to be operonic with *pykF*) was PCR-amplified using pPA1499 F and pPA1499 R primers. The DNA amplicons containing each promoter were digested using *Eco*RI and *Bam*HI and introduced into similarly-digested pLP170. This produced pLP170-*pykA* (*lacZ* transcription driven by the *pykA* promoter) and pLP170-*PA1499* (*lacZ* transcription driven by the *PA1499* promoter).

The pLP170 constructs were introduced into JM109 independently and cells were spread onto LBA containing carbenicillin to select for positive transformants. The desired pLP170 constructs were confirmed using colony PCR and gene sequencing before the plasmids were extracted and re-introduced into PAO1. The pLP170-*pykA* and pLP170-*PA1499* were introduced into PAO1 using electroporation to yield pPykA and pPykF, respectively. PAO1 cells were spread onto LBA containing carbenicillin to select for positive transformants.

2.3.3 Construction of pET19m-*pykA* and pET19m-*pykF* expression vectors

Overexpression of PykA and PykF was driven from the *lac* promoter of the pET19m vector. The *pykA* ORF was PCR-amplified using rPykA F and rPykA R primers and the PCR product was gel-purified. The amplified *pykA* ORF and pET19m were digested with *Nde*I and *Bam*HI restriction endonucleases. The *pykA* amplicon was ligated to the corresponding sites of similarly-digested pET19m and this generated pET19m-*pykA* (able to overexpress PykA upon induction by IPTG). The *pykF* ORF was PCR-amplified using rPykF F and rPykF R primers and the PCR product was gel-purified. The amplified *pykF* ORF and pET19m were digested with *Nde*I and *Hind*III restriction endonucleases. The *pykF* amplicon was ligated to the corresponding sites of similarly-digested pET19m and this generated pET19m-*pykF* (able to overexpress PykF upon induction by IPTG).

The pET19m constructs were first introduced into JM109 and cells were spread onto LBA containing carbenicillin to select for positive transformants. The desired pET19m constructs were confirmed by colony PCR and gene sequencing before the plasmids were extracted and re-introduced into BL21. The pET19m-*pykA* and pET19m-*pykF* were introduced into BL21 using electroporation to yield BL21-PykA and BL21-PykF, respectively. Cells were spread onto LBA containing carbenicillin and chloramphenicol to select for positive transformants.

2.3.4 Construction of PAF0

PAF0 is defective in *pykA* and *pykF* and was generated using generalized phage transduction (ØPA3), in which the genetic material of a *pykF* mutant (donor strain) was transferred into the *pykA* mutant (recipient strain). The following sections show the steps of preparation of the *pykF* genetic material (2.3.4.1), preparation of the *pykA* mutant (2.3.4.2) and phage transduction techniques (2.3.4.3).

2.3.4.1 Preparation of ØPA3 lysates

The ØPA3 is a generalized transducing phage of *P. aeruginosa* and was used for preparation of a phage lysate containing the genetic material of a *pykF* mutant (PW3705). First, a serial dilution of ØPA3 (10^0 to 10^{-7}) was prepared using phage buffer. The ØPA3 lysate of the *pykF* mutant was prepared by mixing 100 µl of an overnight culture of PW3705 with 4 ml of 0.35% molten LBA and 50 µl of each ØPA3 dilution. The mixture was poured on top of a 1.5% (w/v) LBA plate and left to set for 15-30 min. The plate was incubated overnight at 37ºC in upright position (agar at the bottom of the plate). The 0.35% soft agar layer was collected using a spreader from the dilution that showed an incomplete "lacy" surface and the lysate was transferred to a glass bijoux tube. The plate was washed with 3 ml phage buffer and the collected buffer was also transferred to the glass tube containing the lysates. The agar in the glass tube was disrupted by adding 500 µl sodium bicarbonate-treated chloroform and the tube was vortexed for 2 min. The cell lysate was left at room temperature for 30 min before separation from the agar by centrifugation (3,200 x *g*, 4ºC, 20 min). The phage lysate was the supernatant part of the mixture. The lysate was transferred into a fresh bijoux tube. In order to maintain sterility of the lysate, 50 µl of chloroform were added and the bijoux tube was stored at 4ºC.

2.3.4.2 Removal of the antibiotic resistance marker from PW8308

PW8308 and PW3705 are transposon mutants of *pykA* and *pykF*, respectively, in which the genes are disrupted by the insertion of large tetracycline resistance-conferring cassettes. Before phage transduction, the antibiotic resistance of the recipient strain (PW8308) had to be removed to leave the mutant without an antibiotic marker (but still defective in *pykA* function) so that successful phage transduction (transfer of the genetic material from PW3705 into PW8308) could be verified through restoration of antibiotic resistance to PW8308.

The antibiotic marker of the PW8308 was removed using pFLP2-cre, which encodes a Cre-recombinase (enables the excision and recombination of *loxP* sites present on the tetracycline-resistance cassette). pFLP2-cre was introduced into PW8308 by electroporation according to the standard protocol of transformation of *P. aeruginosa* to produce PW8308-cre without an antibiotic marker. Transformants were selected on LBA containing 250 μg/ml carbenicillin and plates were incubated overnight at 37°C. Colonies were picked and streaked first onto LBA with 5% (w/v) sucrose (pFLP2-cre carries *sacB* as a counter-selectable marker) to cure the cells of the pFLP2-cre, and second onto LBA +/- tetracycline to confirm the loss of the tetracycline-resistance cassette. The site-specific excision of the transposon using pFLP2-cre leaves behind a small 64 codon "scar" in place of the antibiotic marker. This small genetic scar was confirmed using PCR.

2.3.4.3 Phage transduction for construction of PAF0

The PAF0 (*pykA pykF* mutant) was generated by transfer of the genetic material from PW3705 (*pykF* mutant, tetracycline resistant) into PW8308-cre (*pykA* mutant, tetracycline sensitive) using phage transduction. This was done by mixing 10 ml overnight culture of PW8308-cre (recipient) with 100 μl of ØPA3 phage lysate containing the genetic material of PW3705 (donor DNA). The mixture was incubated at room temperature for 30 min on a static surface followed by incubation for 20 min on a rotating drum at 37°C. Cells were pelleted by centrifugation (3,200 x *g*, 5 min) and the pellet was washed with 10 ml fresh LB. The cells were re-pelleted and resuspended in 1 ml LB from which 75 μl of the cell suspension was spread onto an LBA plate containing tetracycline.

PAF0 was verified to contain a small scar within the *pykA* (indicative of a *pykA* mutation) and a tetracycline transposon within the *pykF* (indicative of a *pykF* mutation) using PCR.

2.4 Expression and purification of proteins

2.4.1 Expression of PykA and PykF

BL21-PykA (containing pET19m-*pykA*) and BL21-PykF (containing pET19m-*pykF*) were used for overexpression of PykA and PykF, respectively. The BL21 strains containing the pET19m constructs were able to overexpress PykA and PykF recombinantly upon induction of the *lac* promoter (present in pET19m constructs) by isopropyl-β-D-thiogalactopyranoside (IPTG). For expression of the PK proteins, the *E. coli* cells were grown in 1 litre of LB supplemented with 50 μg/ml carbenicillin and 34 μg/ml chloramphenicol. When the cells reached OD_{600} of 0.5-0.6, filter-sterilized IPTG was added at a final concentration of 1 mM. The BL21 cells were incubated overnight at 20°C and the cell pellet was collected by centrifugation (5170 x *g*, 30 min, 4°C) and stored at -20°C until purification.

2.4.2 Purification of PykA and PykF

The BL21 pellet was left to thaw at room temperature before being resuspended in 20 ml cell equilibration buffer containing an EDTA-free protease inhibitor cocktail tablet (Sigma). The cell suspension was sonicated for 3 min (30 sec, 6 rounds, 13 amps) and cell debris was removed by centrifugation (14,636 x *g*, 30 min, 4°C). Protein lysates (containing PykA and PykF) were collected from the supernatant fraction and loaded onto a Ni-NTA column that was pre-washed with equilibration buffer. After the sample was loaded, the Ni-NTA column was washed with equilibration buffer overnight at 4°C. Protein was eluted by passing 10-20 ml elution buffer through the column. The eluted protein His-tags were subsequently removed using TEV protease excision.

For removal of the His-tags from PykA and PykF, each protein was mixed with His-tagged TEV protease and the mixture was loaded in a dialysis bag. Dialysis was performed overnight against dialysis buffer and the protein and TEV mixture was transferred into a falcon tube. Ni-NTA beads (100 μl) were added to the tube in order to capture the protease and uncleaved PK, while leaving the untagged PK enzyme free in solution. The

tube containing the mixture was incubated for 30 min at 4°C on a rotating drum before centrifugation (3,200 x g, 4°C, 30 min) to pellet the Ni-NTA. The purified untagged protein was collected from the supernatant fraction and concentrated using a Vivaspin column (MWCO 30,000 Da, Sartorius). Proteins were dispensed into aliquots, snap-frozen in liquid nitrogen and stored at -80°C.

2.5 Quantification of proteins

2.5.1 Quantification of purified proteins

Concentration of the purified proteins was measured by direct UV absorbance at 280 nm using Eppendorf Biospectrometer. The protein concentration was determined using the calculated extinction coefficients of PykA (24410 $M^{-1}cm^{-1}$) and PykF (25440 $M^{-1}cm^{-1}$).

2.5.2 Quantification of total proteins in cell lysates

2.5.2.1 Preparation of cell lysates

Cells were grown in M9 Minimal media containing the desired carbon source until reaching stationary phase. Cells were sedimented (3,200 x g, 4°C, 10 min) and the pellets were solubilized in 2 ml of lysis buffer containing an EDTA-free protease inhibitor cocktail tablet (Sigma). The cell suspensions were sonicated on ice for 30 sec and centrifuged at 14,636 x g, 4°C for 5 min. Whole-cell protein extracts were collected from the supernatant fraction and proteins were quantified using the Bio-Rad protein assay.

2.5.2.2 Bio-Rad protein assay

The Bio-Rad protein assay is based on the Bradford method (Bradford, 1976) and was used in this study for quantification of total protein in cell lysates. Bradford reagent (1X) was prepared by mixing one part of the Bradford stock reagent (Bio-Rad Protein Assay Dye Reagent Concentrate, 500-0006) with four parts of dH$_2$O. Protein standards of ɣ-globulin ranging from 0.2 to 1.4 mg/ml were prepared using PBS. The Bradford reagent (1X, 980 µl) was mixed with each ɣ-globulin dilution (20 µl) and a standard ɣ-globulin calibration curve was produced.

For preparation of the samples, 20 μl of the sample protein lysate (diluted in PBS if needed) was mixed with 980 μl of the diluted Bradford reagent. PBS buffer was used for preparation of the blank and all reactions were incubated at room temperature for 10 min for colour development. Readings were measured by spectrophotometer at 595 nm and compared with the standard curve. The assay was performed in triplicate.

2.6 Preparation of protein gels

2.6.1 SDS-polyacrylamide gel electrophoresis

Protein samples were mixed with SDS loading buffer and boiled for 5-10 min at 95°C. The samples were loaded on 15% (v/v) SDS-PAGE gels for purified proteins or 9% (v/v) SDS-PAGE gels for cell lysates as described in Table 2.6. Samples were separated by electrophoresis at 20 V cm^{-1} for 80 min. Gels of purified proteins were stained with Coomassie Brilliant Blue and gels of cell lysates were used in western blot analysis.

2.6.2 Coomassie staining

Components of the Coomassie Brilliant Blue stain and destaining solutions are described in Table 2.6. After gel electrophoresis, the gels were incubated overnight in Coomassie Brilliant Blue stain. The stain was decanted and the gels were incubated in Destain I for 1h followed by Destain II for 3 h. The Destain II was replaced with a fresh solution every hour. Staining and destaining were performed with gentle rotation on a moving platform.

2.7 Western blot analysis

Polyclonal antibodies were raised in rabbit against purified PykA and PykF proteins (Biogenes.De). The anti-PykA and anti-PykF antibodies were pre-adsorbed against an acetone extract of *pykA* and *pykF* mutants, respectively. The acetone extraction step was essential in order to minimize non-specific binding. The cleaned antibodies were dispensed in 20 μl aliquots and stored at -20°C.

After gel electrophoresis, proteins were transferred from the SDS-PAGE gels to the polyvinylidene difluoride membrane (PVDF) using transfer buffer (25 mM Tris, 190 mM glycine, 20% methanol). The transfer of proteins was performed at 25 V for 120 min. The PVDF membrane containing the transferred proteins was incubated in blocking buffer (5% w/v semi-skimmed milk in PBS) overnight. The blocking buffer was decanted and the membrane was washed twice in wash buffer (PBS with 0.1% v/v tween). The primary antibody (anti-PykA or anti-PykF) was added (at dilution of 1:2000 in blocking buffer) to the membrane and this was followed by incubation for 1 h. The membrane was washed four times in wash buffer, with 5 min washing intervals and the secondary HRP-coupled goat anti-rabbit antibody was added to the membrane (at dilution of 1:10,000 in blocking buffer). This was followed by incubation for 30 min and then the membrane was washed three times in wash buffer. The membrane was developed using Clarity Western Blotting substrate (Bio-Rad) and chemiluminescence was detected on an x-ray film. All incubation steps were performed at room temperature on a rotating platform.

2.8 Measurements of pyruvate kinase (PK) activity

2.8.1 LDH-coupled assay

The PK activity was measured using an LDH-coupled assay (Figure 2.1). In the assay, PK catalyses the de-phosphorylation of PEP into pyruvate, and LDH converts the pyruvate into lactate along with consumption of NADH. The decline of the NADH at 340 nm indicates PK enzymatic activity.
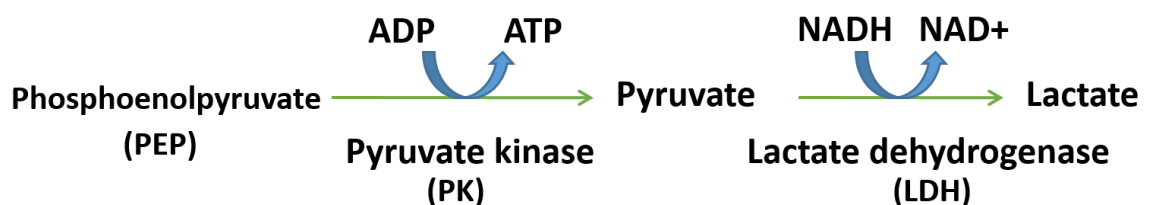
Figure 2.1: LDH-coupled assay. The PK activity is measured by the decline of the NADH concentration which is measurable at 340 nm.

2.8.2 Components and measurement of the reaction

Components of the LDH-coupled assay can be found in Table 2.11. Stock solutions were prepared in dH$_2$O, divided into aliquots and stored at -20°C. The reaction mixture was prepared in 1 ml and incubated for 10 min at 37°C before measurement to ensure optimum enzymatic activity. PykA and PykF were freshly diluted to 0.1 μg/μl in dialysis buffer and these stocks were kept on ice throughout the time of the experiment. The reaction was initiated by the addition of 2 μl of PykA stock or 2.5 μl of PykF stock to the reaction mixture followed by gentle pipetting for mixing. The reaction was measured immediately at 340 nm and 37°C after the addition of the purified enzymes using the Eppendorf Biospectrometer. Each reaction was carried out in triplicate. Data were analysed using GraphPad prism 7 for extraction of the kinetic constants. One unit of PK enzymatic activity was defined as the reduction of 1 μM of NADH per second per milligram of protein.

Table 2.11: Components of the LDH-coupled assay.

Standard reactions	Up to 1 ml
Basic mixture (without PEP or ADP)	50 mM Tris-HCl pH 7.5
	10 mM MgCl$_2$
	0.2 mM NADH
	10 units L-LDH (rabbit muscle)
Standard titration of PEP	Basic mixture
	2 mM ADP
	Variable PEP (0-6 mM)
Standard titration of ADP	Basic mixture
	Variable ADP (0-2.5 mM)
	5 mM PEP
Regulators	**Up to 1 ml**
Screening of regulators at low PEP concentration	Basic mixture
	2 mM ADP
	0.3 mM PEP
	1 mM regulator (unless otherwise stated)

Table 2.11: Continued	
Screening of regulators at high PEP concentration	Basic mixture 2 mM ADP 2 mM PEP 1 mM regulator (unless otherwise stated)
Titration of PEP with regulators	Standard titration of PEP 1 mM regulator (unless otherwise stated)
Titration of ADP with regulators	Standard titration of ADP 1 mM regulator (unless otherwise stated)
Inhibitors	**Up to 1 ml**
Screening of synthetic inhibitors	Basic mixture 2 mM ADP 5 mM PEP 200 μM inhibitor
Titration of PEP with inhibitors	Standard titration of PEP IC25 or IC50 inhibitor
Titration of ADP with inhibitors	Standard titration of ADP IC25 or IC50 inhibitor
Metal ions	**Up to 1 ml**
Screening of divalent ions	Basic mixture without $MgCl_2$ 2 mM ADP 5 mM PEP 10 mM divalent ions
Titration of PEP with monovalent ions	Standard titration of PEP 100 mM monovalent ions
Titration of ADP with monovalent ions	Standard titration of ADP 100 mM monovalent ions

2.8.3 PK activity of cell lysates

PK activity in cell lysates was measured using the same protocol for purified proteins (LDH-coupled assay). Each reaction consisted of the basic mixture (Table 2.11), although PEP (5 mM) and ADP (2 mM) were added at saturation. After quantification of proteins, the concentration of the cell lysates were normalized using lysis buffer. The reaction was initiated by the addition of an equal volume of normalized cell lysates to the reaction mixture. The PK activity was measured immediately after addition of the lysates and each experiment was done three times.

2.8.4 Regulators, synthetic inhibitors and metal ions

Metabolic regulators, synthetic inhibitors and ions used in this study can be found in Table 2.12. Regulators and metal ions were prepared in dH_2O at a final concentration of 50 mM and 1M, respectively, whereas the synthetic inhibitors were dissolved in DMSO at a final concentration of 50 mM. Regulators, inhibitors and ions were kept at -20°C, 4°C and room temperature, respectively.

Table 2.12: List of regulators, ions and inhibitors used in this study.

Regulators	
Sodium acetate	Sodium succinate
Acetyl-CoA	DL-isocitric acid
Adenosine monophosphate (AMP)	Ribose 5-phosphate (R5P)
Adenosine triphosphate (ATP)	Fructose 6-phosphate (F6P)
Citrate	Xylulose 5-phosphate (X5P)
Co-enzyme A	Ribulose 5-phosphate (RL5P)
Fructose 1,6-bisphosphate (F1,6P)	Sodium propionate
Guanosine diphosphate (GDP)	*cis*-aconitic acid
Guanosine triphosphate (GTP)	Ribose
6-phosphogluconate (6PG)	Glucose
Glucose 6-phosphate (G6P)	Fumarate
Glyceraldehyde 3-phosphate (G3P)	Maleic acid
Glycolic acid	Methylglyoxal
Itaconic acid	3-nitropropionic acid
L-glutamic acid	α-ketoglutarate
2-*keto*-3-deoxy-6-phosphogluconate (KDPG)	Malate

Table 2.12: Continued

Monovalent ions	
KCl	
NH_4Cl	
NaCl	

Divalent ions	
$MnCl_2$	$ZnSO_4$
$CaCl_2$	$CoCl_2$
NiSO4	

Inhibitors	
PZ0301	S171204
S7576 (Shikonin)	L334588
R396907	

2.8.5 Kinetic plots and calculations

All data from kinetics analyses were plotted and analysed using GraphPad Prism7. With respect to ADP titration, the kinetic constants (V_{max} and K_M) were obtained using the Michaelis-Menten equation as no cooperativity was observed and the data were hyperbolic. However, the kinetic constants (V_{max}, $S_{0.5}$ and h) with respect to PEP titration were obtained using the allosteric sigmoidal equation as positive cooperativity was apparent. The Michaelis-Menten and the allosteric sigmoidal equations are shown below:

Michaelis-Menten equation: $Y = V_{max} . X/(K_M + X)$

Allosteric sigmoidal equation: $Y = V_{max} . X^h/(S_{0.5}^h + X^h)$

in which V_{max} is the maximum enzyme velocity, X is the variable concentration of the substrate (PEP or ADP), K_M is the Michaelis-Menten constant, $S_{0.5}$ is equivalent to the K_M when sigmoidal kinetics is applied, and h corresponds to the Hill coefficient. The K_M or $S_{0.5}$ is the concentration of the substrate that produces a half-maximal enzyme velocity.

The k_{cat} is the catalytic turnover number and it was calculated from:

$$k_{cat} = V_{max}/E_t$$

where the E_t is the total concentration of the enzyme (monomer) used in the experiments. The E_t for the PykA and the PykF was 3.82 nM and 4.85 nM, respectively.

The catalytic efficiency of each enzyme was calculated as shown:

$$\text{Catalytic efficiency with respect to ADP titration} = k_{cat}/K_M$$
$$\text{Catalytic efficiency with respect to PEP titration} = k_{cat}/S_{0.5}$$

The Lineweaver-Burk plots were used to determine enzyme activation and enzyme inhibition kinetics. The plot results in a straight line with a slope equals to K_M/V_{max}, a Y-intercept equals to $1/V_{max}$ and an X-intercept equals to $-1/K_M$. The plots were calculated from the double-reciprocal of the data as shown below:

$$X = 1/[S]$$
$$Y = (1/V_{max}) . (1 + K_M/[S])$$

in which [S] corresponds to the variable concentration of the substrate used in the experiment. The K_M values were substituted with the $S_{0.5}$ values when investigating changes with respect to PEP titration.

2.9 Analytical ultracentrifugation (AUC)

AUC was performed in collaboration with Biophysics Facility, University of Cambridge Biochemistry Department, in order to determine the oligomeric status of PykA and PykF in solution. The protein sample was dialyzed against 20 mM Tris-HCl pH 7.5, 100 mM NaCl and 0.1 mM EDTA to remove glycerol. The centrepieces of the Epon double-sector of Beckman Optima XL-I (AN-60 Ti rotor) were filled with 400 μl of the protein or blank buffer. The sample was sedimented at 29160 x *g*, for 24 hr at 20°C. Absorbance data were taken every 2 min at 280 nm with interference scans collected every minute. Data analysis and the calculations of buffer viscosity, protein partial specific volumes and frictional ratios were performed using SEDFIT (Schuck, 2000) and SEDNTERP (Hayes et al., 1995).

2.10 X-ray crystallography

2.10.1 Setting up crystallization screens

Crystallization screens were performed using sitting-drop vapour diffusion with ready-to-use screening plates from the X-ray Crystallography Facility, University of Cambridge. Each purified enzyme was adjusted to 20-30 mg/ml final concentration using dialysis buffer and the diluted enzymes were added to the reservoir solution in 1:1 ratio. Screening plates were incubated for 2-3 weeks at 19°C until crystals grew and reached a desirable size. The crystals were mounted on nylon loops and cryoprotected in mother liquor supplemented with 40% (v/v) glycerol before being flash frozen in liquid nitrogen.

2.10.2 Co-crystallization of PykA and PykF

Co-crystallization solutions of PykA and PykF were prepared independently before being added to screening plates. The co-crystallization solutions (25 µl each) were prepared using dialysis buffer and the solutions were incubated for 10 min at room temperature before being added to screening plates in 1:1 ratio.

With respect to PykA, the co-crystallization mixture was made of 22 mg/ml purified PykA, 20 mM $MgCl_2$, 2 mM G6P and 2 mM PEP, and the mother liquor consisted of 20% (w/v) PEG 3350, 0.1 M Bis-Tris propane pH 7.5 and 0.2 M disodium malonate. The co-crystallization solution of PykF consisted of 29 mg/ml purified PykF, 20 mM $MgCl_2$, 200 mM KCl and 2 mM PEP and the mother liquor was made of 25% (w/v) PEG 6000 and 0.1 M Hepes pH 7.5.

2.10.3 X-ray diffraction and structure refinement

Diffraction data were collected remotely at the Diamond Light Source Synchrotron (Didcot, UK) on beamline IO4 (MX14043-47), at a wavelength of 0.9159 Å. The PykA structure was obtained from molecular replacement with BALBES (Long et al., 2008) using PK of *T. brucei* (PDB 4HYV) as a structural template. Model building and refinement of PykA were performed using Coot (Emsley et al., 2010) and *REFMAC5* (Murshudov et al., 1997), respectively. The PykF structure was obtained from molecular replacement with Phaser MR (Adams et al., 2010) using a PykF ensemble generated by

the Swiss model (Waterhouse et al., 2018) as a structural template. Model building and structure refinement was performed using Coot and *phenix.refine* (Adams et al., 2010), respectively.

For both structures, ligands, metal ions and water molecules were added as appropriate. MolProbity (Chen et al., 2010) was used to check the stereochemistry of the structures. PDBePISA (Krissinel and Henrick, 2007) was used for analysis of the inter-protomer and protein-ligand interfaces, while the PDBeFold (Krissinel et al., 2004) was used for analysis of structural alignments. Structural figures were generated using CCP4mg (McNicholas et al., 2011).

2.11 Statistical significance

Where appropriate, an unpaired *t*-test was performed between experimental groups to investigate statistical significance. The *t*-test was based on a two-tailed *p*-value. Asterisks were used as indicated on figures to refer to the degree of significance (*=*p* <0.05, **=*p* <0.01, ***=*p* <0.001).

Chapter 3

3 Genetic characterization of *pykA* and *pykF*

3.1 Introduction

Some Gram-negative bacteria encode *pykA* (pyruvate kinase II) and *pykF* (pyruvate kinase I) instead of a single PK (Ponce et al., 1995; Garcia-Olalla and Garrido-Pertierra, 1987; Hofmann et al., 2013). In these species, *pykF* is the dominant isozyme and inactivation of *pykF* causes major perturbations of the metabolism, growth defects and most importantly diminished virulence (Ponce et al., 1995; Muñoz and Ponce, 2003; Bücker et al., 2014).

P. aeruginosa is an opportunistic pathogen which encodes uncharacterized *pykA* and *pykF* isoforms. Here, I show that *pykA* is the dominant isoform, and that it has a primary role in pyruvate biosynthesis and cell growth on glucose and glycerol carbon sources. In this chapter, I compare *pykA* and *pykF* from *P. aeruginosa* with respect to their locations on the genome and protein classifications. I use β-galactosidase activity assays to investigate the transcription from the *pykA* and *pykF* promoters. I also use Western blots to compare the expression of PykA and PykF. I also examine how inactivation of *pykA*, *pykF* or both genes together impact on pyruvate biosynthesis, cell growth and phenotypic behaviour.

3.2 Bioinformatics

3.2.1 The genomic context of *pykA* and *pykF* in *P. aeruginosa*

PAO1 (a wild-type strain of *P. aeruginosa*) encodes two pyruvate kinase (PK) genes; *pykA* (*PA4329*, 1452 bp) and *pykF* (*PA1498*, 1434 bp). The two genes are placed more than 2500 genes apart on the chromosome of PAO1 (Figure 3.1A). Investigation of the genomic location of *pykA* revealed that it is found downstream of two hypothetical genes (*PA4327* and *PA4328*) which are predicted to be parts of an operon (Figure 3.1B). Protein domain analysis using InterPro revealed that PA4327 contains a tetratricopeptide repeat (TPR) which is known to mediate protein-protein interactions, whereas PA4328 encodes a universal stress protein A (UpsA). The downstream region of

pykA consists of another set of genes that are also predicted to be parts of an operon and this region included *PA4330*, *PA4331* and *sadC* which encode an enoyl-CoA hydratase, a probable ferredoxin reductase and a protein with diguanylate cyclase activity, respectively.

Unlike *pykA*, *pykF* (*PA1498*) is part of a more organized genetic cluster. The upstream region of *pykF* encodes *gcl* (*PA1502*), *PA1501*, *PA1500*, and *PA1499*, which are predicted to encode genes for enzymes that catalyse a series of reactions involved in glyoxylate metabolism (Figure 3.1B, 3.2). *pykF* is also predicted to be operonic with, and to function downstream of *PA1499*. Similarly, *PA1501* and *PA1500* are also predicted to be parts of an operon. The downstream region of *pykF* consists of hypothetical genes with functions unrelated to glyoxylate metabolism. The genetic bioinformatics of *pykA* and *pykF* was generated using Pathway Tools software which is integrated with BioCyc database collection.

A)

B)
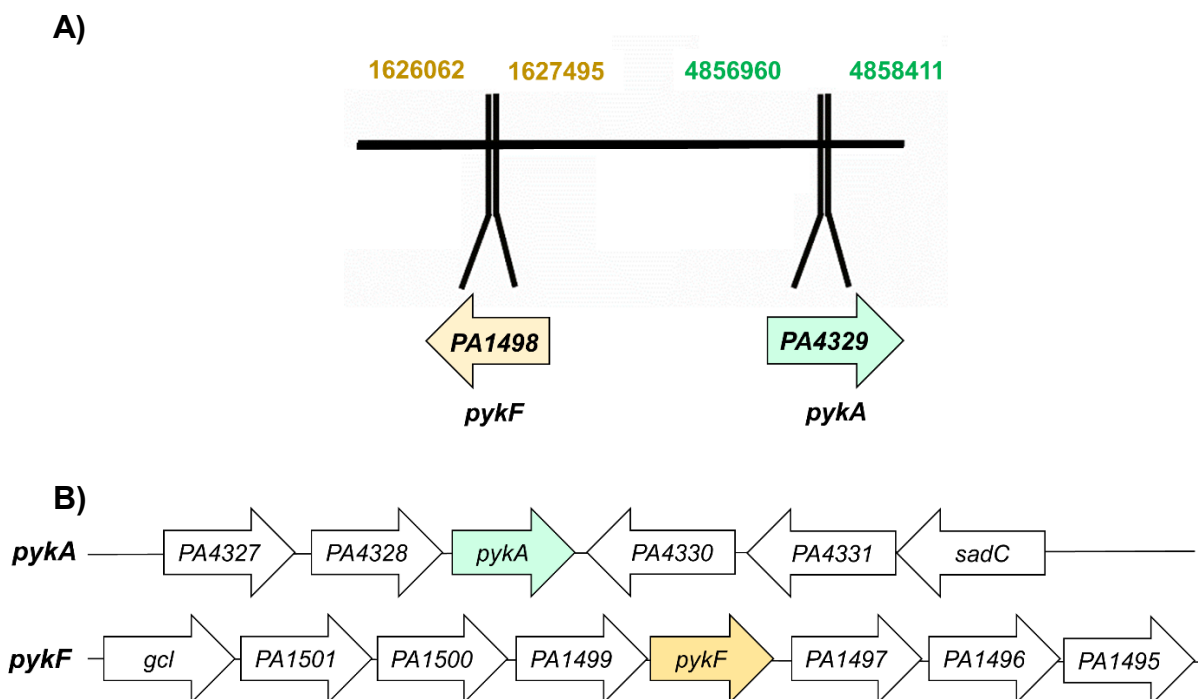
Figure 3.1: The genetic context of *pykA* and *pykF*. A) Location of *pykA* (*PA4329*) and *pykF* (*PA1498*) on the PAO1 chromosome. The numbers shown on the top refer to the coordinates of each gene (PAO1 chromosome numbering) and the arrows point to the direction of the DNA strands. B) Diagram representation of the genetic boundaries of *pykA* (top strand) and *pykF* (bottom strand).
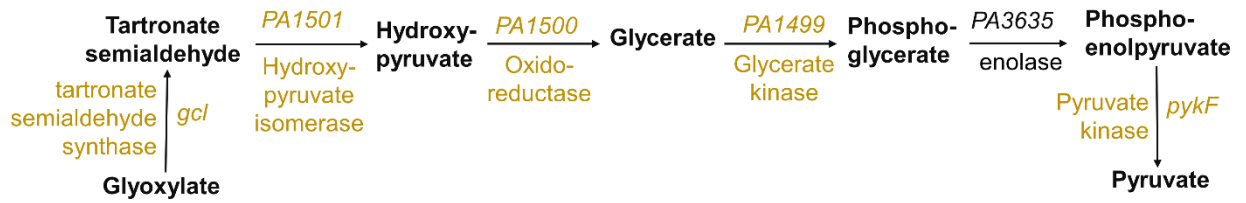
Figure 3.2: Predicted reactions catalysed by gene products from the *pykF* cluster. *pykF* lies within a genetic cluster that is predicted to catalyse a series of reactions involved in the conversion of glyoxylate to pyruvate. Enolase is not part of the genetic cluster, but is inferred to complete the sequence of reactions.

3.2.2 Phylogenetic classification

Before performing any genetic characterization, I wanted to verify that PykA and PykF in *P. aeruginosa* were correctly annotated. Therefore, I investigated the phylogenetic classification of PykA and PykF using PANTHER Tree Viewer, which is a system for classification of proteins and prediction of their functions based on amino acid sequences. Phylogenetic analysis revealed that PykA and PykF from *P. aeruginosa* are different isozymes and that they belong to two independent subfamilies of pyruvate kinase (Figure 3.3). The PykA of *P. aeruginosa* is a member of the pyruvate kinase II subfamily and is in the same cluster with other PykA enzymes from *E. coli*, *S. enterica* Serovar Typhimurium and *Y. pestis*. By contrast, the PykF from *P. aeruginosa* is a member of PKM subfamily together with PykF enzymes from other species.

The PANTHER protein classification was confirmed by performing a second phylogenetic analysis using selected species that are known to encode PykA and PykF together. The amino acid sequences of PykA and PykF from *P. aeruginosa, E. coli*, *S. enterica* Serovar Typhimurium and *Y. pestis* were first aligned using the ClustalOmega webserver, then the aligned sequences were used to generate a new phylogenetic classification using JalView. Results of the new phylogenetic analysis were almost in good overall agreement with the PANTHER classification (Figure 3.4). PykA and PykF were grouped into two independent branches, with PykA and PykF from *P. aeruginosa* placed correctly in their respective groups.
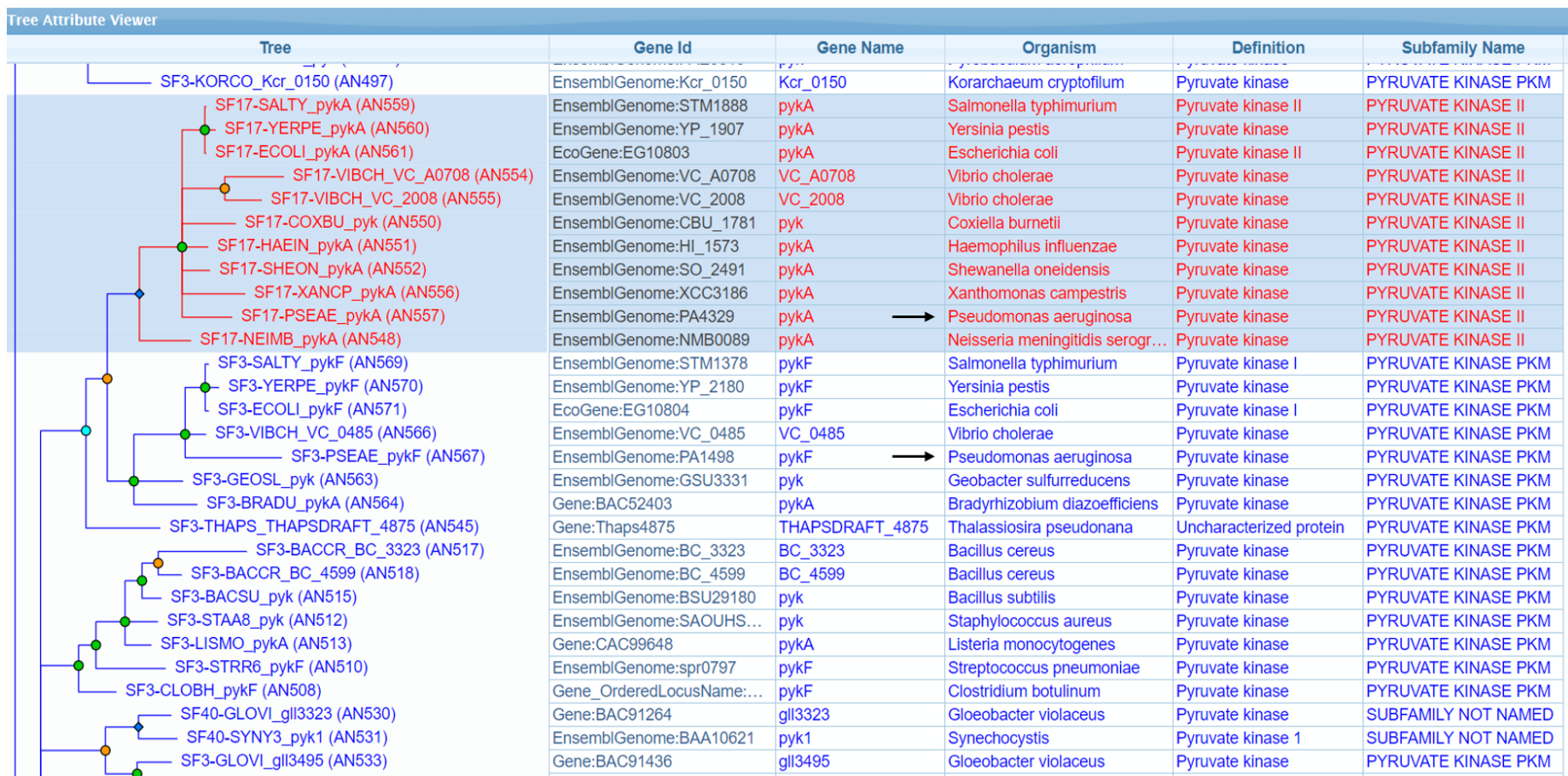
Figure 3.3: A snapshot of PANTHER classification system for a subset of PK enzymes. The PykA and PykF of *P. aeruginosa* (black arrows) belong to two independent subclasses of PK enzymes.
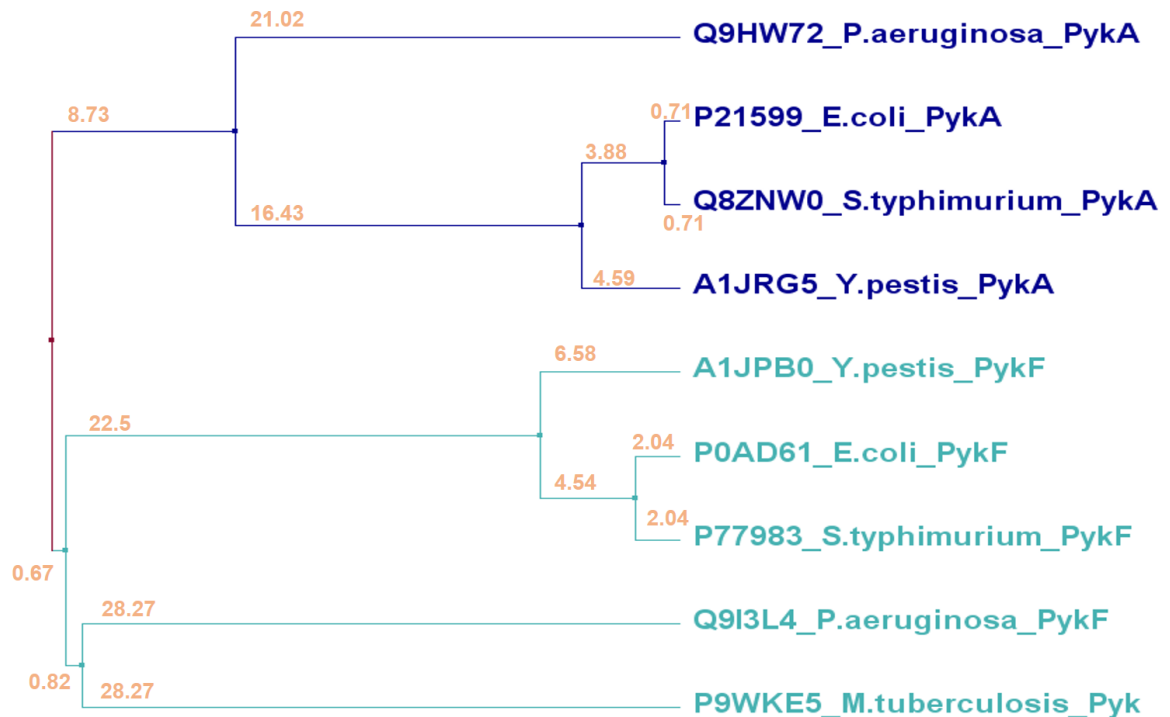
Figure 3.4: Phylogenetic analysis of PykA and PykF in selected bacterial species. The enzymes are identified by their Uniprot ID, bacterial origin and gene name. Phylogeny analysis was done by alignment of the amino acid sequence using ClustalOmega, and the average distances were then calculated from percentage sequence identity using JalView. The shown distances represent the length of branches (or leaves) from their nodes.

3.2.3 Motif analysis

Motif analysis provided a more detailed reassurance that PykA and PykF in *P. aeruginosa* were correctly annotated. Motif analysis was done using the ScanProsite server. My approach was to find if there were any motifs that distinguish PykA from PykF in *P. aeruginosa* and then to check if the distinguishable motifs were present in PykA and PykF from other bacteria.

Results from ScanProsite revealed that most of the motifs are identical in PykA and PykF from *P. aeruginosa*, however, there are a few distinguishable motifs which could discriminate each enzyme (Table 3.1). Motif analysis of PK enzymes from *P. aeruginosa*

showed that PykA has a unique predicted tyrosine kinase phosphorylation (TKP) site that is absent in PykF, whereas PykF encodes a unique predicted cAMP/cGMP dependent protein kinase phosphorylation (CAG-DPKP) site that is absent in PykA. With this, I carried out a motif analysis of PykA from other species to see if they encode a TKP site similar to PykA$_{PA}$. Likewise, I analysed the PykF from other species to see if they encode a CAG-DPKP site similar to PykF$_{PA}$. The ScanProsite results revealed that the PykA enzymes from these species are similar to PykA$_{PA}$ and they encode the TKP site that is absent in the PykF enzymes (Table 3.2). Also, the PykF enzymes from these species has a unique CAG-DPKP that is absent in the PykA enzymes. This confirmed further that the PykA$_{PA}$ and the PykF$_{PA}$ were correctly annotated PykA and PykF enzymes, respectively.

Table 3.1: Motif analysis of PykA and PykF from *P. aeruginosa*. Analysis was performed by ScanProsite webserver. Red asterisks refer to the distinguishable motif for each enzyme. Consensus patterns of the predicted motifs are shown.

Predicted Sites	PykA	PykF
Pyruvate kinase active site signature [LIVAC]-x-[LIVM](2)-[SAPCV]-K-[LIV]-E-[NKRST]-x-[DEQHS]- [GSTA]-[LIVM]	Yes	Yes
Protein kinase C phosphorylation site [ST]-x-[RK], S or T is the phosphorylation site	Yes	Yes
N-myristoylation site G-{EDRKHPFYW}-x(2)-[STAGCN]-{P}, G is the N-myristoylation site	Yes	Yes
N-glycosylation site N-{P}-[ST]-{P}, N is the glycosylation site	Yes	Yes
Casein kinase II phosphorylation site [ST]-x(2)-[DE], S or T is the phosphorylation site	Yes	Yes
Tyrosine kinase phosphorylation site [RK]-x(2)-[DE]-x(3)-Y or[RK]-x(3)-[DE]-x(2)-Y, Y is the phosphorylation site	Yes*	____
Cell attachment sequence R-G-D	Yes	Yes
cAMP- and cGMP-dependent protein kinase phosphorylation site [RK](2)-x-[ST], S or T is the phosphorylation site	____	Yes*

Table 3.2: Motif analysis of PykA and PykF in different bacterial species. Motifs are predicted by ScanProsite webserver based on the amino acid sequence of each enzyme. TKP and CAG-DPKP refer to tyrosine kinase phosphorylation site and cAMP/cGMP dependent protein kinase phosphorylation site, respectively. The subfamily classification of each enzyme is according to PANTHER Tree Viewer.

Origin	UnitProt ID	TKP	CAG-DPKP	Subfamily
PykA (*P. aeruginosa*)	Q9HW72	Present	Absent	Pyruvate kinase II
PykA (*Y. pestis*)	Q0WF92	Present	Absent	Pyruvate kinase II
PykA (*E. coli*)	P21599	Present	Absent	Pyruvate kinase II
PykA (*S. typhimurium*)	Q8ZNW0	Present	Absent	Pyruvate kinase II
PykF (*P. aeruginosa*)	Q9I3L4	Absent	Present	PKM
PykF (*Y. pestis*)	Q0WEC9	Absent	Present	PKM
PykF (*E. coli*)	P0AD61	Absent	Present	PKM
PykF (*S. typhimurium*)	P77983	Absent	Present	PKM

3.3 β-galactosidase activity of the *pykA* and the *pykF* promoters

3.3.1 Construction of the *pykA* and the *pykF* transcriptional reporters

For identification of environmental factors which might modulate the expression of *pykA* and *pykF*, transcriptional reporter strains were constructed using the promoterless pLP170-*lacZ* vector. For measurement of *pykA* transcription, the *pykA* promoter was cloned upstream of the *lacZ* reporter yielding pLP170-*pykA*. For measurement of *pykF* transcription, the promoter preceding the gene upstream of *pykF* (promoter of *PA1499*) was cloned in front of the *lacZ* gene, generating pLP170-*PA1499*. The *lacZ* reporter constructs were introduced into PAO1 to generate PpykA and PpykF which were used in transcription experiments.

3.3.2 Transcription of *pykA* was consistently higher than *pykF*

The β-galactosidase activity was measured in the PpykA and the PpykF grown in minimal media with different carbon sources. Glucose and glycerol were used as representative carbon sources feeding into the upper part of the EDP, whereas acetate and succinate were used as representative carbon sources feeding into metabolism after the EDP. Transcription of *pykA* and *pykF* was measured in cells grown in aerobic (Figure 3.5) and limited oxygen conditions (Figure 3.6). Additionally, to check the effect of low temperature on the transcription of *pykA* and *pykF*, the β-galactosidase activity was also measured in the PpykA and the PpykF grown at 28ᵒC in minimal media supplemented with glucose (Figure 3.7).

The promoter activity of *pykA* was found to be consistently higher than that of *pykF* in all tested carbon sources, oxygen conditions and temperatures. Moreover, *pykA* transcription displayed a trend when cells grew in the presence of limiting oxygen. When the cells grew in glucose and glycerol at limited oxygen levels, transcription of *pykA* was high during exponential growth (1-6 hr) and tailed off during the stationary phase (up to 31 hr). In contrast, the promoter activity of *pykA* seemed to reach its highest levels after 24-25 hr of growth in acetate or succinate at limited oxygen levels. The control strain harbouring empty pLP170 did not show any β-galactosidase activity in all cases when compared with the PpykA or the PpykF.
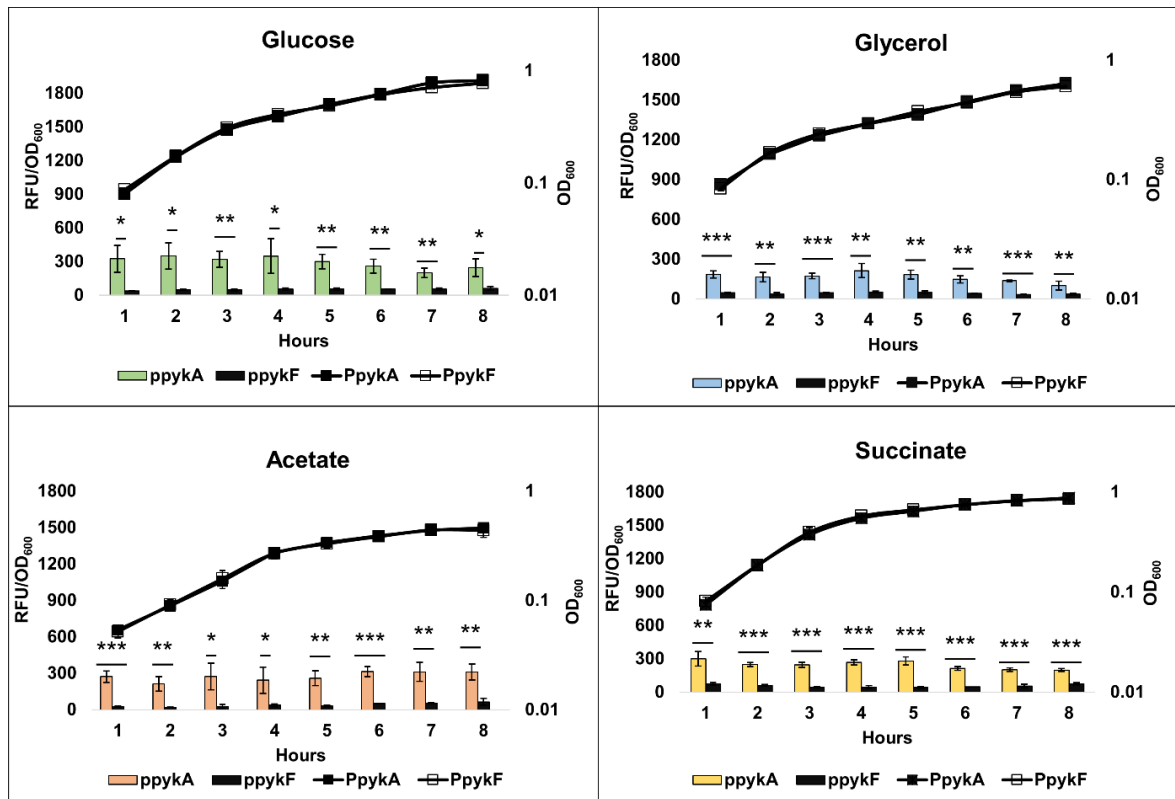
Figure 3.5: Transcription of *pykA* and *pykF* in aerobic conditions. PpykA (PAO1 harbouring pLP170-*pykA*) and PpykF (PAO1 harbouring pLP170-*PA1499*) were grown in minimal media with 20 mM glucose, 30 mM glycerol, 40 mM acetate or 20 mM succinate (as indicated) in aerobic conditions at 37°C. The β-galactosidase activity (as a proxy of transcriptional levels) and cell growth are represented in bars and lines, respectively. The β-galactosidase activity was measured in three biological replicates and the error bars represent standard error. Abbreviations: RFU, relative fluorescence units; OD_{600}, optical density measured at 600 nm. Statistical significance was performed using an unpaired *t*-test (*=*p* <0.05, **=*p* <0.01, ***=*p* <0.001).
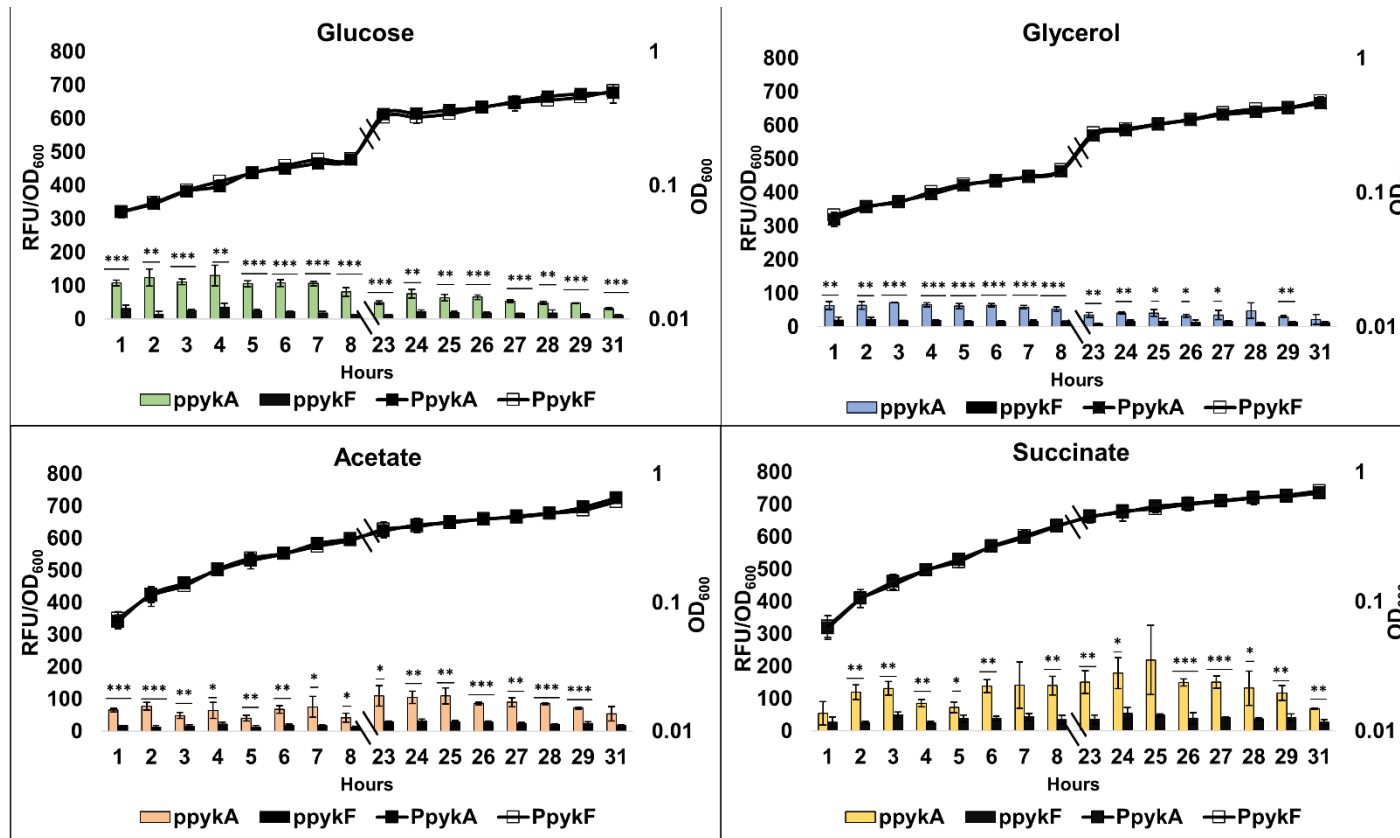
Figure 3.6: Transcription of *pykA* and *pykF* in limited oxygen levels. PpykA (PAO1 harbouring pLP170-*pykA*) and PpykF (PAO1 harbouring pLP170-*PA1499*) were grown in minimal media with 20 mM glucose, 30 mM glycerol, 40 mM acetate or 20 mM succinate (as indicated) at 37°C, under a layer of mineral oil. The β-galactosidase activity (as a proxy of transcriptional levels) and cell growth are represented in bars and lines, respectively. The β-galactosidase activity was measured in three biological replicates and the error bars represent standard error. Abbreviations: RFU, relative fluorescence units; OD_{600}, optical density measured at 600 nm. Statistical significance was performed using an unpaired *t*-test (*=p <0.05, **=p <0.01, ***=p <0.001).
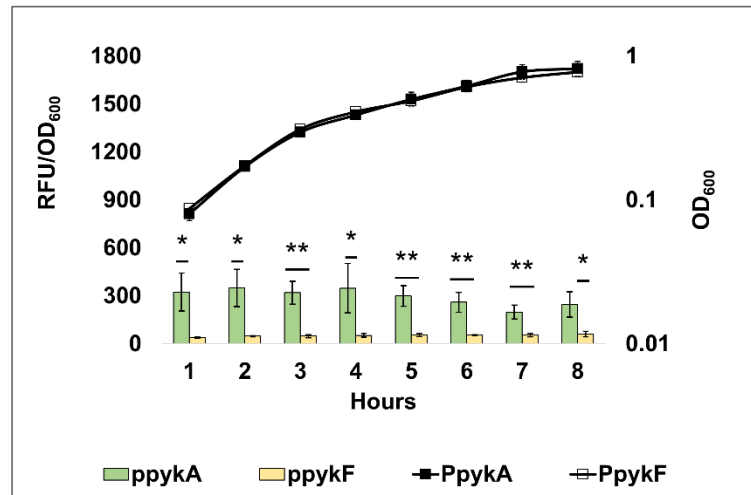
Figure 3.7: Transcription of *pykA* and *pykF* at 28°C. PpykA (PAO1 harbouring pLP170-*pykA*) and PpykF (PAO1 harbouring pLP170-*PA1499*) were grown in minimal media with 20 mM glucose in aerobic condition. The β-galactosidase activity (as a proxy of transcriptional levels) and cell growth are represented in bars and lines, respectively. The β-galactosidase activity was measured in three biological replicates and the error bars represent standard error. Abbreviations: RFU, relative fluorescence units; OD_{600}, optical density measured at 600 nm. Statistical significance was performed using an unpaired *t*-test (*=p <0.05, **=p <0.01, ***=p <0.001).

3.4 Protein expression and enzymatic activity of PykA and PykF

3.4.1 Generation of the PAF0 double mutant

The PW8308 and PW3705 are transposon mutants of *pykA* and *pykF*, respectively, which were purchased from the UWGC PAO1 mutant bank. The two single mutants were used in generation of a double mutant defective in both genes (PAF0). This was done using phage transduction (Figure 3.8). The tetracycline resistance marker was first removed from PW8308 using pFLP2-cre plasmid, producing PW8308-cre mutant. Excision of the transposon from *pykA* left behind a 64-codon scar within the *pykA* ORF and this was confirmed using PCR (Figure 3.9). PW8308-cre (*pykA⁻ pykF⁺*) was then infected by a phage which contains the genetic material of PW3705 (*pykA⁺ pykF⁻*), generating a double *pykA pykF* mutant (PAF0). I used PCR to verify that PAF0 contains a transposon within the *pykF* ORF (indicative of *pykF* mutation) and a small genetic scar within the *pykA* ORF (indicative of *pykA* mutation).
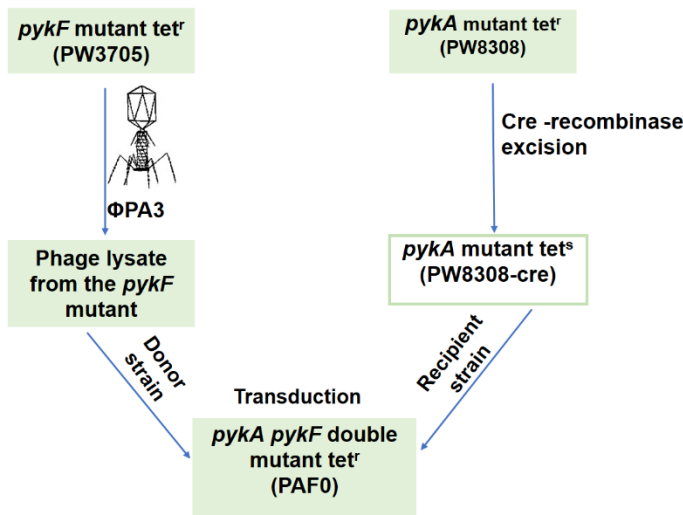
Figure 3.8: Construction of the PAF0 (*pykA*·*pykF*·) double mutant using phage transduction. The antibiotic marker was first removed from the tetracycline resistant PW8308 (*pykA* mutant) using Cre-recombinase excision producing a tetracycline sensitive PW8308-cre mutant. The latter (tetracycline sensitive) was mixed with phage lysate of ØPA3 containing the genetic material of PW3705 (*pykF* mutant, tetracycline resistant) to generate PAF0 (double mutant, tetracycline resistant) using generalized phage transduction.
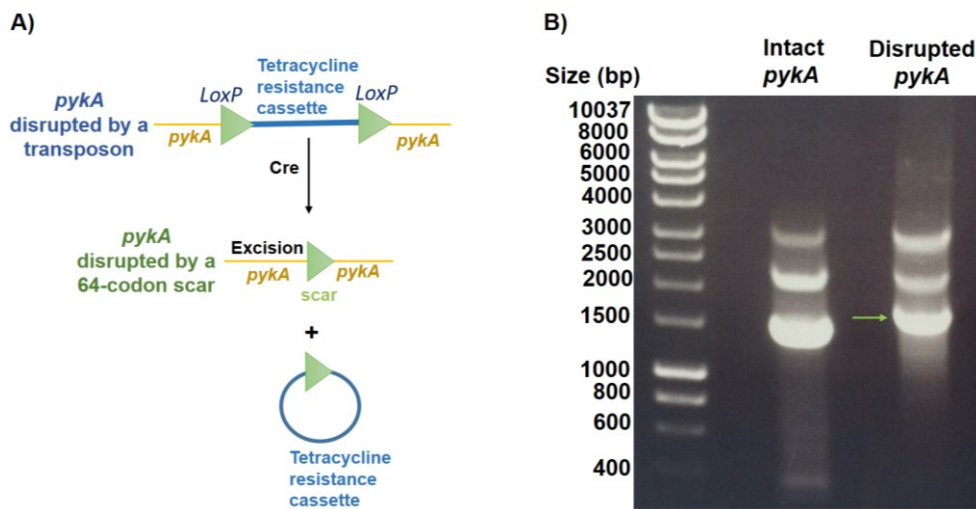
Figure 3.9: Excision of the transposon from the *pykA* mutant. A) Cartoon representation of the mechanism of excision of the antibiotic marker from the *pykA* mutant using Cre-recombinase following introduction of pFLP2-cre. B) Image of an agarose gel showing a DNA band of *pykA* disrupted with 64-codon scar after removal of the transposon (green arrow). The intact *pykA* gene band (1452 bp) is shown for comparison. The shown DNA bands were produced from PCR amplification of genomic DNA from the wild-type (generated intact *pykA* band) and PW8308-cre (generated disrupted *pykA* band), using rPykA R and rPykA F primers. Other bands (2000 bp and 3000 bp) were generated non-specifically.

3.4.2 Complementation of the *pykA* and *pykF* mutants

To confirm that observed phenotypes were truly caused by dysfunction of *pykA* and *pykF*, PW8308 (*pykA⁻ pykF⁺*), PW3705 (*pykA⁺ pykF⁻*) and PAF0 (*pykA⁻ pykF⁻*) were complemented using pUCP20 constructs. For complementation with *pykA*, the upstream region (500 bp) and the ORF of *pykA* were ligated into compatible sites of pUCP20 generating pUCP20-*pykA*. The plasmid was introduced into PW8308 and PAF0 to produce PW8308C and PAF1, respectively. For complementation with *pykF*, the region spanning 500 bp upstream of *PA1499* to the 3' end of *pykF* was ligated into compatible sites of pUCP20 producing pUCP20-*pykF*. The generated pUCP20-*pykF* was introduced into PW3705 and PAF0, generating PW3705C and PAF2, respectively.

3.4.3 Protein expression of the PykA was turned on in all tested carbon sources

To investigate if the transcription profiles of *pykA* and *pykF* correlate with their protein expression levels, Western blot analysis was performed using anti-PykA and anti-PykF antibodies. First, cell lysates from PAO1, PW8308, PW3705 and PAF0 were prepared from cells grown in minimal media with glucose, glycerol, acetate, succinate or ribose as sole carbon source, in aerobic conditions. The concentration of the total protein was measured using Bradford assay and normalized for each Western blot. Anti-PykA and anti-PykF primary antibodies were used for detection of PykA and PykF, respectively.

Consistent with the transcription results, a band of 52.3 kDa corresponding to PykA was clearly seen on the Western blots of PAO1 grown in all carbon sources. PykA expression was also seen in PW3705 (*pykA⁺ pykF⁻*) and was absent from PW8308 (*pykA⁻ pykF⁺*) and PAF0 (*pykA⁻ pykF⁻*) in all tested carbon sources (Figure 3.10). This was expected given that PW3705 encodes intact *pykA*, whereas PW8308 and PAF0 encode a disrupted *pykA* gene. Interestingly, the intensity of the PykA band was nearly doubled in the PW3705 compared with the PAO1 when cells grew in glucose and glycerol. Most likely, the elevated PykA expression was essential to compensate for the loss of the PykF in PW3705. Repeat Western blot analysis using cell lysates from the *pykA* complemented strains (PW8308C and PAF1) revealed that PykA expression was fully recovered (Figure 3.10).

Although PykA was expressed in measurable ranges, the expression of PykF (51.5 kDa) was undetectable. The Western blots from PAO1 and PW8308 (both encoding intact *pykF*) revealed no PykF band when blotted with anti-PykF antibodies. Moreover, no PykF expression was seen in any tested carbon sources. Western blot analysis of the *pykF* complemented strains (PW3705C and PAF2) revealed clear PykF bands against anti-PykF antibodies (Figure 3.10). The detectable PykF expression in the latter strains confirmed that the quality of the antibodies were in fact good. This also indicates that the basal levels of the PykF expression in PAO1 and P8308 were low, beyond the detection limit using Western blot analysis.
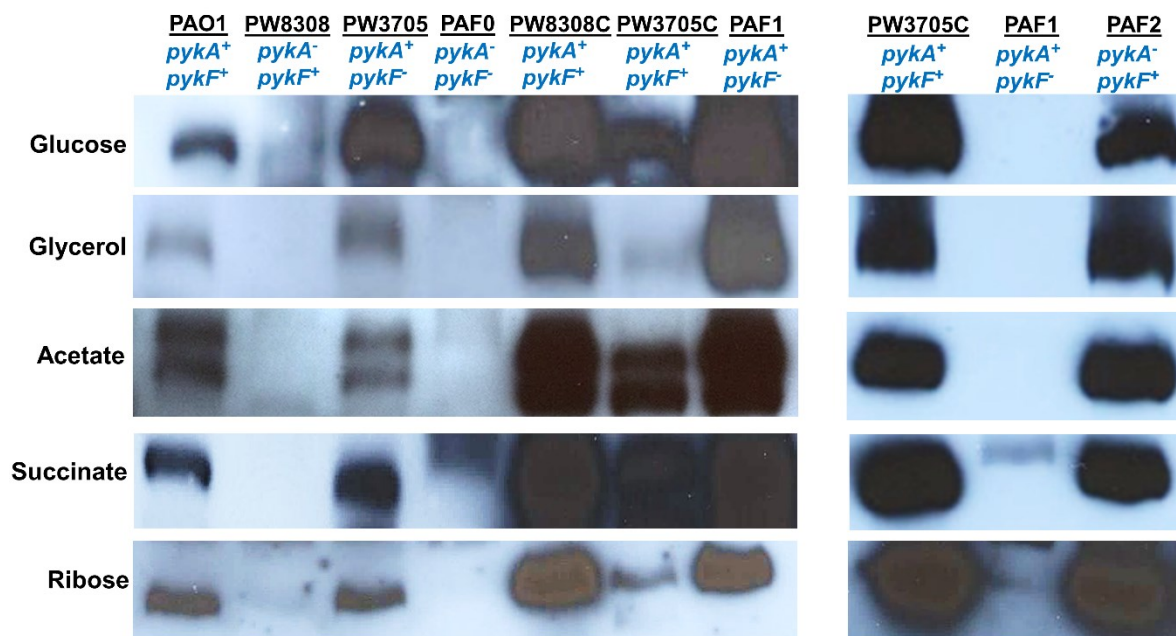
Figure 3.10: Western blot analysis using anti-PykA (left panel) and anti-PykF (right panel) antibodies. Cell lysates were collected from stationary phase cultures grown in minimal media with 20 mM glucose, 30 mM glycerol, 40 mM acetate, 20 mM succinate or 15mM ribose as sole carbon sources, aerobically at 37°C. Protein concentration was quantified using Bradford assay and normalized for each blot. The left panel shows lysates of the wild-type and the indicated mutants blotted using anti-PykA antibodies, whereas the right panel shows lysates of the indicated mutants complemented with *pykF* and blotted using anti-PykF antibodies.

3.5 Enzyme activity of PykA and PykF

3.5.1 LDH-coupled assay

The function of PK is to convert ADP and phospho*enol*pyruvate into ATP and pyruvate, respectively. Thereby, pyruvate biosynthesis is directly correlated with ATP production. In order to investigate the contribution of *pykA* and *pykF* to pyruvate biosynthesis, PK enzymatic activity was measured in bacterial cells using an LDH-coupled assay. The assay is an indirect measurement of PK activity which quantifies the consumption of NADH (needed for conversion of the produced pyruvate into lactate). The enzymatic activity of PK was measured in cell lysates from PAO1, PW8308, PW3705 and PAF0 (Table 3.3). Cell lysates were collected from bacteria grown to stationary phase in M9 minimal media with different carbon sources in aerobic conditions. The concentration of total protein was quantified and normalized before each experiment.

3.5.2 *pykA* contributes more to pyruvate biosynthesis than *pykF*

The LDH-coupled assay revealed that pyruvate biosynthesis was associated with the availability of *pykA* (Table 3.3). The wild-type and PW3705 (both encode an intact *pykA*) exhibited high PK activity in all carbon sources. The highest levels of activity were reached when cells grew on succinate, which is a preferred carbon source for *P. aeruginosa* (Magasanik, 1961). In contrast, the measured PK activity was lower in PW8308 and PAF0 (both are *pykA* mutants) in all carbon sources. These findings indicate that PK activity correlates primarily with expression of PykA in the cell.

Although the PK activity in PW8308 (*pykA⁻ pykF⁺*) was low in almost all carbon sources, there was moderate enzymatic activity in the lysates of cultures grown in ribose. This was unexpected because there was no detected PykF expression on Western blots of lysates of cultures grown in ribose. Thus, it is likely that growth in ribose activates PykF, present in the background of PW8308.

Progression of CF disease is associated with accumulation of thick mucus in the airways of CF patients, changing the aerobic environment of the lungs into microaerobic or anaerobic (Worlitzsch et al., 2002). To see if low oxygen levels had an effect on PK enzymes, I measured the PK activity in cell lysates of cultures grown in microaerobic

conditions with glucose (Figure 3.11). Again, the LDH-assay revealed that lysates from PAO1 and PW3705 (both have intact *pykA*) had substantial PK activity compared with lysates from PW8308 and PAF0 (both are *pykA* mutants). Given that the pattern of PK activity was similar in aerobic and low oxygen levels, it seems that in *P. aeruginosa*, the regulation of PK activity is independent on the oxygen condition.

Complementation of the *pykA* mutants (PW8308 and PAF0) by expression of *pykA* *in trans* fully restored PK activity. However, the enzymatic activity in the complemented strains (PW8308C and PAF1) was significantly higher than the basal PykA activity in the wild-type, which was unsurprising given the high copy number vector employed.

Table 3.3: PK activity in cells grown in different carbon sources. Bacteria were grown to stationary phase in M9 minimal media with 20 mM glucose, 30 mM glycerol, 40 mM acetate, 20 mM succinate or 15 mM ribose as sole carbon sources, aerobically at 37ºC. PK activity was measured using an LDH-coupled assay. The values represent samples from three biological replicates and the standard error is indicated.

Pyruvate kinase activity (µM pyruvate/min/mg)					
PAO1	**PW8308**	**PW3705**	**PAF0**	**PW8308C**	**PAF1**
pykA+	*pykA-*	*pykA+*	*pykA-*	*pykA+*	*pykA+*
pykF+	*pykF+*	*pykF-*	*pykF-*	*pykF+*	*pykF-*
Glucose 89 ± 6	7 ± 1	91 ± 5	2 ± 1	583 ± 38	510 ± 16
Glycerol 127 ± 12	7 ± 1	99 ± 9	3 ± 1	1078 ± 111	1406 ± 85
Acetate 108 ± 6	2 ± 2	107 ± 6	3 ± 2	1136 ± 123	526 ± 31
Succinate 170 ± 3	0	209 ± 5	0	1360 ± 10	1243 ± 41
Ribose 122 ± 12	36 ± 7	103 ± 16	9 ± 4	538 ± 28	770 ± 49
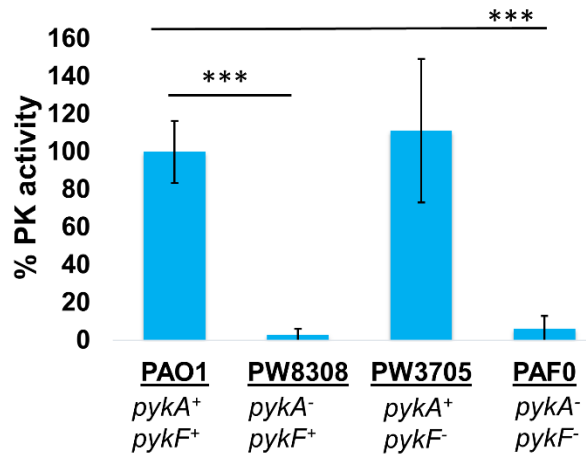
Figure 3.11: PK activity in cells grown in glucose in low oxygen levels. Bacteria were grown until stationary phase in M9 minimal media with 20 mM glucose in microaerobic conditions at 37°C, using an LDH-coupled assay. PK activity was measured in three biological replicates and error bars represent standard error. Statistical significance was performed using an unpaired t-test (*=p <0.05, **=p <0.01, ***=p <0.001).

3.6 Growth analysis of *pykA* and *pykF* mutants

To see if *pykA* and *pykF* were essential for growth, I compared the growth of PAO1 to the PK mutants (PW8308, PW3705, PAF0) in different carbon sources. Growth rates were measured in liquid minimal media supplemented with 20 mM glucose, 30 mM glycerol, 40 mM acetate or 20 mM succinate. Growth was also compared using M9 minimal agar supplemented with the same carbon sources. Growth in liquid cultures and agar was measured in aerobic conditions at 37°C.

3.6.1 Growth in glucose and glycerol

Growth in liquid media containing glucose and glycerol revealed that *pykA* contributes to growth of PAO1. Whereas, deletion of *pykA*, as in PW8308 and PAF0, caused a decline in the growth rate compared with the wild-type or PW3705 (figure 3.12). Moreover, PAF0 (*pykA⁻ pykF⁻*) was the most impaired for growth in glucose and glycerol. Interestingly, PW3705 (*pykA⁺ pykF⁻*) also showed slight impairment of growth in these carbon sources, indicating that *pykF* also seemed to have little effects on growth in glucose and glycerol. After 10 hr of growth in glucose, both PAO1 and PW3705 reached the same final OD_{600}, whereas PW8308 and PAF0 reached an endpoint OD_{600} that was

clearly lower. In glycerol, the mutants could not reach the same final OD_{600} of the wild-type, indicating that *pykA* and *pykF* combined seemed to be important for growth in glycerol. Growth on agar media was in agreement with the measured growth rates in liquid media. On glucose and glycerol minimal agar, PW8308 and PAF0 showed less growth compared with the wild-type, whereas the growth of PW3705 was comparative to the wild-type (figure 3.14).
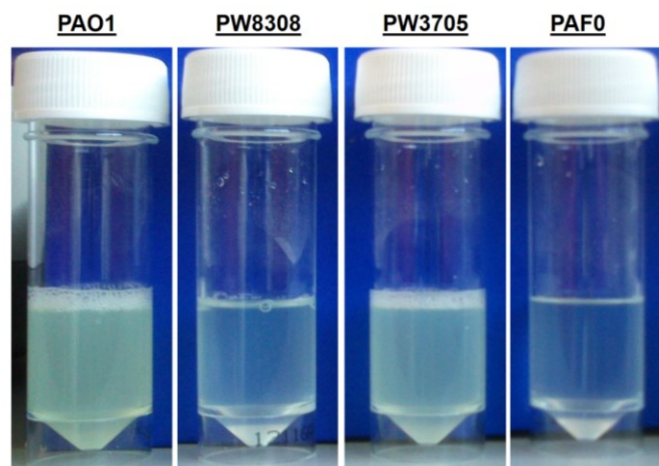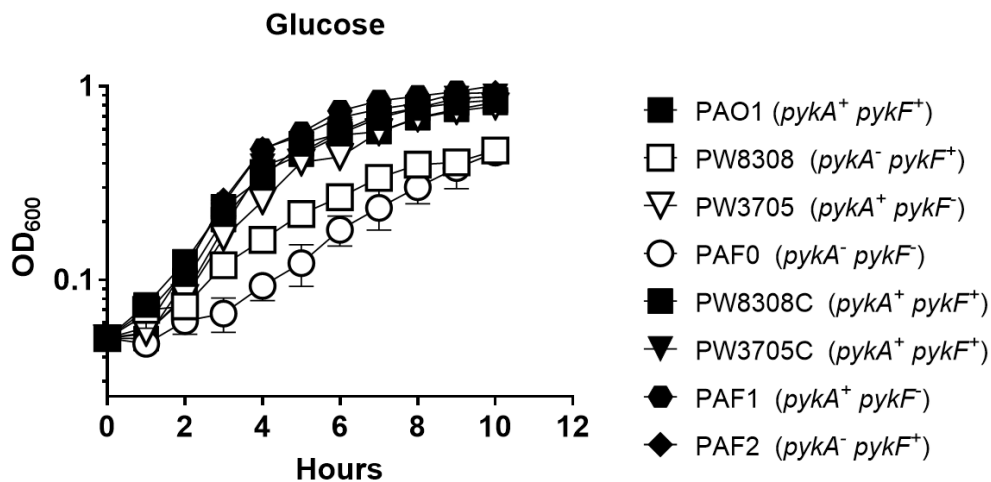
Figure 3.12: Impaired growth of the *pykA* defective mutants in glucose liquid media. Top figure: Growth curve in M9 minimal media with 20 mM glucose. Cells were grown in aerobic conditions at 37°C. Data represent the mean of three biological replicates ± standard error. Bottom figure: Image of bacterial cultures collected at the end of the growth curve (after 10 hr). The photograph represents a subset of three biological replicates.

Compared with glucose, all cells grew much slower in glycerol liquid media with a prolonged lag phase at the beginning of the growth rate (figure 3.13). On solid media, the lag phase extended to almost 24 hr as none of the cells grew, so the agar plates were left until 48 hr before growth was checked. The observed lag phase during growth of cells in glycerol was mostly due to the expression of GlpR regulator which represses the *glp* gene operon responsible for glycerol metabolism. The negative effects of GlpR on the glp genes are alleviated by the increase of the G3P pool in the cell (Schweizer and Po, 1996; Nikel et al., 2015b).
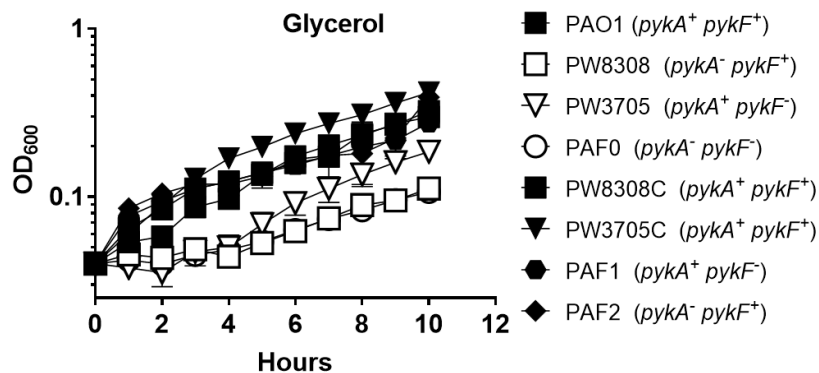
Figure 3.13: Impaired growth of *pykA* defective mutants in glycerol liquid media. Bacterial cells were grown in M9 minimal media with 30 mM glycerol in aerobic conditions at 37°C. Data represent the mean of three biological replicates ± standard error.
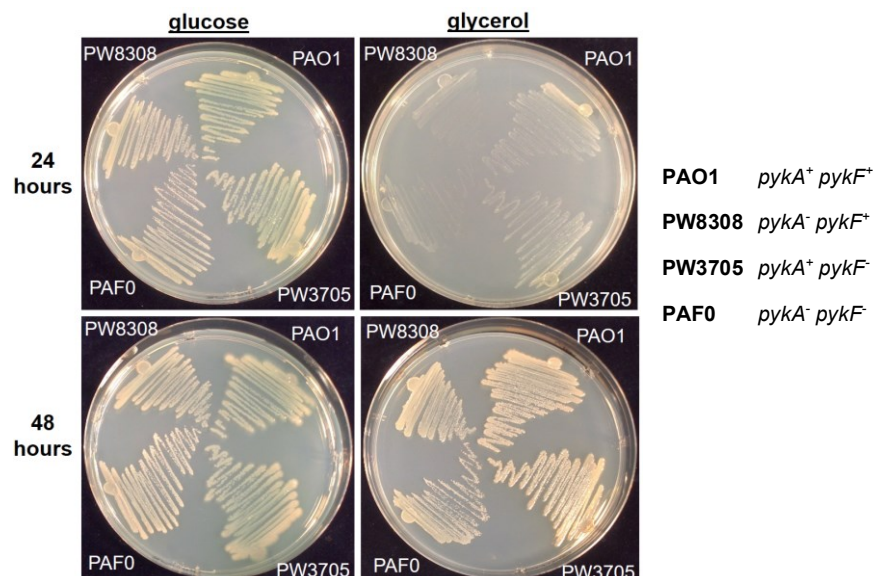
Figure 3.14: Impaired growth of *pykA* defective mutants on minimal agar. The cells were grown on M9 minimal agar with 20 mM glucose or 30 mM glycerol in aerobic conditions at 37°C.

3.6.2 Growth in acetate and succinate

Growth of PAO1 and the PK mutants was also compared in minimal media containing acetate or succinate. In these media, PW8308 and PW3705 grew with comparable rates, although slightly slower than the growth of the wild-type (Figure 3.15). PAF0 again showed the slowest growth among all cells in these carbon sources. After 8-10 hr of growth in acetate or succinate, all mutants reached the same final OD_{600} that was slightly below the final OD_{600} of the wild-type. The growth rates of the PK mutants in acetate and succinate indicated that *pykA* and *pykF* have little effects on growth with carbon sources that comes after the PK step in the EDP. These carbon sources will most likely feed directly into the TCA cycle, bypassing the PK reaction. Complementation of the *pykA* and *pykF* mutants restored the slightly impaired growth rates to wild-type levels.
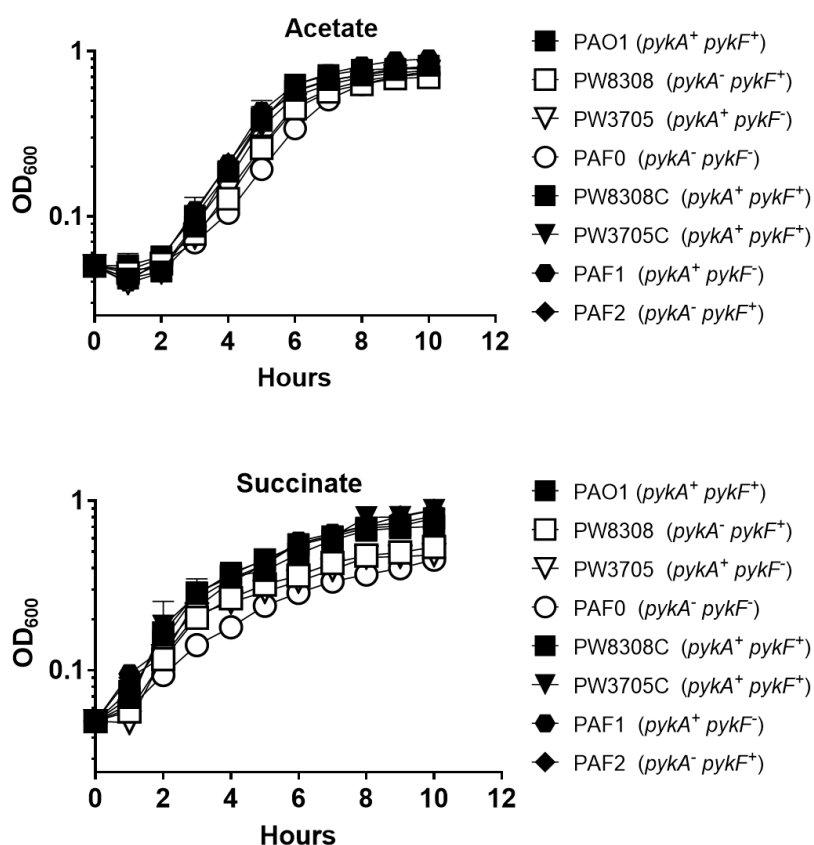
Figure 3.15: Growth of PK mutants in acetate and succinate. Cells were grown in M9 minimal media with 40 mM acetate or 20 mM succinate aerobically at 37°C. Data represent the mean of three biological replicates ± standard error.

3.7 Phenotypic analysis of the *pykA* and *pykF* mutants

P. aeruginosa contains a plethora of virulence factors which enable the pathogen to cause tissue destruction, evade antimicrobial treatment and promote its own survival. In some bacteria, PK was found to have an impact on many of these pathogenic traits. I therefore investigated if *pykA* and *pykF* were associated with virulence phenotypes in *P. aeruginosa*.

3.7.1 Secretion of exoenzymes

P. aeruginosa secretes proteases which facilitate invasion of the host tissue (Sakata et al., 1996). To test for secretion of proteases, the wild-type and the PK mutants (PW8308, PW3705 and PAF0) were spotted onto agar media containing gelatin or casein as substrates for the proteolytic activity. Caseinase and gelatinase activity was detected as a hydrolysed clear zone around the bacterial colony, indicating degradation of the substrates. The wild-type and the mutants were able to secrete caseinase and gelatinase efficiently and to form clear zones of proteolysis surrounding the growing colonies (Figure 3.16). Therefore, the production of proteases seemed to be independent of *pykA* and *pykF*.

3.7.2 Production of rhamnolipids

Rhamnolipids are glycolipids produced intracellularly and secreted to the exterior of *P. aeruginosa*. They play an important role in maintenance of biofilm architecture, inhibition of phagocytosis and in promoting swarming motility (Davey et al., 2003; McClure and Schiller, 1996; Caiazza et al., 2005). To test for rhamnolipid production, PW8308, PW3705 and PAF0 were spotted onto PPGAS agar. Formation of clear blue halos indicated positive rhamnolipid production (Figure 3.17). Although the spreading of colonies from PW8308 (*pykA⁻ pykF⁺*) and PAF0 (*pykA⁻ pykF⁻*) seemed less, both were still able to produce clear blue halos comparable with the wild-type (*pykA⁺ pykF⁺*) and PW3705 (*pykA⁺ pykF⁻*). Apparently, the production of rhamnolipids was not influenced by mutation of PK genes.
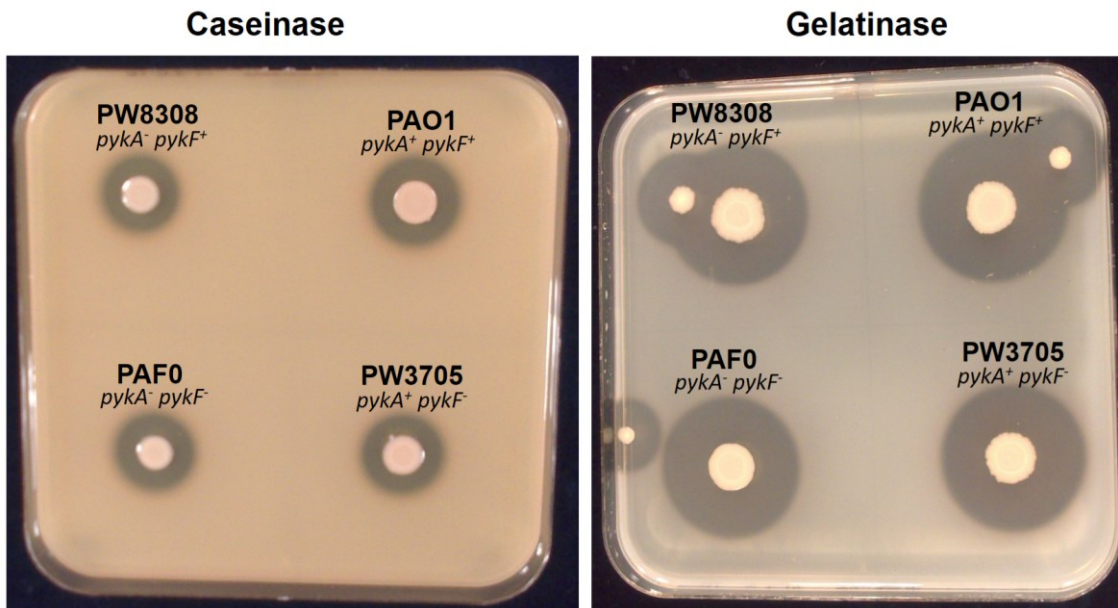
Figure 3.16: Production of caseinase and gelatinase. Bacteria were spotted onto plates containing skim milk or gelatin. Secretion of proteolytic enzymes was visualized by a clear halo formation around the growing colonies. The production of the exoenzymes was seen in the wild-type and the PK mutants.
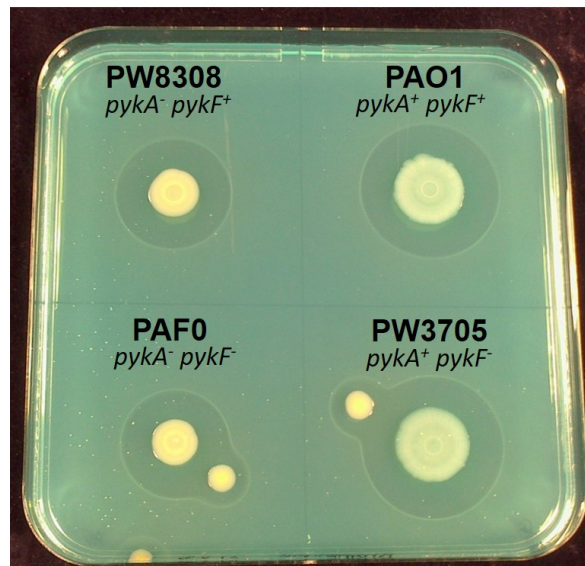
Figure 3.17: Production of rhamnolipids. Clear halos surrounding the colonies indicate production of the rhamnolipids. The wild-type and the PK mutants were both capable of producing rhamnolipids.

3.7.3 Biofilm formation

It is the aggregation of bacterial cells on a biotic or non-biotic surface (Abdallah et al., 2014). *P. aeruginosa* has been speculated to grow in biofilms in the cystic fibrosis lungs (Høiby et al., 2010). By forming biofilms, *P. aeruginosa* can potentially evade the host immune response and become more resistant to antimicrobial agents (Bielen et al., 2017; Drenkard, 2003). To see if the PK genes contribute to biofilm formation, I screened PW8308, PW3705 and PAF0 for their ability to form biofilms.

The PK mutants were able to form biofilms to varying degrees in LB media (Figure 3.18). Unexpectedly, the biofilm formed by PW8308 and PAF0 that were deficient in *pykA*, was denser than that formed by wild-type and PW3705. Moreover, the same pattern was seen following growth in minimal media with glucose, where PW8308 and PAF0 again exhibited greater biofilm formation than the wild-type and PW3705 (Figure 3.18). The increased biofilm formation of PW8308 and PAF0 may be an indication that these cells were experiencing some stress (which could be due to loss of *pykA*). Future work should investigate this further.
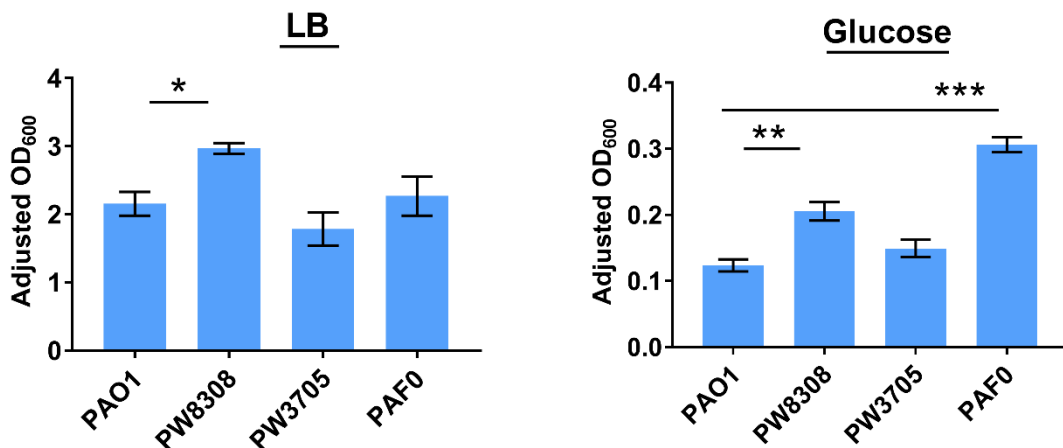
Figure 3.18: Biofilm formation by PK mutants. Biofilms were grown in 96-well plates for 24 hr at 37°C. Biofilm formation was measured by the intensity of the crystal violet staining of the adherent cells on the sides of the wells. The data represents the mean of three biological replicates (Adjusted OD_{600} = OD_{600} of sample-OD_{600} of blank) and error bars represent standard error. Statistical significance was performed using an unpaired *t*-test (*=p <0.05, **=p <0.01, ***=p <0.001).

3.7.4 Motility assays

P. aeruginosa has a single polar flagellum which enables the bacteria to perform swimming and swarming activities. From clinical perspective, severe and acute infections of *P. aeruginosa* are primarily associated with motile strains (Wolfgang et al., 2004). To test if *pykA* and *pykF* have an effect on motility, overnight cultures of PW8308, PW3705 and PAF0 were spotted onto swim and swarm agar plates. Swimming and swarming activities were detected by formation of concentric halos and branch-spreading patterns on the semi-solid agar, respectively. Results of the motility assays can be seen in Figure 3.19.

Motility assays revealed that PW8308 and PW3705 were able to swim and swarm similar to the wild-type after 15 hr of incubation (Figure 3.19). However, PAF0, which was defective in both *pykA* and *pykF*, was unable to swim even after prolonged incubation for 48 hr. In addition, the double mutant strain also had decreased swarming motility. This decreased motility of PAF0 indicated either that the combined effects of *pykA* and *pykF* were necessary for motility, or that there might be unrelated secondary phenotypes. Consistent with this possibility motility assays using PAF1 (expressing *pykA in trans*) and PAF2 (expressing *pykF in trans*) failed to restore motility on the swim or swarm agar plates.

PAO1 $pykA^+ pykF^+$

PW8308 $pykA^- pykF^+$

PW3705 $pykA^+ pykF^-$

PAF0 $pykA^- pykF^-$
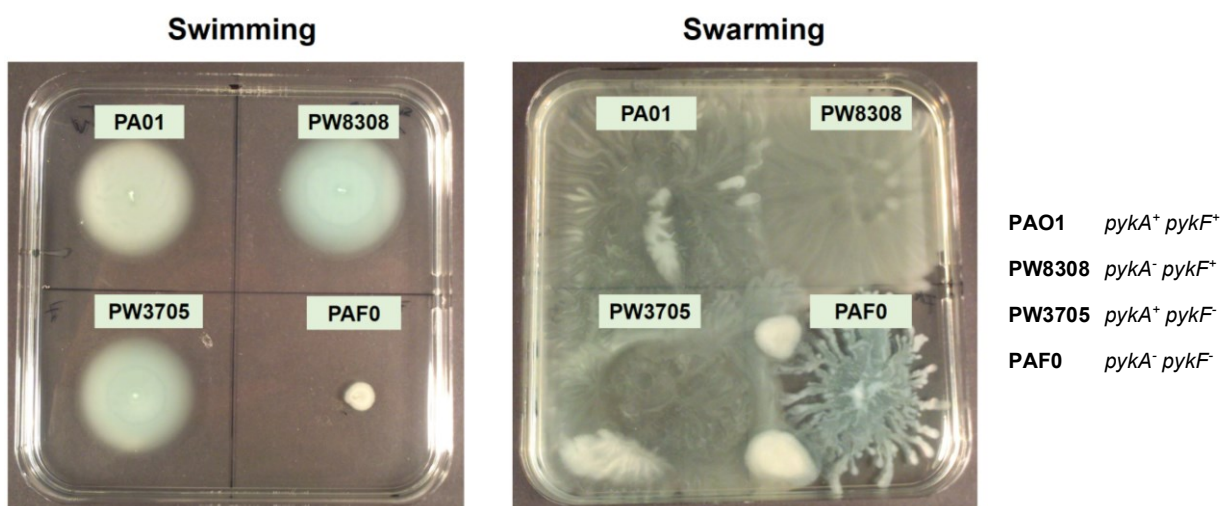
Figure 3.19: Motility of the PK mutants. Overnight cultures of PK mutants were spotted onto swarm and swim agar, where motility was visualized as concentric halos indicative of swimming activity or branch-spreading patterns indicative of swarming activity.

3.8 Discussion

3.8.1 *pykA* is the dominant PK in *P. aeruginosa*

P. aeruginosa encodes *pykA* and *pykF* isozymes, similar to a group of Enterobacteriaceae including *E. coli*, *S. enterica* serovar Typhimurium and *Y. pestis*. Prior work done on *pykA* and *pykF* from the latter species revealed that *pykF* is the dominant enzyme and that the PykF activity has been linked with pyruvate biosynthesis, cell metabolism and virulence, whereas *pykA* was dispensable in these species (Ponce et al., 1995; Muñoz and Ponce, 2003; Garcia-Olalla and Garrido-Pertierra, 1987; Bücker et al., 2014). Nonetheless, findings from this chapter revealed that *pykA* is certainly the dominant PK in *P. aeruginosa*, whereas *pykF* plays a minor role. The LDH-coupled assay demonstrated that *pykA* was responsible for more than 90% of the PK enzymatic activity in lysates of cultures grown in all carbon sources and that inactivation of *pykA* caused a significant decline in the enzymatic activity. Moreover, *pykA* was essential for metabolism of carbon sources that feed into the EDP, so growth in glucose and glycerol was affected when *pykA* was inactivated. Whereas, *pykA* seemed to have little impact on metabolism of carbon sources that feed into the EDP but after the PK step (acetate and succinate). This is apparently why growth in acetate and succinate was not affected by inactivation of *pykA* as these carbon sources can feed directly into the TCA cycle, bypassing the PK reaction. In *P. aeruginosa*, *pykF* seemed to contribute very little mainly to partially rescue the growth of cells, when *pykA* was non-functional. Thus, finding a metabolic target such as *pykA* with direct and major impacts on metabolism and cell growth, is immensely important especially when there is an ongoing global call aiming to identify new drugs to treat *P. aeruginosa* infections.

3.8.2 Up-regulated transcription of *pykA*

The main reason for the dominance of *pykA* over *pykF* in *P. aeruginosa* is related to its great transcription and protein expression. Measurement of β-galactosidase activity associated with a *pykA* transcriptional reporter gene fusion revealed that the promoter of *pykA* was persistently active in all tested carbon sources, oxygen levels and temperatures. On the other hand, the promoter of *PA1499* which is predicted to also drive the transcription of *pykF*, was low in all tested conditions. The Western blots were in

agreement with the transcriptional profiles and indicated that PykA is constantly expressed, whereas PykF expression is negligible.

The up-regulated transcription of *pykA* in *P. aeruginosa* was considered unusual as compared with other bacteria that encode *pykA* and *pykF* enzymes, where the transcription of *pykA* in the latter species is usually lower than *pykF* (Al-Zaid Siddiquee et al., 2004). The unusual transcription of *pykA* in *P. aeruginosa* could be related to its genomic location in this organism compared with other species. *pykA* from the Enterobacteriaceae is present downstream of HexR/YebK which probably alters *pykA* transcription in these species (Figure 3.20). The HexR/YebK is a member of the RpiR family and is characterized in *P. putida* as a negative transcriptional regulator for glucose metabolism. Analysis of taxonomic distribution of HexR-regulated genes in Proteobacteria revealed that *pykA* is regulated by HexR in at least 30 species from six different lineages (Leyn et al., 2011). Gel shift assays showed that HexR binds to genes of glucose metabolism causing significant repression of their activity (Daddaoua et al., 2009). In some organisms, inactivation of HexR was also found to cause global changes to glucose metabolism and most importantly up-regulation of *pykA* transcription (Antunes et al., 2016). Therefore, it is likely that HexR, upstream gene of *pykA* in Enterobacteriaceae, has a negative impact on the transcription of *pykA* in these species.

PA3184 is the HexR homologue in *P. aeruginosa* that regulates transcription of metabolic enzymes involved in glucose degradation (Udaondo et al., 2018). In *P. fluorescens* and *P. putida*, HexR primarily targets the promoters of glucose 6-phosphate dehydrogenase (*zwf*), 6-phosphogluconate dehydratase (*edd*) and glyceraldehyde 3-phoshpate dehydrogenase (*gap*) (Campilongo et al., 2017; Daddaoua et al., 2009). However, *pykA* has not been identified as one of the Hex-regulon genes in *Pseudomonas* species (Udaondo et al., 2018; Kim et al., 2008). Moreover, the negative effects of HexR on its target genes are alleviated by binding of HexR to 2-*keto*-3-deoxy-6-phosphogluconate (KDPG), which is a key metabolite of the EDP (Kim et al., 2009). Taken together, the transcription of *pykA* in *P. aeruginosa* seems to be unaffected by HexR, whereas the transcription of *pykA* homologues in other Gram-negative bacteria is probably suppressed by HexR.
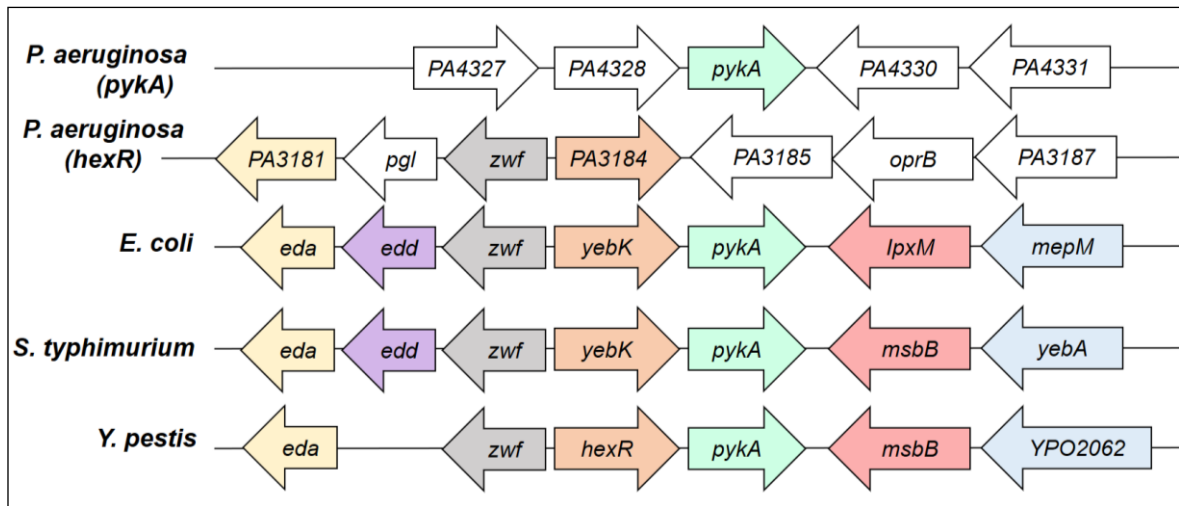
Figure 3.20: The genomic location of *pykA* in selected bacterial species. The genomic position of *pykA* is shown in *P. aeruginosa* (PAO1 NC-002516), *E. coli* (K-12 MG1655), *S. enterica* Serovar Typhimurium (LT2 NC_003197) and *Y. pestis* (CO92 NC-003143) on the basis that they encode *pykA* and *pykF* genes. The genetic cluster of HexR analogue (PA3184) in *P. aeruginosa* is included for clarity. Colours refer to similar genes and sizes of genes are not represented.

3.8.3   Transcription and function of PykF

Whilst *pykA* was clearly the dominant PK in all tested conditions, the role of *pykF* was unclear. In this study, there was no condition identified that could have triggered the transcription of *pykF*, except when the gene was overexpressed using a high copy plasmid such as pUCP20. Complementation using pUCP20-*pykF* was able to boost the dormant transcription and expression of *pykF* in *P. aeruginosa*. Moreover, the gene expression of *pykF* was most likely driven by the activity of the *lacZ* promoter in pUCP20, and not by the promoter of *PA1499* (predicted to be operonic with *pykF*).

The *pykF* is found among an organized genetic cluster on the *P. aeruginosa* chromosome. The gene is present downstream and predicted to be operonic with *PA1499* as shown in Figure 3.1B. Moreover, the two genes are part of an organized gene cluster where all of the encoded genes are annotated as hypothetical, except for *pykF*. The possible function of this operon, including *pykF*, is to catalyse a series of reactions involved in glyoxylate metabolism. This is in agreement with a recent study involving the equivalent *pykF* genetic cluster in *P. putida*, where the corresponding genes encode

enzymes that catabolize ethylene glycol (a precursor of glyoxylate) (Franden et al., 2018). Likewise, *pykF* from *P. aeruginosa* may be important for metabolism of ethylene glycol.

The second probable function of *pykF* in *P. aeruginosa* could be correlated with ribose metabolism. This is because the PK activity of PW8308 (*pykA⁻ pykF⁺*) was higher when cells grew in ribose as compared with negligible PK activity when cells grew in other carbon sources. This was particularly interesting because there was no detectable PykF on the Western blots from cells grown in ribose. It is likely that although PykF expression was undetectable or little in ribose, the activity of PykF was enhanced by ribose or ribose-related metabolites. To investigate this further, the enzymatic activity of purified PykF has to be measured in the presence of ribose and ribose-derivatives.

3.8.4   Motif analysis of PykA and PykF

Findings from the evolutionary and motif analyses demonstrated that the PykA and PykF from *P. aeruginosa* belong to different PK subclasses and that they were correctly annotated. Furthermore, motif analysis revealed that each isozyme is predicted to have a unique phosphorylation site that can be used for identification. A TKP site was predicted for identification of PykA group members, whereas a CAG-DPKP site was predicted for identification of PykF group members.

In fact, this raised the question of whether bacterial PK can actually undergo phosphorylation. In prokaryotes, there is some evidence that enzymes can be phosphorylated including pyruvate kinases. For example in *S. aureus*, functional analysis revealed that the PK is phosphorylated by PknB protein kinase leading to a drop in the PK activity (Vasu et al., 2015). Likewise, PK from *M. tuberculosis* is also a substrate of a PknJ protein kinase which can also phosphorylate key residues of PK in this organism (Arora et al., 2010). Motif analysis of PK from *S. aureus* dictates that the enzyme has a CAG-DPKP phosphorylation site (Vasu et al., 2015) similar to PykF group members, whereas PK of *M. tuberculosis* alternatively encodes a TKP site similar to PykA group members. Thus, it is likely that PykA and PykF from *P. aeruginosa* and the Enterobacteriaceae may also be subjected to phosphorylation that possibly influences their activity.

3.9   Conclusion

In Gram-negative bacteria which have PykA and PykF enzymes, PykF is generally the dominant isozyme and PykA has little contribution. The results presented in this chapter reveal that *P. aeruginosa*, unlike other previously studied species, has a dominant PykA enzyme and a PykF of unclear function. My findings have shown that the gene transcription and expression of *pykA* were turned on in all tested conditions, whereas *pykF* transcription was persistently lower. The work here revealed that PykA was essential for pyruvate kinase activity and growth in glucose and glycerol. These phenotypes were produced from a true PykA enzyme that is evolutionary related to PykA from other bacteria. The successful complementation with *pykA* highlights the importance of this gene for metabolism and cell growth.

Chapter 4

4 Biochemical characterization of PykA and PykF

4.1 Introduction

P. aeruginosa has two PK isoforms; *pykA* and *pykF* similar to few bacteria. The genetic characterization in chapter 3 revealed that unlike other bacteria, *pykA* is the dominant enzyme in *P. aeruginosa*. Whereas in other species, *pykF* is the dominant PK. Given that *P. aeruginosa* is an exclusive EDP-dependent organism, it is likely that PykA and PykF from *P. aeruginosa* are regulated differently than PK isoforms in other species.

In this chapter, I overexpress PykA and PykF from *P. aeruginosa* using *E. coli* as a host, and use the purified proteins to characterize the biochemical properties of these enzymes. I used an LDH-coupled assay for determination of the kinetic parameters for each enzyme and I was able to find a set of metabolic regulators. Moreover, in collaboration with the Department of Pharmacology (University of Cambridge), I was able to identify a ligand that can inhibit PykA activity and alter the cell growth in glucose.

4.2 Overexpression and purification of PykA and PykF

The genes encoding PykA and PykF from *P. aeruginosa* were cloned using an IPTG-inducible pET19m vector to generate pET19m-*pykA* and pET19m-*pykF*, respectively. The pET-19m constructs were then introduced into *E. coli* BL21 (DE3) to generate BL21-PykA and BL21-PykF, which were used for the overexpression of PykA and PykF, respectively. Protein expression was induced by the addition of 1 mM IPTG to the *E. coli* cultures at mid-exponential phase and the bacterial cultures were then incubated overnight at 20°C for large-scale protein production.

Protein lysates of PykA and PykF (with TEV-cleavable His-tags) were extracted from BL21 cell pellets and loaded onto a Ni-NTA column. After elution of the proteins from the Ni-NTA column, His-tags were removed using TEV protease. Therefore, each protein was mixed with His-tagged TEV protease and the mixture was loaded in a dialysis bag. After dialysis and collection of the protein-protease mixture into a falcon tube, Ni-

NTA beads were added to the mixture in order to capture the protease and uncleaved PK, while leaving the untagged PykA or PykF free in solution. The tube containing the mixture was incubated and centrifuged, before PykA or PykF were collected from the supernatant fraction.

The purity of the enzymes was confirmed by SDS-PAGE (Figure 4.1). The total yield of PykA (6.3 mg/L of culture) was less than the total yield of PykF (29 mg/L of culture). Protein aliquots were stored at -80°C and used as needed for PykA and PykF biochemical characterization (this chapter), x-ray crystallography (chapter 5), AUC (chapter 5) and production of antibodies (chapter 3).
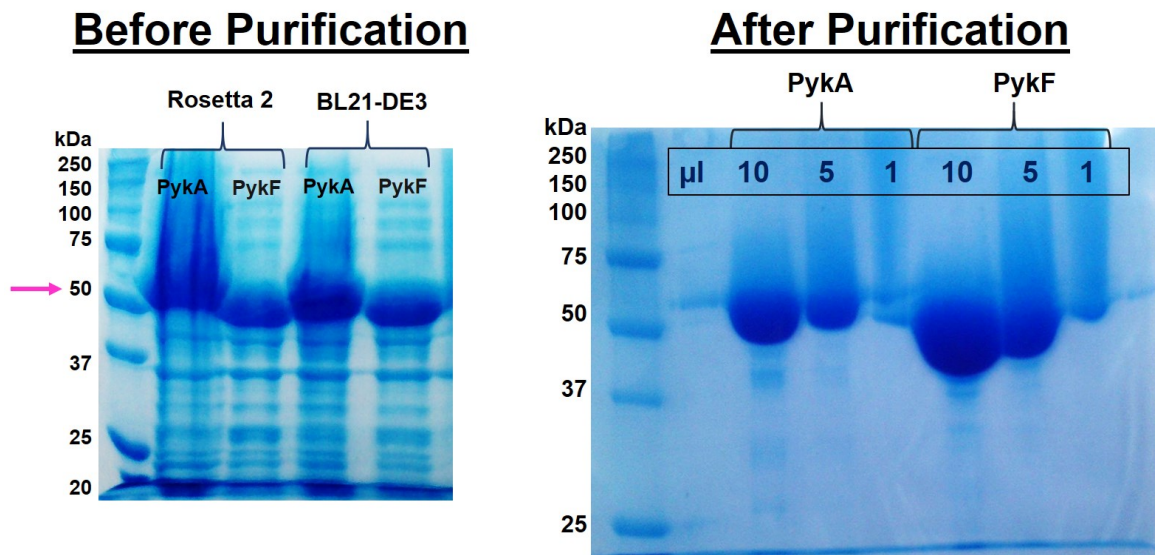
Figure 4.1: SDS-PAGE of PykA (52.3 kDa) and PykF (51.5 kDa). The left figure shows an SDS-PAGE gel of crude cell lysates from two *E. coli* strains (Rosetta 2 and BL21-DE3), after overexpression of PykA and PykF (pink arrow) using pET19m constructs. The right figure shows an SDS-PAGE gel of PykA and PykF after Ni-NTA purification and His-tag removal. Samples of PykA (3 mg/L) and PykF (5 mg/L) were loaded at different volumes on the SDS-PAGE gel as indicated. Both gels were prepared at 12% acrylamide concentration and stained using Coomassie stain.

4.3   Kinetic properties of PykA and PykF

The kinetic properties of PykA and PykF were determined using an LDH-coupled assay. In the assay, PK catalyses the de-phosphorylation of PEP into pyruvate, and LDH converts the pyruvate into lactate along with consumption of NADH. The decline of the NADH at 340 nm indicates PykA or PykF activity. For calculation of $S_{0.5}$ (concentration of PEP required to achieve a half-maximum enzyme activity) with respect to [PEP], PEP was used at variable concentrations (0 - 6 mM) and ADP at saturation (2 mM). Whereas for calculation of kinetic parameters (K_M, V_{max}, k_{cat}, k_{cat}/K_M)) with respect to [ADP], ADP was used at variable concentrations (0 – 2.5 mM) and PEP at saturation (5 mM). PK enzymes are tetramers with four active sites per unit. However, they mostly show steady-state kinetics (Giles et al., 1976; Giles and Poat, 1980), so the four active sites can be treated as one active site. Using this assumption, the enzymatic turnover number (k_{cat}) was calculated by dividing the maximal velocity for each enzyme (V_{max}) by the molar concentration of the enzyme in the assay.

Figure 4.2 shows that PykA and PykF from *P. aeruginosa* responded to titration of PEP and ADP with similar kinetics compared with other PK. With respect to PEP titration, PykA and PykF showed sigmoidal kinetics with a Hill coefficient (*h*) of 2.14 and 2.8, respectively. In enzymes with multiple subunits like PK, the sigmoidal response (*h*>1) to PEP titration is common and this sigmoidal behaviour reflects the positive cooperativity of the enzymes to the substrate so that binding of one substrate molecule to the enzyme improves the binding of the next molecule. With respect to ADP titration, both enzymes responded with hyperbolic kinetics, which is typical for PK.

Kinetic parameters were then calculated from the PEP and ADP titration curves using the sigmoidal allosteric and Michaelis-Menten models, respectively. Table 4.1 shows the calculated kinetic parameters of PykA and PykF. The enzymatic turnover number (k_{cat}) of PykA (k_{cat}^{PEP} = 393 S^{-1}, k_{cat}^{ADP} = 356 S^{-1}) and PykF (k_{cat}= 378 S^{-1} for PEP and ADP) was almost the same given that the two enzymes have almost similar maximal activity (V_{max}) and were used at equal molar concentrations in each assay (4-5 nM). Despite this, PykA showed half the $S_{0.5}$ and K_M values with respect to PEP and ADP titration, respectively compared with PykF. The $S_{0.5}^{PEP}$ and the K_M^{ADP} of PykA were 0.67

mM and 0.07 mM, respectively, whereas PykF had an $S_{0.5}^{PEP}$ of 1.03 mM and the K_M^{ADP} of 0.11 mM. Therefore, the apparent catalytic efficiency ($k_{cat}/S_{0.5}$ or k_{cat}/K_M) which is dependent on the $S_{0.5}$ and the K_M values was higher in PykA.
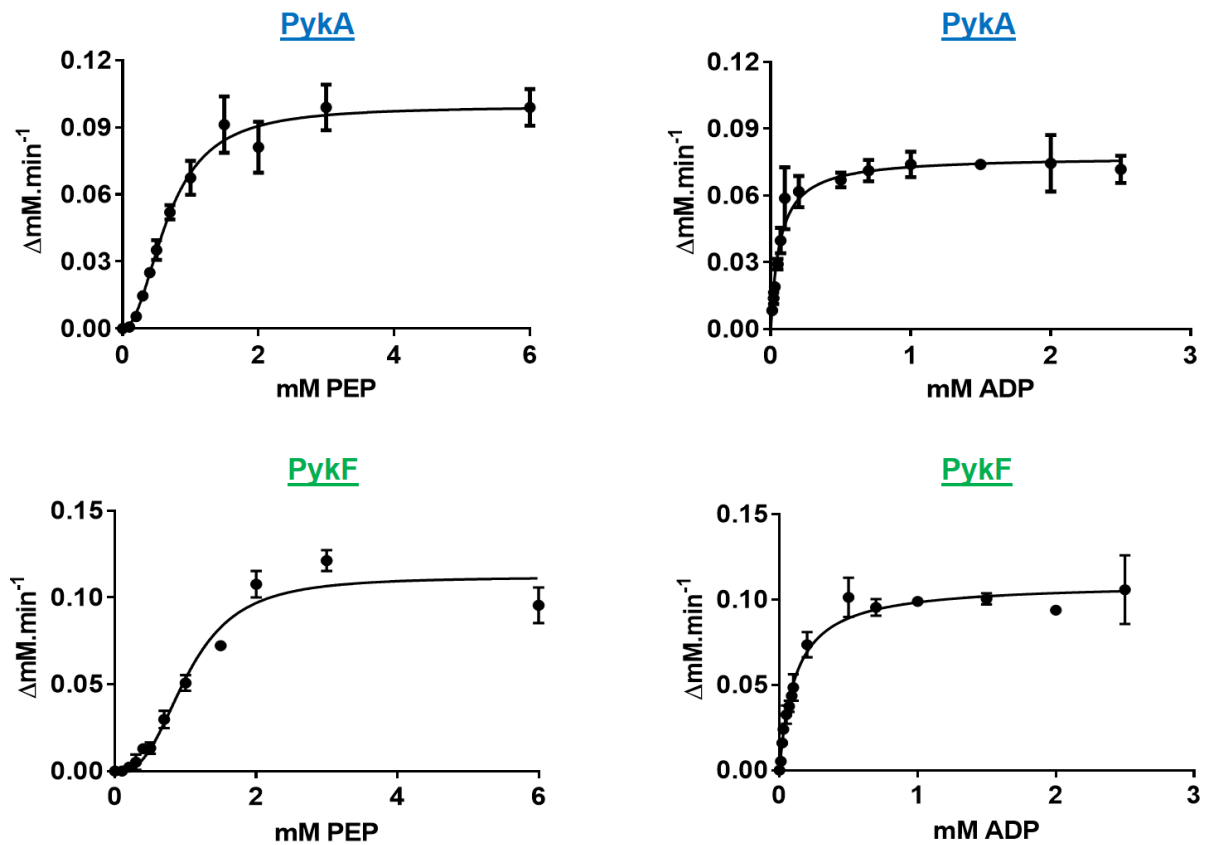
Figure 4.2: Kinetic response curves of PykA and PykF to titration of PEP and ADP. The PEP kinetics were measured at variable PEP concentrations and 2 mM ADP, whereas ADP kinetics were measured at variable ADP concentrations and 5 mM PEP. The enzymatic activity was measured using an LDH-coupled assay at 37°C and each reaction was initiated after the addition of 0.2 μg PykA or 0.25 μg PykF. Graphs were generated using GraphPad Prism 7 (n=3, standard errors are shown).

Table 4.1: Kinetic properties of PykA and PykF. The PEP kinetics were measured at variable PEP concentrations and 2 mM ADP, whereas ADP kinetics were measured at variable ADP concentrations and 5 mM PEP. The enzymatic activity was measured using an LDH-coupled assay at 37°C and each reaction was initiated after the addition of 0.2 µg PykA or 0.25 µg PykF. The kinetic parameters were calculated using GraphPad Prism 7 (n=3, ± standard error).

PEP titration	PykA	PykF
$S_{0.5}$ (mM)	0.67 ± 0.03	1.03 ± 0.006
Hill coeff (h)	2.14 ± 0.2	2.8 ±0.3
V_{max} (ΔmM.min^{-1})	0.09 ± 0.003	0.11 ± 0.004
k_{cat} (s^{-1})	392.6	378
$k_{cat}/S_{0.5}$ (s^{-1}.mM^{-1})	585.9	366.9
ADP titration	**PykA**	**PykF**
K_M (mM)	0.07 ± 0.008	0.11 ± 0.01
V_{max} (ΔmM.min^{-1})	0.08 ± 0.002	0.11 ± 0.02
k_{cat} (s^{-1})	335.9	378
k_{cat}/K_M (s^{-1}.mM^{-1})	5167.6	3436.4

4.4 Metabolic regulation of PykA

P. aeruginosa lacks the key enzymes of the EMPP and the oxidative-PPP, so it is mainly dependent on the EDP for metabolism (Lessie and Phibbs, 1984). Moreover, the EDP in *Pseudomonas* species operates in a special cyclic mode in which metabolites of the EDP can be redirected from the linear EDP pathway and feed into the reversal of the EMPP and the non-oxidative PPP (Conway, 1992). Using this knowledge, I tested PykA activity against a library of intermediates from the EDP, EMPP, PPP and TCA cycle. First, I screened the effect of these metabolites on PykA at 2 mM PEP (high [PEP]) in order to identify potential metabolic inhibitors and then I screened their effects on PykA at 0.3 mM PEP (low [PEP]) to identify potential activators. When a positive "hit" was identified, the kinetic parameters of PykA was re-measured in the presence of this metabolite.

4.4.1 Screening of PykA regulators

Figure 4.3 shows the effect of 1 mM metabolites on PykA activity at high PEP concentrations. No inhibitors were identified, however, PykA activity was increased by some metabolites including ribulose 5-phosphate (RL5P), xylulose 5-phosphate (X5P), fructose 6-phosphate (F6P), ribose 5-phosphate (R5P), and glyceraldehyde 3-phosphate (G3P). In fact, the PykA activity was great when F6P, R5P, and X5P were added at 1 mM concentration as these metabolites seemed to have induced strong PykA activation. Therefore, I added the F6P, R5P and X5P at 0.2 mM, 0.15 mM and 0.5 mM, respectively in all experiments as indicated.

The screen of metabolites at low PEP concentration confirmed that the above candidates were indeed activators of PykA (Figure 4.4). The greatest PykA activation was achieved with F6P and X5P. At low PEP concentration, glucose 6-phosphate (G6P) and 2-*keto*-3-deoxy-6-phosphogluconate (KDPG) also seemed to increase PykA activity, although with lower potency compared with the above metabolites. Figure 4.4 also shows that guanosine triphosphate (GTP) and adenine triphosphate (ATP) seem to decrease the PykA activity. On the other hand, there is no effect of any TCA cycle metabolites on PykA activity either on the high or the low PEP screenings.
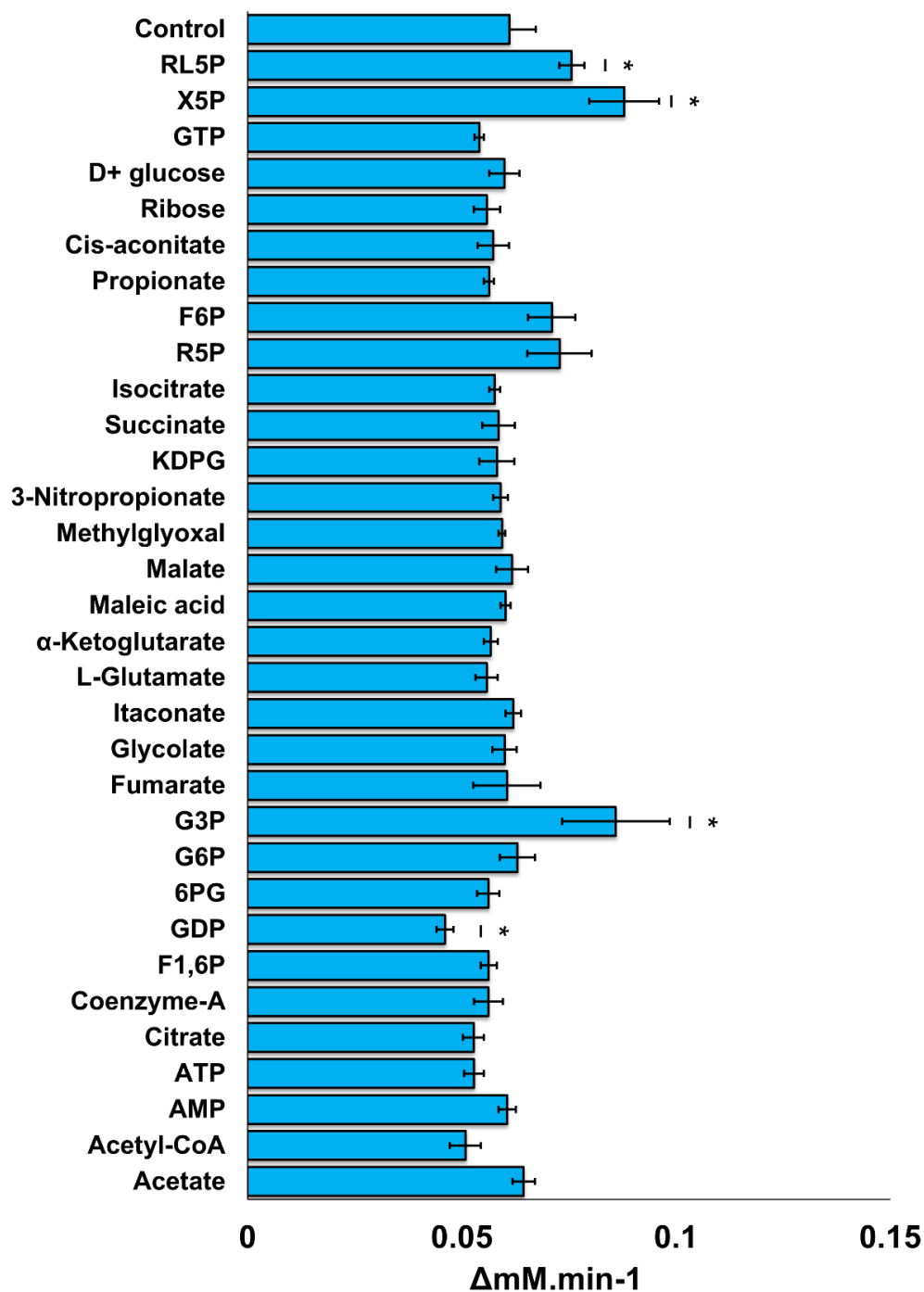
Figure 4.3: The effect of regulators on PykA activity at high PEP concentration. PykA activity was measured at 2 mM PEP and 2 mM ADP using an LDH-coupled assay. Regulators were used at final concentration of 1 mM except for F6P, R5P and X5P which were used at 0.2 mM, 0.15 mM and 0.5 mM, respectively. The represented values are mean of three replicates ± standard error. Statistical significance was performed between control group and test groups using an unpaired *t*-test (*=*p* <0.05, **=*p* <0.01, ***=*p* <0.001).
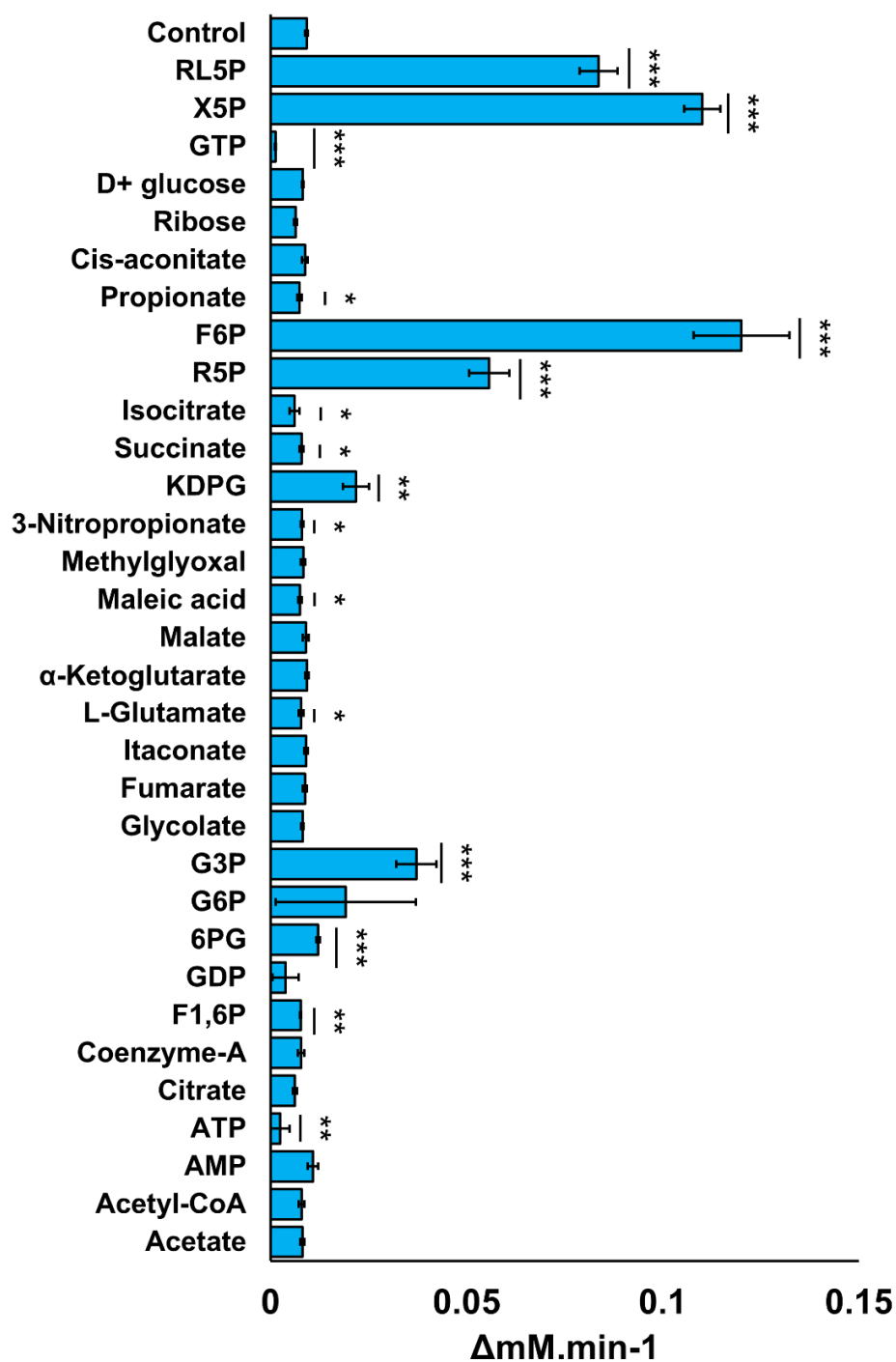
Figure 4.4: The effect of regulators on PykA activity at low PEP concentration. PykA activity was measured at 0.3 mM PEP and 2 mM ADP using an LDH-coupled assay. Regulators were used at final concentration of 1 mM except for F6P, R5P and X5P which were used at 0.2 mM, 0.15 mM and 0.5 mM, respectively. The represented values are mean of three replicates ± standard error. Statistical significance was performed between control group and test groups using an unpaired t-test (*=p <0.05, **=p <0.01, ***=p <0.001).

4.4.2 Effect of regulators on the kinetic properties of PykA

4.4.2.1 Activation of PykA by EDP metabolites

G3P, G6P and KDPG are metabolites from the EDP and were found to enhance PykA activity. I re-measured the kinetics of PykA with respect to [PEP] by using variable PEP concentrations (0-6 mM), 2 mM ADP and 1 mM of each candidate regulator. The addition of G3P, G6P and KDPG caused a drop in PykA cooperativity as indicated by the decrease of the Hill coefficient (h) compared with the control. Along with this, PykA kinetics became less sigmoidal and more hyperbolic to variable degrees according to the potency of each regulator (Figure 4.5). The three metabolites also decreased the apparent binding affinity of PykA to the substrate ($S_{0.5}$), whilst maintaining comparable V_{max} values. Therefore, the addition of these metabolites improved the catalytic efficiency ($k_{cat}/S_{0.5}$) of PykA to variable degrees; G6P > G3P > KDPG.

4.4.2.2 Activation of PykA by EMPP and PPP metabolites

It was surprising to find that metabolites from the PPP (RL5P, R5P, X5P) and the EMPP (F6P, from EMPP operating in gluconeogenic direction) were among the candidate activators of PykA, given that *P. aeruginosa* is an exclusively EDP-dependent organism. Moreover, these intermediates seemed to be potent activators of PykA and exerted their effects at lower concentrations compared with other regulators. Therefore, I re-measured the PykA kinetics at various concentrations of PEP (0-6 mM), 2 mM ADP, in the presence of these metabolites. Given the strong effects of these metabolites on PykA, I added them at concentrations lower than 1 mM (0.2 mM F6P, 0.15 mM R5P, 0.5 mM X5P) except for RL5P which was used at 1 mM. Metabolites of the PPP and gluconeogenic EMPP enhanced PykA activity more strongly than the EDP metabolites (Table 4.2, Figure 4.6). They caused decrease of $S_{0.5}$ values of PykA as compared with the control, whereas they had almost no effect on V_{max}. As shown in Table 4.2, the addition of these metabolites improved the catalytic efficiency ($k_{cat}/S_{0.5}$) of PykA to variable degrees; F6P > X5P > R5P > RL5P.
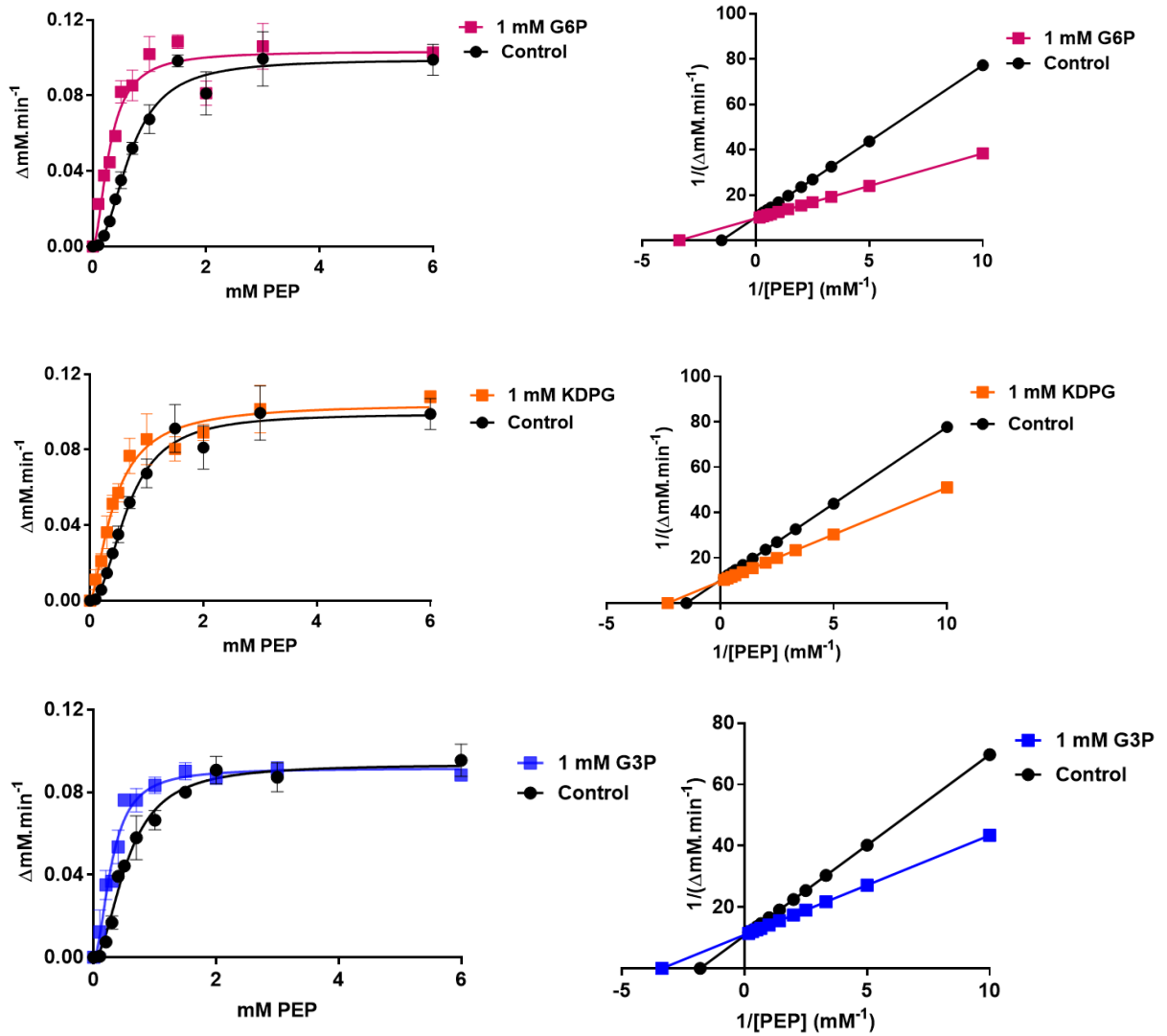
Figure 4.5: Activation of PykA by EDP metabolites. Figures on the left show the effects of metabolites on the sigmoidal kinetics of PykA, whereas figures on the right illustrate Lineweaver-Burk plots of each regulator (y-intercept and the x-intercept indicate $1/V_{max}$ and $-1/S_{0.5}$, respectively). The enzymatic activity of PykA was measured at various PEP concentrations (0-6 mM), 2 mM ADP and 1 mM of each regulator. Values represent mean of three replicates ± standard error. All figures were generated using GraphPad Prism7.
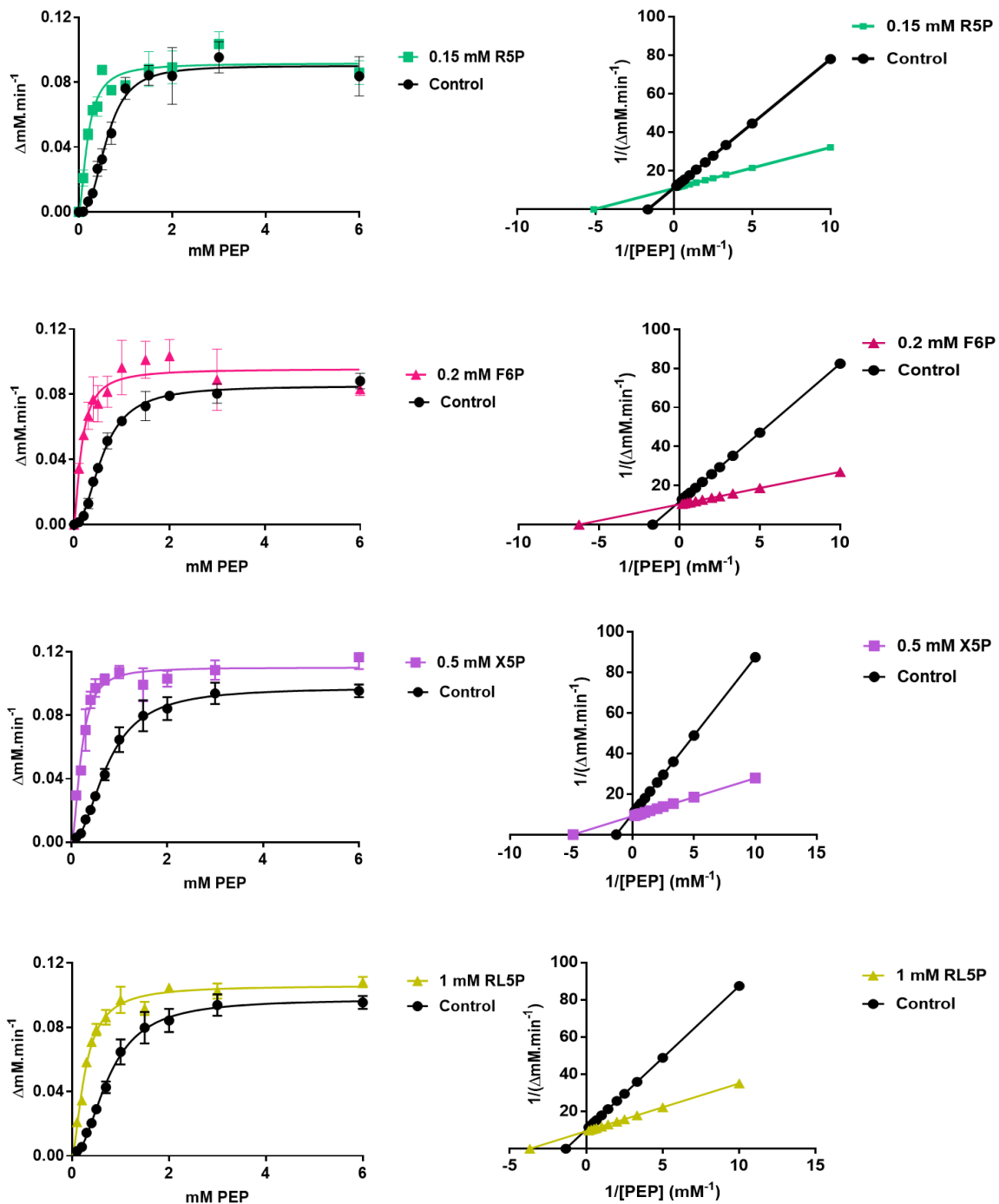
Figure 4.6: Activation of PykA by PPP and EMPP (gluconeogenic direction) metabolites. Figures on the left show the effects of metabolites on the sigmoidal kinetics of PykA, whereas figures on the right illustrate Lineweaver-Burk plots of each regulator (y-intercept and the x-intercept indicate $1/V_{max}$ and $-1/S_{0.5}$, respectively). The enzymatic activity of PykA was measured at various PEP concentrations (0-6 mM), 2 mM ADP, and regulators as indicated. Values represent mean of three replicates ± standard error. All figures were generated using GraphPad Prism7.

Table 4.2: Changes in PykA kinetics caused by metabolic activators.

PEP titration	None	0.2 mM F6P	0.15 mM R5P	0.5 mM X5P	1 mM RL5P	1 mM G3P	1 mM G6P	1 mM KDPG
$S_{0.5}$ (mM)	0.67 ± 0.03	0.16 ± 0.02	0.195 ± 0.01	0.21 ± 0.013	0.27 ± 0.012	0.29 ± 0.01	0.29 ± 0.02	0.43 ± 0.03
Hill Coeff (h)	2.14 ± 0.2	1.44 ± 0.31	1.65 ± 0.24	1.8 ± 0.22	1.6 ± 0.12	1.8 ± 0.21	1.78 ± 0.31	1.51 ± 0.18
V_{max} (ΔmM.min^{-1})	0.09 ± 0.003	0.095 ± 0.004	0.0916 ± 0.002	0.11 ± 0.002	0.10 ± 0.002	0.091 ± 0.002	0.1 ± 0.003	0.1 ± 0.004
k_{cat} (s^{-1})	392.6	414.4	399.6	479.93	462.47	399.2	436.3	436.3
$k_{cat}/S_{0.5}$ (s^{-1}.mM^{-1})	585.9	2590	2049.2	2285.4	1712.9	1376.5	1504.4	1014.6
ADP titration	**None**	**0.2 mM F6P**	**0.15 mM R5P**	**0.5 mM X5P**	**1 mM RL5P**	**1 mM G3P**	**1 mM G6P**	**1 mM KDPG**
K_M (mM)	0.07 ± 0.008	N/D	N/D	N/D	N/D	N/D	N/D	N/D
V_{max} (ΔmM.min^{-1})	0.08 ± 0.002	N/D	N/D	N/D	N/D	N/D	N/D	N/D
k_{cat} (s^{-1})	335.9	N/D	N/D	N/D	N/D	N/D	N/D	N/D
$k_{cat}/S_{0.5}$ (s^{-1}.mM^{-1})	5167.6	N/D	N/D	N/D	N/D	N/D	N/D	N/D

N/D: Not Determined (initial tests suggested that the regulator had no effect on PykA kinetics compared with the control).

4.4.2.3 Effect of ATP and GTP on PykA activity

When regulators were screened at low PEP concentration, ATP and GTP showed some inhibitory effects on PykA. To confirm that these metabolites were inhibitors of PykA, I re-measured the PykA kinetics with respect to [PEP] at variable PEP concentrations (0-6 mM), 2 mM ADP and 1 mM of ATP or GTP. The addition of these nucleotides caused almost no change in the kinetics of PykA (Figure 4.7). The PykA kinetics with ATP ($S_{0.5}$ of 0.58 s^{-1}, V_{max} of 0.09 mM/min) were almost comparable with those of GTP ($S_{0.5}$ of 0.47 s^{-1}, V_{max} of 0.08 mM/min) and the control ($S_{0.5}$ of 0.67 s^{-1}, V_{max} of 0.09 mM/min). Values of the $k_{cat}/S_{0.5}$ with ATP (676.8 s^{-1}mM^{-1}) and GTP (714.6 s^{-1}mM^{-1}) were also close to the control (585.9 s^{-1}mM^{-1}). Therefore, it seemed that the addition of these nucleotides does not have an impact on PykA activity, at least at the tested concentrations.
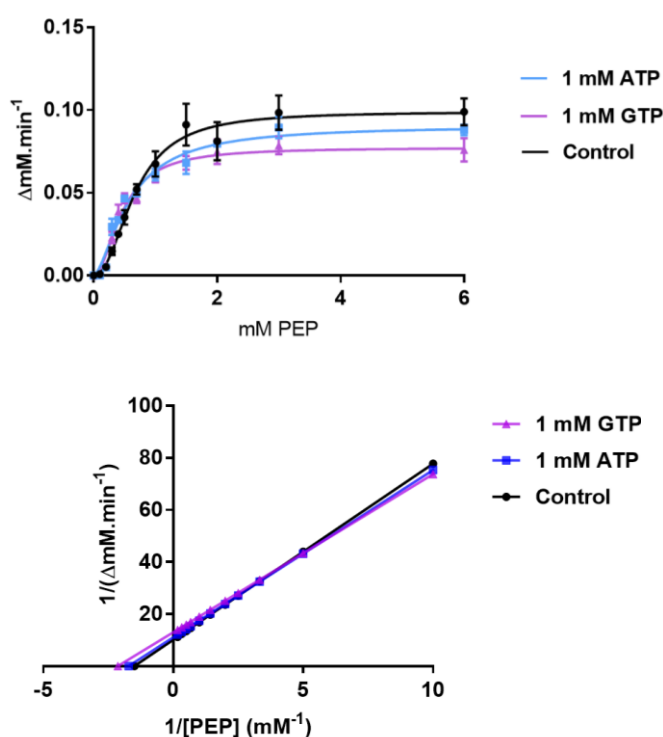
Figure 4.7: The effects of ATP and GTP on PykA activity. The upper panel shows the effects of 1 mM ATP or 1 mM GTP on the sigmoidal kinetics of PykA, whereas the lower panel shows Lineweaver-Burk plots of the two nucleotides (y-intercept and the x-intercept indicate $1/V_{max}$ and $-1/S_{0.5}$, respectively). The enzymatic activity of PykA was measured at various PEP concentrations (0-6 mM), 2 mM ADP and 1 mM of each nucleotide. Values represent mean of three replicates ± standard error. All figures were generated using GraphPad Prism7.

4.4.2.4 Effect of regulators on the ADP-dependency of PykA

I showed above that the EDP and the PPP (including gluconeogenic EMPP) metabolites can change the PykA kinetics with respect to [PEP]. In order to investigate if these activators can also influence the PykA response to ADP, I measured the PykA kinetics with respect to [ADP] with these metabolites present. The enzymatic reaction of PykA was measured at variable concentrations of ADP (0.02, 0.03, 0.07 and 0.5 mM) and 5 mM PEP with PykA activators added at the same concentrations used for the PEP titration experiments; 1 mM G6P, 1 mM KDPG, 1 mM G3P, 0.2 mM F6P, 0.15 mM R5P, 0.5 mM X5P, 0.1 mM RL5P. Figure 4.8 shows that none of the PykA activators changed the PykA responses to [ADP]. This was expected as most of the regulators that activate PK enzymes improve the enzyme kinetics with respect to [PEP] only.
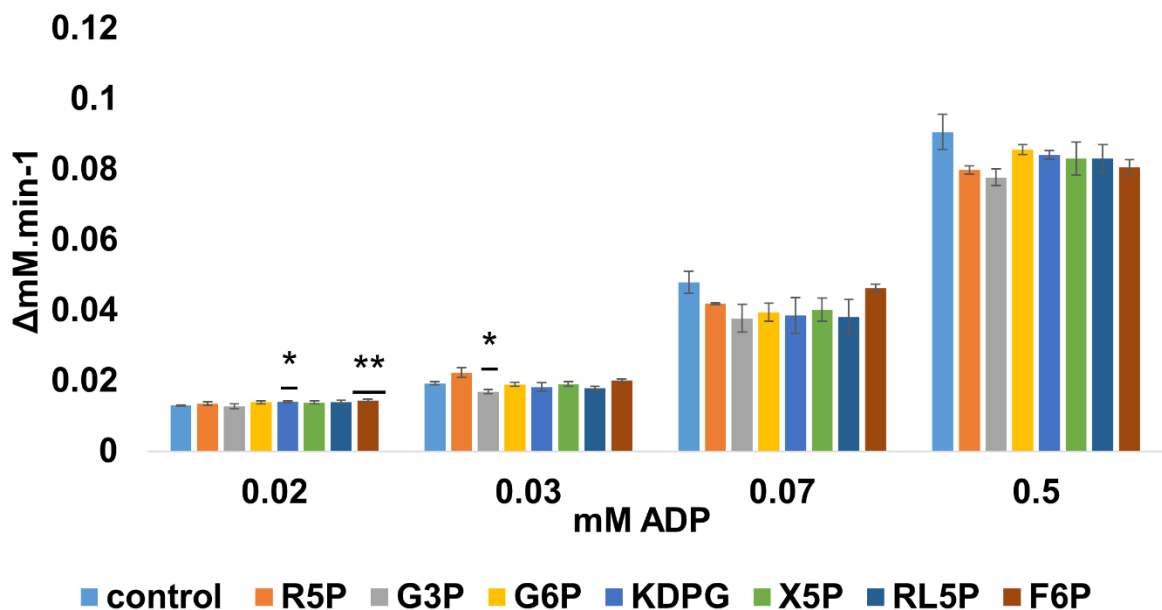
Figure 4.8: The effect of metabolites on the ADP kinetics of PykA. PykA activity was measured at various concentrations of ADP, 5 mM PEP and different metabolites (1 mM G3P, 1 mM G6P, 1 mM KDPG, 0.2 mM F6P, 0.15 mM R5P, 0.5 mM X5P, 1 mM RL5P). Each bar represents the mean of three replicates and standard errors are shown. Statistical significance was performed between control group and test groups using an unpaired t-test (*=p <0.05, **=p <0.01, ***=p <0.001).

4.5 Metabolic regulation of PykF

4.5.1 Screening of PykF regulators

Similar to PykA, I tested the effect of metabolic regulators on PykF activity at high (2 mM) and low PEP (0.3 mM) concentrations in order to identify PykF inhibitors and activators, respectively. In these experiments, the ADP was used at saturation (2 mM) and the regulators were added at 1 mM or less if they showed large effects on PykF activity. The effects of metabolites on PykF can be found in Figure 4.9 and 4.10. At high PEP concentrations, PykF seemed to be activated by R5P, RL5P and X5P which were also found to be activators of PykA. No metabolites were seen to inhibit PykF activity.

At low PEP concentration, PykF activity ($0.02 \, \Delta mM.min^{-1}$) was at least seven fold higher when R5P ($0.139 \, \Delta mM.min^{-1}$), RL5P ($0.14 \, \Delta mM.min^{-1}$) and X5P ($0.17 \, \Delta mM.min^{-1}$) were present. Moreover, the three metabolites activated PykF even when present at less than 0.5 mM. At low PEP concentration, PykF was also activated moderately by G3P, G6P and AMP. Interestingly and compared with PykA, F6P could not enhance PykF, indicating that these activators are very selective for each isozyme. No PykF activation was seen by any TCA cycle metabolites and also no inhibitors of PykF could be detected.

4.5.2 Effect of regulators on the kinetic properties of PykF

Using these potential activators (R5P, RL5P, X5P, G6P, G3P, AMP), the PykF kinetics were re-calculated (with respect to PEP and ADP titrations) in order to see the effects of these metabolites on PykF enzymatic properties ($S_{0.5}$, K_M, Hill coef (h), V_{max}, k_{cat}, $k_{cat}/S_{0.5}$).
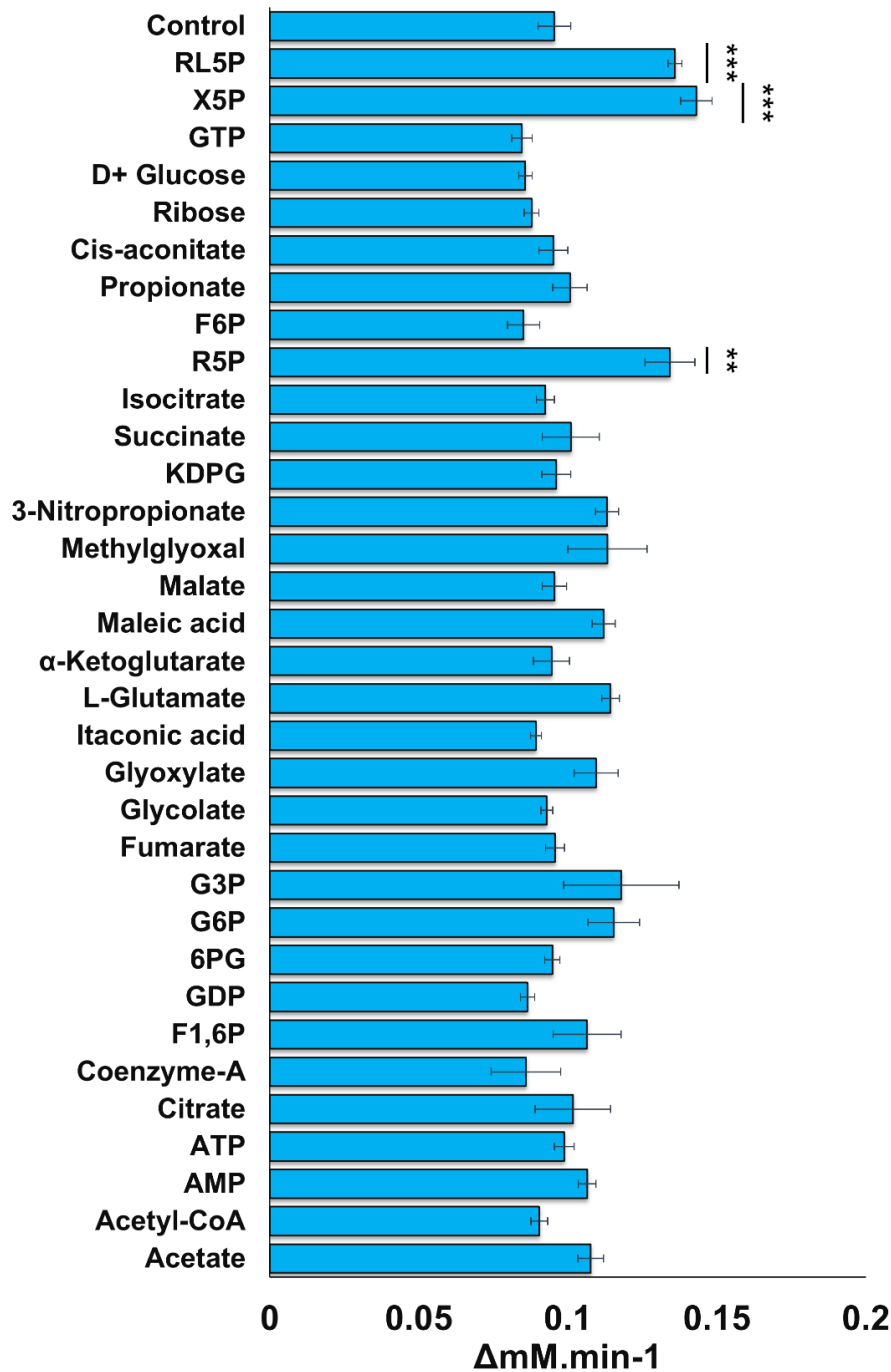
Figure 4.9: The effect of regulators on PykF activity at high PEP concentration. PykF activity was measured at 2 mM PEP and 2 mM ADP using an LDH-coupled assay. Regulators were used at final concentration of 1 mM except for R5P, RL5P and X5P which were used at 0.15 mM, 0.5 mM and 0.5 mM, respectively. The represented values are mean of three replicates ± standard error. Statistical significance was performed between control group and test groups using an unpaired *t*-test (*=p <0.05, **=p <0.01, ***=p <0.001).
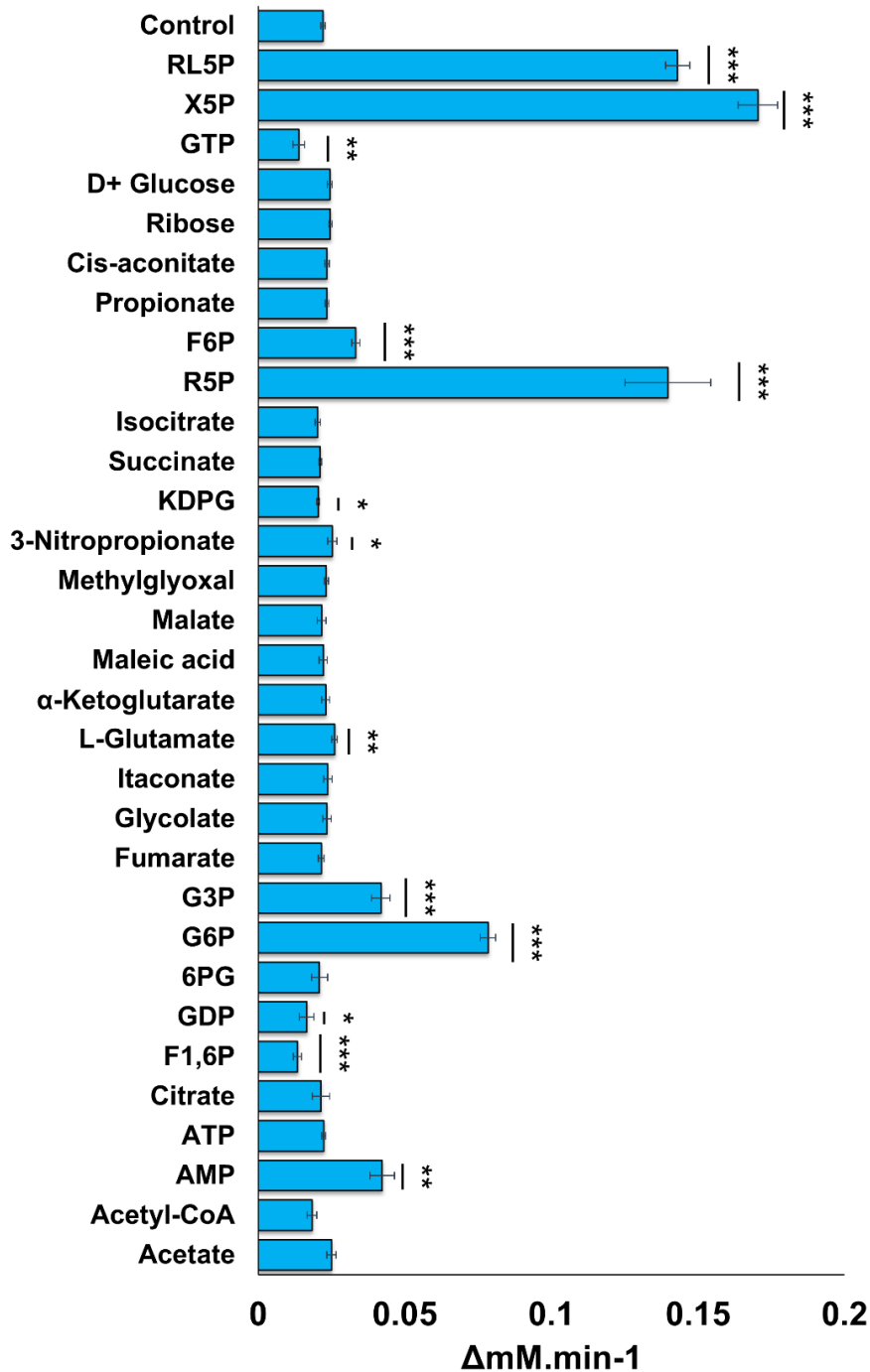
Figure 4.10: The effect of regulators on PykF activity at low PEP concentration. PykF activity was measured at 0.3 mM PEP and 2 mM ADP using an LDH-coupled assay. Regulators were used at final concentration of 1 mM except for R5P, RL5P and X5P which were used at 0.15 mM, 0.5 mM and 0.5 mM, respectively. The represented values are mean of three replicates ± standard error. Statistical significance was performed between control group and test groups using an unpaired *t*-test (*=*p* <0.05, **=*p* <0.01, ***=*p* <0.001).

4.5.2.1 Effect of metabolites on the PEP-dependency of PykF

PykF activity was measured at variable concentrations of PEP (0-6 mM), 2 mM ADP and one of the candidate activators (0.15 mM R5P, 0.5 mM RL5P, 0.5 mM X5P, 1 mM G6P, 1 mM G3P, 1 mM AMP). The resulting kinetic data can be found in Table 4.3, Figure 4.11 and Figure 4.12. In the presence of these metabolites, the sigmoidal kinetics of PykF with respect to [PEP] was decreased and became more hyperbolic, as indicated by the lower Hill coefficients (h) compared with the control. Moreover, the $S_{0.5}$ value of PykF was also decreased, indicating that the apparent binding affinity of PykF to the substrate was improved. There was no accompanying change in V_{max}. Similar to PykA, metabolites from the PPP (X5P, R5P, RL5P) were more potent activators of PykF than those from the EDP (G6P and G3P). AMP also decreased the $S_{0.5}$ and the Hill coefficient of PykF, but less than other PPP metabolites. All the PykF activators improved the catalytic efficiency of the enzyme to variable degrees; X5P > RL5P > R5P > G6P > AMP > G3P.
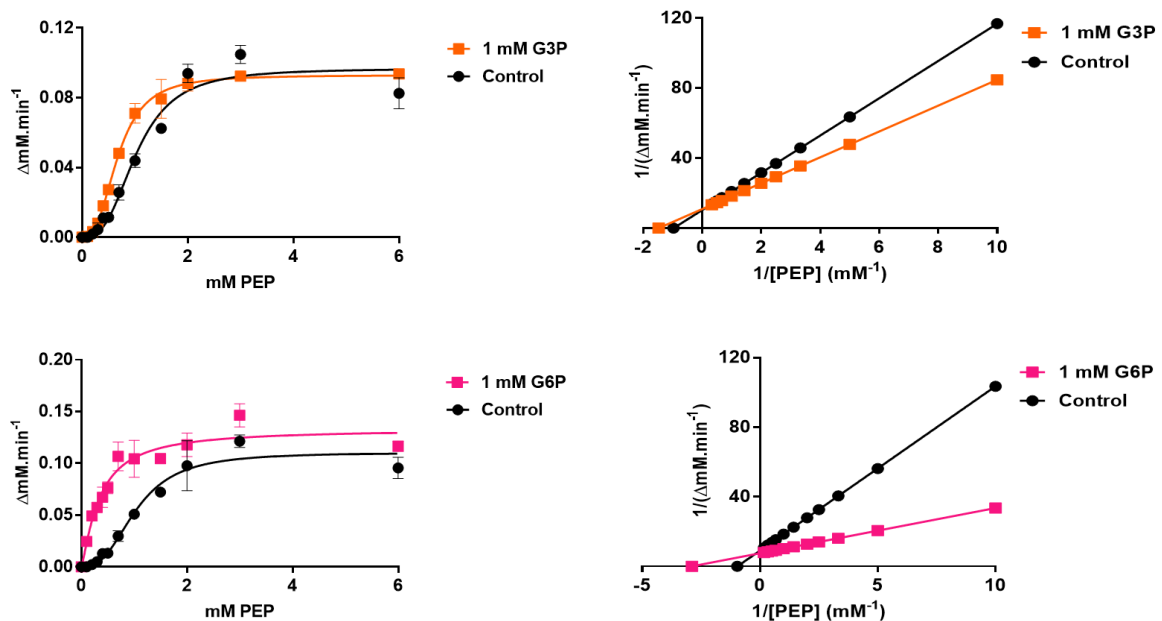
Figure 4.11: Activation of PykF by EDP metabolites. Figures on the left show the effects of metabolites on the sigmoidal kinetics of PykF, whereas figures on the right illustrate Lineweaver-Burk plots of each regulator (y-intercept and the x-intercept indicate $1/V_{max}$ and $-1/S_{0.5}$, respectively). The enzymatic activity of PykF was measured at various PEP concentrations (0-6 mM), 2 mM ADP, and regulators as indicated. Values represent mean of three replicates ± standard error. All figures were generated using GraphPad Prism7.
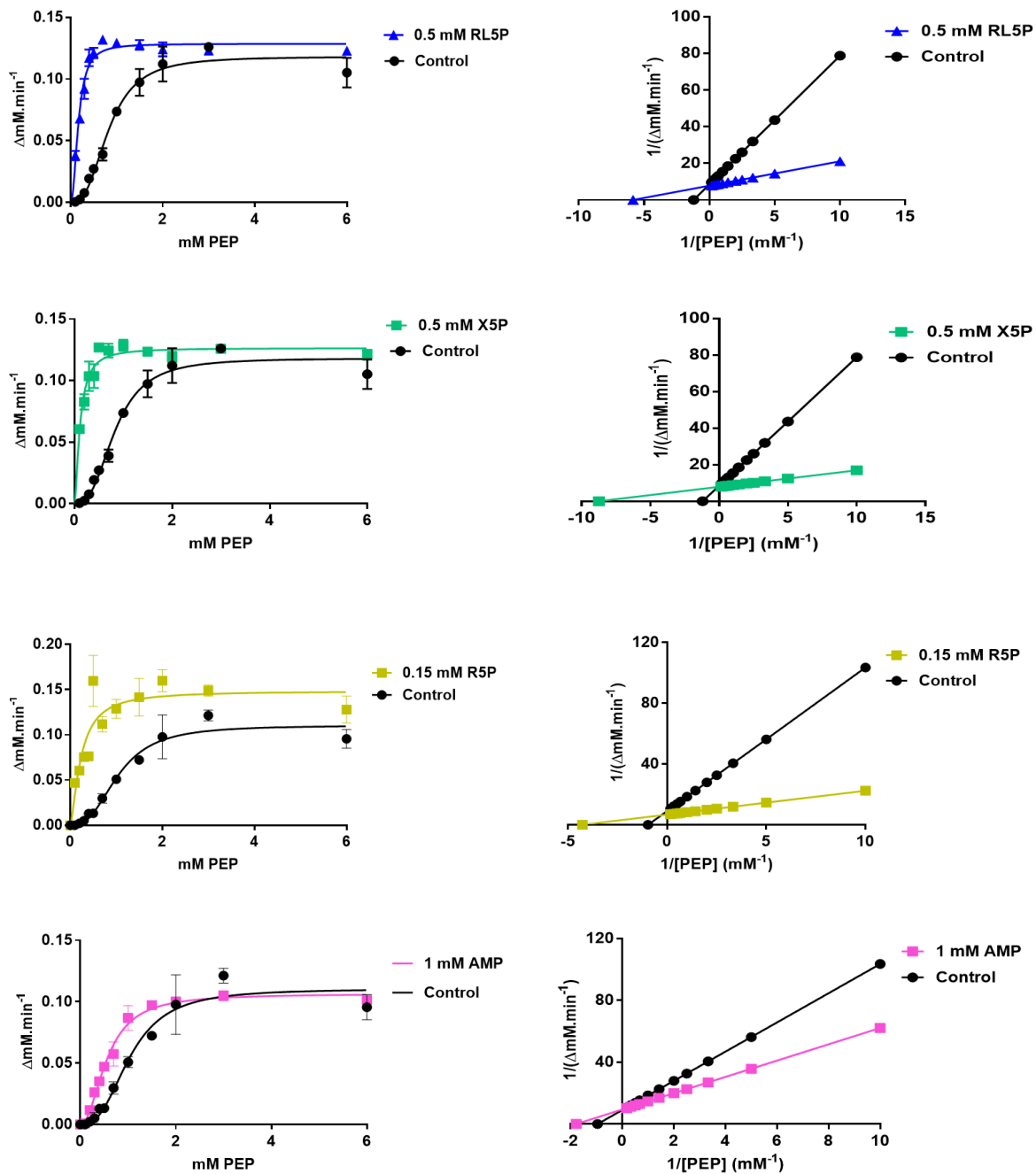
Figure 4.12: Activation of PykF by PPP metabolites. Figures on the left show the effects of metabolites on the sigmoidal kinetics of PykF, whereas figures on the right illustrate Lineweaver-Burk plots of each regulator (y-intercept and the x-intercept indicate $1/V_{max}$ and $-1/S_{0.5}$, respectively). The enzymatic activity of PykF was measured at various PEP concentrations (0-6 mM), 2 mM ADP, and regulators as indicated. Values represent mean of three replicates ± standard error. All figures were generated using GraphPad Prism7.

Table 4.3: Changes in PykF kinetics caused by metabolic activators.

PEP titration	None	0.15 mM R5P	1 mM G6P	1 mM AMP	1 mM G3P	0.5 mM X5P	0.5 mM RL5P
$S_{0.5}$ (mM)	1.03 ± 0.006	0.23 ± 0.03	0.34 ± 0.04	0.56 ± 0.02	0.68 ± 0.02	0.11 ± 0.008	0.17 ± 0.008
Hill Coeff (h)	2.8 ±0.3	1.47 ± 0.3	1.25±0.2	2 ± 0.15	2.7 ± 17	1.58±0.21	2.15±0.2
V_{max} (ΔmM.min^{-1})	0.11 ± 0.004	0.15 ± 0.009	0.13 ± 0.007	0.1064 ± 0.002	0.092 ± 0.001	0.126 ± 0.002	0.128 ± 0.002
k_{cat} (s^{-1})	378	515.4	446.7	365.6	316.15	432.9	439.8
$k_{cat}/S_{0.5}$ (s^{-1}.mM^{-1})	366.9	2240.8	1313.9	652.9	464.9	3935.4	2587
ADP titration	**None**	**0.15 mM R5P**	**1 mM G6P**	**1 mM AMP**	**1 mM G3P**	**0.5 mM X5P**	**0.5 mM RL5P**
K_M (mM)	0.11 ± 0.01	N/D	N/D	N/D	N/D	N/D	N/D
V_{max} (ΔmM.min^{-1})	0.11 ± 0.02	N/D	N/D	N/D	N/D	N/D	N/D
k_{cat} (s^{-1})	378	N/D	N/D	N/D	N/D	N/D	N/D
k_{cat}/K_M (s^{-1}.mM^{-1})	3436.4	N/D	N/D	N/D	N/D	N/D	N/D

N/D: Not Determined (initial tests suggested that the regulator had no effect on PykA kinetics compared with the control).

4.5.2.2 Effect of metabolites on the ADP-dependency of PykF

In order to see if regulators of PykF modify the ADP-dependency of the enzyme kinetics, I again measured the PykF kinetics with respect to [ADP] in the presence of PykF activators (X5P, R5P, RL5P, G3P, G6P and AMP). PykF activity was measured at variable concentrations of ADP (0.02, 0.03, 0.07 and 0.5mM), 5 mM PEP with activators added at the same concentrations used for the PEP titration experiments. Similar to PykA regulators, none of the PykF regulators changed the ADP-dependency of PykF (Figure 4.13).
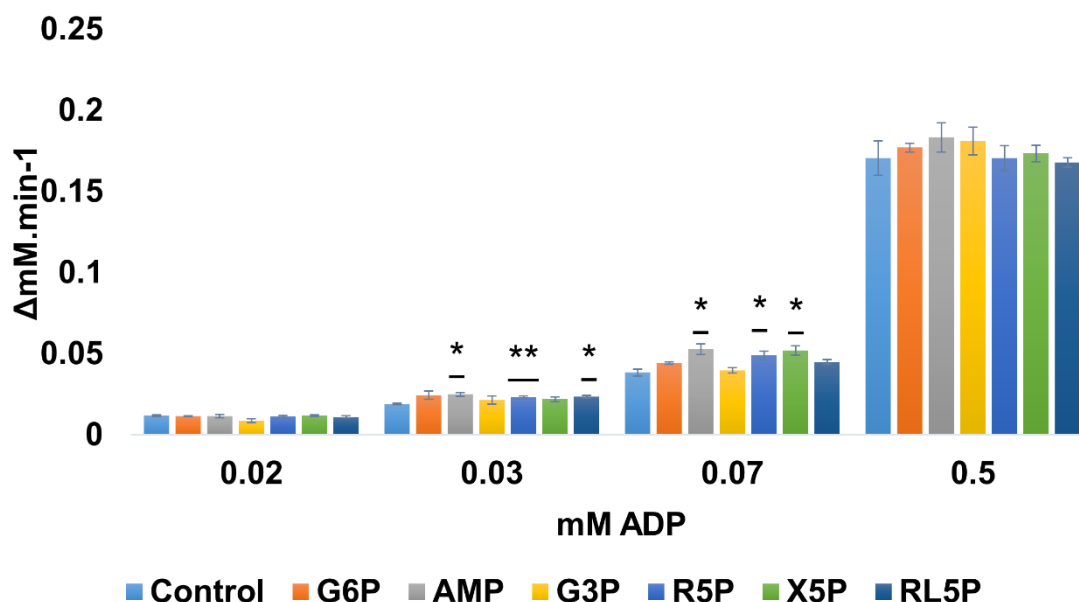
Figure 4.13: The effect of metabolites on the ADP kinetics of PykF. PykF activity was measured at various concentrations of ADP, 5 mM PEP and different metabolites (1 mM G3P, 1 mM G6P, 1 mM AMP, 0.15 mM R5P, 0.5 mM X5P, 0.5 mM RL5P). Each bar represents the mean of three replicates ± standard error. Statistical significance was performed between control group and test groups using an unpaired t-test (*=p <0.05, **=p <0.01, ***=p <0.001).

4.6 Effect of metal ions on PykA and PykF activity

4.6.1 The effect of divalent cations on PykA and PykF

All PK enzymes require a source of divalent cation for catalysis and this ion is mostly Mg^{2+}. However, some PK enzymes reach higher activity levels when divalent ions other than Mg^{2+} are present. Therefore, I compared the enzymatic activity of PykA and PykF using a selection of divalent ions; $MnCl_2$, $CoCl_2$, $CaCl_2$, $ZnSO_4$, $NiSO_4$ and $MgCl_2$. The activity of each isozyme was measured at saturating concentrations of PEP (5 mM), ADP (2 mM), and divalent ions (10 mM).

Figure 4.14 shows the effect of divalent cations on the PykA and PykF activity. Similar to the majority of PK enzymes, PykA and PykF reached maximal activity with $MgCl_2$ as compared with other sources of divalent ions. Both enzymes were partly activated by $MnCl_2$ and reached around 40% of their maximal activities in the presence of this salt. $CoCl_2$ also induced partial activity of PykA and PykF. With $CoCl_2$, the enzymatic activities of PykA and PykF were 45% and 92%, respectively compared with their maximal activity with $MgCl_2$. There was no detectable PykA or PykF activity with $CaCl_2$, $ZnSO_4$ or $NiSO_4$.
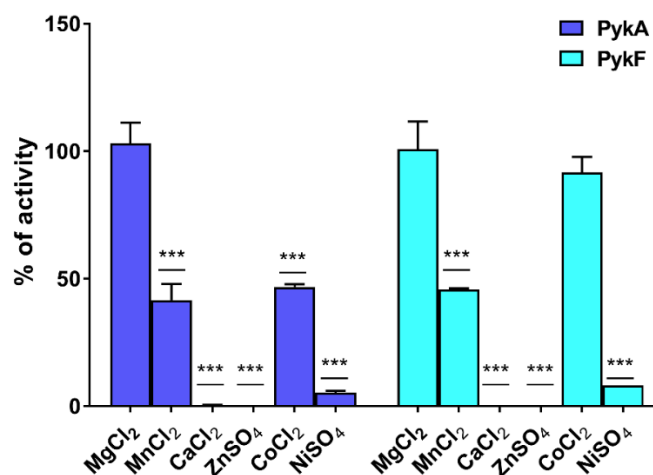
Figure 4.14: The effect of divalent ions on PykA and PykF activity. The activity of each enzyme was measured using 5 mM PEP, 2 mM ADP and 10 mM of divalent ion. The reaction was initiated by the addition of 0.2 µg PykA or 0.25 µg PykF. Bars represent mean of three replicates ± standard error. Statistical significance was performed between control group ($MgCl_2$) and test groups using an unpaired t-test (*=p <0.05, **=p <0.01, ***=p <0.001).

4.6.2   PykA and PykF are K⁺-independent

While there is an obligate requirement for cations to be present during PK catalysis, some PK enzymes require an additional source of monovalent ions, mostly K⁺, in order to achieve maximal activity. To investigate whether PykA and PykF required a source of K⁺ along with Mg^{2+}, I compared the enzyme activity of PykA and PykF with and without KCl. The enzyme activity of each isozyme was measured at 5 mM PEP, 2 mM ADP, 10 mM $MgCl_2$ and 100 mM KCl. Figure 4.15 shows that the PykA and PykF activities were entirely dependent on $MgCl_2$ and there was no activity of either enzyme with KCl alone. Moreover, the combination of $MgCl_2$ and KCl did not increase the activity of the isozymes and it seems that the addition of KCl even caused some minor negative impacts on the PykF. This suggests that PykA and PykF are K⁺-independent enzymes.

4.6.3   The effect of monovalent ions on PykA and PykF

As shown in the previous section, the addition of K⁺ seemed to slightly reduce the enzyme activity of PykF. In fact, it was unclear whether the modification of the PykF activity by K⁺ was specific to the ion itself or it was a change that can be caused by any cation. To compare the effect of K⁺ and other monovalent ions on PykA and PykF activity, I measured the kinetics of PykA and PykF in the presence of 100 mM of KCl, NH_4Cl or NaCl as monovalent ion sources. With respect to [PEP], I measured the activity of each isozyme at variable PEP concentrations (0-6 mM) and 2 mM ADP, whereas with respect to [ADP], I used variable concentrations of ADP (0-2 mM) and 5 mM PEP. Figure 4.16 and Table 4.4 show the effect of monovalent ions on the kinetics of PykA and PykF.

With monovalent ions added, the $S_{0.5}^{PEP}$ and the K_M^{ADP} values increased for both isozymes. Additionally, the maximal enzyme activity (V_{max}) was also decreased in all reactions catalysed by PykF, whereas the V_{max} of PykA was variable depending on the type of substrate and type of cation. The overall catalytic efficiencies of PykA and PykF for both substrates were decreased noticeably with all sources of monovalent ions when compared with control reactions.
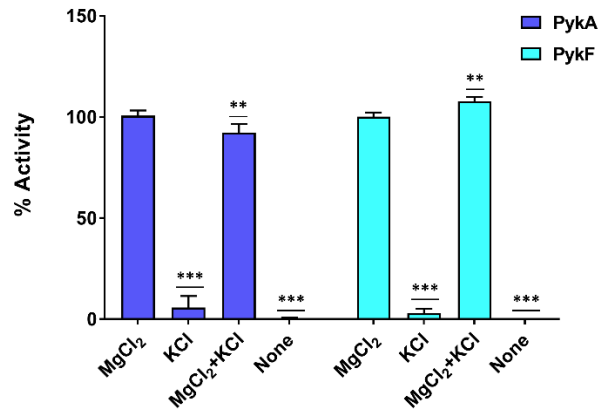
Figure 4.15: The effect of MgCl$_2$ and KCl on the activity of PykA and PykF. The activity of PykA and PykF was measured using 5 mM PEP, 2 mM ADP, 10 mM MgCl$_2$ and 100 mM KCl. The reaction was initiated by the addition of 0.2 µg of PykA or 0.25 µg of PykF. Values represent the mean of three replicates ± standard error. Statistical significance was performed between control group (MgCl$_2$) and test groups using an unpaired *t*-test (*=p <0.05, **=p <0.01, ***=p <0.001).
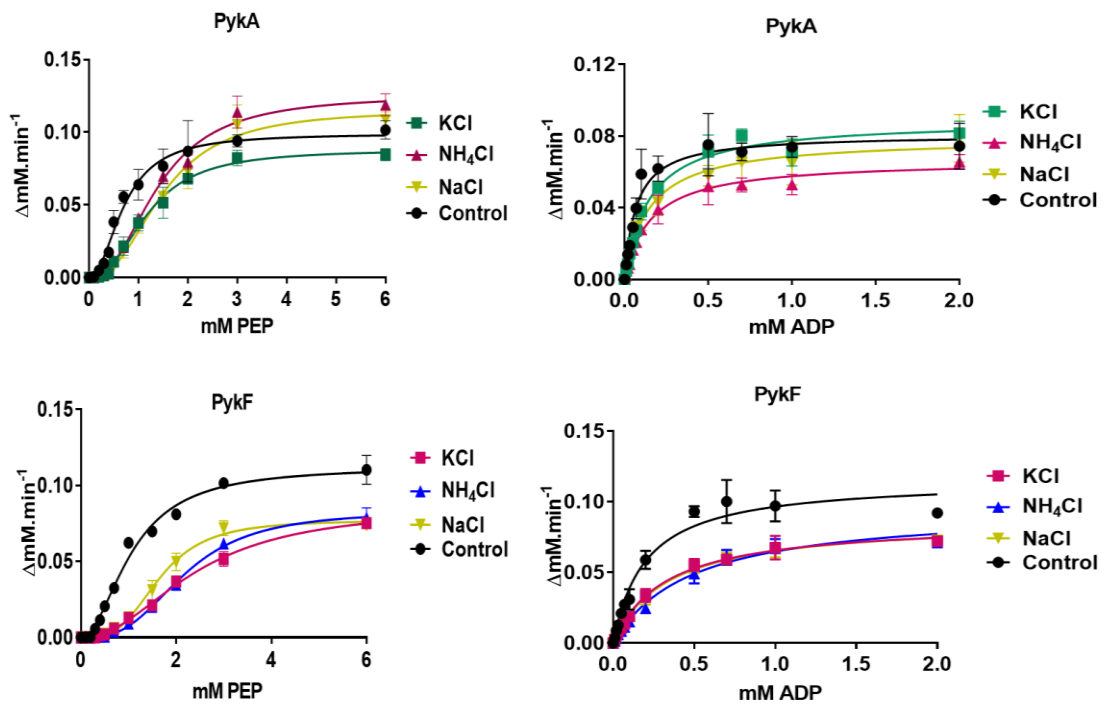
Figure 4.16: The effect of monovalent ions on PykA and PykF. Top panel shows the effect of monovalent ions on PykA and bottom panel shows the effect of monovalent ions on PykF. Titration of PEP was performed using variable PEP concentrations (0-6 mM) and 2 mM ADP, whereas titration of ADP was performed using variable ADP concentrations (0-2 mM) and 5 mM of PEP. Monovalent ions were added at 100 mM concentration. Values represents mean of three replicates ± standard error.

Table 4.4: The effect of monovalent ions on PykA and PykF activity. The activity of each enzyme was measured in the presence of 100 mM monovalent ions. With respect to [PEP], ADP was used at 2 mM and PEP was used at variable concentrations (0-6 mM), whereas with respect to [ADP], PEP was used at 5 mM and ADP was used at variable concentrations (0-2 mM). Values represents mean of three replicates ± standard error. The kinetic parameters shown were calculated using GraphPad Prism7.

PEP titration	PykA				PykF			
	None	KCl	NH$_4$Cl	NaCl	None	KCl	NH$_4$Cl	NaCl
S$_{0.5}$ (mM)	0.67 ± 0.03	1.18 ± 0.05	1.4 ± 0.05	1.49 ± 0.07	1.03 ± 0.006	2.4 ± 0.09	2.18 ± 0.05	1.64 ± 0.04
Hill Coeff (*h*)	2.14 ± 0.2	2.36 ± 0.18	2.3 ± 0.15	2.4 ± 0.2	2.8 ± 0.3	2.13 ± 0.1	2.9 ± 0.1	3.3 ± 0.2
V$_{max}$ (ΔmM.min^{-1})	0.09 ± 0.003	0.087 ± 0.002	0.12 ± 0.003	0.11 ± 0.004	0.11 ± 0.004	0.085 ± 0.002	0.083 ± 0.001	0.077 ± 0.001
k$_{cat}$ (s^{-1})	392.6	379.5	523.5	479.9	378	292	285.2	264.6
k$_{cat}$/S$_{0.5}$ (s^{-1}.mM^{-1})	585.9	321.6	373.9	322	366.9	121.6	130.8	161.3
ADP titration	**None**	**KCl**	**NH$_4$Cl**	**NaCl**	**None**	**KCl**	**NH$_4$Cl**	**NaCl**
K$_M$ (mM)	0.07 ± 0.008	0.148 ± 0.01	0.156 ± 0.01	0.147 ± 0.02	0.11 ± 0.01	0.31 ± 0.02	0.47 ± 0.05	0.34 ± 0.02
V$_{max}$ (ΔmM.min^{-1})	0.08 ± 0.002	0.088 ± 0.002	0.066 ± 0.002	0.078 ± 0.003	0.11 ± 0.02	0.086 ± 0.002	0.095 ± 0.04	0.087 ± 0.002
k$_{cat}$ (s^{-1})	335.9	383.9	287.9	340.3	378	295.5	326.4	298.9
k$_{cat}$/K$_M$ (s^{-1}.mM^{-1})	5167.6	2593.9	1845.5	2314.9	3436.4	953.2	694.4	879.1

4.7 Inhibitors of PykA

In Chapter 3, I showed that *pykA* was the dominant PK that has primary contributions to pyruvate kinase activity and cell growth in glucose and glycerol. A mutant defective in *pykA* had lower pyruvate kinase activity and struggled to grow normally compared with the wild-type cells. Moreover, successful complementation using *pykA* restored the defective phenotypes and this highlights the essential role of this isozyme for these systems. Using this knowledge, I aimed to identify PykA inhibitors that have the potential to be used as antimicrobial drugs against *P. aeruginosa*. This was challenging given that the pathogen is intrinsically resistant to many antimicrobials due to its multiple drug efflux pumps and a very low outer membrane permeability (Livermore, 1984; Schweizer, 2003). In collaboration with the Department of Pharmacology, University of Cambridge, I was able to identify two PykA inhibitors, one of which can penetrate the cell and displays antimicrobial activity *in vivo.*

4.7.1 Screening of inhibitors

A computational prediction of potential PykA inhibitors was performed by the Dept. of Pharmacology using GOLD software (Jones et al., 1997) based on the amino acid sequence of PykA. The enzyme docking produced a list of predicted inhibitors and the top five compounds (PZ0301, S7576, R396907, L334588 and S171204) were selected and purchased from Sigma-Aldrich. I tested the effect of these compounds on PykA to check if they really could inhibit its activity. PykA activity was measured at 5 mM PEP, 2 mM ADP and 200 μM of each inhibitor. I found that PykA was inhibited by S7576 (also known as shikonin) and R396907, whereas the three other compounds seemed to have no effect on the enzyme (Figure 4.17). Moreover, PykA inhibition by shikonin was more profound than that of R396907. The two compounds were analysed further to investigate the types of PykA inhibition caused by them.
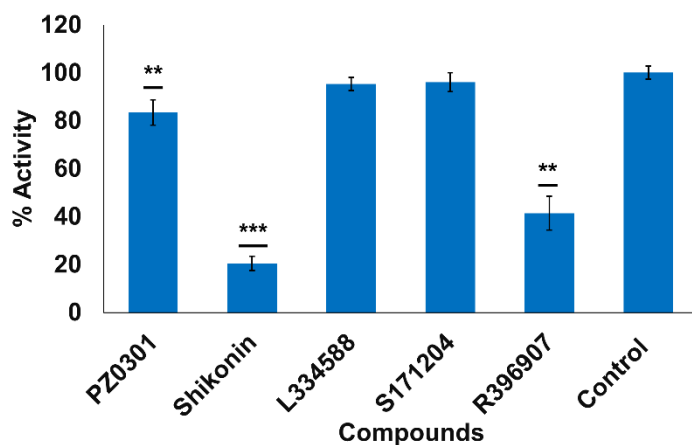
Figure 4.17: Effects of potential inhibitors on PykA activity. PykA activity was measured at 5 mM PEP, 2 mM ADP and 0.05 µg PykA. Compounds were dissolved in DMSO and used at 200 µM concentration. The figure represents mean values of three replicates ± standard error. Statistical significance was performed between control group and test groups using an unpaired t-test (*=p <0.05, **=p <0.01, ***=p <0.001).

4.7.2   Dose-response curves of shikonin and R396907

To determine the mechanism by which shikonin and R396907 can inhibit PykA activity, the PykA kinetics with respect to [PEP] and [ADP] needed to be measured in the presence of IC25 and IC50 of these compounds. Therefore, to establish the IC25 and IC50 of shikonin and R396907, dose-response curves were performed in which PykA activity was measured against an increasing concentration of each inhibitor. From each dose-response curve, I calculated the IC50. Then, I used the IC50 and the Hill slope of that curve (steepness of the curve) to calculate the IC25 (the inhibitor concentration which can inhibit 25% of the maximal activity of the enzyme).

The dose-response curves showed that inhibitory concentrations of shikonin were much lower than the ones of R396907 (Figure 4.18). With Shikonin, the dose-response curve extrapolated an IC50 of 23.2 µM (Hill slope of -1.86 ± 0.7), whereas the IC50 of R396907 was nearly four times more than that (IC50 of 95.5 µM, Hill slope of -1.567 ± 0.29). Based on these figures, the IC25 of shikonin and R396907 were calculated; 13.4 µM and 47.4 µM, respectively.

119
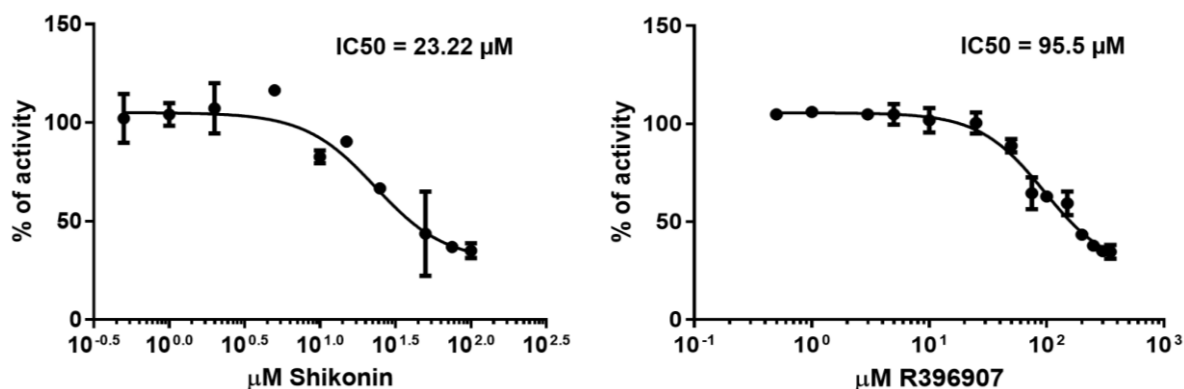
Figure 4.18: Dose-response curves of PykA with shikonin and R396907. PykA activity was measured at 2 mM ADP, 5 mM PEP, and increasing concentrations of shikonin (0-100 µM) or R396907 (0-350 µM). The X-axis of each graph represents the logarithmic concentrations of the inhibitor and the Y-axis represents the percent of PykA activity remaining. The shown values are mean of three replicates ± standard error. The curves and the shown IC50 values were produced using GraphPad Prism 7.

4.7.3 Inhibitory effects of shikonin on PykA kinetics

In this section, I investigated the effects of shikonin on the PEP- and ADP-dependency of PykA kinetics. Therefore, I repeated the PEP and ADP titration experiments whereas using shikonin at the identified IC25 (13.4 µM) and IC50 (23.2 µM) concentrations. The [PEP] was (0-6 mM as indicated), 2 mM ADP and 13.4 µM or 23.2 µM of shikonin, whereas the [ADP] was (0-2.5 mM as indicated), 5 mM PEP and 13.4 µM or 23.2 µM of shikonin.

The inhibitory effects of shikonin on PykA can be seen in Figure 4.19 and Table 4.5. Non-competitive inhibition is achieved when the inhibitor binds either the free enzyme or the enzyme substrate complex causing a drop in the maximal enzyme activity without changing the $S_{0.5}$. With respect to [PEP], shikonin induced non-competitive inhibition of PykA that was indicated by the decline of V_{max} and the unchanged $S_{0.5}$. The non-competitive inhibition of PykA by shikonin was observed at both IC25 and IC50.

Shikonin also induced changes of the ADP-dependency of PykA, however these changes were concentration-dependent. At IC25, the V_{max} of PykA was decreased, while the K_M was unchanged and this was consistent with non-competitive inhibition. Whereas, at IC50, the V_{max} was decreased but the K_M was increased which was consistent with mixed type inhibition. The latter type of inhibition is achieved due to conformational change of the active site (caused by ligand binding) which interferes with substrate binding and eventually leads to increase of the K_M. Moreover, the newly formed conformation of the enzyme also inhibits the overall performance of the enzyme, thus the V_{max} is decreased. In the presence of shikonin, both the catalytic turnover and the catalytic efficiency of PykA was reduced for PEP and ADP. The decline of these parameters was dependent on shikonin concentration; the higher the concentration of shikonin, the more the decline of the catalytic turnover number and the catalytic efficiency.

Table 4.5: Changes in the kinetic parameters of PykA in the presence of shikonin. The inhibitor was used at 0 µM (control), 13.4 µM (IC25) or 23.22 µM (IC50). [PEP] was (0-6 mM) and 2 mM ADP, whereas [ADP] was (0-2.5 mM) and 5 mM of PEP. Values represent the mean of three replicates ± standard error. Kinetics were calculated using GraphPad Prism7.

		Control	IC25	IC50
PEP	$S_{0.5}$ (mM)	0.79 ± 0.06	0.87 ± 0.39	0.95 ± 0.53
	Hill coeff. (h)	1.7 ± 0.2	1.08 ± 0.37	1.38 ± 0.87
	V_{max} (ΔmM.min^{-1})	0.1 ± 0.004	0.076 ± 0.01	0.037 ± 0.01
	k_{cat} (s^{-1})	454.5	334	161.4
	$k_{cat}/S_{0.5}$ (s^{-1}.mM^{-1})	575.3	383	169.8
ADP	K_M (mM)	0.05 ± 0.005	0.058 ± 0.005	0.095 ± 0.01
	V_{max} (ΔmM.min^{-1})	0.11 ± 0.002	0.074 ± 0.001	0.067 ± 0.001
	k_{cat} (s^{-1})	500	322	292.3
	k_{cat}/K_M (s^{-1}.mM^{-1})	10000	5551.7	3076.8
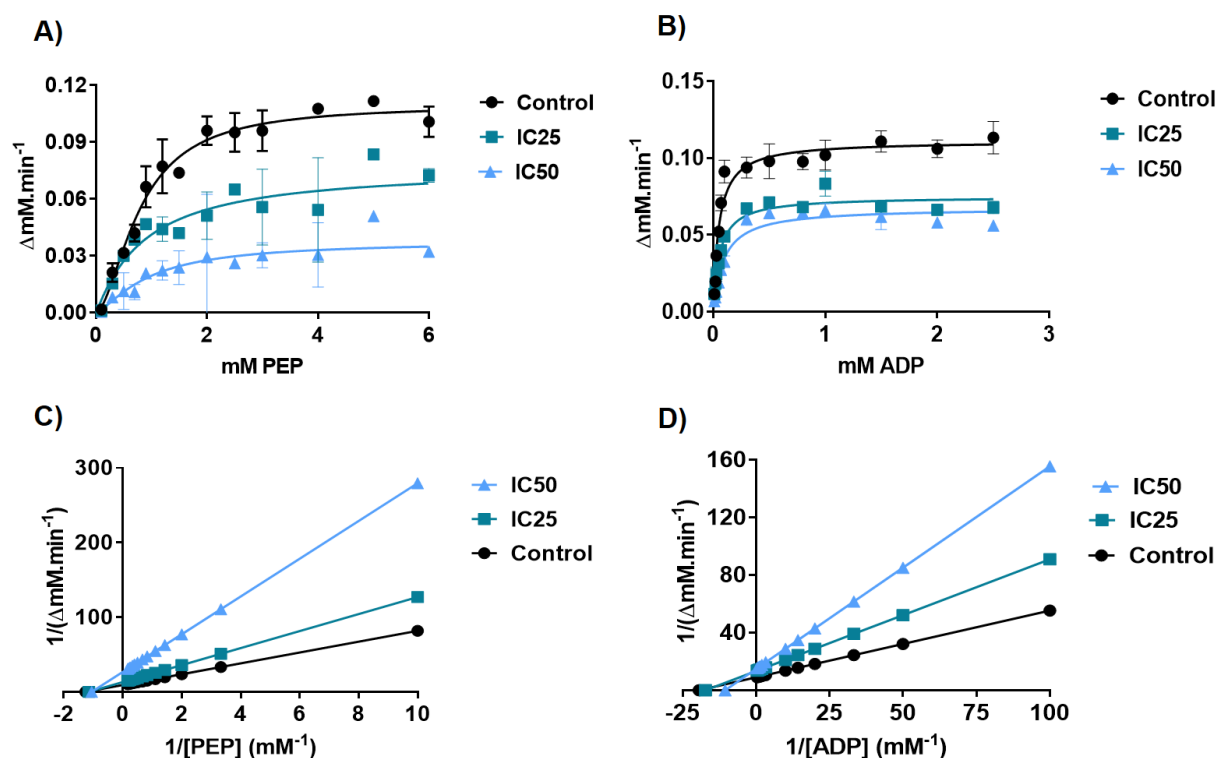
Figure 4.19: Inhibitory effects of shikonin on PykA kinetics. A, B: The effects of shikonin on the PEP- and ADP-dependency of PykA kinetics. PykA kinetics were measured at 13.4 µM (IC25) and 23.22 µM (IC50) of shikonin. With respect to [PEP], ADP was used at 2 mM and PEP was used at variable concentrations, whereas with respect to [ADP], PEP was used at 5 mM and ADP was used at variable concentrations. The experiments were performed in triplicates and standard errors are shown. **C, D:** Lineweaver-Burk plots showing the effects of shikonin on PEP and ADP titration kinetics. The y-intercept and the x-intercept indicate $1/V_{max}$ and $-1/S_{0.5}$, respectively. All graphs were generated using GraphPad Prism.

4.7.4 Inhibitory effects of R396907 on PykA kinetics

Similar to shikonin, I investigated the effects of IC25 (47.4 µM) and IC50 (95.5 µM) of R396907 on PykA kinetics. Experiments were repeated with respect to PEP titration (variable PEP concentration and 2 mM ADP) and ADP titration (at variable ADP concentrations and 5 mM PEP). The PykA kinetics with R396907 revealed that this compound seemed to inhibit PykA using different mechanisms than the ones identified for shikonin (Figure 4.20 and Table 4.6).

With respect to [PEP], R396907 inhibited the PykA activity primarily by competitive inhibition. At IC25 and IC50 of R396907, $S_{0.5}$ of PykA was increased, whereas V_{max} was almost unchanged and this pattern was consistent with competitive inhibition. This type of enzyme inhibition is achieved when the inhibitor binds to the active site of the enzyme causing a decline in the binding affinity of the enzyme to its substrate without changing the maximal activity, thereby the $S_{0.5}$ of the enzyme increases while the V_{max} is not changed. Competitive inhibition is considered a reversible type of inhibition that can be abolished by the addition of more substrate molecules.

With respect to [ADP], R396907 inhibited PykA by two types of inhibition according to the concentration of R396907. At IC25, the K_M of PykA was unchanged but the V_{max} was decreased consistent with non-competitive inhibition. Whereas at the IC50 dose, the K_M of PykA was increased and the V_{max} was decreased indicating mixed type of inhibition. Overall with respect to both substrates, R396907 caused a decline of the catalytic turnover number and the catalytic efficiency of PykA, in a dose-dependent manner.

Table 4.6: Changes in the kinetic parameters of PykA in the presence of R396907. The inhibitor was used at 0 μM (control), 47.4 μM (IC25) or 95.5 μM (IC50). [PEP] was performed by using variable concentrations of PEP (0-6 mM) and 2 mM ADP, whereas [ADP] was performed by using variable concentrations of ADP (0-2.5 mM) and 5 mM of PEP. Each experiment was performed in triplicates and standard errors are shown. Kinetics were calculated using GraphPad Prism7.

		Control	IC25	IC50
PEP	$S_{0.5}$ (mM)	0.73 ± 0.01	1.76 ± 0.09	3.2 ± 0.3
	Hill coeff. (h)	3 ± 0.23	2.43 ± 0.22	2.01 ± 0.18
	V_{max} (ΔmM.min^{-1})	0.0811 ± 0.001	0.08166 ± 0.003	0.074 ± 0.006
	k_{cat} (s^{-1})	368.6	356.2	323
	$k_{cat}/S_{0.5}$ (s^{-1}.mM^{-1})	504.9	202.4	100.9
ADP	K_M (mM)	0.06 ± 0.007	0.065 ± 0.007	0.098 ± 0.007
	V_{max} (ΔmM.min^{-1})	0.09 ± 0.002	0.0652 ± 0.001	0.065 ± 0.001
	k_{cat} (s^{-1})	409.09	284.4	286.2
	k_{cat}/K_M (s^{-1}.mM^{-1})	6818.1	4375.3	2920.5
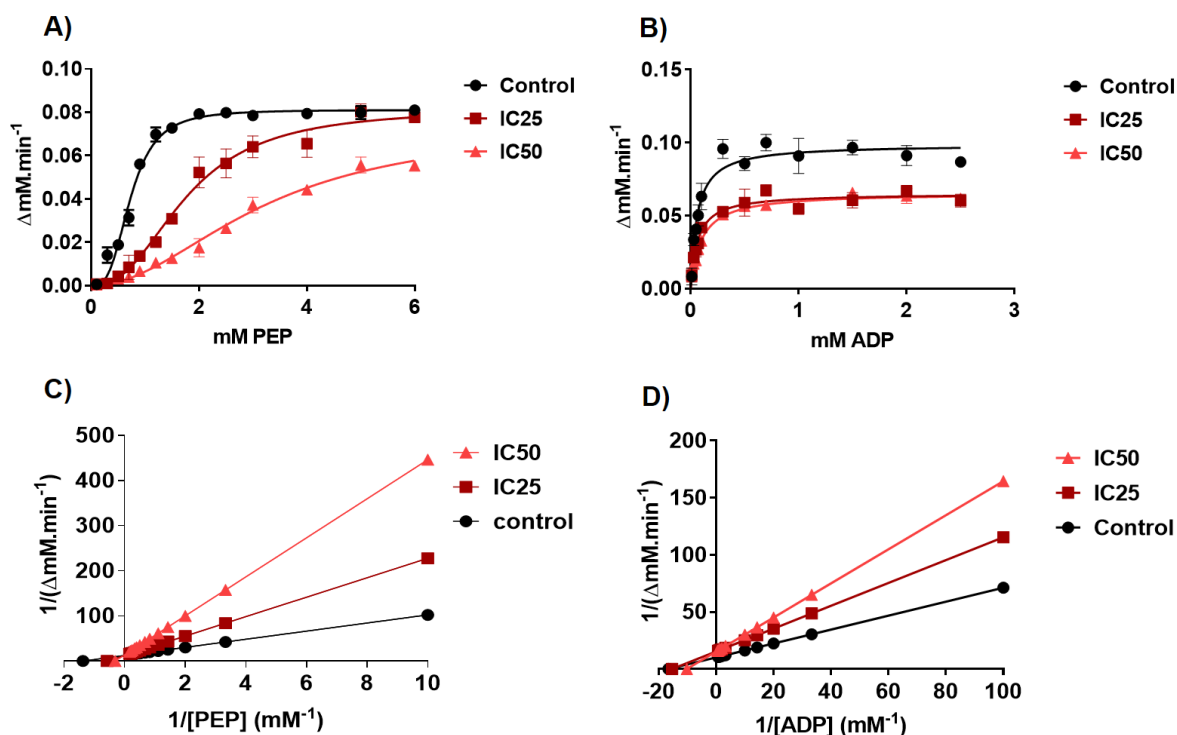
Figure 4.20: Inhibitory effects of R396907 on PykA kinetics. A, B: The effects of R396907 on the PEP- and ADP-dependency of PykA kinetics. PykA kinetics were measured at 45.4 μM (IC25) and 95.5 μM (IC50) of R396907. With respect to [PEP], ADP was used at 2 mM and PEP was used at variable concentrations, whereas with respect to [ADP], PEP was used at 5 mM and ADP was used at variable concentrations. The experiments were performed in triplicates and standard errors are shown. **C, D:** Lineweaver-Burk plots showing the effects of R396907 on PEP and ADP titration kinetics. The y-intercept and the x-intercept indicate $1/V_{max}$ and $-1/S_{0.5}$, respectively. All graphs were generated using GraphPad Prism

4.7.5 The effects of PykA inhibitors on cell growth

To investigate the effect of PykA inhibitors *in vivo*, I measured the growth rate of PAO1 across a range of concentrations of shikonin (0.19 μM to 50 μM) and R396907 (0.48 μM to 500 μM). I used R396907 at higher doses than shikonin because as shown before, R396907 was a less potent inhibitor of PykA compared with shikonin. Cells were grown in 96-well plates containing LB or minimal media with glucose and growth was monitored following the addition of the inhibitors for 20 hr at 37°C.

Figure 4.21 shows that neither shikonin nor R396907 altered the growth of the cells in LB. This was unsurprising given that the LB is a very rich media with many ingredients that can promote growth. Cell growth was temporarily delayed at mid-exponential phase with 50 μM of shikonin, however growth soon took over and cells reached the same final OD_{600} similar to the wild-type.

Whilst growth in LB is not expected to be affected by PykA inhibitors, growth in minimal media with glucose as a sole carbon source is expected to be impaired since *pykA* has previously been shown to be important for growth on this substrate. Figure 4.22 shows that growth of cells in minimal media with glucose was clearly inhibited by shikonin, whereas no growth change was seen with R396907. The growth inhibition by shikonin was concentration-dependent from 50 μM to 6.25 μM, whereas doses of less than 6.25 μM concentration were ineffective. In the presence of shikonin, cells could not reach the same growth endpoint as those of the wild-type. On the other hand, R396907 failed to inhibit the growth in minimal media with glucose even at its maximum dose of 500 μM. Apart from that, the growth in minimal media with glucose had a prolonged lag phase for the first ten hours as compared with growth in LB, where the lag phase lasted only for five hours. This is acceptable given the limitation of nutrients in minimal media compared with the nutrient-rich LB.

4.7.5.1 Inhibition of growth of clinical isolates by shikonin

Because PAO1 is a laboratory strain and might not be representative of clinical strains, I tested the effect of shikonin on the growth of two clinical isolates. The isolates were collected from cystic fibrosis patients (Papworth Hospital, Cambridge) who were infected with *P. aeruginosa*. The strains were classified as fast growers in LB (personal communication with Dr. Emem-Fong Ukor).

Growth of the clinical isolates was performed in minimal media with glucose and at 50 μM shikonin and growth was monitored for 48 hr at 37ºC. Figure 4.23 shows that shikonin was able to inhibit the growth of the two isolates. With shikonin, the isolates failed to reach the same growth endpoint compared with the control cells without shikonin added.
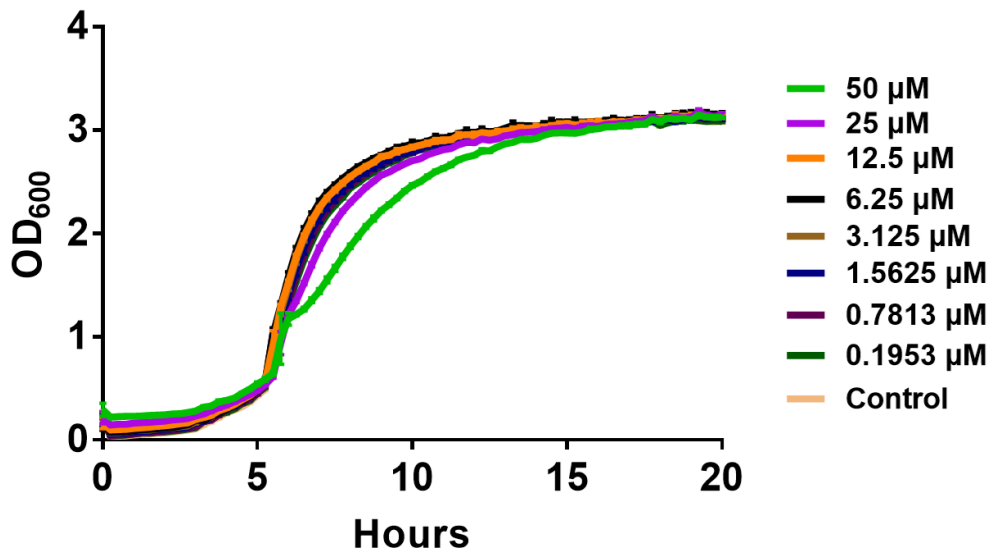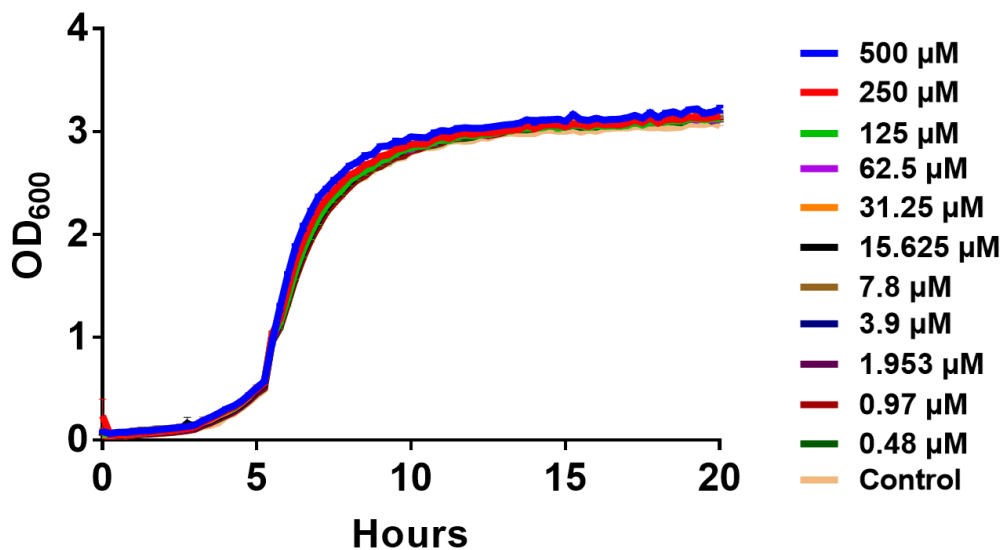
Figure 4.21: The effect of PykA inhibitors on growth of cells in LB. Growth of PAO1 was measured in LB across a range of concentrations of shikonin **(A)** and R396907 **(B)**. Cells were inoculated at OD_{600} of 0.05 in a 96-well plate containing LB and growth was monitored for 20 hr at 37°C using a microtiter plate reader. The data were collected from three biological replicates and error bars represent standard errors.
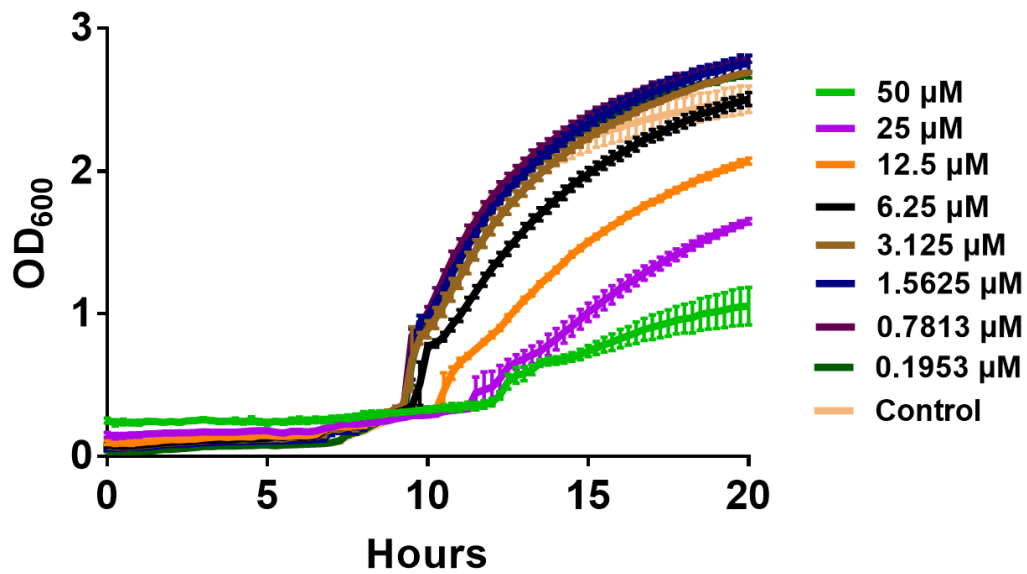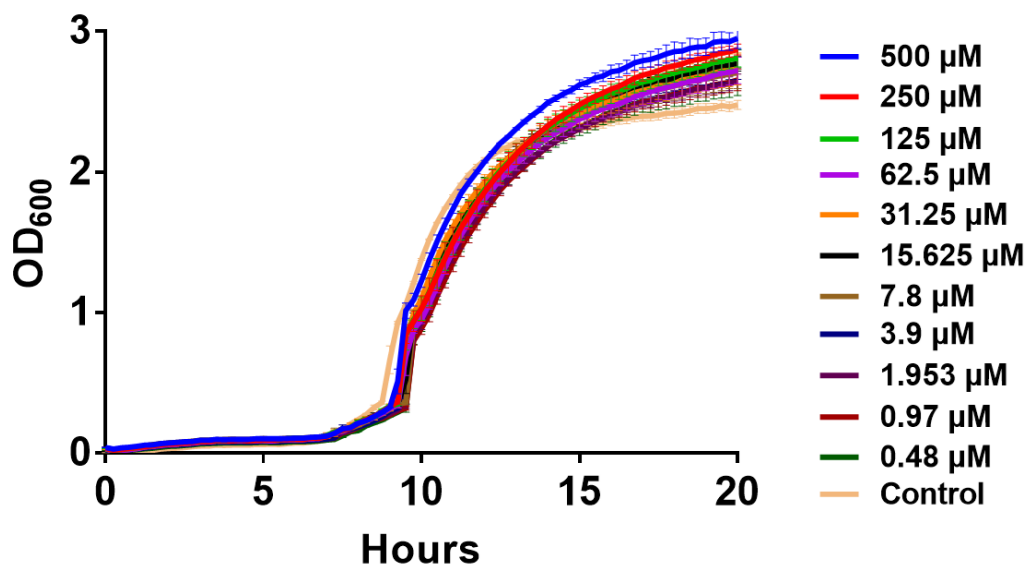
Figure 4.22: The effect of PykA inhibitors on growth of cells in minimal media with glucose. Growth of PAO1 was measured in minimal media with 20 mM glucose across a range of concentrations of shikonin **(A)** and R396907 **(B)**. Cells were inoculated at OD_{600} of 0.05 in a 96-well plate containing the media and growth was monitored for 20 hr at 37°C using a microtiter plate reader. The data were collected from three biological replicates and error bars represent standard errors.
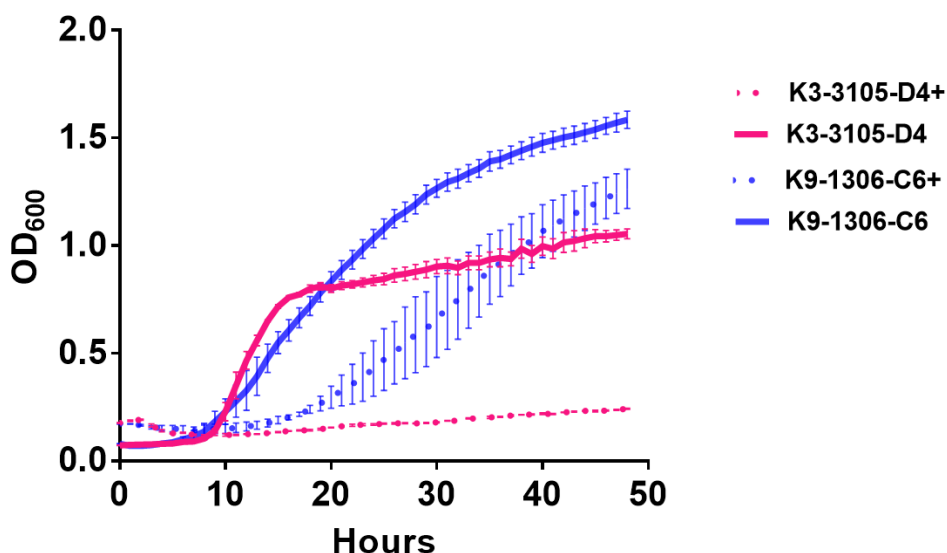
Figure 4.23: Inhibition of growth of clinical isolates by shikonin. Clinical isolates were grown in minimal media with 20 mM glucose in the presence of 50 μM shikonin. Cells were inoculated at OD_{600} of 0.05 in a 96-well plate and growth was measured at 37°C for 48 hr using a microtiter plate reader. Solid lines represent growth of cells without shikonin and dotted lines represent growth with shikonin. The data represent the mean of three biological replicates and standard errors are shown.

4.8   Discussion

4.8.1   Kinetic properties of PykA and PykF

PykA and PykF responded equally to titration of PEP (with sigmoidal kinetics) and to titration of ADP (with hyperbolic kinetics). However, the kinetic constants revealed that PykA was intrinsically more active than PykF. This was clearly demonstrated by the lower $S_{0.5}^{PEP}$ and K_M^{ADP} of PykA compared with PykF. Given the catalytic turnover number (k_{cat}) was almost equal for both isozymes, the catalytic efficiency ($k_{cat}/S_{0.5}$) of PykA was substantially higher than PykF for both substrates. The higher activity of PykA compared with PykF is consistent with findings of chapter 3 which showed that *pykA* was the dominant isozyme and not *pykF*.

Many PK enzymes require the presence of monovalent ions, particularly K^+, in order to achieve 100% catalytic activity (Kachmar and Boyer, 1953). For example, the activity of PykF in *E. coli* greatly increases with monovalent ions (NH_4^+, K^+, Ti^+, Rb^+, Cs^+,

Li$^+$, Na$^+$) and reaches maximum activity when K$^+$ is added (Waygood et al., 1976). The main function of K$^+$ during catalysis by PK is to participate in neutralization of the negatively charged active site and this facilitates the transfer of the phosphoryl group from PEP to ADP (Westheimer, 1987).

Findings of this chapter revealed that K$^+$ was not required for PykA or PykF catalytic activity. The K$^+$-independence of PykA and PykF can be attributed to the amino acid sequence of these enzymes. K$^+$-dependent enzymes were found to encode a glutamate equivalent to Glu117 in rabbit PK, whereas K$^+$-independent PK often encode a lysine equivalent to Glu117 in rabbit PK (Laughlin and Reed, 1997; Oria-Hernández et al., 2006). Structural data revealed that these residues lie in a hinge region which contributes to the acquisition of the active conformation of PK enzymes. Amino acid sequence alignment of PykA and PykF using rabbit PK as a reference revealed that both isozymes encode a lysine in the position of Glu117 in rabbit PK (Figure 4.24). This verifies my findings that PykA and PykF were independent on K$^+$. The lysine residue in K$^+$-independent PK enzymes (such PykA and PykF from PAO1) acts as an integral positive ion and replaces the function of K$^+$ in the active site (Laughlin and Reed, 1997). Moreover, the perturbations of PykA and PykF activities after the addition of K$^+$ and other monovalent ions can be due to disturbance of the ionic strength in the reaction following the increase of these positive charges. This question can be answered in future work.

```
                           110       120       130       140       150       160
                           |         |         |         |         |         |
P11974_Rabbit_PKM/1-530          PVAVALDTKGPEIRTGLIKGSGTAEVELKKGATLKITLDNAYMEKCDENILWLDYKNICKVVDV
Q9HW72_P.aeruginosa_PykA/1-483   FVALLGDLQGPKIRIAKFANKR---IELQVGDKFRFSTSHAR-DAGTQEVVGIDYPDLVKDCGV
Q9I3L4_P.aeruginosa_PykF/1-477   PIGVLMDLQGPKLRVGRFAAGA---VQLQRGQTFTLDLSDA---PGDERRVNLPHPEIIHALEP
A1JRG5_Y.pestis_PykA/1-480       HVAILGDLQGPKIRVSTFKEGK---VFLNIGDKFLLDANMAK-GEGDKEKVGIDYKGLPADVVP
A1JPB0_Y.pestis_PykF/1-470       KAGILLDTKGPEIRTMKLEGGK--DAALIAGQTFTFTTDQSVIG--NNNIVAVTYPGFAADLKI
P21599_E.coli_PykA/1-480         HVAILGDLQGPKIRVSTFKEGK---VFLNIGDKFLLDANLGK-GEGDKEKVGIDYKGLPADVVP
P0AD61_E.coli_PykF/1-470         TAAILLDTKGPEIRTMKLEGGN--DVSLKAGQTFTFTTDKSVIG--NSEMVAVTYEGFTTDLSV
Q8ZNW0_S.typhimurium_PykA/1-480  HVAILGDLQGPKIRVSTFKEGK---VFLNIGDKFLLDANLGK-GEGDKEKVGIDYKGLPADVVP
P77983_S.typhimurium_PykF/1-470  KAAILLDTKGPEIRTIKLEGGN--DVSLKAGQTFTFTTDKSVVG--NNEIVAVTYEGFTSDLSV
```

Figure 4.24: Amino acid sequence alignment using PK from rabbit as a reference. The figure shows Glu117 in rabbit PK (highlighted in blue) and its equivalent residues in other species which dictate whether an enzyme is K$^+$-dependent (if the equivalent residue is glutamate) or K$^+$-independent (if the equivalent residue is lysine). Each enzyme is identified using its Uniprot ID, species of origin and gene name. The amino acid sequence alignment was performed using JalView.

4.8.2   Metabolic regulation of PykA and PykF

The most striking finding in this chapter was the unusual metabolic regulation of PykA and PykF from *P. aeruginosa*. Functional characterization revealed that PykA is activated by metabolites from the EDP (KDPG, G6P, G3P), PPP (R5P, RL5P, X5P) and EMPP (F6P from EMPP operating in gluconeogenic direction), whereas it was insensitive to AMP. Moreover, the PykF from PAO1 was also activated by metabolites from the EDP (G6P, G3P) and PPP (R5P, RL5P, X5P, AMP) and it was insensitive to F6P and F1,6P. These findings contradict the established regulation of PykA and PykF in other bacteria. In other species, PykA is activated by R5P and AMP, whereas PykF is activated primarily by F1,6P (Waygood et al., 1975; Garcia-Olalla and Garrido-Pertierra, 1987).

The observed discrepancy of PykA and PykF regulation is mostly governed by the mechanism of glycolysis and the dominant isozyme in a given bacteria. In Enterobacteriaceae, the EMPP is the main glycolytic pathway and the EDP plays a marginal role. Moreover, PykF in these species is the dominant isozyme, whereas PykA is the less important one. Therefore, it is sensible to conclude that PykF in these bacteria is activated by metabolic signals (such as F1,6P) from the EMPP, whereas PykA can be only activated by metabolites (R5P and AMP) from the peripheral metabolic pathways (PPP).

The same principle can be applied to explain the regulation of PykA and PykF in *P. aeruginosa*. This pathogen lacks the phosphofructokinase and 6-phosphogluconate dehydrogenase that are required for operation of the EMPP and the upper arm of the reductive PPP, respectively (Lessie and Phibbs, 1984; Temple et al., 1998; Berger et al., 2014). Thus, *P. aeruginosa* is exclusively reliant on the EDP for glycolysis similar to some 13% of species for which a genome sequence is available (Flamholz et al., 2013). Moreover, pseudomonads have the capability to recycle metabolites from the main EDP into the side branches of the EMPP and the lower arm of the PPP (known as the EDEMP or the cyclic EDP) (Conway, 1992; Lee et al., 2015a; Nikel et al., 2015a). I conclude that metabolites from the three pathways may be signals to activate the dominant PK. Given that PykA is the dominant isozyme in *P. aeruginosa*, it is not surprising that it is activated by metabolites from the EDP and the PPP (Figure 4.25), while PykF is regulated primarily by metabolites from the PPP.
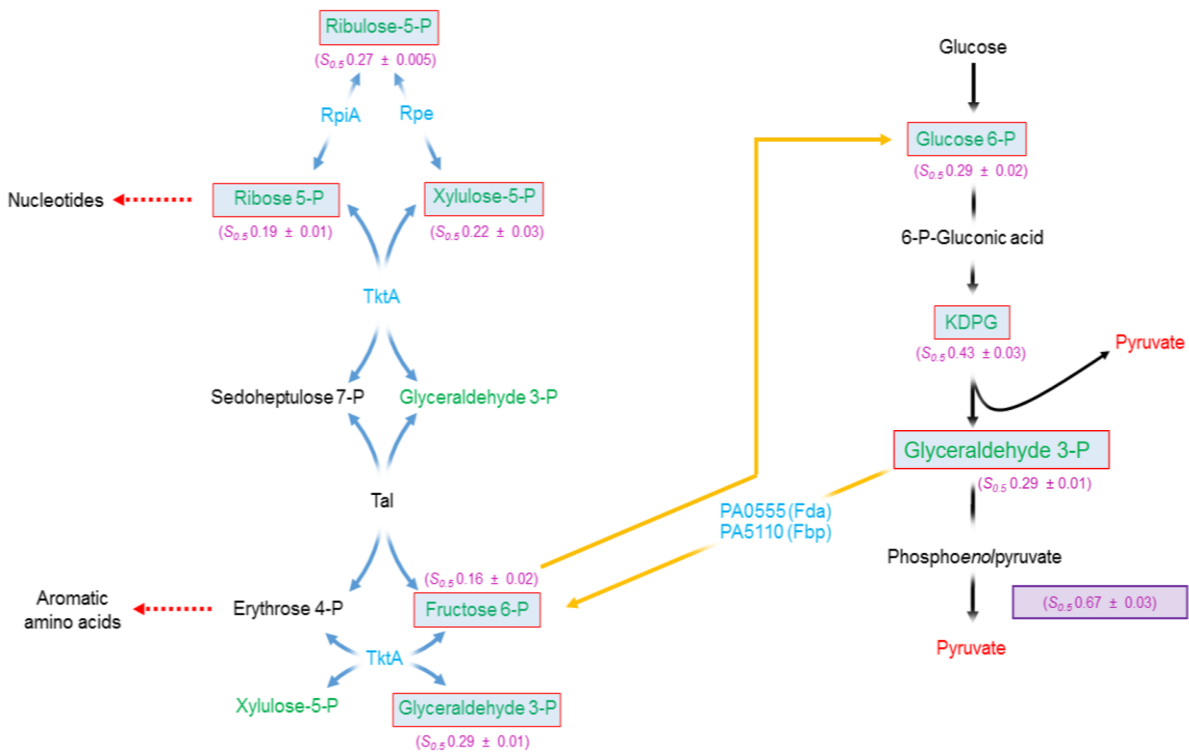
Figure 4.25: The metabolic regulation of PykA. Metabolic pathways are shown by black (EDP), blue (PPP) and yellow (EMPP operating in gluconeogenic direction) arrows, respectively, whereas pathways involved in biosynthetic processes are shown by red dotted arrows. Fructose 6-phosphate is shown as part of the PPP as the gluconeogenic EMPP and PPP are tightly connected. The regulators of PykA are shown in red boxes and the respective $S_{0.5}$ of PykA is shown as indicated. The $S_{0.5}$ of PykA without regulators is shown in a violet box. The $S_{0.5}$ values were calculated from titration of [PEP] at 2 mM ADP and 1 mM regulator except for F6P (0.2 mM), R5P (0.15 mM) and X5P (0.5 mM). GraphPad Prism7 was used for calculation of the $S_{0.5}$ according to the best-fit nonlinear regression using the allosteric sigmoidal equation. Each experiment was done in triplicates and standard errors are shown. Abbreviations: RpiA, ribose 5-phosphate isomerase; Rpe, ribulose phosphate 3-epimerase; TktA, transketolase; Tal, transaldolase; Fda, fructose 1,6-bisphosphate aldolase; Fbp, fructose 1,6-bisphosphatase; KDPG, 2-*keto*-3-deoxy-6-P-gluconate.

There seem to be many benefits for the cell during operation of the EDEMP pathway. One of these is the continuous supply of F6P which is a crucial component in production of exopolysaccharides. In EDEMP, F6P is supplied at a relatively low energy cost compared with its direct production from the EMPP (May et al., 1991). Besides F6P,

other metabolites from the EDEMP such as G6P, F1,6P, and DHAP are known to be essential for biomass production (Nikel et al., 2015a). Also, intermediates from the PPP (R5P, X5P, RL5P) which strongly activate PykA and PykF, are essential for production of nucleotides precursors and the redox equivalents required to cope with stressful conditions (Juhnke et al., 1996; Christodoulou et al., 2018). Therefore, it seems that *P. aeruginosa* has evolved to coordinate glucose oxidation with production of essential biosynthetic precursors mainly through activation of PykA.

4.8.3 The anti-*Pseudomonas* effects of shikonin

Shikonin is a natural product that is extracted from the *Arnebia euchroma* plant and is commonly used in the traditional Chinese medicine (Liu et al., 2013). The compound and its derivatives are known for their broad therapeutic effects including promotion of wound healing, anti-inflammatory and anti-microbial properties, inhibition of free radicals and more recently, anti-cancer effects (Kourounakis et al., 2002; Papageorgiou et al., 2008; Chen et al., 2011; Zhao et al., 2018; Lee et al., 2015b). As far as I am aware, there has been no work done to investigate the mechanism by which shikonin confers its antimicrobial properties. Here, I have shown that shikonin has anti-*Pseudomonas* effects which are promoted by targeting PykA.

Comparison between shikonin and R39607 revealed that the inhibitory properties of shikonin by far outweigh those of R396907. My findings revealed that shikonin inhibits PykA activity by non-competitive and mixed inhibition mechanisms, whereas R396907 inhibits PykA competitively. This means that shikonin binds to the enzyme-substrate complex in an irreversible manner and increasing [substrate] cannot displace the bound shikonin. On the other hand, R396907 is a competitive inhibitor, anticipated to bind to the active site in a reversible fashion. In addition, dose-response curves revealed that the IC50 of R396907 (95.5 μm) is four times more than the IC50 of shikonin (23.4 μm) and this highlights the potency of shikonin as a robust PykA inhibitor compared with R396907. Furthermore, shikonin has demonstrated inhibitory properties *in vivo* compared with R396907, which was ineffective.

One of the main reasons for the failure of antimicrobials in *P. aeruginosa* is due to the low outer membrane permeability of the organism (Westbrock-Wadman et al., 1999). Having said that, the cell surface of *P. aeruginosa* seemed to be permeable to shikonin allowing the compound to enter the cells and to exert its inhibitory effects. *In vivo*, shikonin inhibited the growth of *P. aeruginosa* in glucose minimal media and this was consistent with findings of chapter 3 showing that loss of PykA function resulted in a reduction of growth in glucose minimal media. Moreover, shikonin was also able to decrease the growth of some clinical isolates that were previously identified as fast-growers. However, there was no detectable *in vivo* effect of R396907. There are many factors that possibly contribute to the failure of R396907 during *in vivo* studies. Firstly, it is a competitive inhibitor of PykA meaning that its inhibitory effects might have been abolished if the PEP concentration was high so that PEP can displace R396907 from the active site of PykA. Secondly, it could be possible that the cell surface of *P. aeruginosa* was impermeable to R396907 and that the inhibitor was unable to enter into the cell. Thirdly, it is possible that R396907 successfully enters the cell but is pumped out again, given that surface of *P. aeruginosa* is equipped with multiple drug efflux pumps (Westbrock-Wadman et al., 1999; Schweizer, 2003). These possibilities can be addressed in future research.

Future work should investigate further if *P. aeruginosa* is an actual microbial target for shikonin. From an experimental perspective, a rich broth such as LB is not the best comparator for glucose minimal media. Therefore, future experiments should measure the effects of shikonin during the growth of PAO1 and mutants in glucose and other less-rich media such as acetate minimal media where the growth of PAO1 and the PK mutants is supported equally well (chapter 3). Future work should also investigate if overexpression of PykA can reduce the drug efficacy of shikonin. Moreover, the efficacy of shikonin should also be checked in an animal model of *P. aeruginosa* infection. Finally, the amino acid sequence (or crystal structure) of PykA can be used for docking of PykA using shikonin as a ligand and this should help identify the potential binding site(s) of shikonin in PykA. Once a binding site is detected, site-directed mutagenesis of PykA can be used to identify the essential residues for shikonin binding.

4.9 Conclusion

P. aeruginosa encodes PykA and PykF isozymes which were uncharacterized (until this study). Here, I investigated the biochemical properties of purified PykA and PykF from *P. aeruginosa*. My findings reveal that PykA is intrinsically more active than PykF. I have also shown that unlike many PK, these enzymes are K^+-independent owing to the fact that they encode a lysine residue at a position equivalent to Glu117 in rabbit PK which can replace the function of the K^+ in the active site. Moreover, I identified activators of PykA and PykF, with the most potent ones derived from the PPP. This highlights that *P. aeruginosa* has possibly evolved to coordinate glucose oxidation with production of essential biosynthetic precursors. Moreover, findings of this chapter has have shown that PykA is likely to be a potential target for antimicrobial intervention.

Chapter 5

5 Crystal structures of PykA and PykF

5.1 Introduction

More than 80% of PK structures in the PDB belong to eukaryotes, whereas the number of PK structures from prokaryotes is limited. So far, there is only one bacterial PK structure with metabolites (apart from metal ions) bound to the allosteric site which belongs to the PK of *M. tuberculosis*. Most importantly, there is no structure of any PykA isozyme, whereas the PykF isozyme from *E. coli* has been previously determined.

In this chapter, I demonstrate the first x-ray crystal structures of PykA and PykF from *P. aeruginosa*. The PykA was modelled with a G6P bound in the allosteric site, and a malonate and a Mg^{2+} bound in the active site. By contrast, PykF was modelled in the apo state. Analysis of the PykA and PykF structures show that they both have different properties than the previously modelled PKs from prokaryotes. I found that the G6P binding site in PykA is distinct from the previously identified G6P binding site in the PK of *M. tuberculosis*, meaning that the G6P regulation of PykA is likely to be different compared with *M. tuberculosis* PK. Likewise, comparison of *P. aeruginosa* PykF and *E. coli* PykF demonstrates an extra short helix (Cα1') present only in PykF from *P. aeruginosa* and absent in the *E. coli* isozyme, and this helix is apparently important for enzyme stability as well as for the transmission of conformational signals between the subunits.

5.2 Crystallization, data collection and model building

5.2.1 Crystallization of PykA and PykF

PykA and PykF crystals were obtained from screening using sitting drop vapour diffusion, where the protein and mother solution were mixed in 1:1 ratio. The PykA structure was obtained from co-crystallization of PykA with PEP, G6P and $MgCl_2$, and a mother solution consisting of 20% (w/v) PEG 3350, 200 mM sodium malonate and 100 mM Bis-Tris propane at pH 7.5. This mixture was essential for obtaining a PykA crystal that diffracted and any change in the ingredients caused either no growth or no diffraction of the crystal (Figure 5.1). Also, other co-crystallization trials of PykA with PEP

alone, MgCl$_2$ alone, F6P, R5P, Shikonin, R396907, KCl or using His-tagged PykA were unsuccessful.

The PykF crystals were also produced from screening after co-crystallization of PykF with PEP, KCl and MgCl$_2$, and a mother solution containing 25% (w/v) PEG 6000 and 0.1 M Hepes pH 7.5. Co-crystallization components were also essential for both development of the PykF crystal and for obtaining a good diffraction data (Figure 5.2). Similar to PykA, other co-crystallization trials of PykF with PEP alone, MgCl$_2$ alone, G6P, R5P or using His-tagged PykF were unsuccessful. PykA and PykF crystals both appeared after two days of setting up the crystallization plates and crystals were harvested at the sixth day.

PEP	+	-	+	+	-
MgCl$_2$	+	+	+	-	-
G6P	+	+	-	-	-
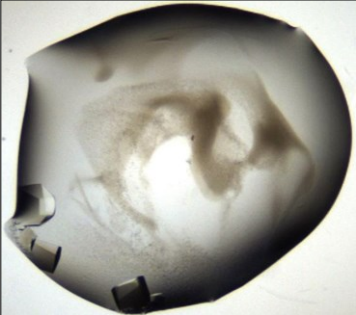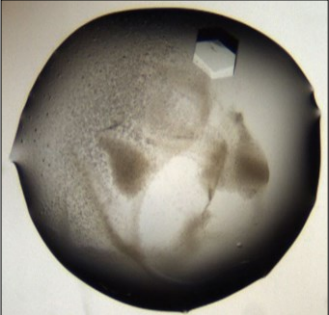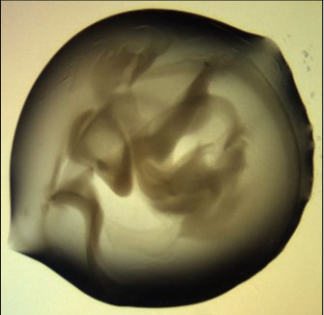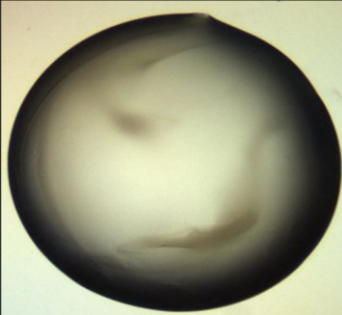
2.43 Å	No diffraction	No crystals	No crystals	No crystals
(used in this study)				

Figure 5.1: The effect of co-crystallization conditions on growth and diffraction of PykA crystals. Light microscope images of PykA crystallization drops taken after five days of incubation in a mother solution containing 20% (w/v) PEG 3350, 200 mM sodium malonate and 100 mM Bis-Tris propane pH 7.5. The PykA (22.4 mg/ml) was mixed with 2 mM PEP, 2 mM G6P, or 20 mM MgCl$_2$ (as indicated) before being added to the mother solution. Drops were visualized using ROCK IMAGER.

PEP	+	-	+	+	-
KCl	+	+	-	-	-
MgCl$_2$	+	+	+	-	-
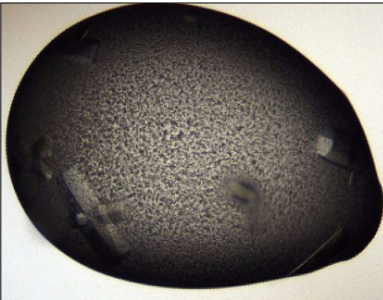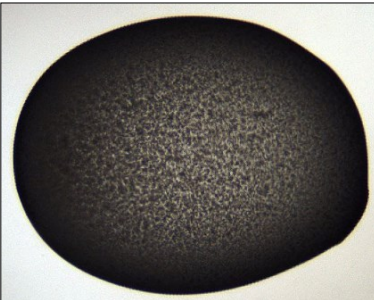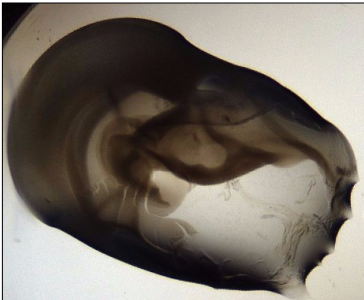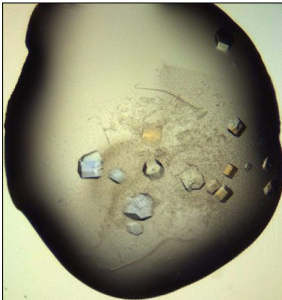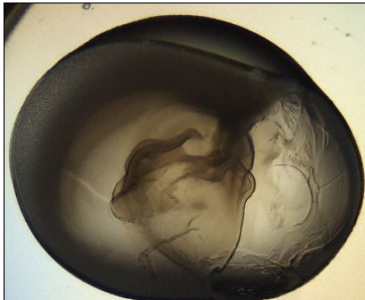
3 Å	No crystals	No crystals	No diffraction	No crystals
(used in this study)				

Figure 5.2: The effect of co-crystallization conditions on growth and diffraction of PykF crystals. Light microscope images of PykF crystallization drops taken after six days of incubation in a mother solution containing 25% (w/v) PEG 6000 and 100 mM Hepes pH 7.5. The PykF (29 mg/ml) was mixed with 2 mM PEP, 200 mM KCl, or 20 mM MgCl$_2$ (as indicated) before being added to the mother solution. Drops were visualized using ROCK IMAGER.

5.2.2 Data collection and model building of PykA

The full length (483 residues) PykA crystal diffracted to 2.43 Å, untagged. The data were processed with space group P3$_1$21, with 100% completeness. Statistical data of PykA and PykF are shown in Table 5.1. Molecular replacement of PykA was performed using the BALBES Pipeline (Long et al., 2008), and *T. brucei* (32% amino acid identity) was used as a search model. The asymmetric unit of PykA comprised 12 chains, denoted as chain A to chain L. After several rounds of manual model building using Coot and *REFMAC5* for refinement, the crystallographic R factor and free R of PykA reached 0.23 and 0.26, respectively, indicating agreement of the PykA model with the experimental diffraction data.

Generally, the PykA model fitted well in the electron density, except for a weak signal noted in chain J (residue 70-175). This region of chain J was far from any crystal contacts and was left unmodelled. Geometrical analysis of PykA revealed that Thr282 was a consistent Ramachandran outlier across all chains. This residue had a well-defined electron density, although it was consistently plotted as an outlier on the phi and psi geometrical plots (Appendix 1). The unusual geometry of Thr282 was observed before in the corresponding threonine of many PK structures. In these structures, they considered the odd geometry of this residue acceptable, given its location in the active site of the enzyme, within a highly restricted environment. This threonine is also known to facilitate the interaction between the active site and the substrate in other PykF structures.

5.2.3 Data collection and model building of PykF

The full length (477 residues) PykF crystal diffracted to 3 Å, untagged. The PykF data were processed with space group P321 with 99.7% completeness (Table 5.1). Phases of PykF structure were obtained using Phaser MR (McCoy et al., 2007) against a PykF ensemble that was generated using a Swiss model (Waterhouse et al., 2018). The asymmetric unit of PykF comprised two chains, denoted as chain A and B. After several rounds of model building (using Coot) and refinement (using PHENIX), the crystallographic R factor and free R of PykF reached 0.23 and 0.27, respectively, indicating agreement of the PykF model with the experimental data. Geometrical analysis demonstrated that the PykF model was generally acceptable with more than 99% of

residues present within the allowed Ramachandran regions. Similar to PykA, the active site residue Thr275 of PykF (corresponding to Thr282 in PykA) was also depicted as an outlier on the geometrical plots of the two chains of PykF (Appendix 2).

Table 5.1: Data collection and refinement statistics of PykA and PykF.

	PykA/G6P/MLI/Mg^{2+}	Apo PykF
Radiation source	Diamond (UK), I04-1	Diamond (UK), I04-1
Data collection		
Wavelength	0.9159	0.9159
Resolution range (Å)	405.44-2.43 (2.49-2.43)	115.14-3.01 (3.09-3.01)
Space groups	P3$_1$ 2 1	P3 2 1
Cell dimensions		
a, b, c (Å)	182.48, 182.48, 405.04	169.05, 169.05, 115.11
α, β, ɣ (º)	90, 90, 120	90, 90, 120
Total reflections	4318494 (226510)	1772874
Unique reflections	292996 (21477)	37859
Multiplicity	14.7 (10.5)	46.8 (21.2)
Completeness (%)	100.0 (100.0)	99.7 (94.0)
Mean I/sigma(I)	11.1 (1.1)	16.3 (1.2)
Wilson B-factor	55.5	115.96
R-merge	0.143 (2.210)	0.139 (3.014)
R-meas	0.148 (2.324)	0.140 (3.088)
CC half	0.999 (0.642)	1.000 (0.846)
Refinement		
Resolution range (Å)	158.03 – 2.43 (2.49-2.43)	73.20-3.01 (3.09-3.01)
Reflections used in refinement	275231 (19691)	37564 (2728)
Reflections used for R-free	14353 (1061)	1859 (110)
R-work	0.235 (0.438)	0.237 (0.505)
R-free	0.261 (0.456)	0.275 (0.502)
No. of molecules in the ASU	12	2

Table 5.1: Continued

	PykA/G6P/MLI/Mg^{2+}	Apo PykF
No. of non-hydrogen atoms		
Macromolecules	43,349	7213
Ligands	1075	n/a
Protein residues		
RMS (bonds) (Å)	0.01	0.01
RMS (angles) (°)	1.64	1.6
Ramachandran favoured (%)	96.98	94
Ramachandran allowed (%)	2.79	5.9
Ramachandran outliers (%)	0.23	0.1
Average B-factor		
Macromolecules	55.5	124
Ligands	55.65	n/a
Solvent	62.51	n/a

5.3 PykA tetramer and domain organization

The asymmetric unit of PykA comprised 12 subunits (Chain A to Chain L), in which four of the chains were already assembled into a homotetramer (Figure 5.3) and the rest of the chains were related by non-crystallographic symmetry. This was in agreement with analytical ultracentrifugation (AUC) analysis of PykA which demonstrated that the enzyme was a tetramer in solution (Appendix 3). The surface area of the complete PykA tetramer (Chains L, I, K, C) was 70240 Å^2 with accessible solvent area of 14490 Å^2. The tetramer assembly was stable in solution with a solvation free energy gain (ΔG) of -102 kcal/mol. Each subunit of PykA consisted of three domains; A, B and C (Figure 5.3, 5.4). The PykA tetramer contains four inter-protomer interfaces, two of which are between adjacent A domains (A-A interface) and two between adjacent C domains (C-C interface).
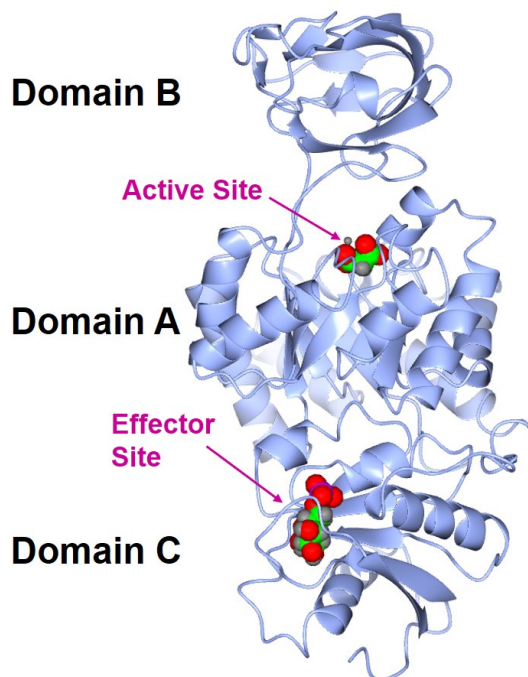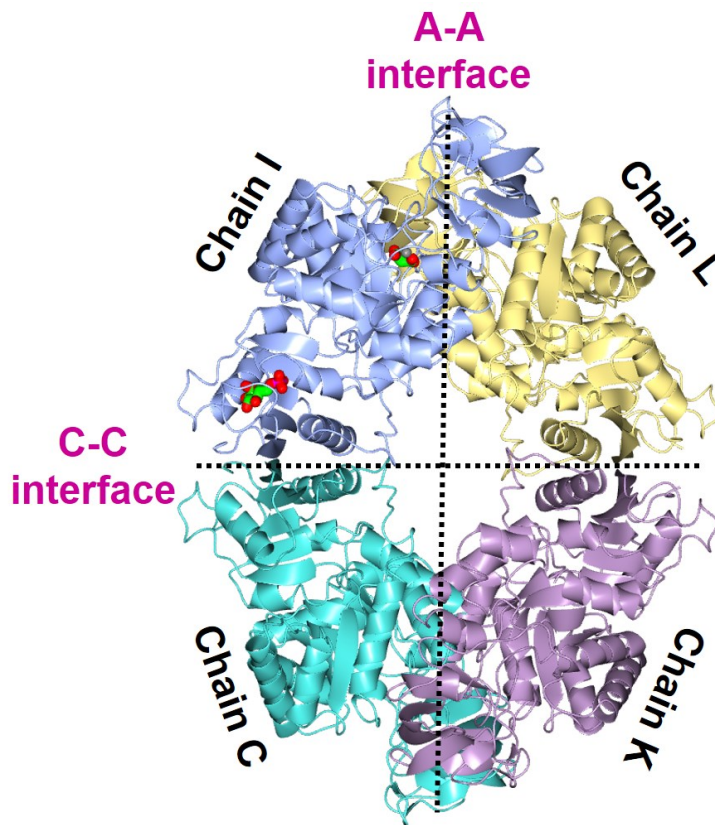
Figure 5.3: Structure of PykA. Top figure: Cartoon representation of a PykA tetramer. The dashed lines highlight the position of the A-A and the C-C interfaces within the tetramer. Bottom figure: Cartoon representation of a single PykA protomer with sodium malonate and Mg^{2+} bound in the active site (PykA-MLI-Mg complex) and G6P bound in the allosteric/effector site.

The A domain is located in the centre between the B and C domains and it is composed of two stretches of amino acids (residues 1-69 and 174-346) that are interrupted by the B domain. The A domain consists of eight alternating α-helices and β-strands forming a TIM barrel, where the α-helices encircle the β-barrel core. The Aα6 and Aα8 helices were subdivided into shorter segments; Aα6' and Aα8' which preceded Aα6 and Aα8, respectively. The B domain (residues 73-163) is present at the C-terminus of the A domain. It consists of nine β-strands (Bβ1...Bβ9) and a short α-helix (Bα1) that is positioned between the fourth and the fifth β-strands. The active site of PykA is found between the A and B domains and each active site is occupied by a malonate (MLI) and a Mg^{2+}, forming a PykA-MLI-Mg complex. The C domain (residues 360-480) is located at the N-terminus of the A domain and is composed of four alternating (α/β) structures with an additional terminal β-strand that runs antiparallel to the previous four ones. The allosteric site of PykA is present in the middle of the C domain and each allosteric site was occupied by a glucose 6-phosphate (G6P) molecule. Interactions of PykA with the bound ligands are detailed in the upcoming sections of this chapter.

In some PKs, the transition from the inactive (T-state) to the active (R-state) state is associated with movement of the B domain (Donovan et al., 2016). Motion of the B domain causes closure of the active site in these enzymes leading to improvement of enzyme substrate binding. However, in some cases such as the PK of *Toxoplasma gondii*, the B domain can have variable positions among the chains of the same model (Bakszt et al., 2010). Thus, in order to investigate if the B domain has variable positions among the PykA chains, I superposed the 12 chains of PykA to each other using PDBeFold. Superposition of the PykA chains generated an rmsd (root mean square deviations of atomic positions) range of 0.17 to 1.56Å, meaning that there is some movement seen among the chains (Appendix 4). However, the PDBeFold analysis does not define the movable part of the structure. Further domain motion analysis using the DynDom webserver was performed to depict the exact movable domain. In this analysis, chain E was used as a fixed model and its atomic position was compared with the rest of the chains. Domain motion analysis revealed that all the PykA chains pivot around the B domain region and that the B domain rotates to variable degrees (Appendix 5). This indicates that the B domain motion was likely the reason for the relatively high rmsd ranges. To verify this further, I deleted the B domains from all the chains, superposed the

chains on each other and re-measured the rmsd ranges using PDBeFold. After deletion of the B domain, the rmsd ranges declined (0.088 to 0.531Å) (Appendix 6) which confirms that the B domain has variable positions in the PykA structure.
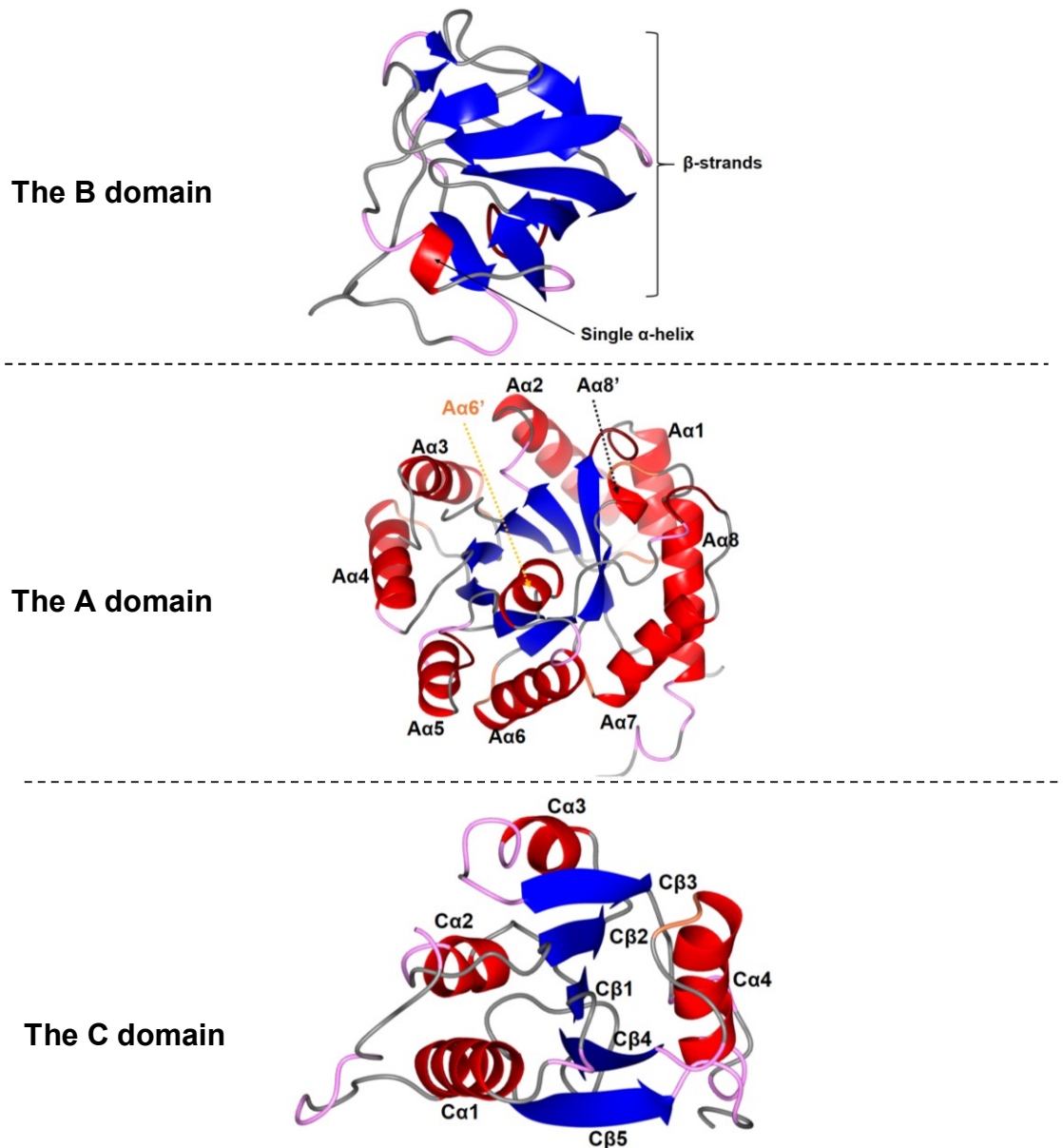
Figure 5.4: Secondary structures of PykA. Cartoon representation of secondary structures of a single PykA protomer. The α-helices and the β-strands are shown in red and blue, respectively. All ligands were removed for clarity. The B domain is β-rich and is found at the C-terminus of the A domain. The A domain is found at the core of the enzyme and is characterized by the presence of the active site helix Aα6'. The C domain is found at the N-terminus of the A domain and contains the allosteric site of the enzyme.

5.4   The active site of PykA

So far, there is one PK structure that has the active site occupied by PEP (the natural substrate of the enzyme) and this structure belongs to PK of *T. brucei* (PDB 4HYV). The PykA from *P. aeruginosa* (PykA$_{PA}$) was co-crystallized with PEP and Mg^{2+} in a mother solution containing MLI (an analogue of PEP). However, the crystal structure of PykA revealed that the active site did not contain PEP and instead, was complexed with MLI and Mg^{2+}, which I refer to here as the "PykA-MLI-Mg complex." The presence of MLI instead of PEP in the active site of PykA was likely due to the MLI (200 mM) in the co-crystallization solution.

5.4.1   The PykA-MLI-Mg complex

The MLI and Mg^{2+} were seen clearly at the cleft between the A and B domains, where the active site of PK structure lies. The electron density was good for this region in all PykA chains with F_o-F_c map of more than 3σ, indicating a clear ligand binding site (Figure 5.5A). Using chain E as a reference, the interface between MLI and PykA was measured to be approximately of 185 Å, burying around 83% of the ligand. The MLI coordinated with the Aα6' helix, Aβ2 strand, Aβ5-Aα5 loop, and the Aβ7-Aα7 loop via a series of hydrogen bonds. These interactions were between the hydroxyl moieties of MLI and the backbone of Gly249 (2.77 Å) and Asp250 (3.06 Å), and the side chains of Arg34 (3.25 Å), Lys221 (2.92 Å) and Thr282 (2.56 Å). Figure 5.5B shows the different interactions in the PykA-MLI-Mg complex.

Mg^{2+} was another component of the complex that seemed to stabilize the bound MLI through further interactions with the active site. The ion had a complete octahedral coordination sphere through six interactions with the surrounding structures, including interactions with the hydroxyl moieties of MLI, the adjacent water molecules and with the side chains of Glu223 and Asp250. The octahedral coordination sphere was confirmed using the metal binding site validation server (CheckMyMetal) and was found to be present in most of the PykA chains.

A)
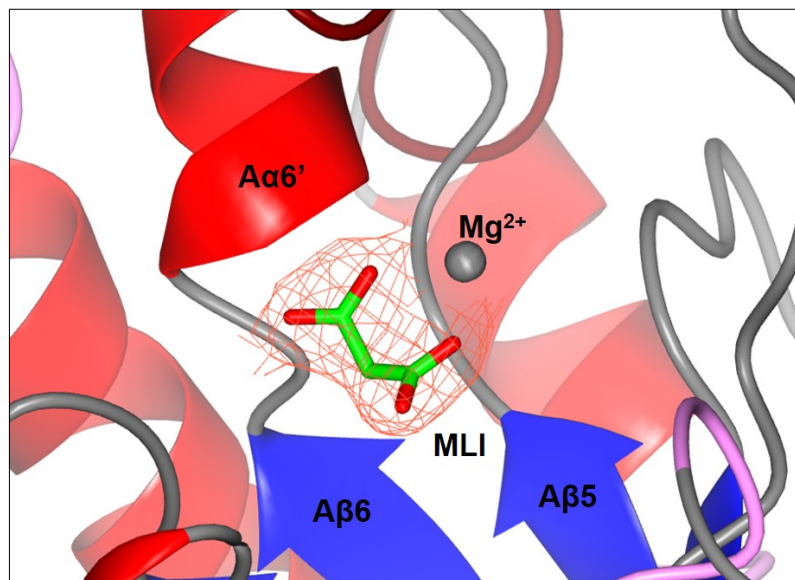
B)
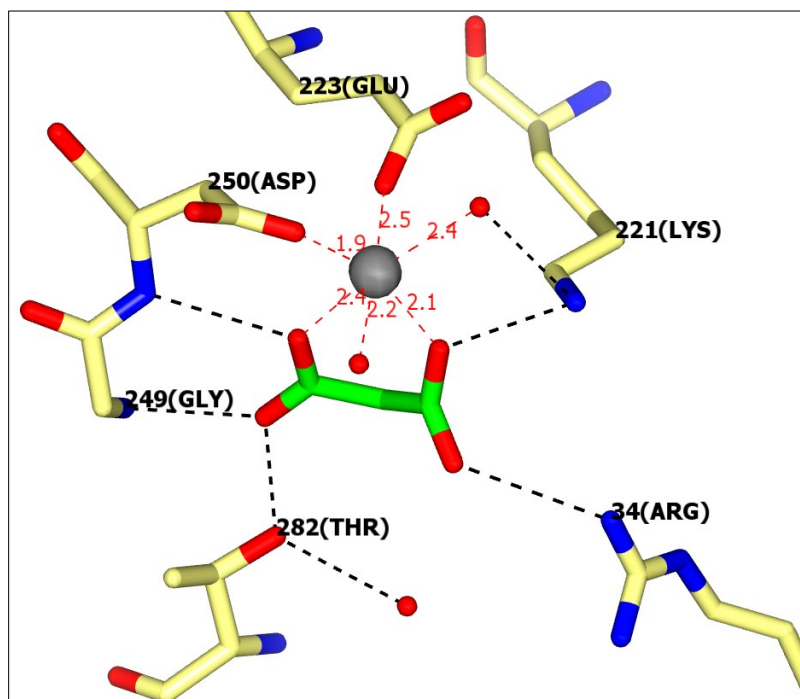
Figure 5.5: The PykA-MLI-Mg complex. A) Cartoon representation of the active site of PykA with bound MLI and Mg^{2+}. The electron density map (F_o-F_c) around the MLI and magnesium is shown as orange mesh and contoured at 3 σ. **B)** Interactions of the PykA-MLI-Mg complex. Active site residues and the bound MLI are shown as yellow and green sticks, respectively. The Mg^{2+} and water molecules are shown as grey and red spheres, respectively. The red dashed lines illustrate the octahedral sphere coordination of Mg^{2+} with the surrounding structures (distances in Angstroms) and the black dashed lines represent the interactions of PykA with MLI or water molecules.

5.4.2 Comparison of the active site of PykA$_{PA}$ with apo and bound PK structures

The ideal situation is to compare a bound enzyme with the apo form of the same enzyme in order to understand the changes associated with ligand binding. When the apo or the bound PK is not available, models from other species are often used instead. The crystal structure of PykF from *E. coli* (PykF$_{EC}$) in the apo state (PDB 1PKY) is suitable and has been used as an unbound model in many studies, when the unbound enzyme is not available. In contrast, PK from rabbit muscle (PKM1) is used as a model of a bound/active PK (PDB 1F3W), when the bound form is not available; this is because PKM1 is physiologically locked in the active state.

Unfortunately, I was not able to obtain a crystal of apo-PykA that diffracted beyond 4 Å in spite of crystallization and optimization trials. Therefore, I compared PykA$_{PA}$ (MLI-Mg-bound) with both PykF$_{EC}$ (PDB 1PKY) and PKM1 (PDB 1F3W) to study conformational changes in the active site. Comparison of bound PykA$_{PA}$ with apo 1PKY revealed that many of the active site residues were shifted in position. These included Arg34, Lys221, Glu223, Gly249 and Asp250 (Figure 5.6A). Additionally, the side chain of Thr282 was in a different orientation in PykA$_{PA}$, with the hydroxyl group facing the bound MLI. In contrast, superposition of the MLI-bound PykA$_{PA}$ and the pyruvate-bound PKM1 (PDB 1F3W) showed that the active site residues of the two structures superimposed well, in the same positions and orientations (Figure 5.6B). Moreover, the bound substrate analogues superposed very well in both structures.

5.4.3 Amino acid sequence alignment of the active site

To determine the degree of conservation of the active site residues in PykA$_{PA}$ with these in other bacterial species, I compared the amino acid sequence of PykA$_{PA}$ with PykF$_{PA}$, and with PykA and PykF from *S. enterica* Serovar Typhimurium, *Y. pestis*, and *E. coli*. These species were selected because they encode both PykA and PykF together, similar to *P. aeruginosa*. Amino acid sequence alignment showed that the active site residues in PykA were 100% conserved. Moreover, the alignment also showed that the active site signature of PykA "[245]MVARGDLGVE[254]" was also present in all included sequences (Figure 5.8).

A)
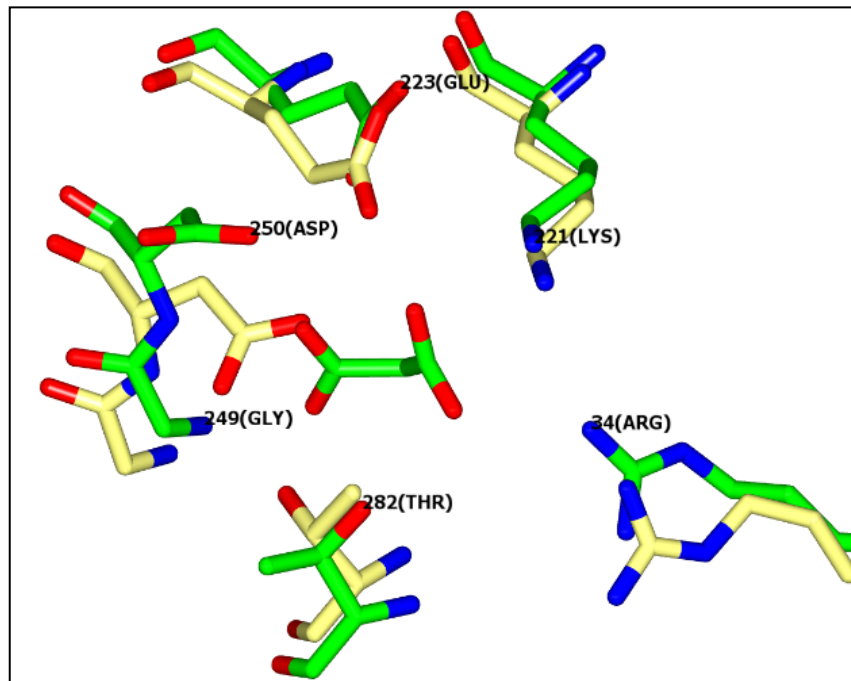
B)
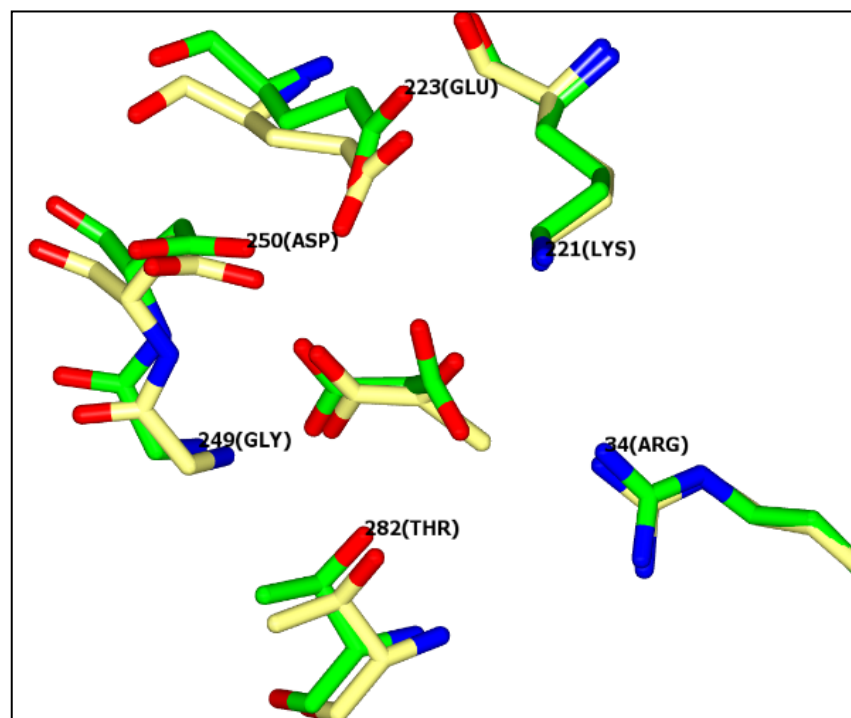
Figure 5.6: Comparison of the active site of PykA$_{PA}$ with apo and bound PK structures. A) Superposition of the active site of MLI-bound PykA$_{PA}$ (green) and the apo 1PKY from *E. coli* (yellow). **B)** Superposition of the active site of MLI-bound PykA$_{PA}$ (green) and pyruvate-bound PKM1 from rabbit muscle (PDB 1F3W, yellow). Residues are annotated using PykA$_{PA}$ numbering.

5.4.4 Elongation of the Aβ5-Aα5 loop in PykA$_{PA}$

While comparing the active site of PykA with other PK structures, I observed that the Aα5 helix of PykA had an outward orientation away from the core of the enzyme (Figure 5.7). This orientation of Aα5 was not apparent in other PK structures from prokaryotes or eukaryotes. Moreover, it was unlikely to be a modelling error given the good electron density signal in this region of PykA (Appendix 7). Analysis of the amino acid sequence revealed that the Aβ5-Aα5 loop which precedes the Aα5 helix was slightly longer in PykA than in certain other PKs, and this might have forced this conformation of the Aα5 helix. The loop contained three additional residues (Ala229, Asp230 and Asp231) which have unbiased electron density (Appendix 7). Alignment of the amino acid sequence revealed that PykA isozymes from other species also encode three extra residues in the same region (Figure 5.8). Presumably, the Aα5 helices of other PykAs most likely adopt a similar conformation of the Aα5 helix of PykA$_{PA}$. Although the three residues which elongate Aβ5-Aα5 loop in PykA$_{PA}$ (Ala229, Asp230 and Asp231) were not directly involved in interactions of the active site, other residues from the same loop participated in formation of the PykA-MLI-Mg complex; including Glu223 (one of the octahedral coordinates of Mg^{2+}) and Lys221 (coordinates directly with MLI).
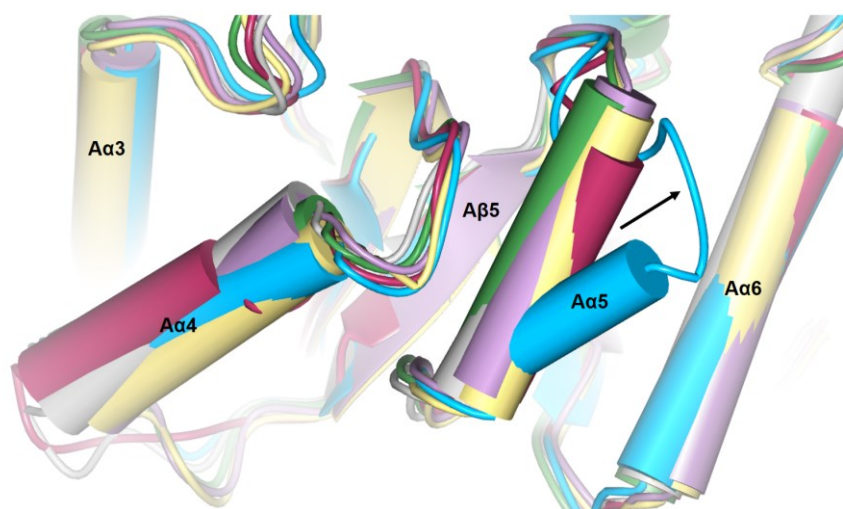
Figure 5.7: Superposition of the Aα5 helix from PykA$_{PA}$ and other PKs. The figure shows superposition of PykA$_{PA}$ (blue), PykF of *E. coli* (PDB 1PKY, green), PK of rabbit muscle (PDB 1F3W, lilac), PK of *S. aureus* (PDB 3T05, grey), PK of *M. tuberculosis* (PDB 5WRP, maroon) and PK of *T. cruzi* (PDB 4KS0, yellow). Alpha helices are shown as coloured tubes and the black arrow points to the elongated Aβ5-Aα5 loop in PykA$_{PA}$.
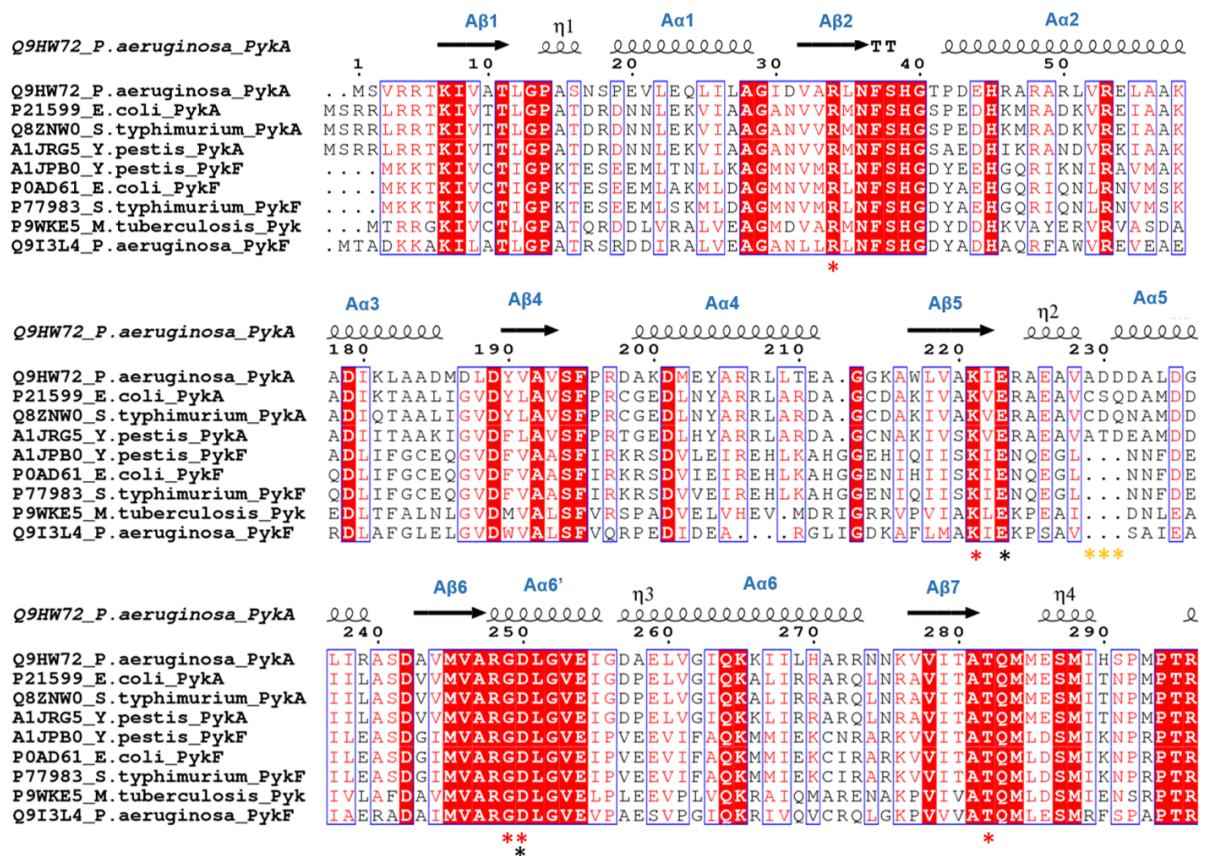
Figure 5.8: Alignment of the amino acid sequence in the active site of PKs. Residues involved in binding of MLI and Mg^{2+} in $PykA_{PA}$ are highlighted in red and black asterisks, respectively. Yellow asterisks indicate the three additional residues that elongate the $A\beta5$-$A\alpha5$ loop in PykA enzymes. Residues highlighted in red are 100% identical, whereas a column is framed in blue if more than 70% of the residues have similar physicochemical properties.

5.5   The allosteric site of PykA

So far, there is only one other prokaryotic PK structure with a bound regulator and this belongs to the PykF subfamily enzyme from *M. tuberculosis*. In that structure, AMP binds to the canonical allosteric site (at the C domain), whereas G6P is present in a different binding pocket (between the A and C domains). In chapter 4, the kinetics of PykA showed that it is allosterically activated by G6P and that the addition of this regulator led to sigmoidal kinetics with respect to PEP titration to become more hyperbolic. Moreover, co-crystallization of PykA with G6P improved the diffraction quality, suggesting that addition of G6P may induce conformational changes in PykA that stabilize the structure

and improve the packing of the crystal. Herein, I present the structure of PykA with G6P bound to the allosteric site. However, the binding site of G6P to PykA is distinct from the G6P binding site in the PK from *M. tuberculosis*, meaning that this regulator is likely to activate PykA via a different allosteric mechanism than the one in *M. tuberculosis* PK.

5.5.1 The binding site of G6P

Analysis of the PykA structure revealed that G6P was present in a clear binding pocket within the C domain, with an average interactive surface area of 275 Å^2. The observed electron density for the bound G6P was unbiased in all chains, with strong F_o–F_c difference (Figure 5.9A). The G6P binding pocket was bordered by the Cβ1-Cα2 loop (residues 383-388), the Cα2 helix (residues 389-393) and the Cβ4-Cβ5 loop (residues 460-471). The Cβ1-Cα2 loop and the first turn of the Cα2 helix anchored the phosphate moiety of G6P, thus the Cβ1-Cα2 loop is referred to as "the phosphate loop", whereas the Cβ4-Cβ5 loop anchored the ring part of G6P and so is referred to as "the ring loop".

G6P was bound tightly in the allosteric pocket of PykA via an extensive network of hydrogen bonds. The phosphate group of G6P coordinated with the side chain of Thr384, the backbone atoms of Glu385, Phe388 and Gly468, and with both the side chains and the backbone atoms of Ser386 and Thr389. In contrast, the ring moiety of G6P bonded with the side chain of Ser463, the backbone atoms of Ala466 and Gly469, and with the side chain and backbone of Glu385 (Figure 5.9B). Interactions of the phosphate group of G6P were present in all 12 chains of PykA, whereas the interactions of the ring part were present in at least nine chains.

5.5.2 The phosphate-ring loop interaction

The phosphate and the ring loops also co-interacted (Figure 5.10). These loops bonded with each other via a pair of electrostatic interactions between Ser386 and Gln467, and between Thr389 and Thr470. The phosphate-ring loop interaction took place primarily near the phosphate moiety of G6P. Additionally, Lys460 and Tyr464 (both from the ring loop) bonded together near the ring moiety of G6P. Taken together, it seems that these interactions keep the allosteric pocket of PykA in a closed conformation covering the bound G6P.
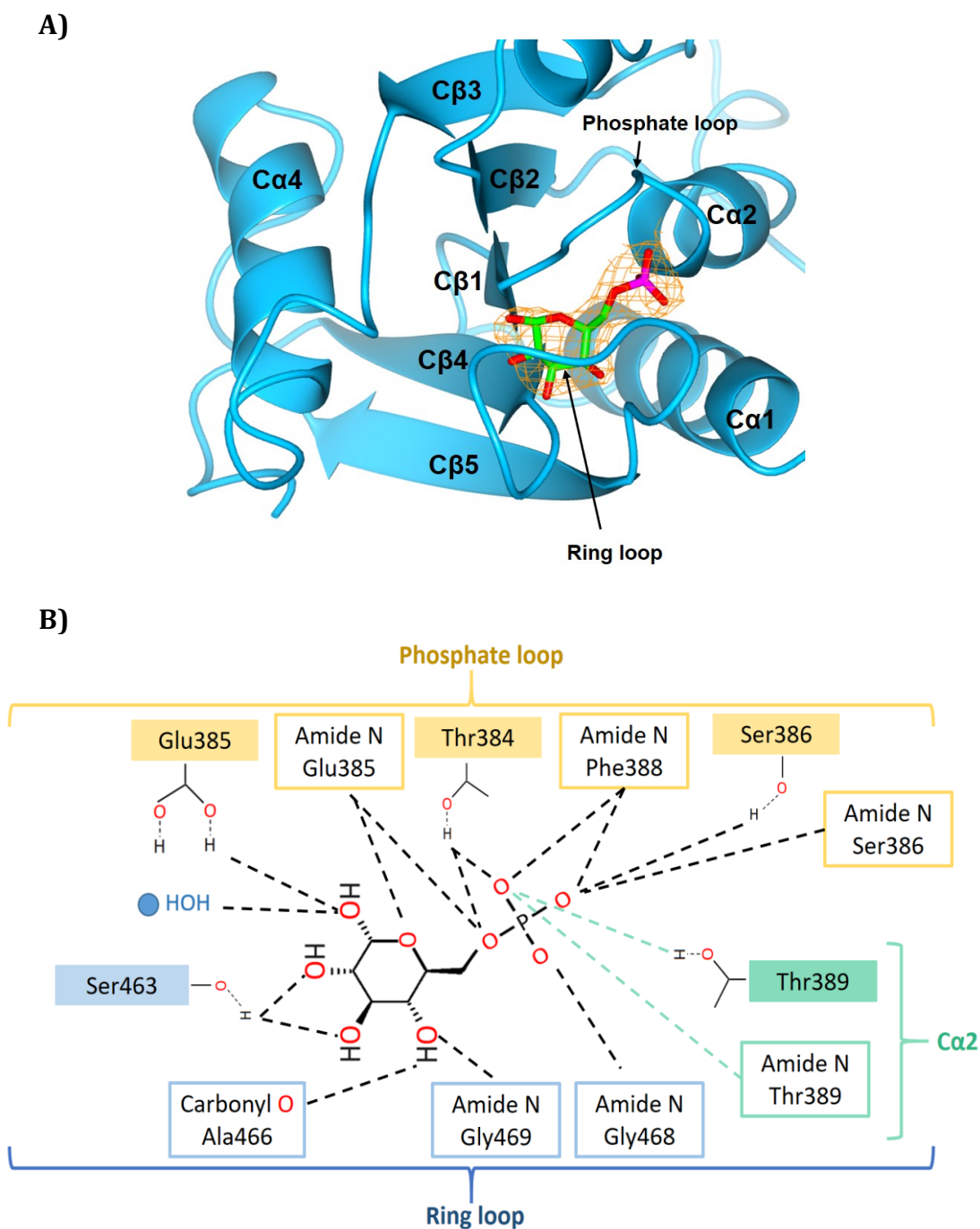
Figure 5.9: The allosteric site of PykA. A) Cartoon representation of the allosteric site of PykA (Chain E) containing bound G6P. The electron density map (F_o-F_c) around the G6P is shown as an orange mesh and contoured at 3σ. The image was generated using CCP4mg. **B)** Schematic diagram of the interactions of G6P with the surrounding residues in the allosteric pocket of PykA. Residues belonging to the phosphate loop, ring loop and Cα2 helix are highlighted in yellow, blue and green colours, respectively. Filled and open squares represent side chain and peptide backbone atoms, respectively. Interactions of the bound G6P were analyzed using PDBePISA.
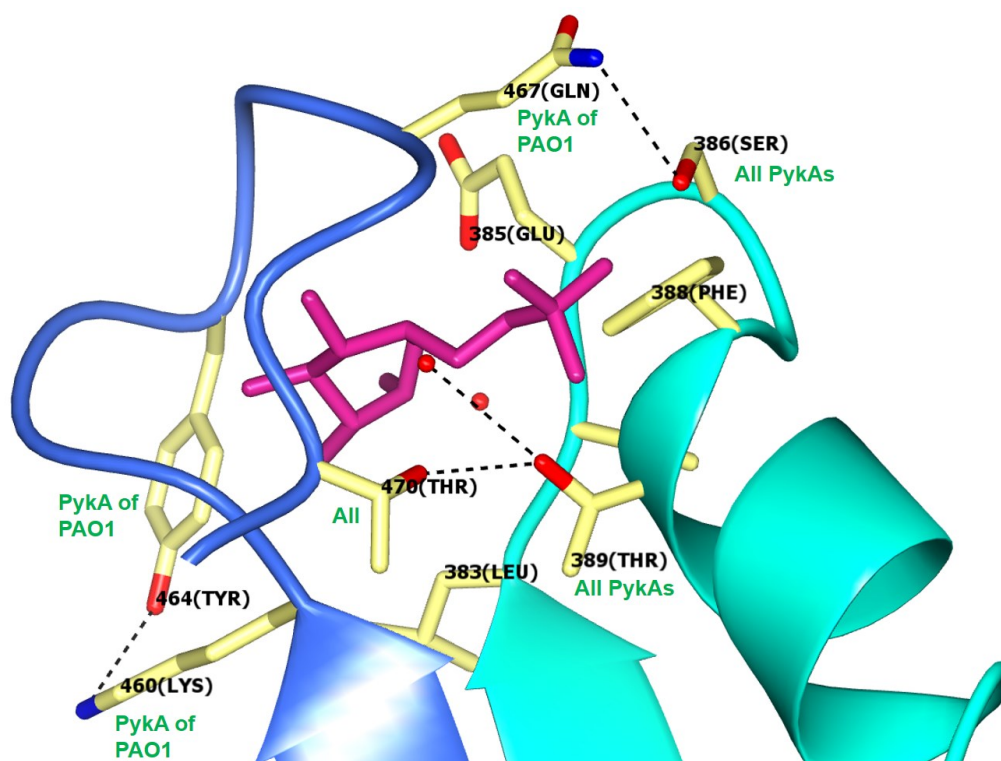
Figure 5.10: Phosphate-ring loop interactions. Cartoon representation of the interactions between the phosphate loop (cyan) and the ring loop (blue) in the allosteric site of PykA. The bound G6P is shown as pink sticks. The conservation of the residues is highlighted in green (All, found in all PykAs and PykFs; All PykAs, found only in PykAs and absent in PykFs; PykA of PAO1, unique to PykA from PAO1 and absent in other PykAs and PykFs). The figure was generated using CCP4mg.

5.5.3 Analysis of the amino acid sequence in the allosteric site

The biochemical analysis in chapter 4 revealed that PykA$_{PA}$ was regulated differently compared with PykA from other species, meaning that it is likely that the allosteric site of PykA$_{PA}$ is built up of different residues (likewise for PykF$_{PA}$). To investigate this further, I compared the amino acid sequence of the allosteric site in PykA$_{PA}$ with PykA and PykF enzymes from other bacteria (Figure 5.11). Amino acid sequence alignment showed that the residues of the phosphate loop and Cα2 helix were highly similar among the PykA enzymes including PykA$_{PA}$ and among the PykF enzymes including PykF$_{PA}$. This indicates that the phosphate loop and the Cα2 helix were apparently unlinked with the unusual allosteric regulation of PykA$_{PA}$ and PykF$_{PA}$.

On the other hand, the amino acid sequence of the ring loop was different in PykA_PA and PykF_PA, despite its high conservation among PykA and PykF from other species. This suggests that the unusual allosteric regulation of PykA_PA and PykF_PA may be related to the distinct composition of their respective ring loops. The amino acid sequence alignment also showed that the phosphate-ring loop interactions seemed to be specific to PykA_PA, as half of the residues involved in these interactions were present only in PykA_PA. The only exception to this was the interaction of Thr389 and Thr470, which was mediated by conserved residues in all PykA enzymes.
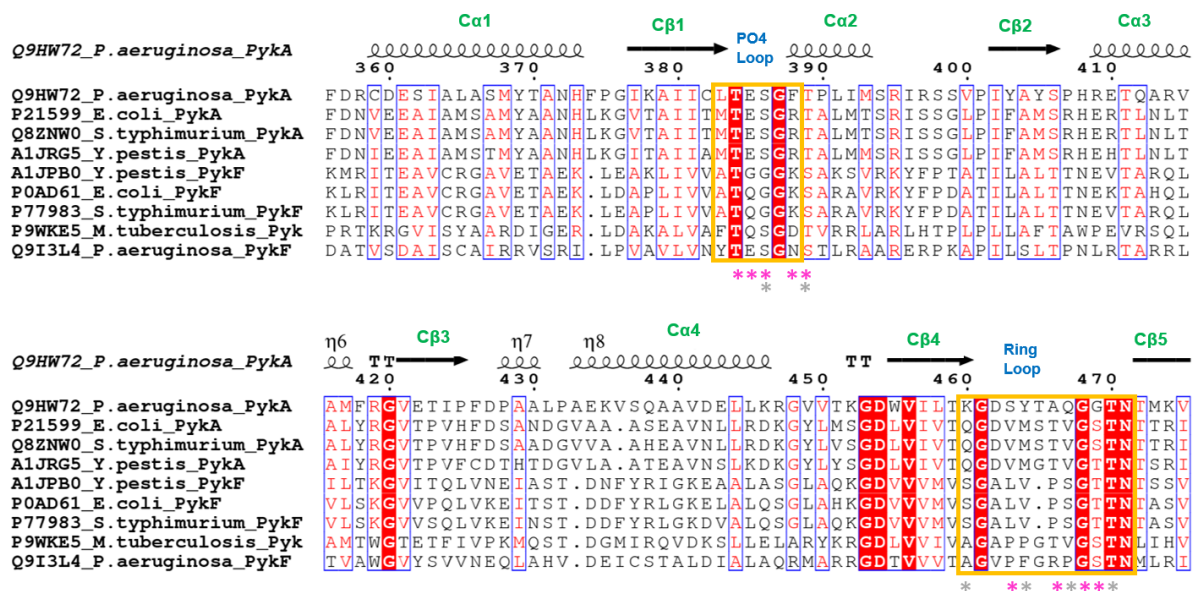
Figure 5.11: Alignment of the amino acid sequence in the allosteric site of PKs. Residues involved in G6P-binding and phosphate-ring loop interactions in PykA_PA are highlighted by pink and grey asterisks, respectively. Residues of the phosphate and ring loops are surrounded by yellow boxes. Residues highlighted in red are 100% identical, whereas a column is framed in blue if more than 70% of the residues have similar physicochemical properties.

5.5.4 Comparison of the allosteric site in PykA$_{PA}$ with apo PykF from *E. coli*

In the allosteric site of PykA$_{PA}$, G6P was anchored by the phosphate loop, the Cα2 and the ring loop. Comparison of the allosteric site in PykA$_{PA}$ with the apo PykF model from *E. coli* (1PKY$_{EC}$) revealed major disparities between the two structures, particularly in the ring loop (Figure 5.12). In PykA$_{PA}$, the ring loop shifted towards the bound G6P, closing the allosteric pocket, whereas in 1PKY$_{EC}$, the ring loop was shifted away from the allosteric pocket and the allosteric site was in a more open conformation. The phosphate loop and the Cα2 helix, however, were in the same conformation in both structures. Although, the Cα4 helix was not involved in interactions of PykA$_{PA}$ with G6P, was partially unwound in PykA$_{PA}$ in comparison with 1PKY.
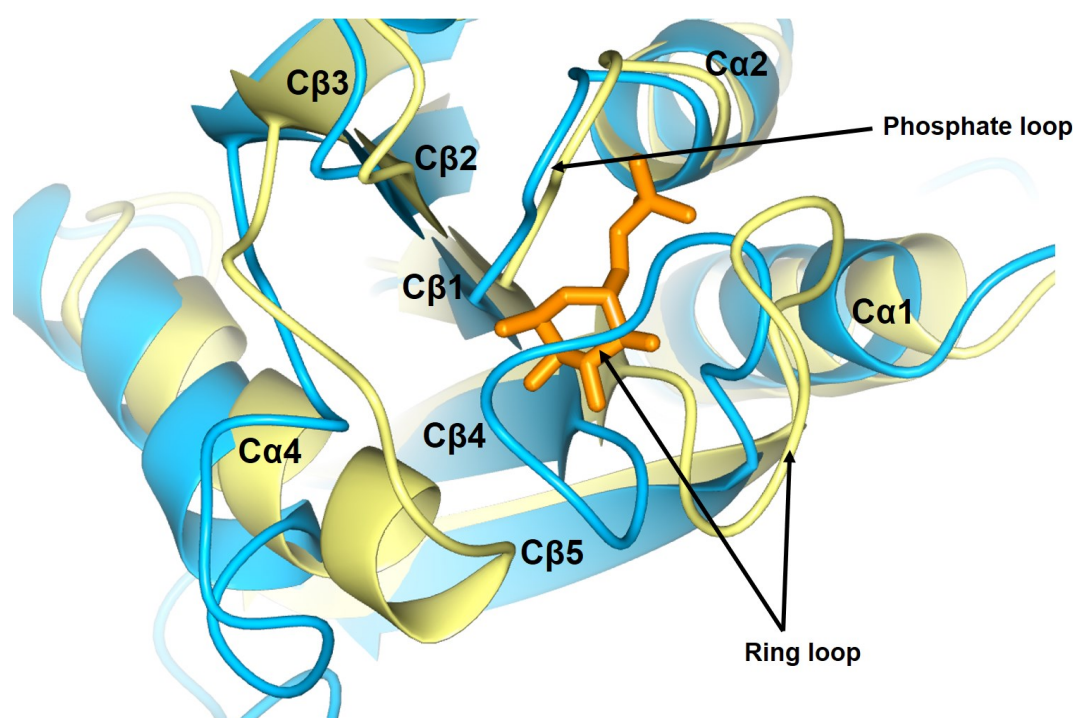
Figure 5.12: Comparison between the allosteric site in PykA$_{PA}$ and 1PKY$_{EC}$. Cartoon representation of the allosteric site of G6P-bound PykA$_{PA}$ (light blue) superposed with 1PKY$_{EC}$ (light yellow). G6P is shown as a coral cylinder. Secondary structures are annotated using PykA$_{PA}$ numbering. The figure was generated using CCP4mg.

5.6. Intersubunit interactions in PykA

Intersubunit interactions are the means by which allosteric or activity signals can be transmitted from one subunit to another. In PykA, the opposing A domains communicate via the A-A interface, whereas the opposing C domains communicate via the C-C interface. I analysed the interactions across the PykA subunits using PDBePISA webserver.

5.6.1 The A-A interface in PykA

The PykA tetramer contained two A-A interfaces; between chains I & L and between chains K & C. However, there were additional A-A interfaces present between the scattered chains in the asymmetric unit of PykA; A-A interface between chains H & E and between chains B & F. The A-A interface was derived from interactions between two protomers, with one being apparently perpendicular to the other (Figure 5.13A). The average surface area of the interface was around 1450 Å^2, burying about 7% of the surface of each subunit.

The A-A interface is stabilized primarily by hydrogen bonds and a small subset of salt bridges (Table 5.2). The interface comprises four helices; Aα6', Aα6, Aα7 and Aα8 and three connecting loops; Aα6- Aα6', Aβ7- Aα7 and Aα8- Cα1 (Figure 5.13B, 5.14). Of these structures, the most important interaction is mediated by the active site helix Aα6'. In this interaction, Arg248 and Gly249 (both from Aα6') which mediate the coordination of MLI and Mg^{2+} to the active site, also bond with Arg296 (Aα7) from the opposing monomer. This suggests that the Aα6' helix is not just important for formation of the active site pocket, it also plays a role in transmission of the activity signals between adjacent subunits.

Figure 5.13: Structures of the A-A interface in PykA. A) Cartoon representation of the A-A interface between two PykA protomers. **B)** Close-up view of the secondary structures forming the A-A interface in PykA. The bound MLI in the active site is shown as a coral cylinder. The figure was generated using CCP4mg.

Table 5.2: Intersubunit interactions in PykA. The table lists the interactions at the A-A and the C-C interfaces in PykA. The shown distances at the A-A interface represent the interactions between chain B & F and those at the C-C interface section represent the interactions between chain I & C. Black and red "plus" marks indicate hydrogen bonds and salt bridges, respectively. The results are based on interface analysis using PDBePISA.

The A-A interface in PykA									
Chain I		**Chain II**		**Å**	**I & L**	**K & C**	**H & E**	**B & F**	
Aα6	Lys265	Aα7	Asn304	2.82	+	+	+	+	
Aα7	Arg296	Loop Aβ7-Aα7	Gln283	3.2	+	+	+	+	
Aα7	Arg296	Aα6'	Arg248	2.86	+	+	+	+	
Aα7	Arg296	Aα6'	Gly249	2.75	+	+	+	+	
Loop Aα8-Cα1	Lys341	Loop Aα6'-Aα6	Glu259	3.68	+	+	+	+	
Aα8	Arg334	Loop Aα6'-Aα6	Asp257	3.21		+	+	+	
Aα7	Arg296	Loop Aα6'-Aα6	Asp257	3.32	+		+		
Loop Aβ7-Aα7	Gln283	Aα7	Ala297	3.79		+	+	+	
Loop Bβ5-Bβ6	Asp129	Aα7	Arg296	3.39				+	
The C-C interface in PykA									
Chain I		**Chain II**		**Å**	**I & C**		**K & L**		
Cα1	Tyr369	Loop Aα8-Cα1	His350	2.7	+		+		
Loop Aα8-Cα1	Phe356	Cα1	His373	2.87	+		+		
Cβ5	Lys474	Loop Cβ4 -Cβ5	Asp462	3.03	+		+		
Cβ5	Val475	Cβ5	Asn471	3.11	+		+		
Cβ5	Lys474	Cβ5	Thr472	3.6	+		+		
Cβ5	Met473	Cβ5	Met473	2.92	+		+		
Cα1	Cys359	Cβ5	Val475	3.62	+		+		
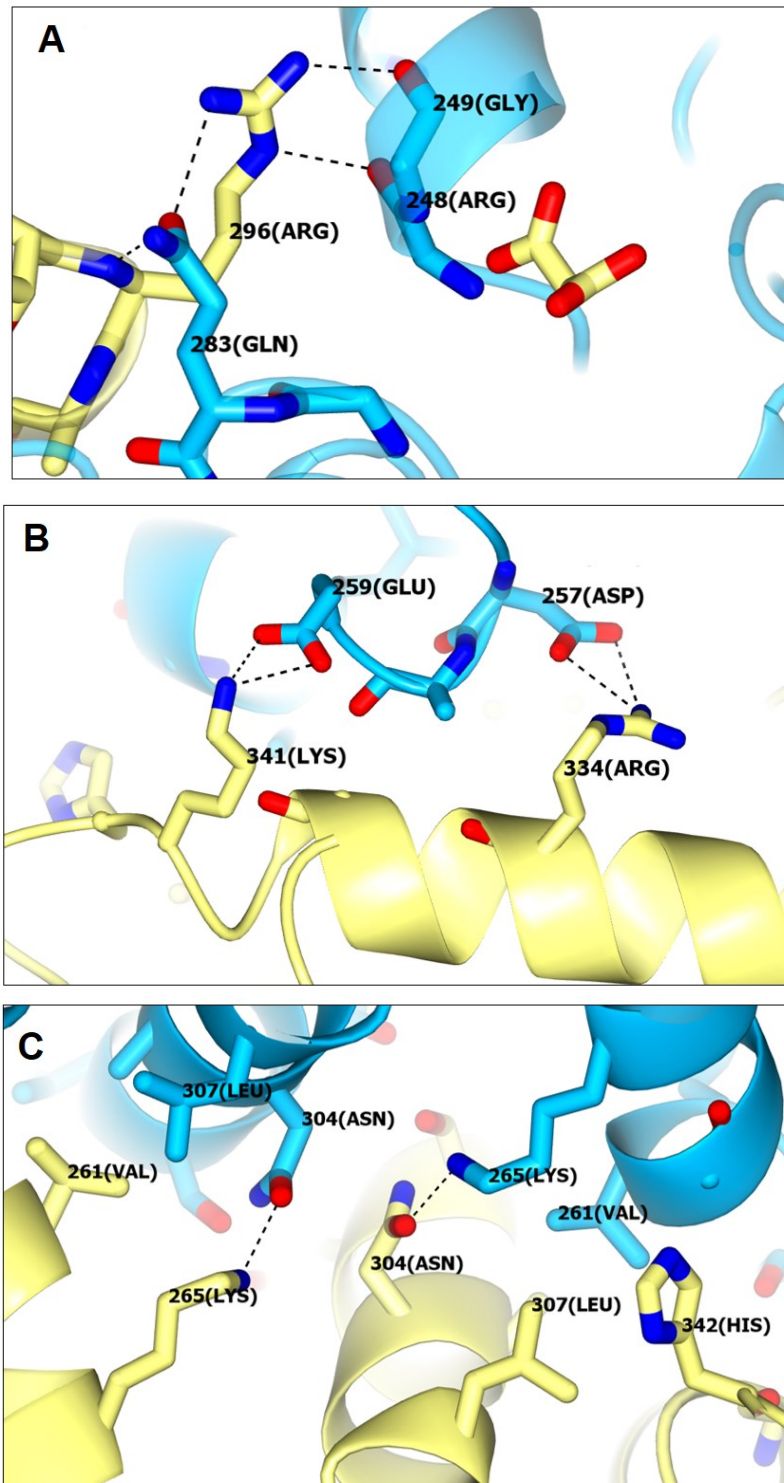
Figure 5.14: Interactions across the A-A interface in PykA. A) Interactions of the active site helix Aα6' (Arg248 and Gly249), Aα7 (Arg296) and loop Aβ7-Aα7 (Gln283). **B)** Formation of salt bridges between Aα8 + loop Aα8-Cα1 (Arg334, Lys341) and loop Aα6'-Aα6 (Asp257, Glu259). **C)** Interactions of Aα6 (Lys265) and Aα7 (Asn304).

5.6.2 Analysis of the amino acid sequence in the A-A interface

Residues in the A-A interface in PykA can be sorted according to their conservation into three groups; strictly-conserved residues, residues that are highly conserved except for PykF$_{PA}$, and residues that are specific to PykA enzymes (Figure 5.15). The 100% conserved residues belong to Aα6', Aα6, loop Aβ7-Aα7 and the first turn of Aα7. This means that the same interactions mediated between Aα7 and Aα6' or Aα6 or loop Aβ7-Aα7 are likely to take place at the A-A interfaces of PykA and PykF in different species. The second group of residues are Glu259 and Asn304 and these are conserved in all enzymes except for PykF$_{PA}$ (replaced by a serine and a threonine, respectively). This indicates that possibly the interactions of the A-A interface in PykF$_{PA}$ are mediated by different mechanisms than they are in other PykA or PykF enzymes. The last group of residues are specific to the PykA enzymes including PykA$_{PA}$ and they are absent in all PykF isozymes. These residues include Asp257, Arg334 and Lys341 (with the exception of Arg334, which is replaced in *S. enterica* Serovar *Typhimurium* by a lysine). The latter three residues are particularly important as they contribute the only two salt bridges at the A-A interface. Altogether, the A-A interface in PykA$_{PA}$ is highly conserved across PykA isoforms.
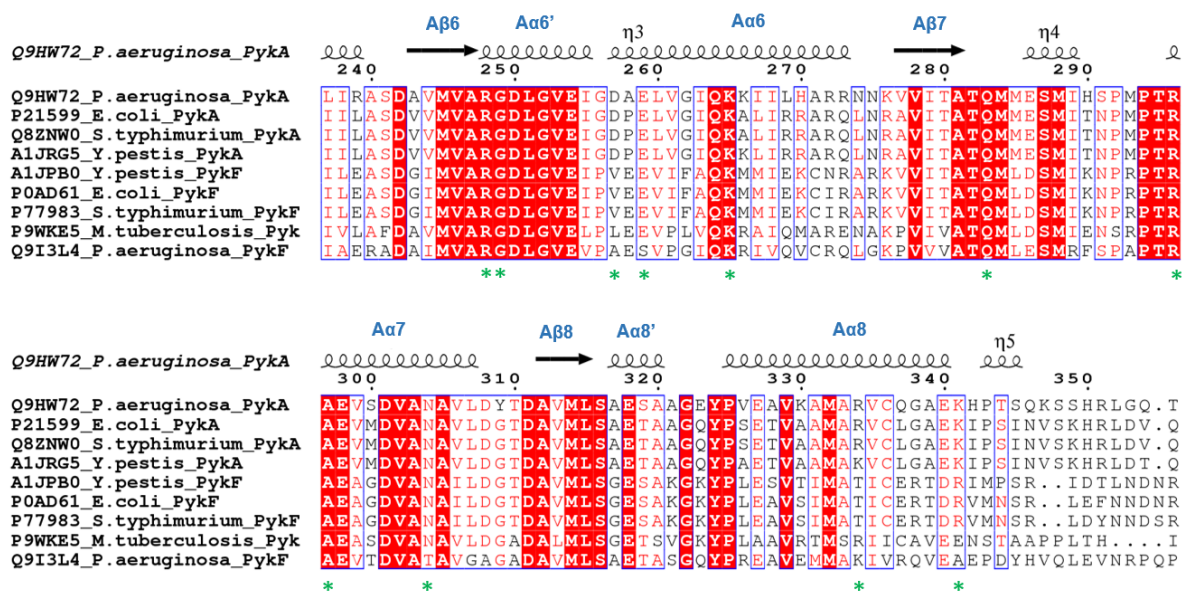
Figure 5.15: The A-A interface in PykA. Amino acid sequence alignment showing the residues that mediate the A-A interface in PykA (green asterisks) compared with other enzymes. Residues highlighted in red are 100% identical, whereas a column is framed in blue if more than 70% of the residues have similar physicochemical properties.

160

5.6.3 The C-C interface in PykA

The C-C interface was formed between the opposing C domains of two protomers (Figure 5.16A, 5.16B). There are two C-C interfaces present in the PykA tetramer; one is formed between chains I & C and the second is formed between chains L & K. The C-C interface had a slightly smaller surface area than the A-A interface (approximately 1200 Å^2) burying around 6 % of each protomer.

The C-C interface in PykA can be viewed as pairing of the Cα1 and Cβ5 from one protomer with the same structures from the opposite protomer (Figure 5.16B). The C-C interface was stabilized by interactions from Cα1, Cβ5, loop Aα8-Cα1 and loop Cβ4-Cβ5 (Figure 5.17). The Aα8-Cα1 loop was also a part of the A-A interface, meaning that this loop apparently contacts two protomers at the same time. Moreover, the Cβ4-Cβ5 loop is also the ring loop anchoring the ring of G6P to the allosteric site. The C-C interface is mediated mainly by hydrogen bonds, with the exception of one salt bridge found between Asp462 (ring loop) and Lys474 (Cβ5). Interactions at the C-C interface in PykA are shown in Table 5.2.

5.6.4 Analysis of the amino acid sequence in the C-C interface

Amino acid sequence alignment of PykA$_{PA}$ and PK enzymes from other species showed that the residues which mediate the C-C interface are apparently less conserved than PykAs and PykFs from other species (Figure 5.18). Apart from Asn471, which is highly conserved in all PK enzymes, the C-C interface in PykA$_{PA}$ is mediated either by residues conserved in all PykA enzymes (His350, Phe356, Tyr369, His373, Asp462, Thr472) or by residues specific to PykA$_{PA}$ (Met473, Lys474, Val475, Cys359). The diversity of residues mediating the C-C interface in PykA$_{PA}$ indicates that the transmission of activity signals across the protomers of this enzyme is likely different compared with the PKs from other bacteria.
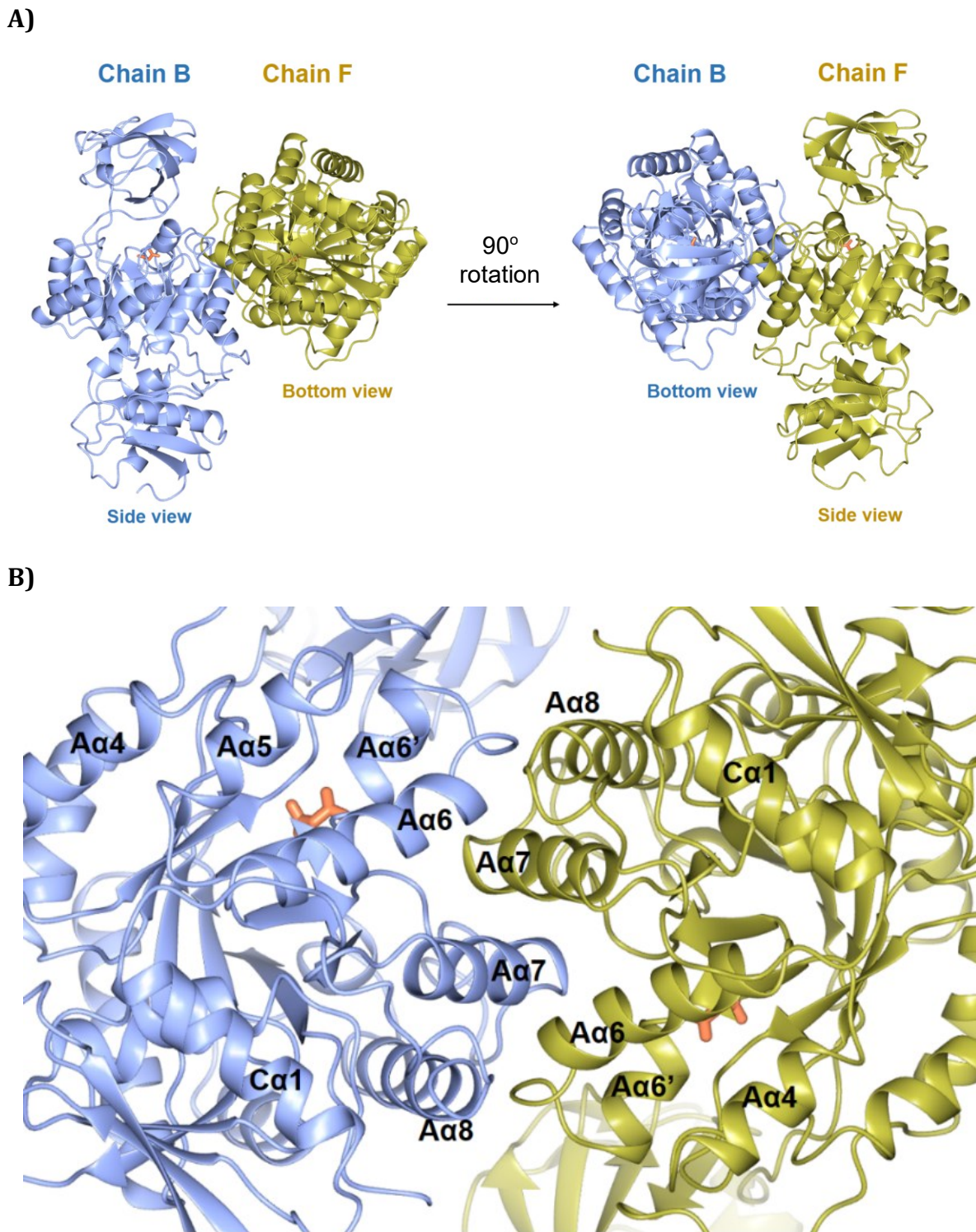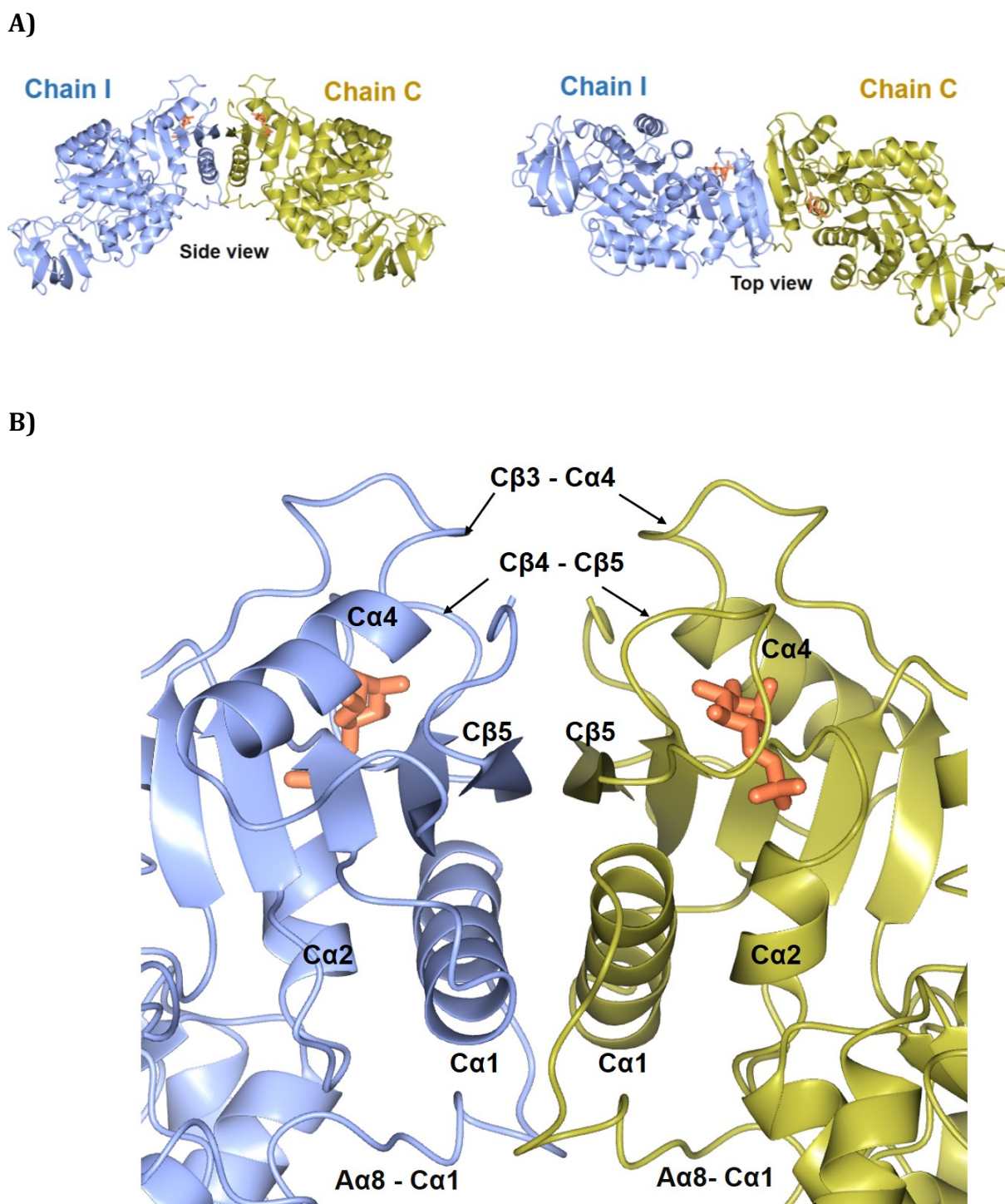
Figure 5.16: Structures of the C-C interface in PykA. A) Cartoon representation of the C-C interface formed between two PykA protomers. **B)** Close-up view of the secondary structures in the C-C interface. The bound G6P at the allosteric site is shown as coral cylinders. The figure was generated using CCP4mg.
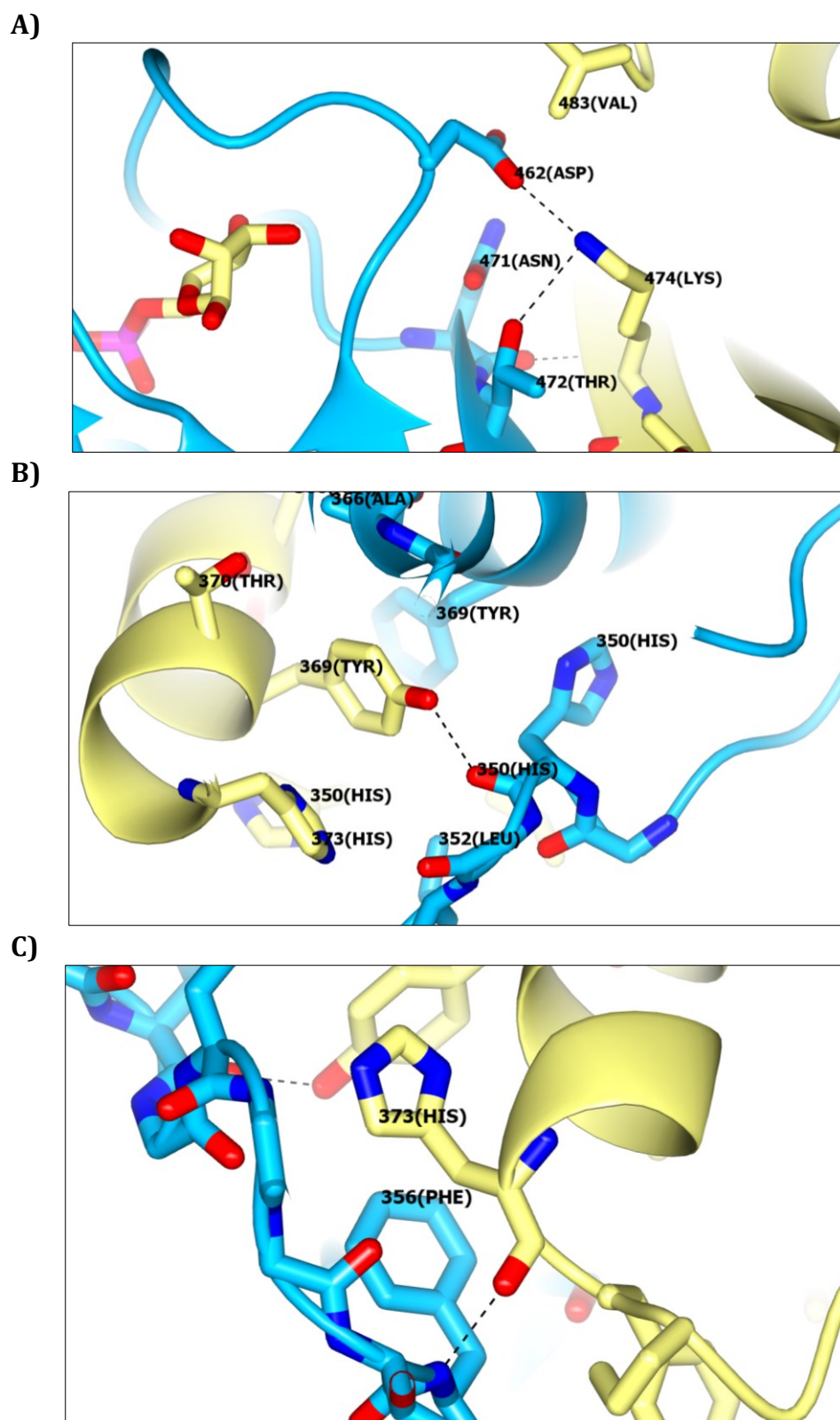
Figure 5.17: Interactions across the C-C interface in PykA. A) Interactions of the Cβ5 (Lys474), loop Cβ4 - Cβ5 (Asp462) and Cβ5 (Thr472). **B) & C)** Interactions between the loop Aα8-Cα1 (His350, Phe356) and Cα1 (Tyr369, His373).
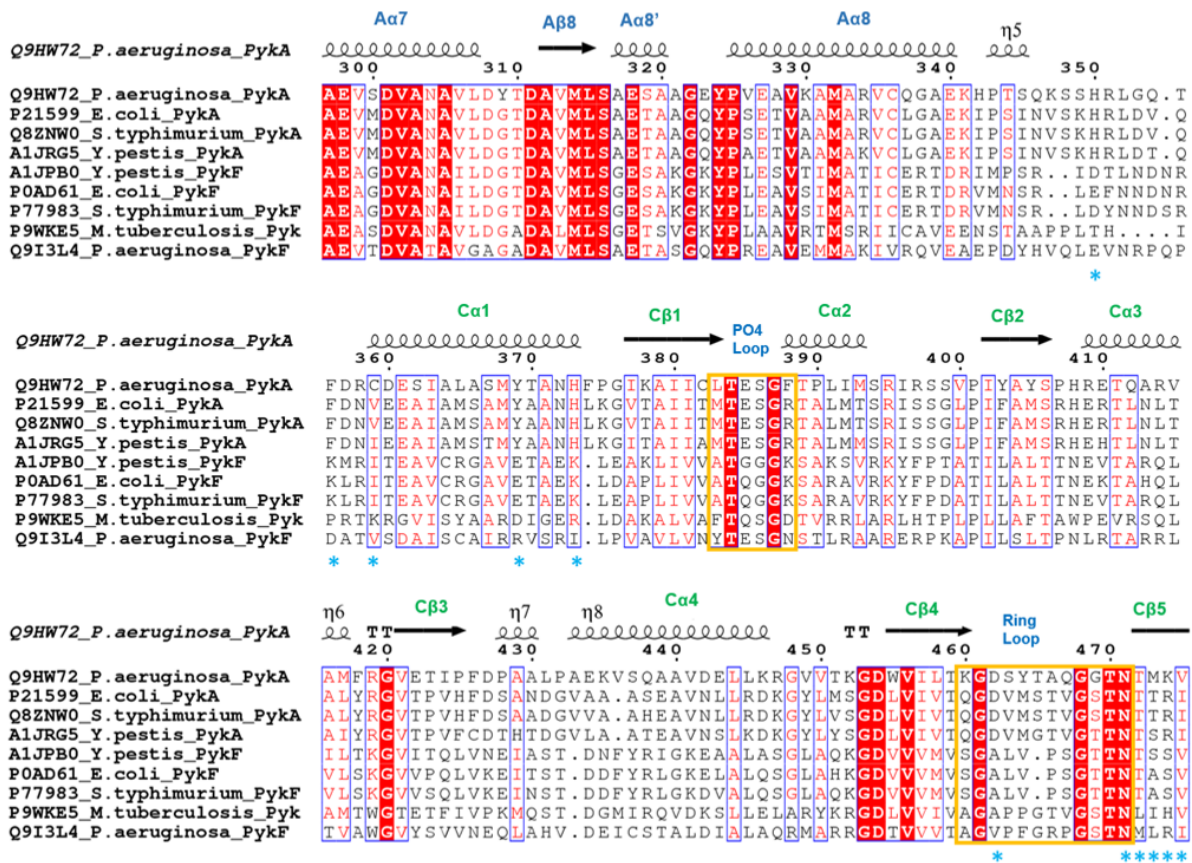
Figure 5.18: The C-C interface in PykA. Amino acid sequence alignment showing the residues mediating the C-C interface in PykA (blue asterisks) compared with other enzymes. The phosphate and the ring loops in the allosteric site are shown in yellow boxes. Residues highlighted in red are 100% identical, whereas a column is framed in blue if more than 70% of the residues have similar physicochemical properties.

5.6.5 Intersubunit interactions in PykA$_{PA}$ compared with 1PKY from *E. coli*

Occupation of the active/allosteric site of a multi-subunit enzyme such as PK is associated with rearrangement of the intersubunit structures in a way which facilitates the transfer of the activity/allosteric signals from one subunit to another. Given that there is no apo PykA$_{PA}$ structure, I again used 1PKY available from *E. coli* as an apo model to compare the intersubunit interactions. I analysed the interactions of the A-A and the C-C interfaces of PykA$_{PA}$ and 1PKY$_{EC}$ using PDBePISA. The interactions are summarized in Figure 5.19.

Analysis of the A-A interface in PykA$_{PA}$ showed that the interface network was primarily mediated by hydrogen bonds and without the co-interaction of opposite Aα7 helices (Figure 5.19). The interaction between Aα7 helices of two adjacent protomers is an indication of unbound PK (Mattevi et al., 1995). Moreover, the Aα6' helix and the Aα8-Cα1 loop contributed to formation of the A-A interface in PykA$_{PA}$. In contrast, the A-A interface in 1PKY$_{EC}$ was mediated by a network of salt bridges and included bonding of the opposite Aα7 helices (Mattevi et al., 1995). In addition, neither the active site helix (Aα6') nor the Aα8-Cα1 loop were part of the A-A interface in 1PKY$_{EC}$. There were also differences between the C-C interface in PykA$_{PA}$ and 1PKY$_{EC}$ (Figure 5.19). In PykA$_{PA}$, the C-C interface included interactions from Cα1 and loop Aα8-Cα1, without interactions from Cα4. By contrast, the C-C interface in 1PKY did not contain interactions from Cα1 or loop Aα8- Cα1, but did include contributions from Cα4.
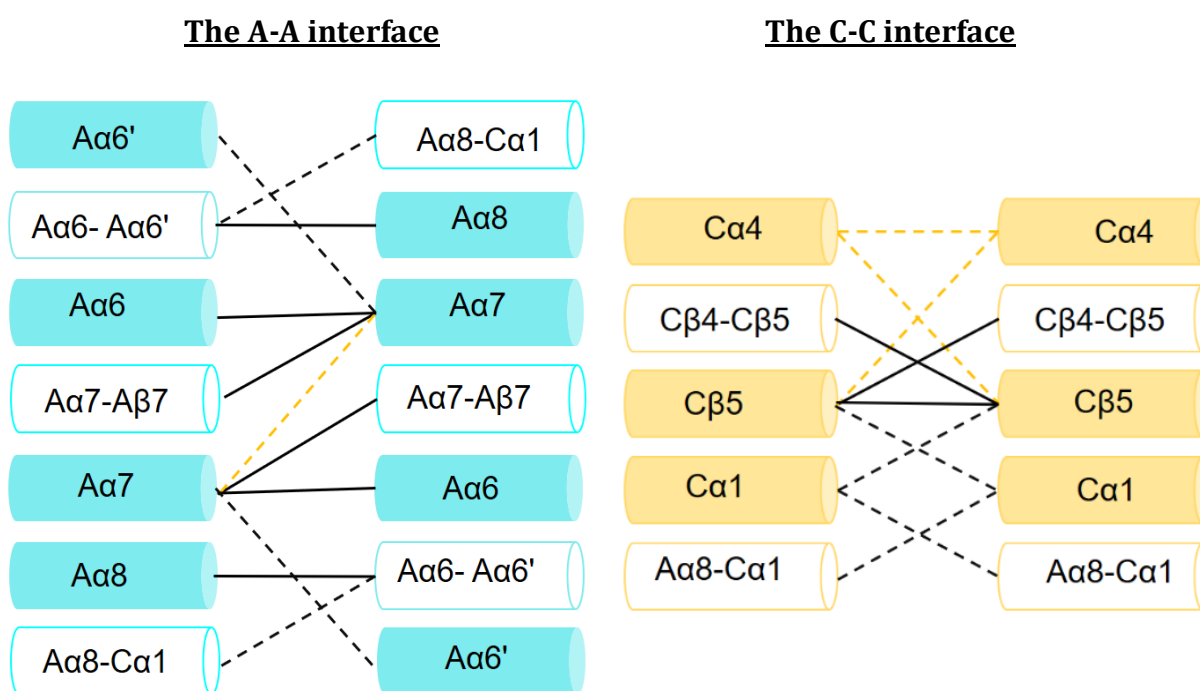
Figure 5.19: Comparison between the intersubunit interactions in PykA$_{PA}$ and 1PKY$_{EC}$. The figure summarizes the interactions of the A-A and the C-C interfaces of PykA$_{PA}$ and 1PKY$_{EC}$. Black dashed, yellow dashed and black solid lines represent interactions of PykA$_{PA}$ only, of 1PKY$_{EC}$ only, and of both structures, respectively. Filled cylinders represent alpha helices or beta strands, whereas empty cylinders represent connecting loops. All interactions were analysed using PDBePISA.

5.7   The PykF tetramer and domain organization

The asymmetric unit of PykF consisted of two chains (chain A & B), whereas a complete PykF tetramer was generated by symmetry coordinates (chain C & D) (Figure 5.20A). This was consistent with AUC analysis of PykF which demonstrated that the enzyme is a tetramer in solution (Appendix 8). Analysis of the PykF tetramer using PDBePISA revealed that the surface area of the PykF tetramer was 75449.9 $Å^2$ with total accessible solvent area of 8474.2 $Å^2$. The tetramer assembly was stable in solution with a solvation free energy gain (ΔG) of -42 kcal/mol. There was no electron density indicative of bound ligands in the active site or in the predicted allosteric site of PykF so it was modelled as an apo PykF.

Each chain of PykF comprised three domains; A, B and C (Figure 5.20B). The A domain was formed of two stretches of residues; 4-72 and 169-336, whereas the B and the C domains ran through 74 -167 and 337-470, respectively. The A domain was placed at the centre of the chain and was comprised of typical eight α/β TIM-barrel structure where the alpha helices span around the core of the beta strands. Similar to PykA, there were an additional two helical fragments preceding the Aα6 and Aα8 and these were annotated as the Aα6' and Aα8', respectively. The B domain was present at the C-terminus of the A domain and was comprised of seven β-strands and a small α-helix. While the C domain was present at the N-terminus of the A domain and was formed of four α-helices alternating with five β-strands, with the fifth strand running anti-parallel to the four other strands. Given the lower resolution of the PykF diffraction data, the electron density of the Cβ3 strand of chain A was weak and the strand was modelled as a loop. Also, the electron density signal was weak at the three terminal residues of chain A and these were left unmodelled.

Although the secondary structures of PykF$_{PA}$ resemble those of PykA$_{PA}$, there is one key difference between the two. The first α-helix of the C domain (Cα1) was preceded by a short helical segment in PykF$_{PA}$ and I denoted this short helix as Cα1' (Figure 5.20). The Cα1' helix is absent in PykA$_{PA}$ and apo PykF from *E. coli* and it seems to be a unique structure present only in PykF$_{PA}$ of the PykF structures solved to date. Cα1' was clearly seen in the two chains of PykF$_{PA}$, in spite of the low resolution of the model. Within the

PykF tetramer, the opposing Cα1' helices are placed close to each other, particularly at the A-A interface region.
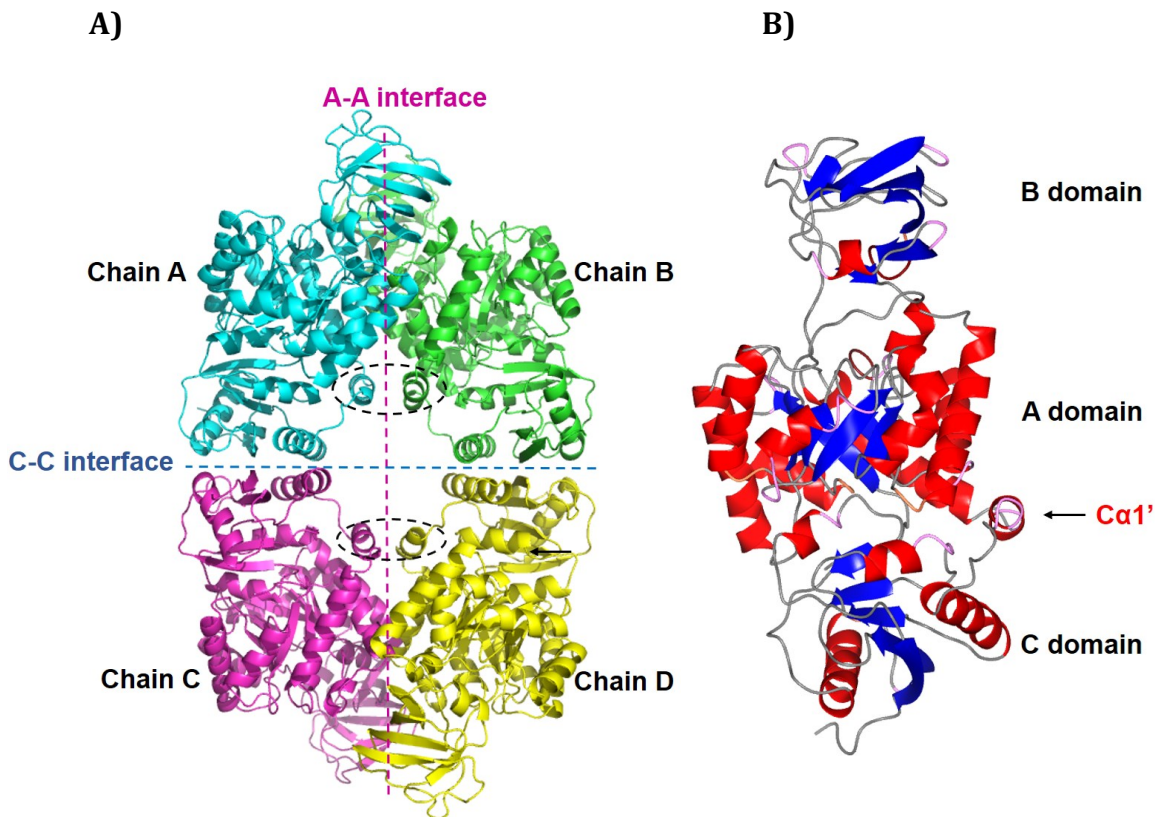
Figure 5.20: Structure of PykF. A) Cartoon representation of the PykF tetramer. Chain A and B were present in the asymmetric unit, whereas chain C and D were generated by symmetry coordinates. The dashed lines and dashed ovals highlight the PykF interfaces and the Cα1' helices, respectively. **B)** Cartoon representation of the secondary structures of a PykF protomer (chain B). Alpha helices and beta strands are presented in red and blue, respectively.

5.8   The active site of PykF

Although the PykF crystal diffracted only following co-crystallization of the enzyme with PEP, Mg^{2+} and KCl, there was no evidence of these in the final PykF model. To investigate the conformation of the active site of $PykF_{PA}$, I compared the active site of $PykF_{PA}$ with the MLI-bound $PykA_{PA}$ (Figure 5.21A). Superposition of the two models revealed that Arg35, Lys217, Glu219, Gly242, Asp243 and Thr275 were the likely active site residues in $PykF_{PA}$. These residues were clearly disorganized in the active site of

PykF$_{PA}$ compared with PykA$_{PA}$, meaning that apparently the active site of PykF$_{PA}$ did not contain any bound ligand. I also superposed PykF$_{PA}$ with unbound 1PKY from *E. coli* and this revealed that the active site residues of the two structures superimposed well, in the same positions and orientations (Figure 5.21B) which indicates that the active site of PykF$_{PA}$ did not contain a bound ligand.

A)

B)
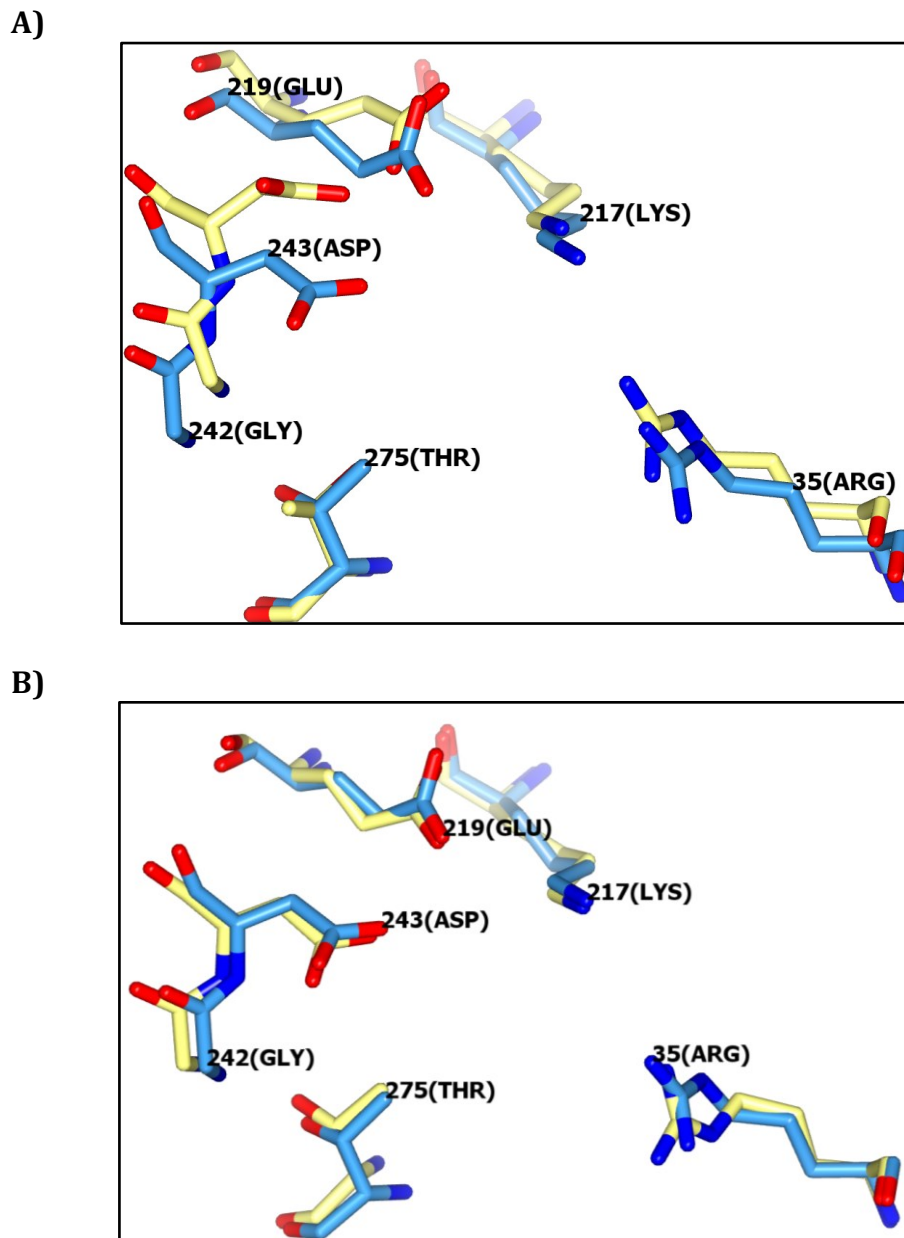
Figure 5.21: The predicted active site in PykF. A) Superposition of the active site in PykF$_{PA}$ (blue, chain B) and PykA$_{PA}$ (yellow, chain E). **B)** Superposition of the active site in PykF$_{PA}$ (blue, chain B) and 1PKY from *E. coli* (yellow, chain C). Residues are annotated according to the PykF$_{PA}$ model.

5.9   The allosteric site of PykF

PykF was crystallized in the absence of heterotropic regulators and it was likely that the conformation of its allosteric site is similar to the allosteric site of the unbound 1PKY from *E. coli*. To investigate this further, I superposed the allosteric site of PykF$_{PA}$ with 1PKY$_{EC}$ (unbound to regulators) and PykA$_{PA}$ (bound with G6P) (Figure 5.22). Alignment of the three models revealed that the allosteric site in PykF$_{PA}$ seemed to adopt a more closed conformation than 1PKY$_{EC}$, as the Cβ4-Cβ5 loop in PykF$_{PA}$ is shifted closer to the allosteric pocket than the corresponding loop in 1PKY$_{EC}$. On the other hand, the position of the Cβ4-Cβ5 loop in PykF$_{PA}$ was not as close to the allosteric pocket as the corresponding loop in PykA$_{PA.}$ Thus, the conformation of the allosteric site of PykF$_{PA}$ was apparently in partial closure, although the allosteric pocket was empty of regulators. The partially closed allosteric site of PykF$_{PA}$ is probably because the Cβ4-Cβ5 loop of PykF$_{PA}$ contains two prolines (Pro455 and Pro459) and these are known to provide flexibility to the structures. In contrast, the Cβ4-Cβ5 loop in 1PKY$_{EC}$ contains just a single proline and is presumably less flexible than the loop in PykF$_{PA}$.
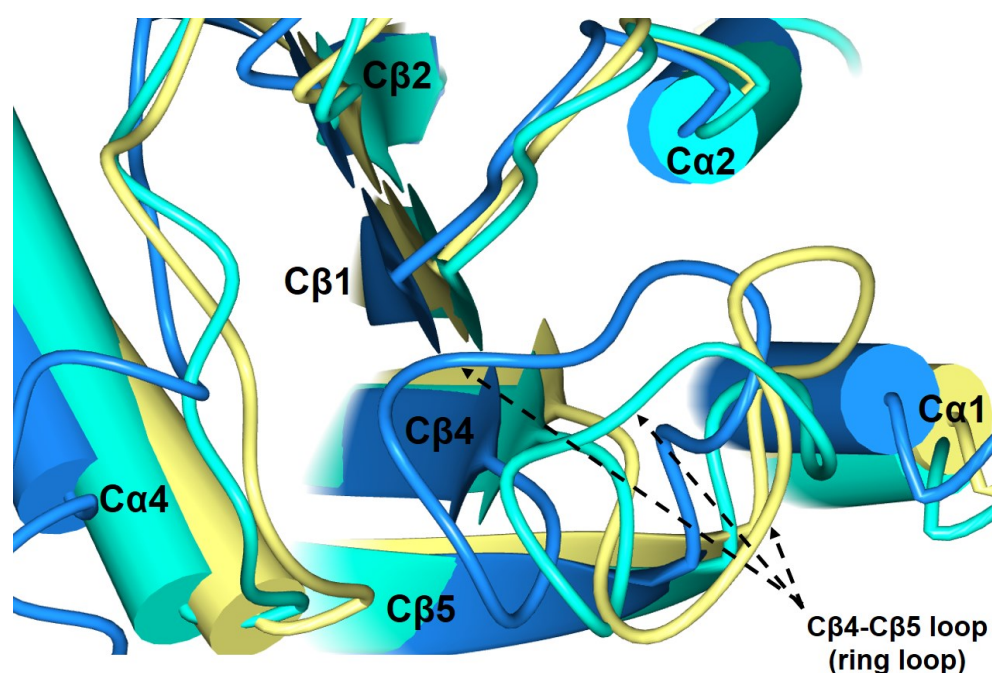
Figure 5.22: The allosteric site in PykF. Superposition of the allosteric site of PykF$_{PA}$ (cyan), PykA$_{PA}$ (blue) and 1PKY from *E. coli* (yellow). The Cβ4-Cβ5 in PykF$_{PA}$ adopts an intermediate conformation between fully opened and closed. Figure was generated using CCP4mg.

5.10 Intersubunit interactions in PykF

5.10.1 The A-A interface in PykF

The A-A interface in PykF is formed between the opposing A domains of chain A and B, and of chain C and D. Interactions of the A-A interface are shown in Table 5.3, Figure 5.23 and Figure 5.24. The interface comprises of a mixed network of hydrogen bonds and salt bridges and is coordinated through interactions from four α-helices (Aα6, Aα7, Aα8 and Cα1') and two loops (Aα7-Aβ7 loop and Aα8-Cα1' loop). Most importantly, Aα6' (the active site helix) is not a part of the A-A interface in PykF$_{PA}$. Also, the Cα1' helix which is unique to PykF$_{PA}$ (absent in PykA$_{PA}$ and apo PykF from *E. coli*), connects the two adjacent A domains of PykF$_{PA}$ through a Cα1'-Cα1' interaction (Figure 5.24).

Amino acid sequence analysis of the A-A interface in PykF$_{PA}$ (Appendix 9) revealed that the interface was mediated equally by bonds provided by conserved and less-conserved residues. Many of the less-conserved residues were only present in PykF$_{PA}$ and absent in PykA or PykF from other species. These residues include Thr297, Lys327, Glu335, Asp337, and Gln341. The coordination of the A-A interface in PykF$_{PA}$ via a set of less-conserved residues indicates that this enzyme may have evolved differently in *P. aeruginosa* compared with PykF from other species. Gln341 is one of the less-conserved residues which is present only in PykF$_{PA}$. At the A-A interface in PykF$_{PA}$, Gln341 forms a glutamine dimer connecting the opposite Cα1' helices together (Figure 5.24). The Gln341-Gln341 interaction (or the Cα1'-Cα1' interaction) is the shortest bond (2 Å) at the A-A interface in PykF$_{PA}$. The rest of the less-conserved residues at the A-A interface in PykF$_{PA}$ (Lys327, Glu335 and Asp337) seem to be of equal importance to Gln341 as they mediate formation of three different salt bridges.

5.10.2 The C-C interface in PykF

As there is no C-C interface present in the asymmetric unit of PykF, the C-C interface was generated by symmetry coordinates from chain A and B. The C-C interface was generated between the opposing C domains of chain A and C, and of chain B and D. The accessible solvent surface area of the C-C interface is 1070 Å^2, burying around 5% of each protomer surface. Table 5.3 and Figure 5.25 illustrate the inter-protomer interactions at the C-C interface in PykF. The arrangement of the structures at the C-C

interface in PykF$_{PA}$ was similar to the same interface in PykF from *E. coli* (PDB 1PKY), in which the adjacent Cα4 and Cβ5 are placed close to the interface and coordinate with the opposite Cα4 and Cβ5, respectively. The Cα1-Cα1' loop (Aα8-Cα1 loop in *E. coli*) is also shifted away from the interface in both structures (Figure 5.25). The configuration of the C-C interface in PykF$_{PA}$ is likely associated with the unbound status of the enzyme.

Table 5.3: Intersubunit interactions in PykF. Each interaction is presented once. Red asterisks refer to the formation of salt bridges. The results are based on interface analysis using PDBePISA.

The A-A interface in PykF					
Chain B	**Secondary structure**	**Distance (Å)**	**Chain A**	**Secondary structure**	
Lys258	Aα6	2.54	Glu335	loop Aα8-Cα1'	*
Arg289	Aα7	2.68	Gln276	loop Aβ7-Aα7	
Arg289	Aα7	2.64	Asp294	Aα7	*
Thr297	Aα7	3.84	Thr297	Aα7	
Asp337	loop Aα8-Cα1'	2.71	Lys258	Aα6	*
Glu251	Aα6	3.10	Lys327	Aα8	*
Gln341	Cα1'	2.07	Gln341	Cα1'	
The C-C interface in PykF					
Chain B	**Secondary structure**	**Distance (Å)**	**Chain C**	**Secondary structure**	
Ile467	Cβ5	2.91	Asn463	Cβ5	
Leu465	Cβ5	2.92	Leu465	Cβ5	
Asp426	Cα4	3.91	His424	Cα4	*
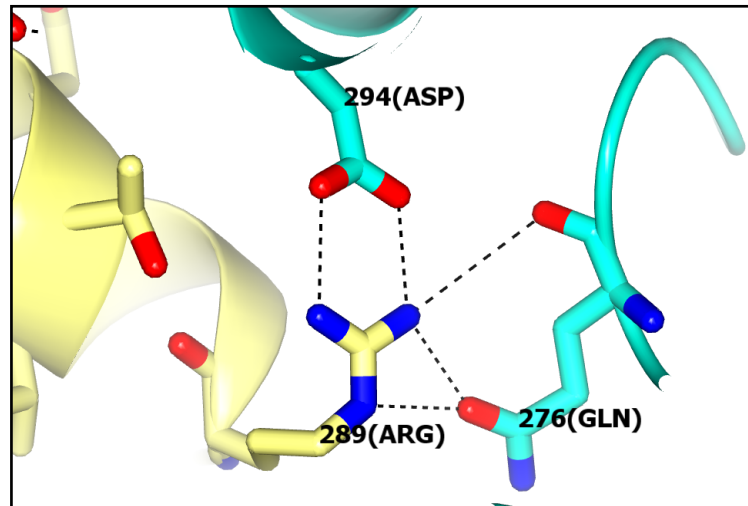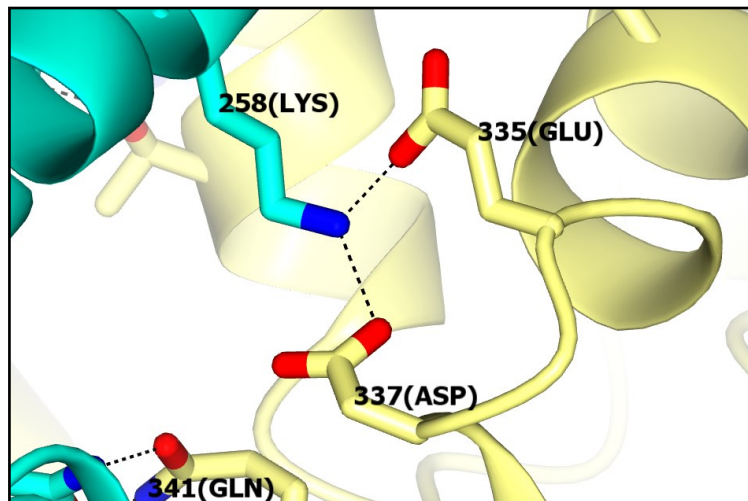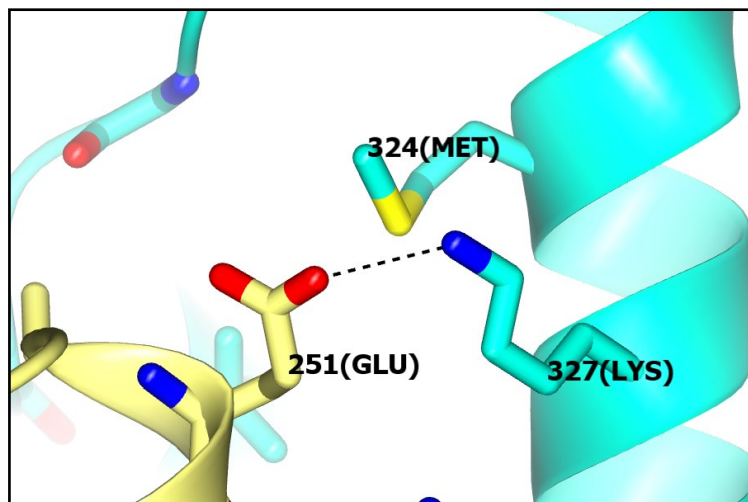
Figure 5.23: Close-up view of the A-A interface in PykF. The figure shows the salt bridge mediated interactions between the A domains of chain A (yellow) and B (cyan). The figure was generated using CCP4mg.

A)
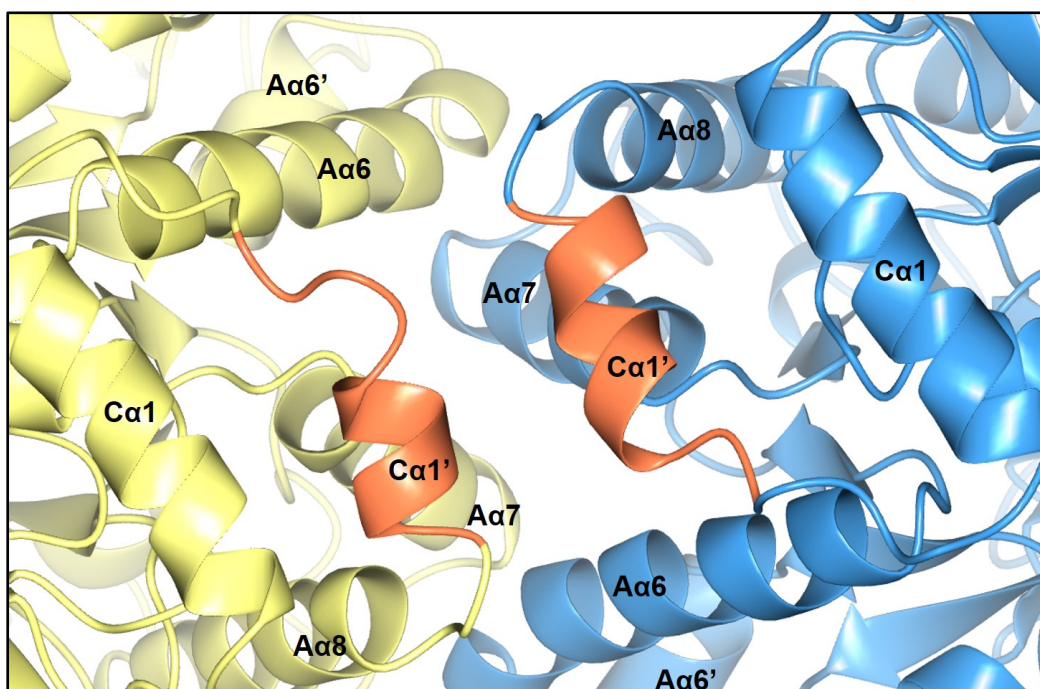
B)
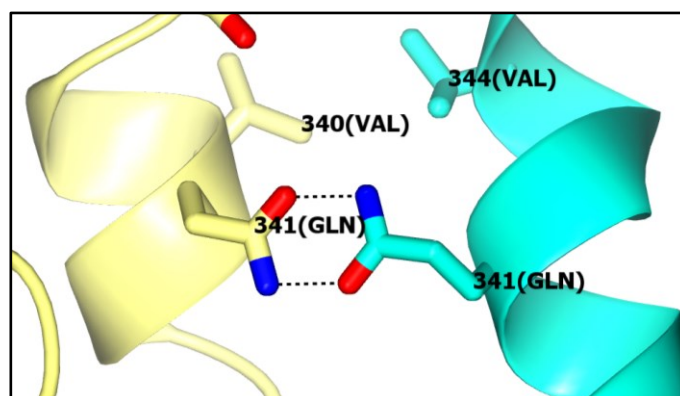
Figure 5.24: The A-A interface in PykF. A) Front view of the A-A interface in PykF. Chain A and B are presented as blue and yellow ribbons, respectively. The adjacent Cα1' helices are shown as coral ribbons. **B)** Close-up view of the A-A interface in PykF showing the glutamine dimer between the adjacent Cα1' helices. Figures were generated using CCP4mg.
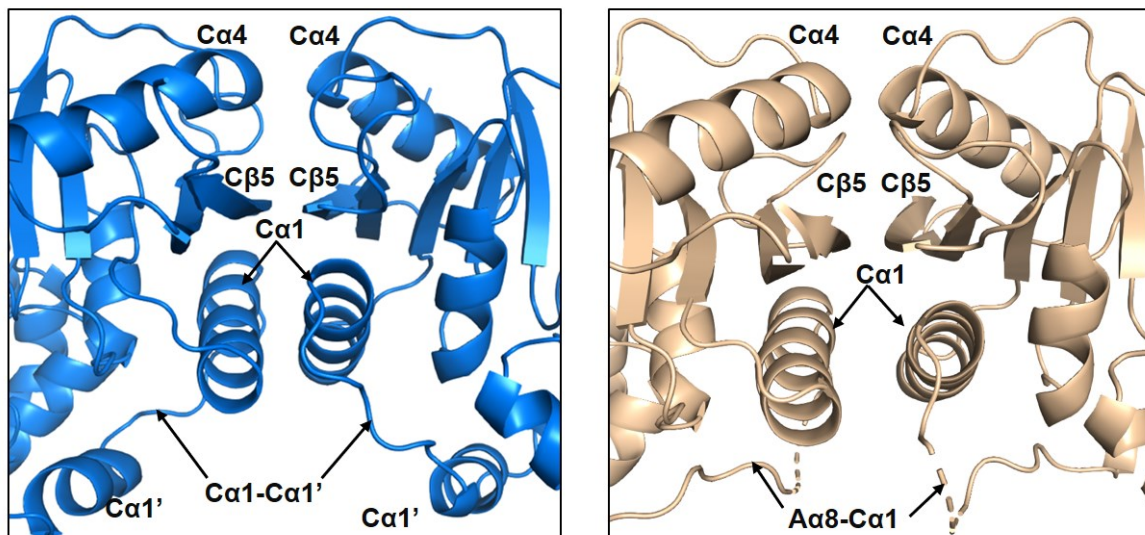
Figure 5.25: Comparison between the C-C interface in PykF$_{PA}$ and 1PKY from *E. coli*. The figure shows cartoon representation of the C-C interface in PykF$_{PA}$ (left, blue) and 1PKY (right, beige). The C-C interface in PykF$_{PA}$ shows the same configuration of the unbound 1PKY. The figure was generated using CCP4mg.

5.10.3 Intersubunit interactions in PykF$_{PA}$ compared with 1PKY from *E. coli*

Although PykF$_{PA}$ and PykF of *E. coli* (PDB 1PKY) were modelled as apo enzymes, investigation of the interactions at inter-protomer spaces revealed many differences between the two models (Figure 5.26). The A-A interface in PykF$_{PA}$ showed a prominent Cα1'-Cα1' interaction, whereas there is no Cα1' structure in 1PKY$_{EC}$ (Figure 5.26A). There is also bonding of Aα6 with the opposite Aα8-Cα1' loop or the Aα8 helix at the A-A interface in PykF$_{PA}$ and these interactions are absent in 1PKY$_{EC}$. By contrast, the A-A interface in 1PKY$_{EC}$ included interactions from the Aα6- Aα6' loop and these were absent in PykF$_{PA}$. Analysis of the PykF$_{PA}$ and 1PKY$_{EC}$ structures demonstrated that the C-C interface in PykF$_{PA}$ is stabilized by salt bridge formation and lacks any interactions from the Cβ4-Cβ5 loop (Figure 5.26B). By contrast, in 1PKY$_{EC}$, the C-C interface is mediated without salt bridges and with contributions from Cβ4-Cβ5 loop. The differences between PykF$_{PA}$ and 1PKY$_{EC}$ structures may partly explain the unusual regulation of PykF in *P. aeruginosa* compared with PykF from *E. coli*.
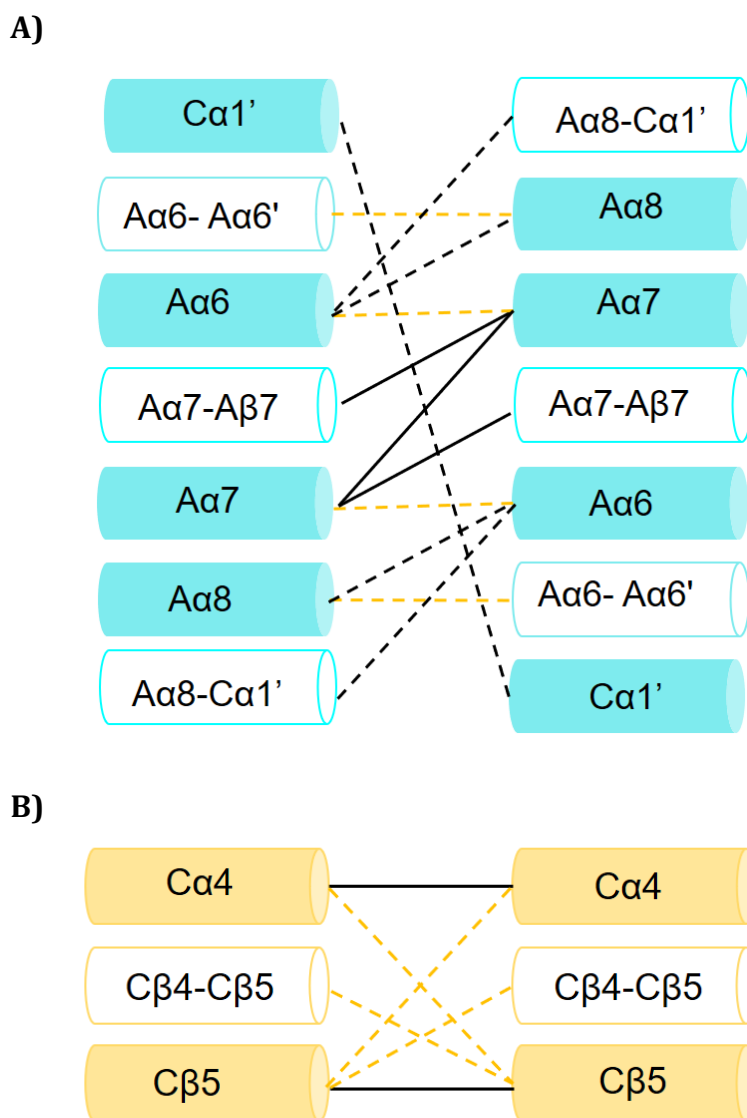
Figure 5.26: Comparison between the intersubunit interactions in PykF$_{PA}$ and 1PKY from *E. coli*. The figure illustrates the interactions at the A-A interface **(A)** and at the C-C interface **(B)** in PykF$_{PA}$ and in the unbound 1PKY from *E. coli*. Black dashed, yellow dashed and black solid lines represent the interactions present in PykF$_{PA}$ only, 1PKY only, and both structures, respectively. Filled cylinders represent alpha helices or beta strands, whereas unfilled cylinders represent the connecting loops. The diagram was based on analysis of inter-protomer interactions using PDBePISA.

5.11 Discussion

Here, I present the first crystal structures of PykA and PykF from *P. aeruginosa*. PykA$_{PA}$ was solved in complex with MLI, Mg^{2+} and G6P, whereas PykF$_{PA}$ was solved in an apo state and at a slightly lower resolution than PykA$_{PA}$. At present, PK of *M. tuberculosis* is the only available bacterial PK structure in the PDB with bound ligands (apart from metal ions). In *M. tuberculosis*, PK displays two ligand binding sites; a G6P-binding site and an AMP-binding site. Analysis of PykA$_{PA}$ revealed that it has a G6P-binding site which corresponds to the AMP-binding site in PK of *M. tuberculosis*, meaning that PykA$_{PA}$ and PK of *M. tuberculosis* presumably have different mechanisms of allosteric regulation by G6P. Likewise, PykF$_{PA}$ also revealed many structural differences when compared with PykF from *E. coli*, although both were modelled as unbound.

5.11.1 The unusual regulation of PykA$_{PA}$ and PykF$_{PA}$ is mostly related to their structures

Findings from chapter 4 showed that PykA$_{PA}$ and PykF$_{PA}$ are regulated differently than the PykA and PykF enzymes from other Gram-negative species. PykA$_{PA}$ was activated by a diverse set of metabolites from the EDP and PPP, whereas regulation of PykA from other species was mainly achieved by R5P and AMP (Waygood et al., 1975; Garcia-Olalla and Garrido-Pertierra, 1987). PykF$_{PA}$ was activated by monophosphorylated metabolites of the PPP, whereas other PykF enzymes are activated by di-phosphorylated metabolites of the EMP pathway (Waygood et al., 1976; Garcia-Olalla and Garrido-Pertierra, 1987; Waygood and Sanwal, 1974). Thus, apparently there are some structural features of PykA$_{PA}$ and PykF$_{PA}$ which could be responsible for their unusual regulation.

Why do PykA$_{PA}$ and PykF$_{PA}$ respond differently to allosteric regulators?. The G6P-binding site in PykA$_{PA}$ corresponds to the predicted allosteric site in other enzymes. In PykA$_{PA}$, the phosphate loop and Cα2 helix bind to the phosphate moiety of G6P, whereas the ring loop anchors the ring moiety of the ligand. Given that the residues of the first region are strictly-conserved among all PykA enzymes including PykA$_{PA}$ ($_{384}$TESGFT$_{389}$, with the exception of the Phe388 in PykA$_{PA}$ which is replaced by an arginine in other PykAs), it is unlikely that this region is behind the unusual regulation of

PykA$_{PA}$. By contrast, the ring loop of PykA$_{PA}$ encodes a unique sequence ($_{462}$DSYTAQ$_{467}$) which is not present in other PykA group members. Likewise, the equivalent ring loop in PykF$_{PA}$ also encodes a distinguishable sequence ($_{454}$VPFGRP$_{459}$). Taken together, it seems that the unusual regulation of PykA and PykF in *P. aeruginosa* may be partly associated with the different amino acid sequence composition of their ring loops.

In PykA$_{PA}$, the ring loop is apparently important for many aspects of the allosteric regulation. Using the ring loop, PykA$_{PA}$ can directly interact with both G6P and the surrounding structures of the C domain (phosphate-ring loop interaction). These interactions of the ring loop likely stabilize the ligand in the allosteric pocket. Moreover, the loop itself forms a salt bridge across the C-C interface, thus the ring loop might also be essential for transmission of allosteric signals across the subunits of PykA$_{PA}$. Future work should study the specific impact of ring loop mutations on the allosteric response of PykA$_{PA}$ and PykF$_{PA}$.

Why is PykF$_{PA}$ not activated by di-phosphorylated metabolites?. Many PK enzymes are known to be allosterically regulated by di-phosphorylated metabolites such as F1,6P (Waygood and Sanwal, 1974; Waygood et al., 1976; Garcia-Olalla and Garrido-Pertierra, 1987; Hofmann et al., 2013). However, PykF$_{PA}$ was unaffected by F1,6P which could also be due to structural factors of PykF$_{PA}$. Analysis of PK enzymes which are activated by F1,6P shows that this bisphosphate binds to the predicted allosteric site of these enzymes. At the allosteric site, the negatively charged 1-phosphate of F1,6P binds to a positively charged residue (mostly arginine) from Cα4 (Jurica et al., 1998). Analysis of PykF$_{PA}$ structure and amino acid sequence reveal that Cα4 lies between Val425 and Ala438 and this region lacks any positively charged residues. This means that the Cα4 helix of PykF$_{PA}$ is apparently less favourable for binding of the 1-phosphate of F1,6P. By contrast, amino acid sequence analysis of PykF from other bacteria shows that there are two conserved positively charged residues (arginine and lysine) in the centre of the Cα4 helix (Figure 5.27). The positively charged residues in the Cα4 helix of these PykF enzymes are likely involved in the binding of F1,6P. However, this needs further investigation as there are no bacterial PykF structures in the PDB bound to F1,6P.
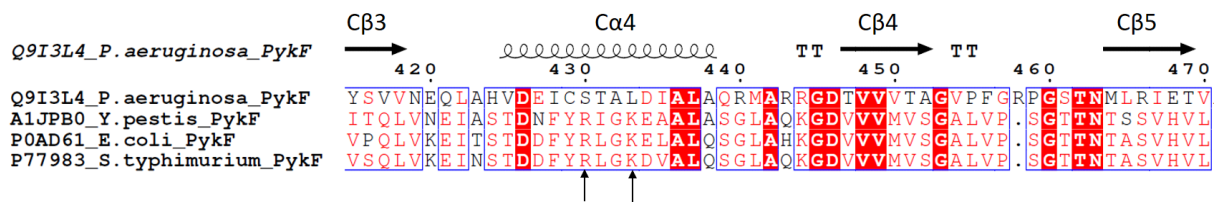
Figure 5.27: Amino acid sequence alignment of PykF enzymes. Secondary structures are annotated according to the structure of PykF$_{PA}$. Black arrows point to the positively charged residues which probably bind to 1-phosphate group of F1,6P (in the Cα4 helix of the PykF enzymes). PykF$_{PA}$ lacks these residues. Residues highlighted in red are 100% identical, whereas a column is framed in blue if more than 70% of the residues have similar physicochemical properties.

5.11.2 The G6P-binding site in PykA

The only published G6P-bound bacterial PK structure belongs to *M. tuberculosis* (PDB 5WSA, 5WSB, 5WSC). Alignment of PykA$_{PA}$ and PK of *M. tuberculosis* reveals that the G6P-binding site in PykA$_{PA}$ is clearly distinct than the one in PK of *M. tuberculosis* (Figure 5.28). Whereas G6P binds to the heart of the C domain of PykA$_{PA}$, it is placed between the A and C domains of PK of *M. tuberculosis*. Moreover, the G6P-binding site of PykA$_{PA}$ overlaps with the AMP-binding site of PK of *M. tuberculosis.* Despite sharing the same allosteric site, the secondary structures that anchor G6P in PykA$_{PA}$ are different than the ones that hold AMP in the PK of *M. tuberculosis*. PykA$_{PA}$ coordinates G6P in the allosteric site using the ring loop, the phosphate loop and the Cα2 helix. By contrast, the AMP in *M. tuberculosis* is anchored using additional residues from Cα1, Cα4 and loop Cβ3-Cα4 (Zhong et al., 2017). Also, the Cα4 helix of PykA$_{PA}$ is partially unwound and placed far from the bound G6P, whereas the Cα4 helix of PK from *M. tuberculosis* is placed closer to the bound AMP. All these structural differences between PykA$_{PA}$ and PK from *M. tuberculosis* highlights that there is likely a different regulatory mechanism by which G6P activates PykA$_{PA}$.
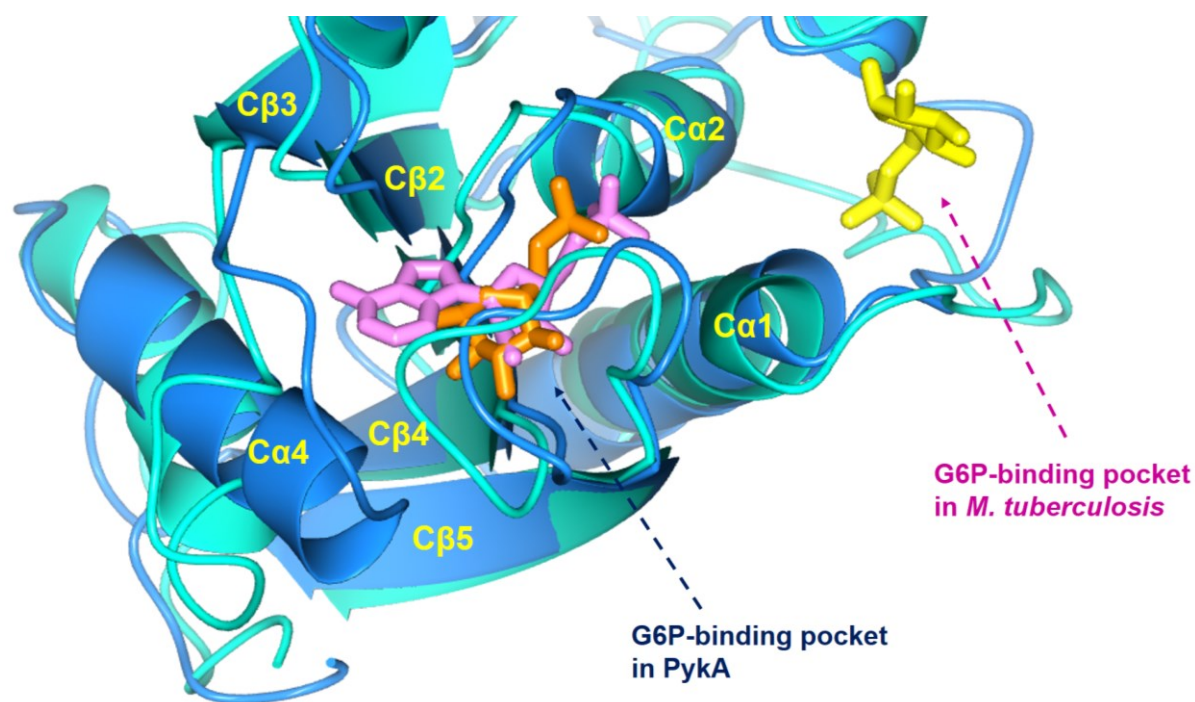
Figure 5.28: The G6P-binding site in PykA$_{PA}$ and PK of *M. tuberculosis*. Cartoon representation of the allosteric site in PykA$_{PA}$ (cyan) and PK of *M. tuberculosis* (PDB 5WSB, blue). G6P bound to PykA$_{PA}$ is shown as a coral cylinder, whereas the G6P and AMP that bind to PK of *M. tuberculosis* are shown in yellow and pink cylinders, respectively. Secondary structures are annotated according to PykA$_{PA}$. The figure was generated using CCP4mg.

5.11.3 Contributions of the Aβ5-Aα5 loop to formation of the active site in PykA

Analysis of the active site in PykA showed a distinguishable outward orientation of Aα5 helix which was attributed to elongation of the preceding Aβ5-Aα5 loop. Although, there was no direct involvement of Aα5 residues to the interactions at the active site, the Aβ5-Aα5 loop clearly contributes to formation of the PykA-MLI-Mg complex (Figure 5.29). In PykA, the Aβ5-Aα5 loop terminates with two strictly-conserved residues; Lys221 and Glu223, which are known to have significance for the enzymatic activity. In other PKs, the equivalent lysine binds to the phosphoryl group of phospho*enol*pyruvate and stabilizes its transfer from PEP to ADP (Bollenbach et al., 1999). In bacteria and yeast, site-directed mutagenesis of the DNA encoding this lysine residue caused a significant drop of catalytic activity compared with wild-type (Suzuki et al., 2008; Bollenbach et al., 1999).

179

Also, Glu223 seems to be of equal importance for the enzymatic activity of PK. In PykA, Glu223 holds Mg^{2+} in the active site pocket. In other enzymes, the equivalent glutamic acid is important for binding of PEP, ADP and ATP in the active site (Muirhead et al., 1986). Moreover, substitution of this glutamic acid with other residues, even aspartate, causes loss of PK enzymatic activity and shutdown of carbohydrate metabolism (Keating et al., 2005). Despite the importance of the Aβ5-Aα5 loop for the enzymatic activity, the impact of its elongation on PykA$_{PA}$ activity is still unclear.
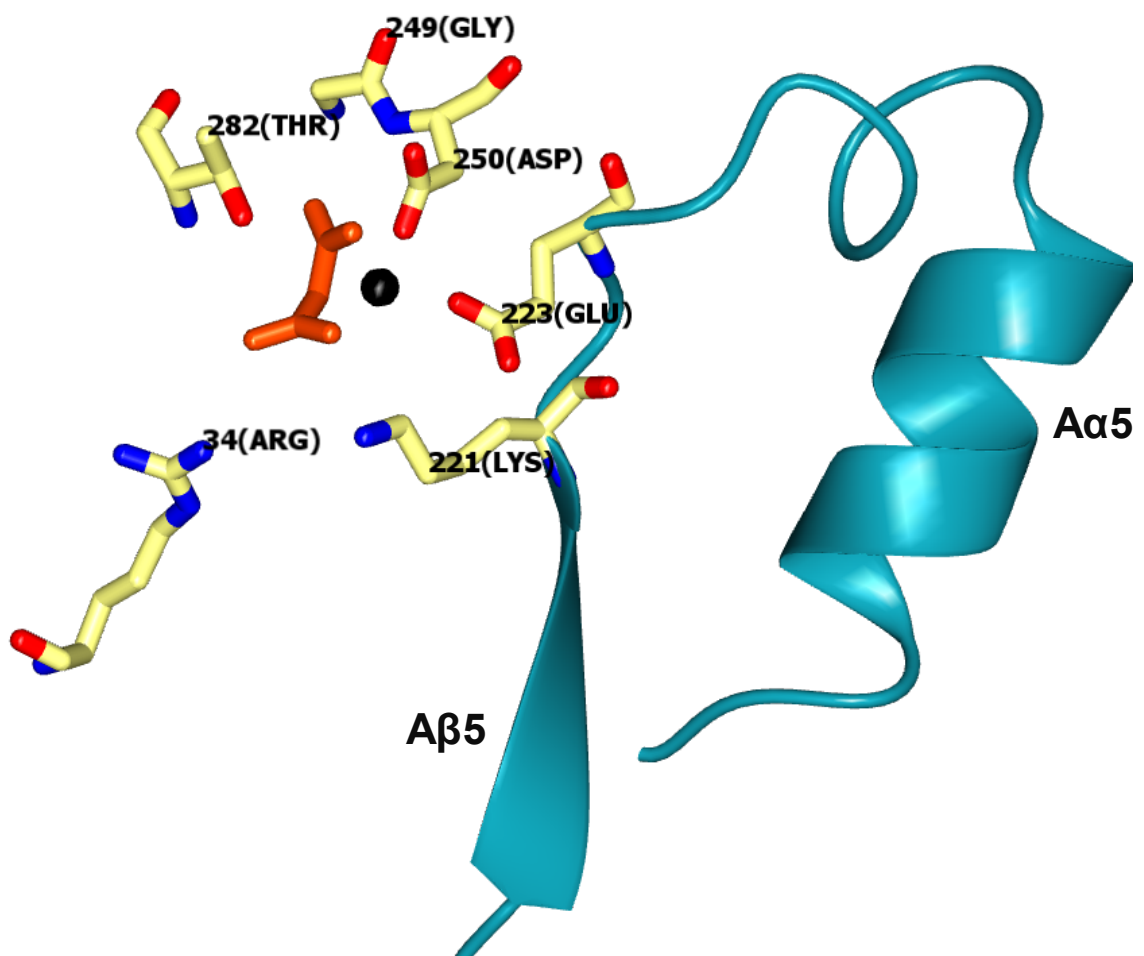
Figure 5.29: Contributions of the Aβ5-Aα5 loop to the active site in PykA. A cartoon diagram showing that the elongated Aβ5 and Aα5 loop terminates with Lys221 and Glu223, which participate in formation of the PykA-MLI-Mg complex in the active site. The bound MLI and Mg^{2+} ion are indicated by a coral cylinder and a black sphere, respectively. The figure was generated using CCP4mg.

5.11.4 Interactions of Aα6' and Aα7 at the A-A interface in PykA

One of the most important interactions across the A-A interface in PykA$_{PA}$ was the pairing of the active site helix Aα6' from one protomer (Arg248 and Gly249) with the Aα7 helix (harbouring Arg296) of the adjacent protomer. This coordination is considered as a hallmark of a bound or active PK conformation (Mattevi et al., 1995) and it is likely primed by movement of Arg296 on Aα7.

Arg296 is strictly-conserved among all PK and the equivalent arginine in PykF of *E. coli* (Arg292) is predicted to have a role in transmission of the activity signal from the active site to the adjacent subunits (Valentini et al., 2000). Moreover, mutagenesis of Arg292 in *E. coli* PykF causes loss of enzymatic activity and disorder of integral structures of the active site (Valentini et al., 2000). Mutagenesis of Arg292 in PykF$_{EC}$, however did not alter the oligomeric state of the enzyme.

Reorientation of Arg292 (equivalent to Arg296 in PykA$_{PA}$) has been proposed to prime the transition of *E. coli* PykF from the unbound to the bound state (Valentini et al., 2000). In unbound PykF, Arg292 forms a salt bridge with Asp297 from the adjacent protomer (Figure 5.30). Upon transition to the bound state, Arg292 is predicted to reorient towards Aα6' (the active site helix). With this, Arg292 brings helix Aα6' to the A-A interface, allowing the newly freed Asp297 to form a salt bridge (intra-protomer) with Arg244 (Valentini et al., 2000). Given that these residues are conserved in *E. coli* PykF and *P. aeruginosa* PykA, the same scenario can be predicted for PykA$_{PA}$ upon transition from the unbound to the bound state. In unbound PykA$_{PA}$, Arg296 likely coordinates with Asp301 via a salt bridge (equivalent to the Arg292-Asp297 interaction in PykF$_{EC}$). Then, upon converting to the bound state, the Arg296-Asp301 interaction is disrupted due to rearrangement of the structures at the active site. Alternatively, Arg296 reorients towards and interacts with helix Aα6' and the free Asp301 forms an intra-protomer salt bridge with Arg248 (Figure 5.30).
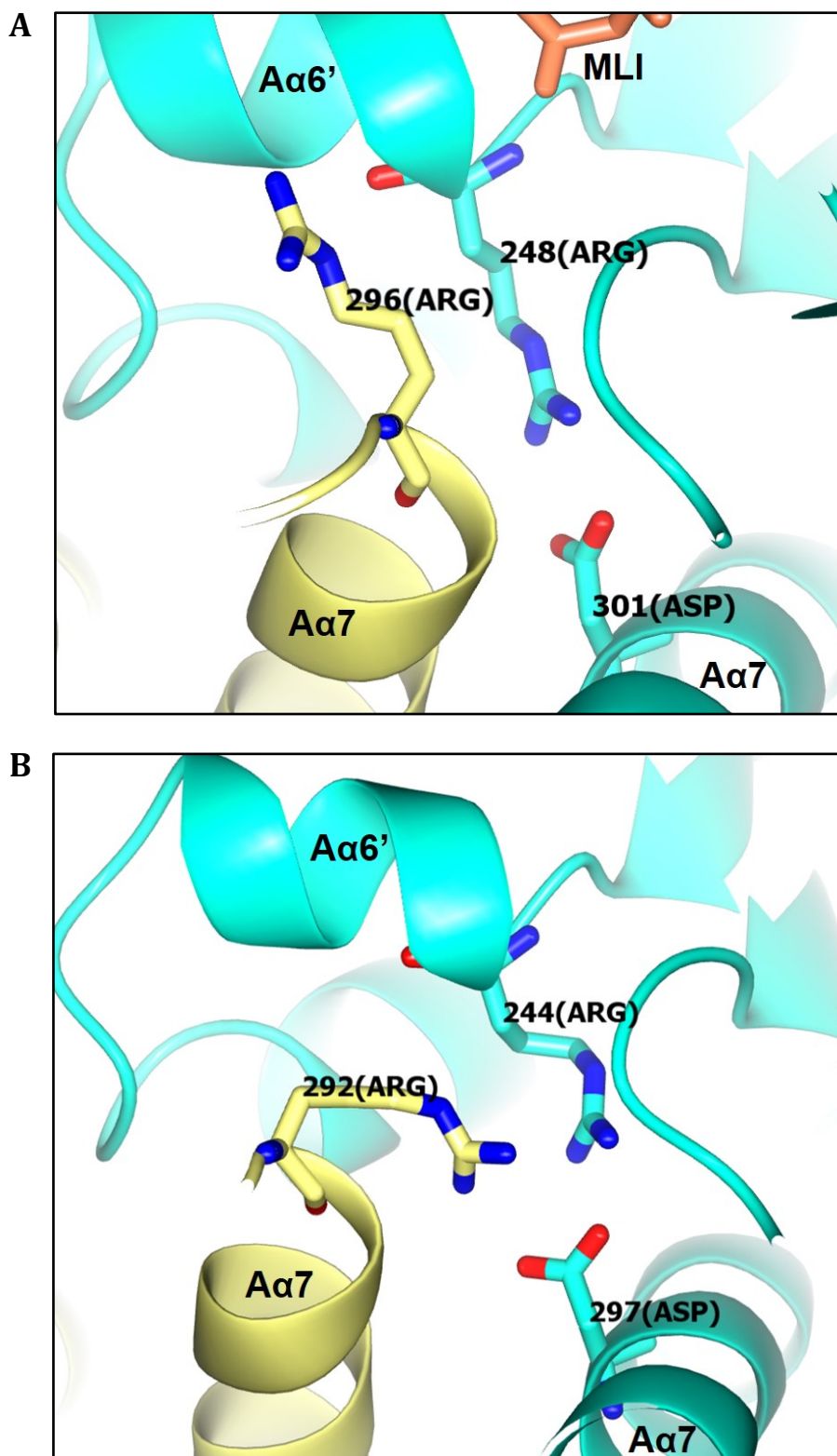
Figure 5.30: Interactions of Aα6' and Aα7 in PykA$_{PA}$ (A) and apo PykF from *E. coli* (B). Protomers are shown in different colours. Sodium malonate is shown as a coral cylinder in the active site of PykA$_{PA}$. PDB 1PKY was used as a model for *E. coli* PykF. Figures were generated using CCP4mg.

5.11.5 A proposed mechanism of PykA regulation by G6P

To understand the mechanism of transmission of allosteric signals from the G6P binding site to the active site in PykA, inter-protomer interactions should be compared in G6P-bound PykA and apo-PykA. However, due to the unavailability of an apo PykA structure, the A-A interfaces and the C-C interfaces were analysed using PykF from *E. coli* as an apo model. Analysis of PykA$_{PA}$ shows that the A-A interface comprises interactions from the Aα6' helix and Aα8-Cα1 loop, whereas these are absent in apo-PykF$_{EC}$. In contrast, the A-A interface in apo-PykF$_{EC}$ has an Aα7-Aα7 interaction which is disrupted in G6P-bound PykA$_{PA}$ (due to mobility of Arg292 towards the active site, Figure 5.30). Analysis of PykA$_{PA}$ and apo-PykF$_{EC}$ demonstrated additional differences in the allosteric site and at the C-C interface. In apo-PykF$_{EC}$, the allosteric pocket is opened (due to movement of the ring loop away from the allosteric site), whereas the allosteric site of PykA$_{PA}$ adopts a closed configuration (due to movement of the ring loop towards the bound G6P). Also, the C-C interface in apo-PykF$_{EC}$ contains interactions from Cα4, whereas Cα4 is replaced by Cα1 and the Aα8-Cα1 loop at the C-C interface in PykA$_{PA}$.

By combining these differences, a mechanism of PykA regulation by G6P can be proposed (Figure 5.31). The proposed sequence of interactions begins with occupation of the allosteric site of PykA by G6P which causes relocation of the ring loop towards the allosteric pocket. This movement of the ring loop promotes closure of the allosteric pocket and facilitates the bonding of G6P with the ring and phosphate loops. Movement of the ring loop also displaces the Cα4-Cα4 at the C-C interface. This new configuration of the allosteric site in PykA promotes disruption of Cα4 interactions at the C-C interface, but also recruits Cα1 and the Aα8-Cα1 loop to the interface. In PykA, the Aα8-Cα1 loop coordinates two protomers simultaneously via the A-A interface and the C-C interface. Therefore, changes at the C-C interface are likely accompanied by changes at the A-A interface via Aα8-Cα1. Given the proximity of the A-A interface with the active site helix (Aα6'), this suggests a likely mechanism by which G6P binding may influence catalysis by PykA.
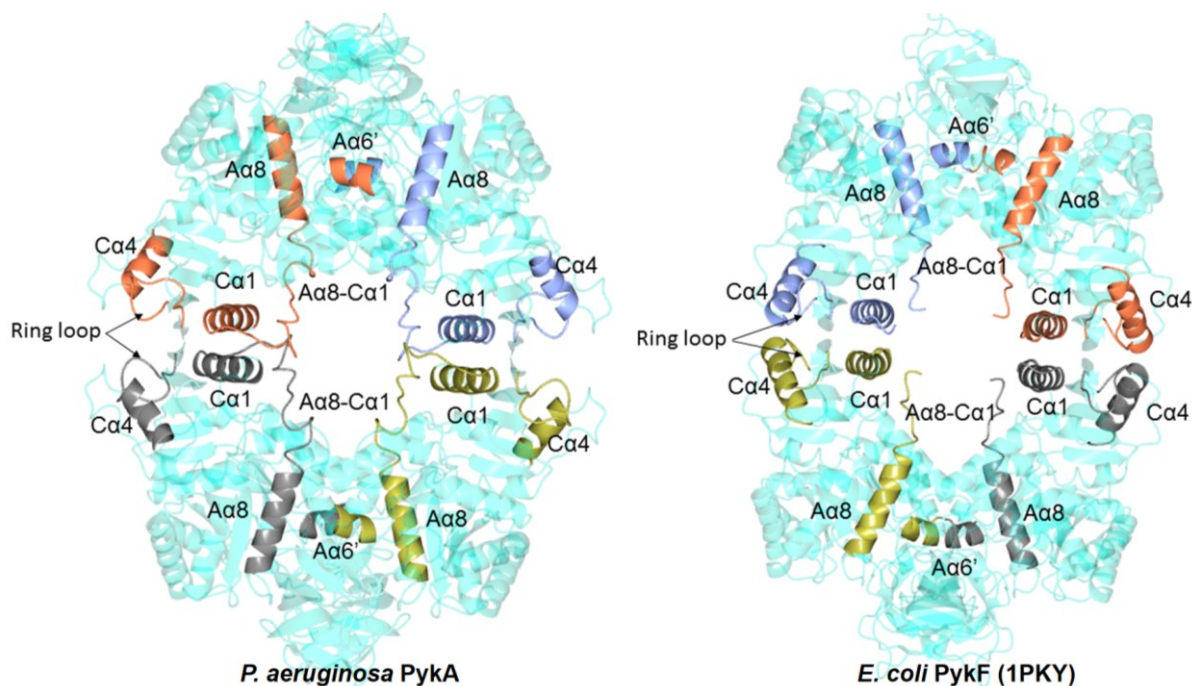
Figure 5.31: Configuration of key secondary structures in PykA$_{PA}$ and PykF$_{EC}$. The proposed mechanism of allosteric regulation of PykA by G6P begins with binding of G6P to PykA which leads to retraction of the ring loop towards the bound ligand. This movement of the ring loop causes disruption of Cα4-Cα4 at the C-C interface, but recruits Cα1 and the Aα8-Cα1 loop to join the interface. These changes cause displacement of Aα8 which subsequently pairs with the Aα6-Aα6' loop at the A-A interface. As the Aα6' helix is a prominent structure of the active site in PykA, this cascade of interactions most likely explains the allosteric activation of PykA by G6P.

5.11.6 The Cα1' helix of PykF

One of the main differences between PykF from *P. aeruginosa* and PykF from *E. coli* is that the former has a Cα1' helix. Cα1' is a short helical fragment that precedes the Cα1 helix, thus it connects between the A and C domains. Cα1' was clearly seen in the electron density of both subunits of PykF. By contrast, Cα1' is absent from the PK structures of other Proteobacteria such as *E. coli* PykF or *P. aeruginosa* PykA. In the latter species, Cα1' is replaced by a long uninterrupted loop connecting the A and C domains (Aα8-Cα1 loop). On the other hand, the crystal structures of PK from some Firmicutes and eukaryotes do contain a helix similar to Cα1' in PykF$_{PA}$. These structures include PK from *Bacillus stearothermophilus* (PDB 2E28), *Staphylococcus aureus* (PDB 3T05 and 3T07)

and *Toxoplasma gondii* (PDB 3EOE). Comparison of the amino acid sequence of these enzymes revealed that residues of Cα1' are diverse, meaning that the function of Cα1' (if any) is likely species-specific.

In PykF$_{PA}$, Cα1' contributes to formation of the A-A interface via reciprocal hydrogen bonds formed between the side chains of opposite Gln341 residues. In crystallography, enthalpic cooperativity is always preferred over entropic interactions in order to achieve structural stability. Hydrogen bonding between side chains of glutamine is considered one of the best interactions which achieves maximum enthalpic cooperativity (Plumley and Dannenberg, 2010). Thus, it is likely that the glutamine dimer across the A-A interface in PykF$_{PA}$ may have a major impact on the stability of the enzyme. Moreover, the shorter the distances between side chains of a "glutamine dimer", the stronger the interaction they stabilize. In PykF, the distance of the Gln341-Gln341 hydrogen bond was just 2 Å. Future work should study the impact of Gln341 on the stability and activity of PykF.

5.12 Conclusion

X-ray crystallography is a powerful tool for determination of biological structures and molecular interactions, and its outputs can serve as a basis for drug-design efforts. Here, I have shown the first x-ray structures of PykA (bound with G6P, MLI and Mg^{2+}) and PykF (unbound) from *P. aeruginosa*. The allosteric site of PykA was bound with its regulator (G6P), however the G6P binding site in PykA was distinct from that previously identified in the PK from *M. tuberculosis*. My data also suggest a plausible mechanism by which the binding of G6P transmits a conformational change to the active site of PykA. Analysis of the PykF structure has also shown many differences compared with *E. coli* PykF. The structure-sequence analysis revealed that the unusual allosteric regulation of PykA and PykF in *P. aeruginosa* is likely related to the amino acid composition of their ring loops.

Chapter 6

6 Final conclusions

PK is a key metabolic enzyme with a central position between glycolysis and the TCA cycle. PK activity has also been linked with physiological changes in many microorganisms, impacting on energy production, survival and virulence (Pan et al., 2008; Bücker et al., 2014; Chai et al., 2016). Thus, PK has become a promising metabolic target in the treatment of antibiotic resistant infections such as those caused by *Staphylococcus aureus* (Axerio-Cilies et al., 2012). Most of bacteria encode one PK, whereas a few have two PK isozymes, denoted as PykA and PykF. In the latter species, PykF is usually the dominant isoform and is activated by F1,6P (an intermediate from the EMPP), whereas PykA plays a less important role and is activated by R5P and/or AMP (intermediates from the PPP). *P. aeruginosa* encodes one PykA and one PykF isoform, and they are uncharacterized to date. Unlike most bacteria, *P. aeruginosa* depends mainly on the EDP for metabolism because it lacks the key enzymes for operation of the EMPP and the PPP. However, this organism can recycle metabolites from the main EDP into the side branches of the EMPP and the lower arm of the PPP (known as the EDEMP or the cyclic EDP). Therefore, it is likely that PykA and PykF behave differently in this organism and that is because of the way in which this organism is "wired up" for the EDP. With this, my main aim was to characterize the genetic, biochemical and structural properties of PykA and PykF in *P. aeruginosa*.

Bioinformatic analysis revealed that the PK isozymes in *P. aeruginosa* have been rightly assigned to the correct PK subclasses. PykA and PykF from *P. aeruginosa* were classified according to their amino acid sequence to the PK II subfamily and PKM subfamily, respectively. Motif analysis further demonstrated that PykA has a predicted tyrosine kinase phosphorylation (TKP) site which is absent in PykF. By contrast, PykF is predicted to have a cAMP/cGMP dependent protein kinase phosphorylation (CAG-DPKP) site which is absent in PykA. These sites were also predicted in PykA and PykF from other species. Given that these sites are more common in eukaryotes, the question as to why they are predicted and conserved among PykA and PykF isoforms still needs to be addressed.

Having verified that PykA and PykF were annotated correctly in *P. aeruginosa*, my first objective was to investigate *pykA* and *pykF* from a genetic perspective and to see if they both contribute to cell physiology. Unlike previously characterized *pykA* and *pykF* isoforms from other species, the transcription of *pykA* was predominant in all tested carbon sources and oxygen levels. In contrast, the transcription of *pykF* was comparatively low throughout. Protein expression data were in agreement with the transcription profiles and revealed that PykA is the dominant isoform expressed in all the tested carbon sources, whereas the expression of PykF was undetectable.

To investigate the contribution of PykA and PykF towards cell physiology, enzymatic activity assays, growth curves and virulence assays were performed using *pykA* and *pykF* mutants and their complements. Results of these indicated that the function of PykA and PykF correlates well with their transcription and protein expression profiles. The data demonstrated that *pykA* was indispensable for pyruvate kinase activity and growth in glucose and glycerol (substrates that require PK catalysis), whereas it had little effect on growth in acetate and succinate (substrates that do not require PK catalysis). On the other hand, mutation of *pykF* did not alter the pyruvate kinase activity or growth phenotypes. These data combined indicates that unlike other species, PykA is the dominant isoform in *P. aeruginosa* and not PykF.

As this work started as an investigation of the *pykA* and *pykF* genetics, my second objective was to characterize the kinetics and regulatory properties of purified PykA and PykF. PykA and PykF were overexpressed in *E. coli* and purified in good yield. Kinetic analysis of PykA and PykF revealed that PykA was intrinsically more active than PykF as the K_M and $S_{0.5}$ values of PykA (with respect to ADP and PEP titration, respectively) were lower than those of PykF. Further analysis revealed that unlike most PK, PykA and PykF were K^+-independent and that they require Mg^{2+} for catalysis. In fact the addition of monovalent ions such as K^+ slightly perturbed their enzymatic activity. Amino acid sequence analysis of PykA and PykF revealed that these isoforms have a lysine residue which could replace the function of K^+ in the active site.

In order to identify potential regulators of PykA and PykF, I measured their activity in the presence of a range of metabolites. Although no inhibitors were identified,

a large set of activators of PykA and PykF was found. The most potent activators of PykA and PykF were X5P, R5P and RL5P, which all belong to the PPP. This was unexpected given that *P. aeruginosa* depends mainly on the EDP for glycolysis and it lacks 6-phosphogluconate dehydrogenase that feeds carbon into the upper arm of the PPP. However, metabolites can be recycled from the main EDP into the side branches of the EMPP and the lower arm of the PPP, such as during gluconeogenesis. Therefore, the activation of PykA and PykF by PPP metabolites highlights that in *P. aeruginosa*, the production of biosynthetic precursors is apparently coordinated with glycolysis.

P. aeruginosa is intrinsically resistant to many conventional antibiotics and it is one of the top-listed pathogens which require urgent development of new antimicrobials. Given that PykA was the dominant PK in *P. aeruginosa*, I aimed to identify PykA inhibitors that have the potential to be used as antimicrobial drugs against *P. aeruginosa*. Drug screening showed that shikonin and R396907 can inhibit the PykA activity, however via different inhibitory mechanisms. Shikonin inhibited PykA non-competitively, whereas R396907 inhibited PykA competitively. Moreover, dose-response curves revealed that the IC50 of shikonin (23.2 μM) was lower than the IC50 of R396907 (95.5 μM), meaning that shikonin was more potent than R396907. Growth curves of wild-type and clinical isolates showed that shikonin was also able to impair the growth of cells in glucose in a dose-dependent manner, whereas R396907 did not have an impact on growth. Although shikonin is known to have antimicrobial properties against *P. aeruginosa* (Al-Mussawi, 2010), there is no currently-identified target for shikonin in this organism. With this work, PykA becomes the first identified microbial target for shikonin in *P. aeruginosa*. Future work should investigate the effects of shikonin in treatment of cells/animals infected by *P. aeruginosa*.

My third objective was to solve the x-ray crystal structures of PykA and PykF in order to link the structure, function and regulation of these enzymes. I solved the structure of PykA (2.43 Å) bound with MLI and Mg^{2+} in the active site and with its activator G6P bound in the allosteric site. The PykF structure (3 Å) was solved as an apo enzyme. Structural analysis of PykA and PykF revealed many distinct properties of these enzymes compared with previously characterized PK structures.

The active site of PykA adopts a similar configuration to the active site of PKM1 from rabbit muscle which is known to be locked to the active state. The active site of PykA also forms a complex with the bound substrate analogue and ion (PykA-MLI-Mg complex) which is mediated by many conserved residues. Interestingly, helix Aα5 was found in an outward orientation away from the active site and this was attributed to elongation of the preceding Aβ5-Aα5 loop. The Aβ5-Aα5 loop was longer in PykA than in other PK structures and it contributes to formation of the active site via Lys221 and Glu223. Based on the amino acid sequence of PykA isozymes from other species, it is predicted that these also have a longer Aβ5-Aα5 loop, although the exact physiological role of this elongation is unclear.

In PykA, G6P was bound to an allosteric pocket which is distinct from the G6P binding site in PK from *M. tuberculosis*. This means that the mechanism by which G6P activates PykA is apparently different compared with the way it activates PK from *M. tuberculosis*. In the allosteric site of PykA, G6P was bound by two loops, denoted as the phosphate and ring loops. The two loops coordinate G6P in the allosteric site and they can also co-interact. The amino acid sequence of the phosphate loop was found to be conserved among PykA and PykF isoforms from many species. By contrast, the ring loop was found to be less conserved in the PKs from *P. aeruginosa*, so it is possible that the atypical regulation of these enzymes in *P. aeruginosa* is related to the amino acid composition of their ring loops.

Additionally, I proposed a mechanism by which G6P activates PykA based on comparisons between PykA (obtained in this study) and apo PykF from *E. coli* (PDB 1PKY). I hypothesized that when G6P binds to the allosteric site of PykA, it retracts the ring loop towards the allosteric site in order to stabilize the binding of the metabolite. Therefore, the ring loop initiates interactions with the G6P and also with the phosphate loop. The movement of the ring loop also disrupts the Cα4-Cα4 interaction at the C-C interface, whereas it recruits Cα1 and the Aα8-Cα1 loop to the C-C interface. The Aα8-Cα1 loop is part of the A-A interface and subsequently recruits the active site helix Aα6' to the A-A interface. This may explain how binding of G6P to the allosteric site enhances PykA activity.

Investigation of PykF showed that this isozyme adopts an inactive configuration. However, there are many differences found between *P. aeruginosa* PykF and *E. coli* apo-PykF. First, PykF from *P. aeruginosa* has a Cα1' helix (a short helical segment preceding Cα1), whereas Cα1' is absent in PykF from *E. coli*. The Cα1' helix in PykF$_{PA}$ connects the two opposite protomers together and also seems to have a role in stabilizing PykF$_{PA}$ by formation of a glutamine-dimer. Second, the allosteric site of PykF$_{PA}$ is partially closed due to disposition of the ring loop, whereas the allosteric site in PykF$_{EC}$ is open. This is likely related to the proline content of the ring loop in these enzymes; the ring loop of PykF$_{PA}$ contains two proline residues so it is likely to be more flexible, whereas the ring loop of PykF$_{EC}$ has one proline. Third, many of the inter-protomer interactions are different in PykF$_{PA}$ compared with PykF$_{EC}$, meaning that the communication between the subunits is likely to be different in the two proteins. This is important because inter-protomer interactions correlate well with the enzyme regulation. These differences combined may explain why PykF$_{PA}$ is regulated differently than PykF$_{EC}$.

In summary, the results presented in this dissertation show that in *P. aeruginosa*, PykA contributes more to cell physiology and growth than does PykF. This is primarily because the transcription and gene expression of *pykA* by far exceed that of *pykF*. However, PykF seems to have a role in glyoxylate metabolism based on its genomic location among the glyoxylate catabolism operon. Further analysis revealed that PykA and PykF are functional enzymes and are strongly activated by metabolites of the PPP. Since PykA and PykF lie downstream of the EDP and not the PPP, the question as to why the PPP metabolites activate PykA and PykF needs an answer. The most probable explanation could be that PykA and PykF are the sources of the energy required to fuel the adaptive processes in *P. aeruginosa*.

P. aeruginosa can thrive under diverse environments including low oxygen, limited nutrients, and industrial areas. Among the three metabolic pathways, the PPP is an excellent choice to support growth in these conditions. The PPP can supply the cell with NADPH and R5P that are used for the alleviation of oxidative stress and repair of damaged DNA, respectively. Also, PPP can provide the cell with E4P which can be used for biosynthesis of amino acids, the building blocks of the cell. Furthermore, various carbon intermediates can enter the metabolism via PPP (through the interconversion

reactions of C3, C4, C5, C6, and C7). Thus, the PPP has a role in promotion of cell adaptation in *P. aeruginosa*. Given that these adaptive processes require energy for operation, it is not surprising that PykA and PykF are strongly activated by most of the PPP intermediates. Moreover, the genetic location of *pykF* within a glyoxylate metabolism operon also supports that PykF is particularly required for adaptation in industrial settings where ethylene glycol and its derivatives are quite abundant.

References

Abdallah M, Benoliel C, Drider D, Dhulster P, Chihib N-E. (2014). Biofilm formation and persistence on abiotic surfaces in the context of food and medical environments. *Archives of Microbiology* 196: 453–472.

Adams PD, Afonine P V., Bunkóczi G, Chen VB, Davis IW, Echols N, Headd JJ, Hung L-W, Kapral GJ, Grosse-Kunstleve RW, McCoy AJ, Moriarty NW, Oeffner R, Read RJ, Richardson DC, Richardson JS, Terwilliger TC, Zwart PH, IUCr. (2010). PHENIX : a comprehensive Python-based system for macromolecular structure solution. *Acta Crystallographica Section D Biological Crystallography* 66: 213–221.

Aires JR, Köhler T, Nikaido H, Plésiat P. (1999). Involvement of an active efflux system in the natural resistance of Pseudomonas aeruginosa to aminoglycosides. *Antimicrobial agents and chemotherapy* 43: 2624–2628.

Al-Mussawi AA. (2010). Isolation and Identification of Shikonin From Arnebia Decumbens L. and its Antibacterial Activity. *Journal of Applied Sciences Research* 6: 1452–1456.

Al-Zaid Siddiquee K, Arauzo-Bravo MJ, Shimizu K. (2004). Metabolic flux analysis of pykF gene knockout Escherichia coli based on 13C-labeling experiments together with measurements of enzyme activities and intracellular metabolite concentrations. *Applied Microbiology and Biotechnology* 63: 407–417.

Alhazmi A. (2015). Pseudomonas aeruginosa-Pathogenesis and Pathogenic Mechanisms. *International Journal of Biology* 7.

Allen SC, Muirhead H. (1996). Refined Three-Dimensional Structure of Cat-Muscle (M1) Pyruvate Kinase at a Resolution of 2.6 Å. *Acta Crystallographica Section D Biological Crystallography* 52: 499–504.

Antunes A, Golfieri G, Ferlicca F, Giuliani MM, Scarlato V, Delany I. (2016). HexR Controls Glucose-Responsive Genes and Central Carbon Metabolism in Neisseria meningitidis. *Journal of Bacteriology* 198: 644–654.

Arora G, Sajid A, Gupta M, Bhaduri A, Kumar P, Basu-Modak S, Singh Y. (2010). Understanding the Role of PknJ in Mycobacterium tuberculosis: Biochemical Characterization and Identification of Novel Substrate Pyruvate Kinase A. *PLoS ONE* 5: e10772.

Axerio-Cilies P, See RH, Zoraghi R, Worral L, Lian T, Stoynov N, Jiang J, Kaur S, Jackson L, Gong H, Swayze R, Amandoron E, Kumar NS, Moreau A, Hsing M, Strynadka NC, McMaster WR, Finlay BB, Foster LJ, Young RN, Reiner NE, Cherkasov A. (2012). Cheminformatics-driven discovery of selective, nanomolar inhibitors for staphylococcal pyruvate kinase. *ACS chemical biology* 7: 350–359.

Baek YH, Nowak T. (1982). Kinetic evidence for a dual cation role for muscle pyruvate kinase. *Archives of Biochemistry and Biophysics* 217: 491–497.

Bakszt R, Wernimont A, Allali-Hassani A, Mok MW, Hills T, Hui R, Pizarro JC. (2010). The crystal structure of Toxoplasma gondii pyruvate kinase 1. *PloS one* 5: e12736.

Bar-Even A, Flamholz A, Noor E, Milo R. (2012). Rethinking glycolysis: on the biochemical logic of metabolic pathways. *Nature Chemical Biology* 8: 509–517.

Baratti JC, Bu'lock JD. (1986). Zymomonas mobilis: a bacterium for ethanol production. *Biotechnology advances* 4: 95–115.

Berger A, Dohnt K, Tielen P, Jahn D, Becker J, Wittmann C. (2014). Robustness and Plasticity of

Metabolic Pathway Flux among Uropathogenic Isolates of Pseudomonas aeruginosa. *PLoS ONE* 9: e88368.

Bianconi I, Jeukens J, Freschi L, Alcalá-Franco B, Facchini M, Boyle B, Molinaro A, Kukavica-Ibrulj I, Tümmler B, Levesque RC, Bragonzi A. (2015). Comparative genomics and biological characterization of sequential Pseudomonas aeruginosa isolates from persistent airways infection. *BMC genomics* 16: 1105.

Bielecki P, Glik J, Kawecki M, Martins dos Santos VAP. (2008). Towards understanding Pseudomonas aeruginosa burn wound infections by profiling gene expression. *Biotechnology Letters* 30: 777–790.

Bielen K, 'S Jongers B, Boddaert J, Raju TK, Lammens C, Malhotra-Kumar S, Jorens PG, Goossens H, Kumar-Singh S. (2017). Biofilm-Induced Type 2 Innate Immunity in a Cystic Fibrosis Model of Pseudomonas aeruginosa. *Frontiers in Cellular and Infection Microbiology* 7: 274.

Blackwood LL, Stone RM, Iglewski BH, Pennington JE. (1983). Evaluation of Pseudomonas aeruginosa exotoxin A and elastase as virulence factors in acute lung infection. *Infection and immunity* 39: 198–201.

Bledig SA, Ramseier TM, Saier MH. (1996). Frur mediates catabolite activation of pyruvate kinase (pykF) gene expression in Escherichia coli. *Journal of bacteriology* 178: 280–283.

Bollenbach TJ, Mesecar AD, Nowak T. (1999). Role of Lysine 240 in the Mechanism of Yeast Pyruvate Kinase Catalysis †. *Biochemistry* 38: 9137–9145.

Boyd A, Chakrabarty AM. (1995). Pseudomonas aeruginosa biofilms: role of the alginate exopolysaccharide. *Journal of industrial microbiology* 15: 162–168.

Bradford MM. (1976). A rapid and sensitive method for the quantitation of microgram quantities of protein utilizing the principle of protein-dye binding. *Analytical biochemistry* 72: 248–254.

Bücker R, Heroven AK, Becker J, Dersch P, Wittmann C. (2014). The pyruvate-tricarboxylic acid cycle node: a focal point of virulence control in the enteric pathogen Yersinia pseudotuberculosis. *The Journal of biological chemistry* 289: 30114–30132.

Caiazza NC, Shanks RMQ, O'Toole GA. (2005). Rhamnolipids modulate swarming motility patterns of Pseudomonas aeruginosa. *Journal of bacteriology* 187: 7351–61.

Campilongo R, Fung RKY, Little RH, Grenga L, Trampari E, Pepe S, Chandra G, Stevenson CEM, Roncarati D, Malone JG. (2017). One ligand, two regulators and three binding sites: How KDPG controls primary carbon metabolism in Pseudomonas. *PLOS Genetics* 13: e1006839.

Chai X, Shang X, Zhang Y, Liu S, Liang Y, Zhang Y, Wen T. (2016). A novel pyruvate kinase and its application in lactic acid production under oxygen deprivation in Corynebacterium glutamicum. *BMC Biotechnology* 16: 79.

Chambost JP, Fraenkel DG. (1980). The use of 6-labeled glucose to assess futile cycling in Escherichia coli. *The Journal of biological chemistry* 255: 2867–2869.

Chavadi S, Wooff E, Coldham NG, Sritharan M, Hewinson RG, Gordon S V., Wheeler PR. (2009). Global Effects of Inactivation of the Pyruvate Kinase Gene in the Mycobacterium tuberculosis Complex. *Journal of Bacteriology* 191: 7545–7553.

Chavarría M, Nikel PI, Pérez-Pantoja D, de Lorenzo V. (2013). The Entner-Doudoroff pathway empowers *Pseudomonas putida* KT2440 with a high tolerance to oxidative stress. *Environmental Microbiology* 15: 1772–1785.

Chen J, Xie J, Jiang Z, Wang B, Wang Y, Hu X. (2011). Shikonin and its analogs inhibit cancer cell

glycolysis by targeting tumor pyruvate kinase-M2. *Oncogene* 30: 4297–4306.

Chen VB, Arendall WB, Headd JJ, Keedy DA, Immormino RM, Kapral GJ, Murray LW, Richardson JS, Richardson DC, IUCr. (2010). MolProbity: all-atom structure validation for macromolecular crystallography. *Acta Crystallographica Section D Biological Crystallography* 66: 12–21.

Chen X, Schreiber K, Appel J, Makowka A, Fähnrich B, Roettger M, Hajirezaei MR, Sönnichsen FD, Schönheit P, Martin WF, Gutekunst K. (2016). The Entner-Doudoroff pathway is an overlooked glycolytic route in cyanobacteria and plants. *Proceedings of the National Academy of Sciences of the United States of America* 113: 5441–5446.

Christodoulou D, Link H, Fuhrer T, Kochanowski K, Gerosa L, Sauer U. (2018). Reserve Flux Capacity in the Pentose Phosphate Pathway Enables Escherichia coli's Rapid Response to Oxidative Stress. *Cell systems* 6: 569–578.e7.

Coburn B, Sekirov I, Finlay BB. (2007). Type III Secretion Systems and Disease. *Clinical Microbiology Reviews* 20: 535–549.

Conway T. (1992). The Entner-Doudoroff pathway: history, physiology and molecular biology. *FEMS microbiology reviews* 9: 1–27.

Cook WJ, Senkovich O, Aleem K, Chattopadhyay D. (2012). Crystal structure of Cryptosporidium parvum pyruvate kinase. *PloS one* 7: e46875.

Craig L, Pique ME, Tainer JA. (2004). Type IV pilus structure and bacterial pathogenicity. *Nature Reviews Microbiology* 2: 363–378.

Daddaoua A, Krell T, Ramos JL. (2009). Regulation of glucose metabolism in Pseudomonas. The phosphorylative branch and Entner-Doudoroff enzymes are regulated by a repressor containing a sugar isomerase domain. *Journal of Biological Chemistry* 284: 21360–21368.

Daldal F, Fraenkel DG. (1983). Assessment of a futile cycle involving reconversion of fructose 6-phosphate to fructose 1,6-bisphosphate during gluconeogenic growth of Escherichia coli. *Journal of bacteriology* 153: 390–394.

Davey ME, Caiazza NC, O'Toole GA. (2003). Rhamnolipid surfactant production affects biofilm architecture in Pseudomonas aeruginosa PAO1. *Journal of bacteriology* 185: 1027–1036.

Donovan KA, Zhu S, Liuni P, Peng F, Kessans SA, Wilson DJ, Dobson RCJ. (2016). Conformational Dynamics and Allostery in Pyruvate Kinase. *Journal of Biological Chemistry* 291: 9244–9256.

Döring G, Pier GB. (2008). Vaccines and immunotherapy against Pseudomonas aeruginosa. *Vaccine* 26: 1011–1024.

Drechsler ER, Boyer PD, Kowalsky AG. (1959). The catalytic activity of carboxypeptidase-degraded aldolase. *The Journal of biological chemistry* 234: 2627–2634.

Drenkard E. (2003). Antimicrobial resistance of Pseudomonas aeruginosa biofilms. *Microbes and infection* 5: 1213–1219.

Eisenberg RC, Dobrogosz WJ. (1967). Gluconate metabolism in Escherichia coli. *Journal of bacteriology* 93: 941–949.

Emsley P, Lohkamp B, Scott WG, Cowtan K. (2010). Features and development of Coot. *Acta Cryst* 66: 486–501.

Entner N, Doudoroff M. (1952). Glucose and gluconic acid oxidation of Pseudomonas saccharophila. *The Journal of biological chemistry* 196: 853–862.

Fenton AW. (2008). Allostery: an illustrated definition for the 'second secret of life.' *Trends in Biochemical Sciences* 33: 420–425.

Fenton AW, Blair JB. (2002). Kinetic and Allosteric Consequences of Mutations in the Subunit and Domain Interfaces and the Allosteric Site of Yeast Pyruvate Kinase. *Archives of Biochemistry and Biophysics* 397: 28–39.

Fett WF, Wells JM, Cescutti P, Wijey C. (1995). Identification of exopolysaccharides produced by fluorescent pseudomonads associated with commercial mushroom (Agaricus bisporus) production. *Applied and environmental microbiology* 61: 513–517.

Finck-Barbançon V, Goranson J, Zhu L, Sawa T, Wiener-Kronish JP, Fleiszig SM, Wu C, Mende-Mueller L, Frank DW. (1997). ExoU expression by Pseudomonas aeruginosa correlates with acute cytotoxicity and epithelial injury. *Molecular microbiology* 25: 547–557.

Flamholz A, Noor E, Bar-Even A, Liebermeister W, Milo R. (2013). Glycolytic strategy as a tradeoff between energy yield and protein cost. *Proceedings of the National Academy of Sciences of the United States of America* 110: 10039–10044.

Fliege R, Tong S, Shibata A, Nickerson KW, Conway T. (1992). The Entner-Doudoroff pathway in Escherichia coli is induced for oxidative glucose metabolism via pyrroloquinoline quinone-dependent glucose dehydrogenase. *Applied and environmental microbiology* 58: 3826–3829.

Flume PA, O'Sullivan BP, Robinson KA, Goss CH, Mogayzel PJ, Willey-Courand DB, Bujan J, Finder J, Lester M, Quittell L, Rosenblatt R, Vender RL, Hazle L, Sabadosa K, Marshall B, Cystic Fibrosis Foundation, Pulmonary Therapies Committee. (2007). Cystic Fibrosis Pulmonary Guidelines. *American Journal of Respiratory and Critical Care Medicine* 176: 957–969.

Fraenkel DG. (1986). Mutants in Glucose Metabolism. *Annual Review of Biochemistry* 55: 317–337.

Franden MA, Jayakody LN, Li W-J, Wagner NJ, Cleveland NS, Michener WE, Hauer B, Blank LM, Wierckx N, Klebensberger J, Beckham GT. (2018). Engineering Pseudomonas putida KT2440 for efficient ethylene glycol utilization. *Metabolic Engineering* 48: 197–207.

Friesen RH, Lee JC. (1998). The negative dominant effects of T340M mutation on mammalian pyruvate kinase. *The Journal of biological chemistry* 273: 14772–14779.

Fry B, Zhu T, Domach MM, Koepsel RR, Phalakornkule C, Ataai MM. (2000). Characterization of growth and acid formation in a Bacillus subtilis pyruvate kinase mutant. *Applied and environmental microbiology* 66: 4045–4049.

Fuhrer T, Fischer E, Sauer U. (2005). Experimental identification and quantification of glucose metabolism in seven bacterial species. *Journal of bacteriology* 187: 1581–1590.

Gacesa P, Wusteman FS. (1990). Plate assay for simultaneous detection of alginate lyases and determination of substrate specificity. *Applied and environmental microbiology* 56: 2265–2267.

Garcia-Olalla C, Garrido-Pertierra A. (1987). Purification and kinetic properties of pyruvate kinase isoenzymes of Salmonella typhimurium. *The Biochemical journal* 241: 573–581.

Garrity-Ryan L, Kazmierczak B, Kowal R, Comolli J, Hauser A, Engel JN. (2000). The arginine finger domain of ExoT contributes to actin cytoskeleton disruption and inhibition of internalization of Pseudomonas aeruginosa by epithelial cells and macrophages. *Infection and immunity* 68: 7100–7113.

Gellatly SL, Hancock REW. (2013). *Pseudomonas aeruginosa* : new insights into pathogenesis and host defenses. *Pathogens and Disease* 67: 159–173.

Giles IG, Poat PC. (1980). A steady-state kinetic analysis of the fructose 1,6-bisphosphate-

activated pyruvate kinase from Carcinus maenas hepatopancreas. *The Biochemical journal* 185: 289–299.

Giles IG, Poat PC, Munday KA. (1976). The kinetics of rabbit muscle pyruvate kinase. Initial-velocity, substrate- and product-inhibition and isotopic-exchange studies of the reverse reaction. *The Biochemical journal* 157: 577–589.

Gilleland LB, Gilleland HE, Gibson JA, Champlin FR. (1989). Adaptive resistance to aminoglycoside antibiotics in Pseudomonas aeruginosa. *Journal of Medical Microbiology* 29: 41–50.

Grady R, Hayes F. (2003). Axe-Txe, a broad-spectrum proteic toxin-antitoxin system specified by a multidrug-resistant, clinical isolate of Enterococcus faecium. *Molecular Microbiology* 47: 1419–1432.

Haiko J, Westerlund-Wikström B. (2013). The role of the bacterial flagellum in adhesion and virulence. *Biology* 2: 1242–1267.

Hancock REW, Speert DP. (2000). Antibiotic resistance in Pseudomonas aeruginosa: mechanisms and impact on treatment. *Drug Resistance Updates* 3: 247–255.

Hattori J, Baum BR, Mchugh SG, Blakele SD, Dennis DT, Miki BL. (1995). Pyruvate kinase isozymes: Ancient diversity retained in modern plant cells. *Biochemical Systematics and Ecology* 23: 773–780.

Hayes D, Laue T, Philo J. (1995). Program Sednterp: Sedimentation Interpretation Program. Alliance Protein Laboratories, Thousand Oaks, CA.

Heine H, Rietschel ET, Ulmer AJ. (2001). The Biology of Endotoxin. *Molecular Biotechnology* 19: 279–296.

Hillman JD, Fraenkel DG. (1975). Glyceraldehyde 3-phosphate dehydrogenase mutants of Escherichia coli. *Journal of bacteriology* 122: 1175–1179.

Hobden JA. (2002). *Pseudomonas aeruginosa* Proteases and Corneal Virulence. *DNA and Cell Biology* 21: 391–396.

Hofmann E. (1976). The significance of phosphofructokinase to the regulation of carbohydrate metabolism. *Reviews of physiology, biochemistry and pharmacology* 75: 1–68.

Hofmann J, Heider C, Li W, Krausze J, Roessle M, Wilharm G. (2013). Recombinant production of Yersinia enterocolitica pyruvate kinase isoenzymes PykA and PykF. *Protein Expression and Purification* 88: 243–247.

Høiby N, Ciofu O, Bjarnsholt T. (2010). *Pseudomonas aeruginosa* biofilms in cystic fibrosis. *Future Microbiology* 5: 1663–1674.

Hollsing AE, Granström M, Vasil ML, Wretlind B, Strandvik B. (1987). Prospective study of serum antibodies to Pseudomonas aeruginosa exoproteins in cystic fibrosis. *Journal of clinical microbiology* 25: 1868–1874.

Huang H, Hancock RE. (1996). The role of specific surface loop regions in determining the function of the imipenem-specific pore protein OprD of Pseudomonas aeruginosa. *Journal of bacteriology* 178: 3085–3090.

Istúriz T, Palmero E, Vitelli-Flores J. (1986). Mutations Affecting Gluconate Catabolism in Escherichia coli. Genetic Mapping of the Locus for the Thermosensitive Gluconokinase. *Microbiology* 132: 3209–3219.

Jacoby GA. (2009). AmpC beta-lactamases. *Clinical microbiology reviews* 22: 161–182.

Jones G, Willett P, Glen RC, Leach AR, Taylor R. (1997). Development and validation of a genetic algorithm for flexible docking. *Journal of Molecular Biology* 267: 727–748.

Juhnke H, Krems B, Kötter P, Entian K-D. (1996). Mutants that show increased sensitivity to hydrogen peroxide reveal an important role for the pentose phosphate pathway in protection of yeast against oxidative stress. *MGG Molecular & General Genetics* 252: 456–464.

Jurica MS, Mesecar A, Heath PJ, Shi W, Nowak T, Stoddard BL. (1998). The allosteric regulation of pyruvate kinase by fructose-1,6-bisphosphate. *Structure* 6: 195–210.

Kachmar J, Boyer P. (1953). Kinetic analysis of enzyme reactions. II. The potassium activation and calcium inhibition of pyruvic phosphoferase. *The Journal of biological chemistry* 200: 669–682.

Keating LA, Wheeler PR, Mansoor H, Inwald JK, Dale J, Hewinson RG, Gordon S V. (2005). The pyruvate requirement of some members of the Mycobacterium tuberculosis complex is due to an inactive pyruvate kinase: implications for in vivo growth. *Molecular Microbiology* 56: 163–174.

Kersters K, De Ley J. (1968). The occurrence of the Entner-Doudoroff pathway in bacteria. *Antonie van Leeuwenhoek* 34: 393–408.

Kim BH, Gadd GM. (2008). Glycolysis. In: Bacterial physiology and metabolism. Cambridge University Press, p 60–80.

Kim J, Jeon CO, Park W. (2008). Dual regulation of zwf-1 by both 2-keto-3-deoxy-6-phosphogluconate and oxidative stress in Pseudomonas putida. *Microbiology* 154: 3905–3916.

Kim J, Yeom J, Jeon CO, Park W. (2009). Intracellular 2-keto-3-deoxy-6-phosphogluconate is the signal for carbon catabolite repression of phenylacetic acid metabolism in Pseudomonas putida KT2440. *Microbiology* 155: 2420–2428.

Klausen M, Heydorn A, Ragas P, Lambertsen L, Aaes-Jørgensen A, Molin S, Tolker-Nielsen T. (2003). Biofilm formation by Pseudomonas aeruginosa wild type, flagella and type IV pili mutants. *Molecular microbiology* 48: 1511–1524.

Koh AY, Priebe GP, Pier GB. (2005). Virulence of Pseudomonas aeruginosa in a Murine Model of Gastrointestinal Colonization and Dissemination in Neutropenia. *Infection and Immunity* 73: 2262–2272.

Kourounakis AP, Assimopoulou AN, Papageorgiou VP, Gavalas A, Kourounakis PN. (2002). Alkannin and Shikonin: Effect on Free Radical Processes and on Inflammation - A Preliminary Pharmacochemical Investigation. *Archiv der Pharmazie* 335: 262–266.

Kovachevich R, Wood WA. (1955a). Carbohydrate metabolism by Pseudomonas fluorescens. III. Purification and properties of a 6-phosphogluconate dehydrase. *The Journal of biological chemistry* 213: 745–756.

Kovachevich R, Wood WA. (1955b). Carbohydrate metabolism by Pseudomonas fluorescens. IV. Purification and properties of 2-keto-3-deoxy-6-phosphogluconate aldolase. *The Journal of biological chemistry* 213: 757–767.

Kresge N, Simoni RD, Hill RL. (2005). Otto Fritz Meyerhof and the elucidation of the glycolytic pathway. *The Journal of biological chemistry* 280: e3.

Krissinel E, Henrick K. (2007). Inference of Macromolecular Assemblies from Crystalline State. *Journal of Molecular Biology* 372: 774–797.

Krissinel E, Henrick K, IUCr. (2004). Secondary-structure matching (SSM), a new tool for fast

protein structure alignment in three dimensions. *Acta Crystallographica Section D Biological Crystallography* 60: 2256–2268.

Kuang Z, Hao Y, Walling BE, Jeffries JL, Ohman DE, Lau GW. (2011). Pseudomonas aeruginosa Elastase Provides an Escape from Phagocytosis by Degrading the Pulmonary Surfactant Protein-A. *PLoS ONE* 6: e27091.

Laarman AJ, Bardoel BW, Ruyken M, Fernie J, Milder FJ, van Strijp JAG, Rooijakkers SHM. (2012). Pseudomonas aeruginosa Alkaline Protease Blocks Complement Activation via the Classical and Lectin Pathways. *The Journal of Immunology* 188: 386–393.

Lam J, Chan R, Lam K, Costerton JW. (1980). Production of Mucoid Microcolonies by Pseudomonas aeruginosa Within Infected Lungs in Cystic Fibrosis. *Infection and immunity* 28: 546–556.

Larsen TM, Benning MM, Wesenberg GE, Rayment I, Reed GH. (1997). Ligand-Induced Domain Movement in Pyruvate Kinase: Structure of the Enzyme from Rabbit Muscle with Mg2+, K+, and L-Phospholactate at 2.7 Å Resolution. *Archives of Biochemistry and Biophysics* 345: 199–206.

Larsen TM, Laughlin LT, Holden HM, Rayment I, Reed GH. (1994). Structure of Rabbit Muscle Pyruvate Kinase Complexed with Mn2+, K+, and Pyruvate. *Biochemistry* 33: 6301–6309.

Laughlin LT, Reed GH. (1997). The monovalent cation requirement of rabbit muscle pyruvate kinase is eliminated by substitution of lysine for glutamate 117. *Archives of Biochemistry and Biophysics* 348: 262–267.

Lee SA, Gallagher LA, Thongdee M, Staudinger BJ, Lippman S, Singh PK, Manoil C. (2015a). General and condition-specific essential functions of Pseudomonas aeruginosa. *Proceedings of the National Academy of Sciences of the United States of America* 112: 5189–5194.

Lee Y-S, Lee D-Y, Kim YB, Lee S-W, Cha S-W, Park H-W, Kim G-S, Kwon D-Y, Lee M-H, Han S-H. (2015b). The Mechanism Underlying the Antibacterial Activity of Shikonin against Methicillin-Resistant Staphylococcus aureus. *Evidence-based complementary and alternative medicine* 2015: 520578.

Lessie TG, Phibbs P V. (1984). Alternative Pathways of Carbohydrate Utilization in Pseudomonads. *Annual Review of Microbiology* 38: 359–388.

Levy HR. (2006). Glucose-6-Phosphate Dehydrogenases. In: Advances in Enzymology - and Related Areas of Molecular Biology. Wiley-Blackwell, p 97–192.

Leyn SA, Li X, Zheng Q, Novichkov PS, Reed S, Romine MF, Fredrickson JK, Yang C, Osterman AL, Rodionov DA. (2011). Control of proteobacterial central carbon metabolism by the HexR transcriptional regulator: a case study in Shewanella oneidensis. *The Journal of biological chemistry* 286: 35782–94.

Li JD, Dohrman AF, Gallup M, Miyata S, Gum JR, Kim YS, Nadel JA, Prince A, Basbaum CB. (1997). Transcriptional activation of mucin by Pseudomonas aeruginosa lipopolysaccharide in the pathogenesis of cystic fibrosis lung disease. *Proceedings of the National Academy of Sciences of the United States of America* 94: 967–972.

Liu T, Ma C, Yang L, Wang W, Sui X, Zhao C, Zu Y, Liu T, Ma C, Yang L, Wang W, Sui X, Zhao C, Zu Y. (2013). Optimization of Shikonin Homogenate Extraction from Arnebia euchroma Using Response Surface Methodology. *Molecules* 18: 466–481.

Livermore DM. (1984). Penicillin-Binding Proteins, Porins Andouter-Membrane Permeability of Carbenicillin-Resistant and -Susceptible Strains of Pseudomonas Aeruginosa. *Journal of Medical Microbiology* 18: 261–270.

Long F, Vagin AA, Young P, Murshudov GN. (2008). BALBES: a molecular-replacement pipeline. *Acta crystallographica. Section D, Biological crystallography* 64: 125–132.

Lyczak JB, Cannon CL, Pier GB. (2000). Establishment of Pseudomonas aeruginosa infection: lessons from a versatile opportunist. *Microbes and Infection* 2: 1051–1060.

Magasanik B. (1961). Catabolite Repression. *Cold Spring Harbor Symposia on Quantitative Biology* 26: 249–256.

Mah T-F, Pitts B, Pellock B, Walker GC, Stewart PS, O'Toole GA. (2003). A genetic basis for Pseudomonas aeruginosa biofilm antibiotic resistance. *Nature* 426: 306–310.

Malcovati M, Valentini G. (1982). AMP- and fructose 1,6-bisphosphate-activated pyruvate kinases from Escherichia coli. *Methods in Enzymology* 90: 170–179.

Mann EE, Wozniak DJ. (2012). *Pseudomonas* biofilm matrix composition and niche biology. *FEMS Microbiology Reviews* 36: 893–916.

Mariencheck WI, Alcorn JF, Palmer SM, Wright JR. (2003). *Pseudomonas aeruginosa* Elastase Degrades Surfactant Proteins A and D. *American Journal of Respiratory Cell and Molecular Biology* 28: 528–537.

Martin DW, Schurr MJ, Mudd MH, Govan JR, Holloway BW, Deretic V. (1993). Mechanism of conversion to mucoidy in Pseudomonas aeruginosa infecting cystic fibrosis patients. *Proceedings of the National Academy of Sciences of the United States of America* 90: 8377–81.

Masuda N, Gotoh N, Ishii C, Sakagawa E, Ohya S, Nishino T. (1999). Interplay between chromosomal beta-lactamase and the MexAB-OprM efflux system in intrinsic resistance to beta-lactams in Pseudomonas aeruginosa. *Antimicrobial agents and chemotherapy* 43: 400–402.

Matsumoto K. (2004). Role of bacterial proteases in pseudomonal and serratial keratitis. *Biological Chemistry* 385: 1007–1016.

Mattevi A, Bolognesi M, Valentini G. (1996). The allosteric regulation of pyruvate kinase. *FEBS letters* 389: 15–9.

Mattevi A, Valentini G, Rizzi M, Speranza ML, Bolognesi M, Coda A. (1995). Crystal structure of Escherichia coli pyruvate kinase type I: molecular basis of the allosteric transition. *Structure* 3: 729–741.

Matz C, Bergfeld T, Rice SA, Kjelleberg S. (2004). Microcolonies, quorum sensing and cytotoxicity determine the survival of Pseudomonas aeruginosa biofilms exposed to protozoan grazing. *Environmental microbiology* 6: 218–226.

May TB, Shinabarger D, Maharaj R, Kato J, Chu L, DeVault JD, Roychoudhury S, Zielinski NA, Berry A, Rothmel RK, al. et. (1991). Alginate synthesis by Pseudomonas aeruginosa: a key pathogenic factor in chronic pulmonary infections of cystic fibrosis patients. *Clinical microbiology reviews* 4: 191–206.

McCaslin CA, Petrusca DN, Poirier C, Serban KA, Anderson GG, Petrache I. (2015). Impact of alginate-producing Pseudomonas aeruginosa on alveolar macrophage apoptotic cell clearance. *Journal of Cystic Fibrosis* 14: 70–77.

McClure CD, Schiller NL. (1996). Inhibition of Macrophage Phagocytosis by Pseudomonas aeruginosa Rhamnolipids In Vitro and In Vivo. *Current Microbiology* 33: 109–117.

McCoy AJ, Grosse-Kunstleve RW, Adams PD, Winn MD, Storoni LC, Read RJ. (2007). Phaser crystallographic software. *Journal of Applied Crystallography* 40: 658–674.

McDaniel CT, Panmanee W, Hassett DJ. (2015). An Overview of Infections in Cystic Fibrosis Airways and the Role of Environmental Conditions on Pseudomonas aeruginosa Biofilm Formation and Viability. In: Cystic Fibrosis in the Light of New Research, D. Wat. InTech, p 171–198.

McNicholas S, Potterton E, Wilson KS, Noble MEM. (2011). Presenting your structures: the CCP4mg molecular-graphics software. *Acta Crystallographica Section D Biological Crystallography* 67: 386–394.

McPhee JB, Bains M, Winsor G, Lewenza S, Kwasnicka A, Brazas MD, Brinkman FSL, Hancock REW. (2006). Contribution of the PhoP-PhoQ and PmrA-PmrB Two-Component Regulatory Systems to Mg2+-Induced Gene Regulation in Pseudomonas aeruginosa. *Journal of Bacteriology* 188: 3995–4006.

Mesecar AD, Nowak T. (1997). Metal-Ion-Mediated Allosteric Triggering of Yeast Pyruvate Kinase. 1. A Multidimensional Kinetic Linked-Function Analysis. *Biochemistry* 36: 6792–6802.

Miyaue S, Suzuki E, Komiyama Y, Kondo Y, Morikawa M, Maeda S. (2018). Bacterial Memory of Persisters: Bacterial Persister Cells Can Retain Their Phenotype for Days or Weeks After Withdrawal From Colony–Biofilm Culture. *Frontiers in Microbiology* 9: 1396.

Monod J, Wyman J, Changeux J-P. (1965). On the nature of allosteric transitions: A plausible model. *Journal of Molecular Biology* 12: 88–118.

Monson R, Foulds I, Foweraker J, Welch M, Salmond GPC. (2011). The Pseudomonas aeruginosa generalized transducing phage PA3 is a new member of the KZ-like group of "jumbo" phages, and infects model laboratory strains and clinical isolates from cystic fibrosis patients. *Microbiology* 157: 859–867.

Morgan HP, McNae IW, Nowicki MW, Hannaert V, Michels PAM, Fothergill-Gilmore LA, Walkinshaw MD. (2010). Allosteric mechanism of pyruvate kinase from Leishmania mexicana uses a rock and lock model. *The Journal of biological chemistry* 285: 12892–12898.

Morgan HP, Zhong W, McNae IW, Michels PAM, Fothergill-Gilmore LA, Walkinshaw MD. (2014). Structures of pyruvate kinases display evolutionarily divergent allosteric strategies. *Royal Society open science* 1: 140120.

Morse SA, Stein S, Hines J. (1974). Glucose Metabolism in Neisseria gonorrhoeae. *Journal of bacteriology* 120: 702–714.

Muirhead H, Clayden DA, Barford D, Lorimer CG, Fothergill-Gilmore LA, Schiltz E, Schmitt W. (1986). The structure of cat muscle pyruvate kinase. *The EMBO Journal* 5: 475–481.

Mulcahy LR, Burns JL, Lory S, Lewis K. (2010). Emergence of Pseudomonas aeruginosa Strains Producing High Levels of Persister Cells in Patients with Cystic Fibrosis. *Journal of Bacteriology* 192: 6191–6199.

Muñoz ME, Ponce E. (2003). Pyruvate kinase: current status of regulatory and functional properties. *Comparative biochemistry and physiology. Part B, Biochemistry & molecular biology* 135: 197–218.

Murshudov GN, Vagin AA, Dodson EJ, IUCr. (1997). Refinement of Macromolecular Structures by the Maximum-Likelihood Method. *Acta Crystallographica Section D Biological Crystallography* 53: 240–255.

Naithani A, Taylor P, Erman B, Walkinshaw MD. (2015). A Molecular Dynamics Study of Allosteric Transitions in Leishmania mexicana Pyruvate Kinase. *Biophysical Journal* 109: 1149–1156.

Nakae T, Nakajima A, Ono T, Saito K, Yoneyama H. (1999). Resistance to beta-lactam antibiotics

in Pseudomonas aeruginosa due to interplay between the MexAB-OprM efflux pump and beta-lactamase. *Antimicrobial agents and chemotherapy* 43: 1301–1303.

Newsom SW, Sykes RB, Richmond MH. (1970). Detection of a beta-lactamase markedly active against carbenicillin in a strain of Pseudomonas aeruginosa. *Journal of bacteriology* 101: 1079–1080.

Nikaido H, Nikaido K, Harayama S. (1991). Identification and characterization of porins in Pseudomonas aeruginosa. *The Journal of biological chemistry* 266: 770–779.

Nikel PI, Chavarría M, Fuhrer T, Sauer U, de Lorenzo V. (2015a). *Pseudomonas putida* KT2440 Strain Metabolizes Glucose through a Cycle Formed by Enzymes of the Entner-Doudoroff, Embden-Meyerhof-Parnas, and Pentose Phosphate Pathways. *Journal of Biological Chemistry* 290: 25920–25932.

Nikel PI, Romero-Campero FJ, Zeidman JA, Goñi-Moreno Á, Lorenzo V de. (2015b). The Glycerol-Dependent Metabolic Persistence of Pseudomonas putida KT2440 Reflects the Regulatory Logic of the GlpR Repressor. *mBio* 6: e00340-15.

Noor E, Eden E, Milo R, Alon U. (2010). Central Carbon Metabolism as a Minimal Biochemical Walk between Precursors for Biomass and Energy. *Molecular Cell* 39: 809–820.

O'Toole G, Kaplan HB, Kolter R. (2000). Biofilm Formation as Microbial Development. *Annual Review of Microbiology* 54: 49–79.

Oria-Hernández J, Cabrera N, Pérez-Montfort R, Ramírez-Silva L. (2005). Pyruvate kinase revisited: the activating effect of K+. *The Journal of biological chemistry* 280: 37924–37929.

Oria-Hernández J, Riveros-Rosas H, Ramírez-Sílva L. (2006). Dichotomic Phylogenetic Tree of the Pyruvate Kinase Family. *Journal of Biological Chemistry* 281: 30717–30724.

Page R, Peti W. (2016). Toxin-antitoxin systems in bacterial growth arrest and persistence. *Nature Chemical Biology* 12: 208–214.

Pan Z, Cunningham DS, Zhu T, Ye K, Koepsel RR, Domach MM, Ataai MM. (2010). Enhanced recombinant protein production in pyruvate kinase mutant of Bacillus subtilis. *Applied Microbiology and Biotechnology* 85: 1769–1778.

Pan Z, Zhu T, Domagalski N, Khan S, Koepsel RR, Domach MM, Ataai MM. (2008). Regulating Expression of Pyruvate Kinase in Bacillus subtilis for Control of Growth Rate and Formation of Acidic Byproducts. *Biotechnology Progress* 22: 1451–1455.

Papageorgiou V, Assimopoulou A, Ballis A. (2008). Alkannins and Shikonins: A New Class of Wound Healing Agents. *Current Medicinal Chemistry* 15: 3248–3267.

Pedersen SS. (1992). Lung infection with alginate-producing, mucoid Pseudomonas aeruginosa in cystic fibrosis. *APMIS. Supplementum* 28: 1–79.

Peekhaus N, Conway T. (1998). What's for dinner?: Entner-Doudoroff metabolism in Escherichia coli. *Journal of bacteriology* 180: 3495–3502.

Periasamy S, Nair HAS, Lee KWK, Ong J, Goh JQJ, Kjelleberg S, Rice SA. (2015). Pseudomonas aeruginosa PAO1 exopolysaccharides are important for mixed species biofilm community development and stress tolerance. *Frontiers in microbiology* 6: 851.

Pertierra AG, Cooper RA. (1977). Pyruvate formation during the catabolism of simple hexose sugars by Escherichia coli: studies with pyruvate kinase-negative mutants. *Journal of bacteriology* 129: 1208–1214.

Phibbs P V. (1988). Genetic analysis of carbohydrate metabolism in Pseudomonas In Microbial

Metabolism and the Carbon Cycle: Scott R. Hagedorn, Richard S. Hanson, Daniel A. Kunz. New York: Harwood Academic Publishers. 413-436 p.

Pier GB. (2007). Pseudomonas aeruginosa lipopolysaccharide: a major virulence factor, initiator of inflammation and target for effective immunity. *International journal of medical microbiology : IJMM* 297: 277–295.

Plumley JA, Dannenberg JJ. (2010). The importance of hydrogen bonding between the glutamine side chains to the formation of amyloid VQIVYK parallel beta-sheets: an ONIOM DFT/AM1 study. *Journal of the American Chemical Society* 132: 1758–1759.

Ponce E, Flores N, Martinez A, Valle F, Bolívar F. (1995). Cloning of the two pyruvate kinase isoenzyme structural genes from Escherichia coli: the relative roles of these enzymes in pyruvate biosynthesis. *Journal of bacteriology* 177: 5719–5722.

Preston MJ, Seed PC, Toder DS, Iglewski BH, Ohman DE, Gustin JK, Goldberg JB, Pier GB. (1997). Contribution of proteases and LasR to the virulence of Pseudomonas aeruginosa during corneal infections. *Infection and immunity* 65: 3086–3090.

Prichard R, Schofield P. (1968). The metabolism of phosphoenolpyruvate and pyruvate in the adult liver fluke Fasciola hepatica. *Biochimica et Biophysica Acta (BBA) - General Subjects* 170: 63–76.

Ramphal R, Vishwanath S. (1987). Why is Pseudomonas the colonizer and why does it persist? *Infection* 15: 281–287.

Ramsay J. (2013). High-throughput β-galactosidase and β-glucuronidase Assays Using Fluorogenic Substrates. *Bio-Protocol* 3: e827–e827.

Ramseier TM, Bledig S, Michotey V, Feghali R, Saier MH. (1995). The global regulatory protein FruR modulates the direction of carbon flow in Escherichia coli. *Molecular microbiology* 16: 1157–1169.

Riordan JR, Rommens JM, Kerem B, Alon N, Rozmahel R, Grzelczak Z, Zielenski J, Lok S, Plavsic N, Chou JL. (1989). Identification of the cystic fibrosis gene: cloning and characterization of complementary DNA. *Science* 245: 1066–1073.

Rogers PL, Lee KJ, Tribe DE. (1979). Kinetics of alcohol production by zymomonas mobilis at high sugar concentrations. *Biotechnology Letters* 1: 165–170.

Romano AH, Conway T. (1996). Evolution of carbohydrate metabolic pathways. *Research in microbiology* 147: 448–455.

Romeo T, Babitzke P. (2018). Global Regulation by CsrA and Its RNA Antagonists. *Microbiology spectrum* 6.

Ronimus RS, Morgan HW. (2001). The biochemical properties and phylogenies of phosphofructokinases from extremophiles. *Extremophiles : life under extreme conditions* 5: 357–373.

Rose IA. (1970). Stereochemistry of pyruvate kinase, pyruvate carboxylase, and malate enzyme reactions. *The Journal of biological chemistry* 245: 6052–6056.

Roy-Burman A, Savel RH, Racine S, Swanson BL, Revadigar NS, Fujimoto J, Sawa T, Frank DW, Wiener-Kronish JP. (2001). Type III Protein Secretion Is Associated with Death in Lower Respiratory and Systemic *Pseudomonas aeruginosa* Infections. *The Journal of Infectious Diseases* 183: 1767–1774.

Sabnis NA, Yang H, Romeo T. (1995). Pleiotropic regulation of central carbohydrate metabolism in Escherichia coli via the gene csrA. *The Journal of biological chemistry* 270: 29096–29104.

Sakata Y, Akaike T, Suga M, Ijiri S, Ando M, Maeda H. (1996). Bradykinin generation triggered by Pseudomonas proteases facilitates invasion of the systemic circulation by Pseudomonas aeruginosa. *Microbiology and immunology* 40: 415–423.

Sambrook J, Fritsch EF, Maniatis T. (1989). Molecular cloning: a laboratory manual. New Work: Cold Spring Harbor Laboratory Press.

Santajit S, Indrawattana N. (2016). Mechanisms of Antimicrobial Resistance in ESKAPE Pathogens. *BioMed research international* 2016: 2475067.

Sawada K, Zen-in S, Wada M, Yokota A. (2010). Metabolic changes in a pyruvate kinase gene deletion mutant of Corynebacterium glutamicum ATCC 13032. *Metabolic Engineering* 12: 401–407.

Schuck P. (2000). Size-Distribution Analysis of Macromolecules by Sedimentation Velocity Ultracentrifugation and Lamm Equation Modeling. *Biophysical Journal* 78: 1606–1619.

Schweizer HP. (2003). Efflux as a mechanism of resistance to antimicrobials in Pseudomonas aeruginosa and related bacteria: unanswered questions. *Genetics and molecular research : GMR* 2: 48–62.

Schweizer HP, Po C. (1996). Characterization of the glpR Repressor Gene. 5215-5221 p.

Scott MG, Yan H, Hancock RE. (1999). Biological properties of structurally related alpha-helical cationic antimicrobial peptides. *Infection and immunity* 67: 2005–2009.

Seeholzer SH, Jaworowski A, Rose IA. (1991). Enolpyruvate: chemical determination as a pyruvate kinase intermediate. *Biochemistry* 30: 727–732.

Siddiquee K, Arauzo-Bravo MJ, Shimizu K. (2004). Effect of a pyruvate kinase (pykF-gene) knockout mutation on the control of gene expression and metabolic fluxes in Escherichia coli. *FEMS Microbiology Letters* 235: 25–33.

Smith CR, Knowles VL, Plaxton WC. (2000). Purification and characterization of cytosolic pyruvate kinase from Brassica napus (rapeseed) suspension cell cultures: implications for the integration of glycolysis with nitrogen assimilation. *European journal of biochemistry* 267: 4477–4485.

Smith RS, Harris SG, Phipps R, Iglewski B. (2002). The Pseudomonas aeruginosa quorum-sensing molecule N-(3-oxododecanoyl)homoserine lactone contributes to virulence and induces inflammation in vivo. *Journal of bacteriology* 184: 1132–1139.

Sprague GF. (1977). Isolation and characterization of a Saccharomyces cerevisiae mutant deficient in pyruvate kinase activity. *Journal of bacteriology* 130: 232–241.

Suzuki K, Ito S, Shimizu-Ibuka A, Sakai H. (2008). Crystal structure of pyruvate kinase from Geobacillus stearothermophilus. *Journal of biochemistry* 144: 305–312.

Tang H, Kays M, Prince A. (1995). Role of Pseudomonas aeruginosa pili in acute pulmonary infection. *Infection and immunity* 63: 1278–1285.

Temple LM, Sage AE, Schweizer HP, Phibbs P V. (1998). Carbohydrate Catabolism in Pseudomonas aeruginosa. In: Pseudomonas. Boston, MA: Springer US, p 35–72.

Tiwari NP, Campbell JJR. (1969). Enzymatic control of the metabolic activity of Pseudomonas aeruginosa grown in glucose or succinate media. *Biochimica et Biophysica Acta (BBA) - General Subjects* 192: 395–401.

Udaondo Z, Ramos J-L, Segura A, Krell T, Daddaoua A. (2018). Regulation of carbohydrate degradation pathways in *Pseudomonas* involves a versatile set of transcriptional regulators.

Microbial Biotechnology 11: 442–454.

Valentini G, Chiarelli L, Fortin R, Speranza ML, Galizzi A, Mattevi A. (2000). The allosteric regulation of pyruvate kinase. *The Journal of biological chemistry* 275: 18145–18152.

Valentini G, Iadarola P, Somani BL, Malcovati M. (1979). Two forms of pyruvate kinase in Escherichia coli a comparison of chemical and molecular properties. *Biochimica et Biophysica Acta (BBA) - Enzymology* 570: 248–258.

Vasu D, Sunitha MM, Srikanth L, Swarupa V, Prasad UV, Sireesha K, Yeswanth S, Kumar PS, Venkatesh K, Chaudhary A, Sarma PVGK. (2015). In Staphylococcus aureus the regulation of pyruvate kinase activity by serine/threonine protein kinase favors biofilm formation. *3 Biotech* 5: 505–512.

Voet D, Voet JG, Pratt CW. (2012). Glucose Catabolism. In: Fundamentals of biochemistry : life at the molecular level. Wiley & Sons, p 472–516.

Waterhouse A, Bertoni M, Bienert S, Studer G, Tauriello G, Gumienny R, Heer FT, de Beer TAP, Rempfer C, Bordoli L, Lepore R, Schwede T. (2018). SWISS-MODEL: homology modelling of protein structures and complexes. *Nucleic Acids Research* 46: W296–W303.

Waygood EB, Mort JS, Sanwal BD. (1976). The control of pyruvate kinase of Escherichia coli. Binding of substrate and allosteric effectors to the enzyme activated by fructose 1,6-bisphosphate. *Biochemistry* 15: 277–282.

Waygood EB, Rayman MK, Sanwal BD. (1975). The control of pyruvate kinases of Escherichia coli. II. Effectors and regulatory properties of the enzyme activated by ribose 5-phosphate. *Canadian journal of biochemistry* 53: 444–454.

Waygood EB, Sanwal BD. (1974). The control of pyruvate kinases of Escherichia coli. I. Physicochemical and regulatory properties of the enzyme activated by fructose 1,6-diphosphate. *The Journal of biological chemistry* 249: 265–274.

West SE, Schweizer HP, Dall C, Sample AK, Runyen-Janecky LJ. (1994). Construction of improved Escherichia-Pseudomonas shuttle vectors derived from pUC18/19 and sequence of the region required for their replication in Pseudomonas aeruginosa. *Gene* 148: 81–86.

Westbrock-Wadman S, Sherman DR, Hickey MJ, Coulter SN, Zhu YQ, Warrener P, Nguyen LY, Shawar RM, Folger KR, Stover CK. (1999). Characterization of a Pseudomonas aeruginosa efflux pump contributing to aminoglycoside impermeability. *Antimicrobial agents and chemotherapy* 43: 2975–2983.

Westheimer FH. (1987). Why nature chose phosphates. *Science* 235: 1173–1178.

Whitchurch CB, Tolker-Nielsen T, Ragas PC, Mattick JS. (2002). Extracellular DNA Required for Bacterial Biofilm Formation. *Science* 295: 1487–1487.

Whiteley M, Lee KM, Greenberg EP. (1999). Identification of genes controlled by quorum sensing in Pseudomonas aeruginosa. *Proceedings of the National Academy of Sciences of the United States of America* 96: 13904–9.

Winstanley C, O'Brien S, Brockhurst MA. (2016). Pseudomonas aeruginosa Evolutionary Adaptation and Diversification in Cystic Fibrosis Chronic Lung Infections. *Trends in microbiology* 24: 327–337.

Wolfgang MC, Jyot J, Goodman AL, Ramphal R, Lory S. (2004). Pseudomonas aeruginosa regulates flagellin expression as part of a global response to airway fluid from cystic fibrosis patients. *Proceedings of the National Academy of Sciences of the United States of America* 101: 6664–6668.

Wood TK, Knabel SJ, Kwan BW. (2013). Bacterial persister cell formation and dormancy. *Applied and environmental microbiology* 79: 7116–21.

Wooll JO, Friesen RH, White MA, Watowich SJ, Fox RO, Lee JC, Czerwinski EW. (2001). Structural and functional linkages between subunit interfaces in mammalian pyruvate kinase. *Journal of molecular biology* 312: 525–540.

Worlitzsch D, Tarran R, Ulrich M, Schwab U, Cekici A, Meyer KC, Birrer P, Bellon G, Berger J, Weiss T, Botzenhart K, Yankaskas JR, Randell S, Boucher RC, Döring G. (2002). Effects of reduced mucus oxygen concentration in airway Pseudomonas infections of cystic fibrosis patients. *Journal of Clinical Investigation* 109: 317–325.

Yamamoto M, Ueda A, Kudo M, Matsuo Y, Fukushima J, Nakae T, Kaneko T, Ishigatsubo Y. (2009). Role of MexZ and PA5471 in transcriptional regulation of mexXY in Pseudomonas aeruginosa. *Microbiology* 155: 3312–3321.

Yanisch-Perron C, Vieira J, Messing J. (1985). Improved M13 phage cloning vectors and host strains: nucleotide sequences of the M13mp18 and pUC19 vectors. *Gene* 33: 103–119.

Yoshimura F, Nikaido H. (1982). Permeability of Pseudomonas aeruginosa outer membrane to hydrophilic solutes. *Journal of bacteriology* 152: 636–642.

Zhao Q, Li XZ, Srikumar R, Poole K. (1998). Contribution of outer membrane efflux protein OprM to antibiotic resistance in Pseudomonas aeruginosa independent of MexAB. *Antimicrobial agents and chemotherapy* 42: 1682–1688.

Zhao X, Zhu Y, Hu J, Jiang L, Li L, Jia S, Zen K. (2018). Shikonin Inhibits Tumor Growth in Mice by Suppressing Pyruvate Kinase M2-mediated Aerobic Glycolysis. *Scientific Reports* 8: 14517.

Zhong W, Cui L, Goh BC, Cai Q, Ho P, Chionh YH, Yuan M, Sahili A El, Fothergill-Gilmore LA, Walkinshaw MD, Lescar J, Dedon PC. (2017). Allosteric pyruvate kinase-based "logic gate" synergistically senses energy and sugar levels in Mycobacterium tuberculosis. *Nature communications* 8: 1986.

Zhong W, Morgan HP, McNae IW, Michels PAM, Fothergill-Gilmore LA, Walkinshaw MD. (2013). `In crystallo' substrate binding triggers major domain movements and reveals magnesium as a co-activator of Trypanosoma brucei pyruvate kinase. *Acta crystallographica. Section D, Biological crystallography* 69: 1768–1779.

Zoraghi R, See RH, Axerio-Cilies P, Kumar NS, Gong H, Moreau A, Hsing M, Kaur S, Swayze RD, Worrall L, Amandoron E, Lian T, Jackson L, Jiang J, Thorson L, Labriere C, Foster L, Brunham RC, McMaster WR, Finlay BB, Strynadka NC, Cherkasov A, Young RN, Reiner NE. (2011). Identification of Pyruvate Kinase in Methicillin-Resistant Staphylococcus aureus as a Novel Antimicrobial Drug Target. *Antimicrobial Agents and Chemotherapy* 55: 2042–2053.

Zoraghi R, See RH, Gong H, Lian T, Swayze R, Finlay BB, Brunham RC, McMaster WR, Reiner NE. (2010). Functional Analysis, Overexpression, and Kinetic Characterization of Pyruvate Kinase from Methicillin-Resistant *Staphylococcus aureus*. *Biochemistry* 49: 7733–7747.

Appendixes

Appendix 1: Geometry of Thr282 in PykA. Left: Image of the PykA model showing that the enzyme has well-defined electron density surrounding Thr282. Right: Ramachandran plot showing that Thr282 (arrow) had unusual phi and psi angles and that it lies in an outlier area. This geometry of Thr282 is seen in the 12 chains of PykA (outliers = 12).
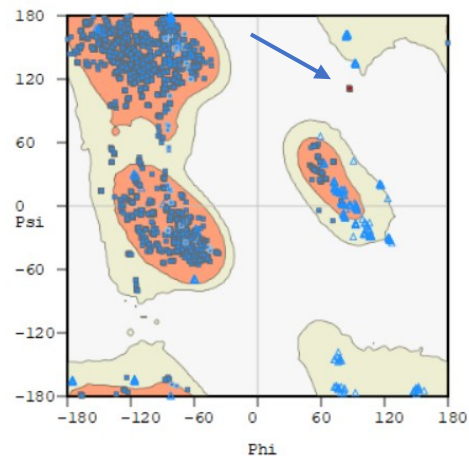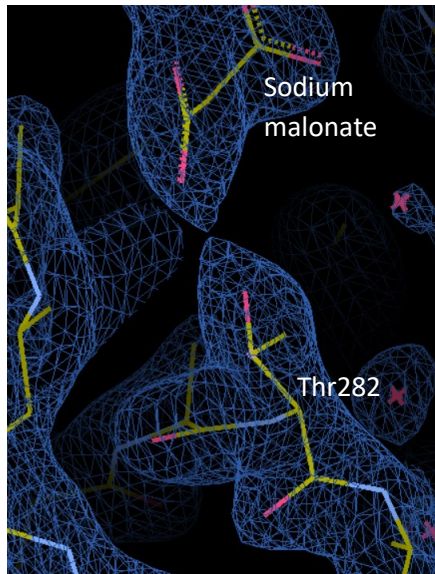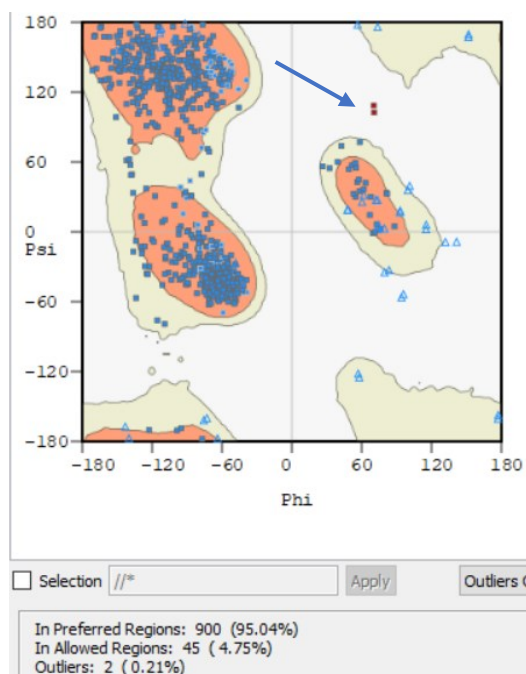
Appendix 2: Geometry of Thr275 in PykF. Left: Image of the PykF model showing that the enzyme has well-defined electron density surrounding Thr275. Right: Ramachandran plot showing that Thr275 had unusual odd phi and psi angles (arrow) and that it lies in an outlier area. This geometry of Thr275 is seen in the two chains of PykF (outliers = 2).

Appendix 3: Analytical ultracentrifugation (AUC) analysis of PykA (52.3 kDa) showing that the enzyme is assembled into a tetramer in solution (196 kDa).
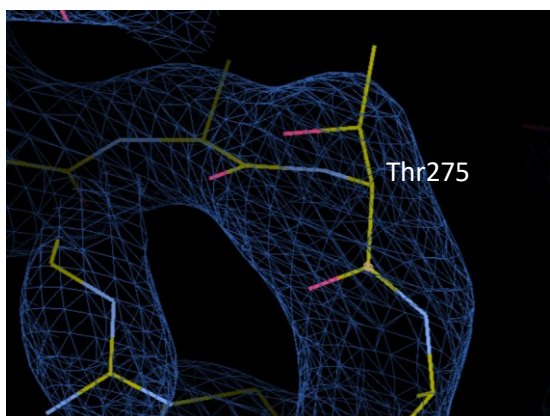
Appendix 4: Superposition of PykA chains. Rmsd values were generated using PDBefold. All chains were assumed as complete except for chain J, where the B domain was unmodelled.

| Rmsd (Å)	A	B	C	D	E	F	G	H	I	J	K	L
A		0.24	0.61	1.2	1.25	1.39	1.54	1	1.27	0.34	1.56	0.72
B	0.24		0.53	1.2	1.21	1.53	1.27	0.88	1.2	0.33	1.45	0.6
C	0.61	0.53		0.92	0.99	1.56	1.32	0.86	0.93	0.39	1.55	0.77
D	1.2	1.2	0.92		0.17	1.1	1.29	0.87	0.32	0.36	1.4	1.04
E	1.25	1.21	0.99	0.17		1.05	1.51	0.92	0.27	0.37	1.42	1.11
F	1.39	1.53	1.56	1.1	1.05		0.44	1.37	1.33	0.59	0.5	1.21
G	1.54	1.27	1.32	1.29	1.51	0.44		1.41	1.48	0.42	0.46	1.54
H	1	0.88	0.86	0.87	0.92	1.37	1.41		0.78	0.19	1.28	0.48
I	1.27	1.2	0.93	0.32	0.27	1.33	1.48	0.78		0.34	1.4	1.05
J	0.34	0.33	0.39	0.36	0.37	0.59	0.42	0.19	0.34		0.48	0.2
K	1.56	1.45	1.55	1.4	1.42	0.5	0.46	1.28	1.4	0.48		1.16
L	0.72	0.6	0.77	1.04	1.11	1.21	1.54	0.48	1.05	0.2	1.16	

Appendix 5: Domain motion analysis of PykA using DynDom. The data represents output results from superposition of all chains to chain E. Note that the bending residues in all moving domains correspond to the B domain region in each chain.

| Moving domain	Rotation angle (°)	Translation (Å)	Closure %	Bending residues
A	18.9	0.6	39.8	71-75
				162-176
B	18.1	0.5	31.7	71-75
				162-171
C	11.5	-0.1	47	71-75
				162-164
D	1.2	0	96.4	70-71
				169-170
F	32.8	0	89.6	71-74
				162-176
G	36.9	-0.2	88.1	70-75
				165-174
H	12.5	0.3	5	71-75
				164-171
I	3.1	0.1	7	71-75
				163-172
K	32.8	-0.4	91.7	69-73
				166-179
L	17.2	0.3	12	71-75
				162-176

Appendix 6: Superposition of PykA chains after deletion of the B domain. Rmsd values were generated using PDBefold.

Rmsd (Å)	A	B	C	D	E	F	G	H	I	J	K	L
A		0.149	0.213	0.234	0.242	0.431	0.359	0.236	0.226	0.218	0.398	0.18
B	0.149		0.151	0.275	0.24	0.48	0.41	0.303	0.259	0.268	0.441	0.245
C	0.213	0.151		0.262	0.221	0.406	0.529	0.358	0.249	0.333	0.418	0.308
D	0.234	0.275	0.262		0.109	0.374	0.269	0.253	0.088	0.271	0.395	0.241
E	0.242	0.24	0.221	0.109		0.394	0.282	0.281	0.097	0.276	0.416	0.267
F	0.431	0.48	0.406	0.374	0.394		0.351	0.508	0.482	0.53	0.359	0.476
G	0.359	0.41	0.529	0.269	0.282	0.351		0.329	0.282	0.348	0.249	0.407
H	0.236	0.303	0.358	0.253	0.281	0.508	0.329		0.254	0.139	0.375	0.123
I	0.226	0.259	0.249	0.088	0.097	0.482	0.282	0.254		0.25	0.432	0.239
J	0.218	0.268	0.333	0.271	0.276	0.53	0.348	0.139	0.25		0.384	0.160
K	0.398	0.441	0.418	0.395	0.416	0.359	0.249	0.375	0.432	0.384		0.415
L	0.18	0.245	0.308	0.241	0.267	0.476	0.407	0.123	0.239	0.160	0.415	

Appendix 7: Close-up view of the three extra residues which elongate the Aβ5-Aα5 loop in PykA. The figure shows that there is unbiased electron density surrounding the three residues.
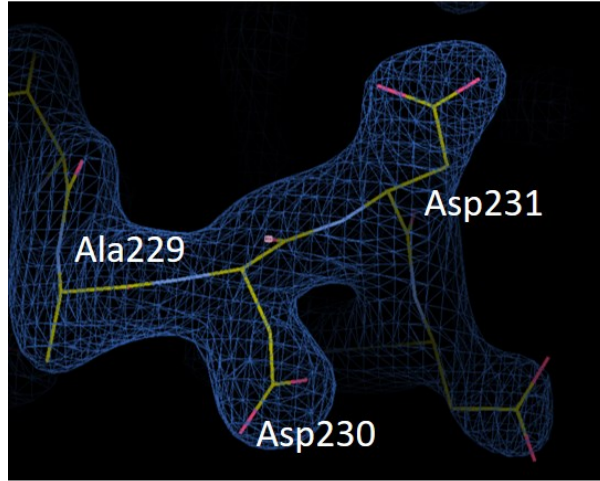
Appendix 8: Analytical ultracentrifugation (AUC) analysis of PykF (51.5 kDa) showing that the enzyme is assembled into a tetramer in solution (192 kDa).
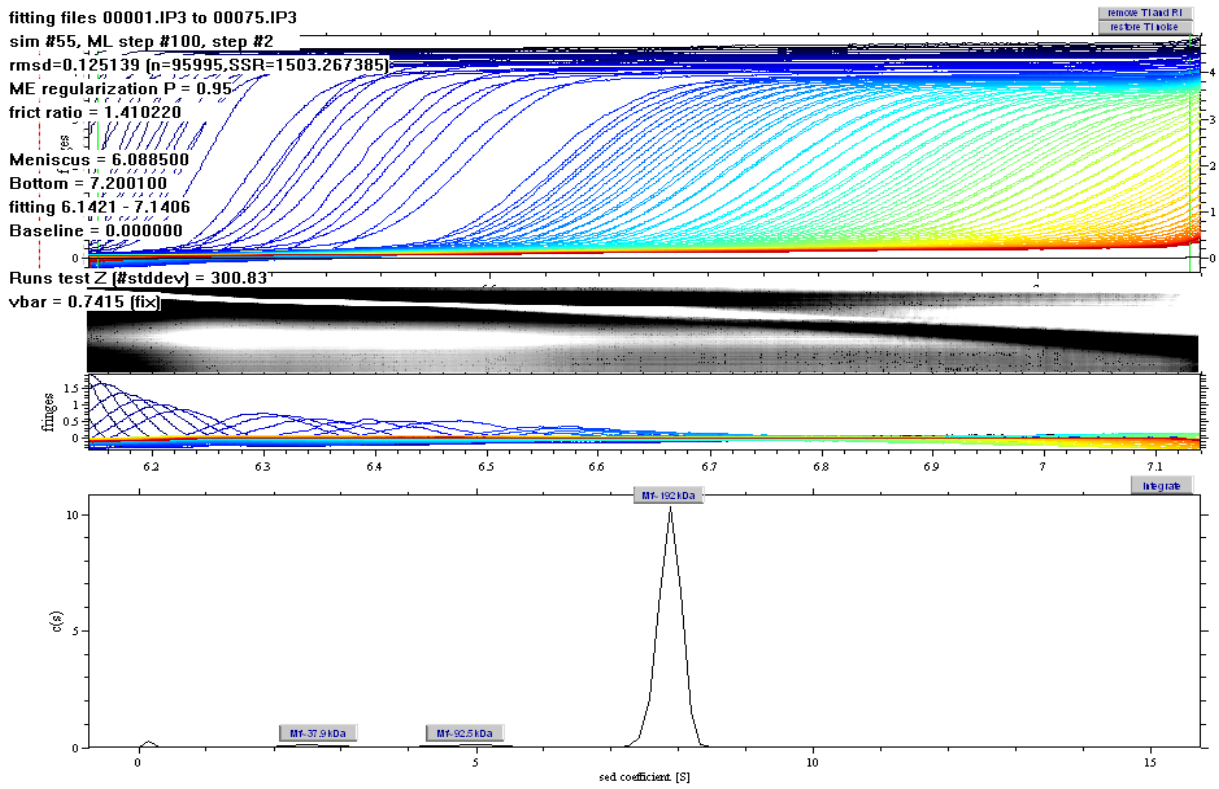
Appendix 9: Alignment of the amino acid sequence at the A-A interface in PykF. Residues involved in the formation of the A-A interface are marked with black asterisks. Residues highlighted in red are 100% identical, whereas a column is framed in blue if more than 70% of the residues have similar physicochemical properties. Residues are annotated according to the amino acid sequence of PykF in *P. aeruginosa*.